Nitrilase 2: insight into its regulation in Arabidopsis and its potential for improving maize salt tolerance

by

Nina-Courtney Foreman

Thesis presented for the degree of **Doctor of Philosophy**

In the Department of Molecular and Cell Biology

University of Cape Town

February 2023

TABLE OF CONTENTS

3.4. Discussion

CHAPTER 4: FUNCTIONAL CHARACTERISATION OF THE MAIZE *NITRILASE 2* HOMOLOG UNDER SALINE CONDITIONS IN ARABIDOPSIS

4.1. Introduction

4.2. Materials and methods

4.3. Results

4.4. Discussion

CHAPTER 5: FINAL DISCUSSION AND SUGGESTIONS FOR A WAY FORWARD

DECLARATION

I hereby declare that this thesis, submitted in fulfilment of the requirements for the degree of Doctor of Philosophy in the Department of Molecular and Cell Biology at the University of Cape Town, is the result of my own investigations, apart from the referenced work of others, and that neither the whole work nor any part of it has been, is being, or is to be submitted for another degree in this or any other university.

_____

Nina-Courtney Foreman

University of Cape Town

11/02/2023

ACKNOWLEDGEMENTS

Firstly, I need to thank the National Research Foundation and the University of Cape Town for their financial support throughout this project, without whom none of this would have been possible.

Next, a huge thank you to Shane Murray and Rob Ingle for inspiring a curiosity within me to alter the path of my life from being set on doing my postgraduate studies in human genetics, to deciding to pursue plant science. Wow – plants are cool! Thankfully, eight years after those formative undergraduate lectures, I still feel this way.

To my supervisors, Lara Donaldson and Rob Ingle, thank you for everything. I am so grateful for all of your guidance and support that have led me to where I am today and will continue to stay with me in my future. I am grateful not only for your part in helping shape this thesis, but also in shaping me into the scientist I am today. Also, to the members of lab 430 over the years, especially to Lee, Paul, Shannon, Grant, and Amy – thank you for all of the shared laughs, (sometimes) tears, troubleshooting discussions, and friendship. I am so glad that I could conduct my research in such a wonderful environment, with colleagues that I can also call friends.

To Katherine Denby, who allowed me to visit her lab at the University of York to complete my yeast one-hybrid experiment, and Fabian Vaistij, who guided me in this protocol, I am so grateful for your assistance and willingness to collaborate.

To my family and friends outside the lab, it's been a ride! Thank you for dealing with all of my PhD-related mood swings and looking at my never-ending plant photos. To my uncle Lawrence, thank you for never hesitating to lend support and encouragement when it was needed. To Jeremy, I don't know if there are words to express how much your support has meant to me. I am so glad that I met you on my first day of university, and that you are the person that I get to spend the rest of my life with. Thank you for always helping me believe in myself and for inspiring me to be a better version of myself. To my Nana, who is no longer with us, thank you for giving me the tools to help me accomplish my dreams. I hope that I have made you proud.

ABSTRACT

By the year 2050, it is estimated that more than 50% of the arable land worldwide will be too saline to sustain the growth and productivity of many crop plants. Soil salinisation threatens food security because it reduces crop yield and quality. Therefore, to increase food production for the growing population, we need to improve crop salt tolerance. To do this, we need a better understanding of inherent plant molecular responses to salt stress in order to engineer crops with enhanced salt tolerance.

Previously, our group has shown that in Arabidopsis, salt-specific genes are enriched in the gene ontology term "response to auxin stimulus", and auxin levels increase under saline conditions. *Nitrilase 2* was identified as the biosynthetic gene possibly responsible for these changes in auxin accumulation as *AtNit2* expression was elevated specifically under saline conditions. Additionally, *AtNit2* overexpression lines were more salt tolerant.

As *AtNit2* is a candidate for enhancing plant growth under saline conditions to improve salt tolerance, it is important to understand how this gene is regulated and this was the main aim of this research project. The *AtNit2* promoter region was analysed and five MYELOBLASTOSIS (MYB) transcription factor (TF) binding sites were identified. Interestingly, two MYB TFs were upregulated specifically in response to salt in our experiments. These two TFs, AtMYB2 and AtMYB30 were functionally characterised in Arabidopsis to investigate whether they might be upstream of *AtNit2* in the plant salt stress response pathway. Overexpression of *AtMYB2* in Arabidopsis did not lead to altered *AtNit2* expression or biomass production under saline conditions, nor was binding of AtMYB2 to the *AtNit2* promoter observed in a yeast one-hybrid (Y1H) assay, suggesting that it may not be involved in *AtNit2* regulation. Although AtMYB30 did not bind directly to the *AtNit2* promoter in the Y1H assay, *AtMYB30* overexpressing plants were more salt tolerant and showed increased expression of *AtNit2* under control and saline conditions. An *atmyb30* T-DNA mutant line also showed a reduction in salt tolerance, however *AtNit2* was still upregulated under saline conditions in the *atmyb30* T-DNA mutant lines. Overall, this data indicates that AtMYB30 might play an indirect role in *AtNit2* regulation.

To identify TFs that can bind to the *AtNit2* promoter, a Y1H TF library screen approach was used. Six TFs were identified: HOMEOBOX PROTEIN 34 (AtHB34), HOMEOBOX PROTEIN 24

(AtHB24), HOMEOBOX PROTEIN 28 (AtHB28), HIGH MOBILITY GROUP BOX PROTEIN 9 (AtHMGB9), GLABRA 2 (AtGL2), and SQUAMOSA PROMOTER BINDING PROTEIN-LIKE 7 (AtSPL7). Two of these TFs were further characterised: AtHMGB9 and AtSPL7. Reporter assays in Arabidopsis mesophyll protoplasts showed that AtHMGB9 was able to bind to and negatively regulate *AtNit2* promoter activity *in planta.* However, *athmgb9* mutant lines displayed only slightly increased *AtNit2* expression under saline conditions. While transfection of protoplasts with AtSPL7 did not lead to changes in *AtNit2* promoter:reporter activity*, atspl7* lines showed slightly increased *AtNit2* expression indicating that AtSPL7 may play a role in negatively regulating *AtNit2* expression but may require other co-factors to do so *in planta*.

To determine whether *Nit2* regulation is also important for maize salt tolerance, preliminary analysis of the maize *Nit2* homolog, *ZmNit2,* showed that *ZmNit2* expression was induced in response to salt in both root and shoot tissue in a dose-dependent manner, implying that auxin might play a role in salt tolerance across different plant species. Overexpressing *ZmNit2* was sufficient to increase salt tolerance of two-week old Arabidopsis plants, indicating that *ZmNit2* may play a role in the maize response to salt stress early in development and therefore suggests that genes identified in Arabidopsis may be appropriate targets for manipulation in crop plants, such as maize.

Overall, this study provides novel insights into the regulation of *AtNit2* by identifying several TFs that may bind to and regulate *AtNit2* expression. It also shows that *ZmNit2* is able to improve Arabidopsis salt tolerance and indicates a potential role in improving maize salt tolerance.

LIST OF SYMBOLS AND ABBREVIATIONS

A	adenine
ABA	abscisic acid
AD	activation domain
ANOVA	analysis of variance
At	*Arabidopsis thaliana*
ATP	adenosine 5-triphosphate
BD	binding domain
BG	background
BLAST	basic local alignment tool
bp	base pair(s)
BS	binding site
˚C	degrees Celsius
C	cytosine
CaMV	cauliflower mosaic virus
cDNA	complementary deoxyribonucleic acid
CDS	coding sequence
Chl	chlorophyll
Col-0	Columbia Arabidopsis ecotype
DBD	DNA-binding domain
dH_2O	deionized water
DNA	deoxyribonucleic acid
dNTPs	deoxy-ribonucleoside triphosphates
$dS.m^{-1}$	decisiemens per metre
EDTA	ethylene glycol tetraacetic acid
EtOH	ethanol
EtBr	ethidium bromide
EV	empty vector

F	forward
FC	fold change
FDR	false discovery rate
FL	full-length
fmol	femtomole(s)
g	gravity constant (9.81 m.s-1)
g	gram
G	guanine
GA	gibberellic acid
GFP	green fluorescent protein
GH3	Gretchen Hagen 3
GO	gene ontology
GOI	gene of interest
GUS	β-glucuronidase
HB	homeobox
HD	homeodomain
His	histidine
HKT	high-affinity K+ channels
hr	hour(s)
IAA	indole-3-acetic acid
IAN	indole-3-acetonitrile
kb	kilobase
KEP	Kalahari Early Pearl
KO	knock-out
L	litre
LB	Luria Bertani
LC-MS/MS	liquid chromatograph coupled with tandem mass spectrometry
Leu	leucine

Luc	luciferase
LucF	firefly luciferase
LucR	*Renilla* luciferase
LR	lateral root
M	molar
m	meter(s)
MES	morpholinoethane sulfonic acid
mg	milligram(s)
min	minute(s)
mL	millilitre(s)
mM	millimolar
mRNA	messenger RNA
MW	molecular weight
n	sample size
N/A	not applicable
NASC	Nottingham Arabidopsis Stock Centre
ng	nanogram
Nit	nitrilase
No-0	Nossen Arabidopsis ecotype
NSCC	non-selective cation channel
nm	nanometer
nM	nanomolar
O/N	overnight
OD_X	optical density at X nanometer wavelength light
OE	overexpressor
p	probability
PCR	polymerase chain reaction
PTM	post-translational modification
PDI	protein-DNA interaction

Phe	phenylalanine
PI	propidium iodide
PM	plasma membrane
PN	plant nutrient
qPCR	quantitative PCR
R	reverse
RM	ready-mix
RNA	ribonucleic acid
RNAi	RNA interference
rpm	revolutions per minute
ROS	reactive oxygen species
RT-qPCR	quantitative reverse transcriptase PCR
s/sec	second(s)
SAUR	small auxin-upregulated RNA
SD	synthetic defined
SDS	sodium dodecyl sulphate
sorb	sorbitol
SOS	salt-overly-sensitive
T	thymine
TAE	tris-acetate
TAIR	The Arabidopsis Information Resource
T-DNA	transfer DNA
Thr	threonine
TF(s)	transcription factor(s)
TFBS	transcription factor binding site
Tris	trisaminomethane
TSS	transcription start site
Trp	tryptophan

U	units
UTR	untranslated region
UV	ultraviolet
vol	volume
v/v	volume/volume
WT	wild type
w/v	weight/volume
Y1H	yeast one-hybrid
Y2H	yeast two-hybrid
Zm	*Zea mays*
µg	microgram(s)
µL	microlitre(s)
µM	micromolar
µmol	micromole(s)
#	number

CHAPTER 1: INTRODUCTION

1.1. The global impact of soil salinisation

As the global population increases exponentially, it is important to increase food production to meet the food demands of the expected population. By 2050, a 50% increase in global food production is required to ensure food security (Chakraborty & Newton, 2011). A variety of plants are extremely important as food and energy sources worldwide and are subject to yield losses primarily due to abiotic stresses (Munns & Tester, 2008; Reynolds & Tuberosa, 2008). Unfortunately, due in large part to climate change and poor agricultural practices, the frequency and severity of these abiotic stresses is increasing, and this is detrimentally affecting yields. Climate change has resulted in shifts in temperatures and weather patterns, often resulting in extreme temperatures, drought, and soil salinisation. These abiotic stresses are particularly devastating as they affect a wide range of plant physiological and biochemical processes, such as osmotic and ionic homeostasis, and nutrient uptake (Wang, Vinocur & Altman, 2003). Therefore, to ensure food security, generating more stress-resistant crop plants is important. Through conventional plant breeding techniques more stress-tolerant varieties of different crop plants have become available. However, conventional breeding is too slow and the success rate is not sufficient to meet the increased food demands (Gong et al., 2015). Therefore, other molecular mechanisms to improve abiotic stress tolerance are becoming more important, such as marker-assisted selection, genome editing, and genetic engineering.

Soil salinity, one of the abiotic stresses negatively affecting global crop productivity, is characterised by soils with an electrical conductivity of saturated soil extract (ECe) above 4 $dS.m^{-1}$. This is approximately equivalent to 40 mM NaCl, with NaCl being the most soluble and abundant salt responsible for soil salinity (Chinnusamy, Jagendorf & Zhu, 2005; Munns & Tester, 2008). Soil salinisation occurs through both natural means, such as wind- and rain-mediated deposition of oceanic salts, and man-made processes, such as irrigation with poor quality water (Gupta & Huang, 2014; van Zelm, Zhang & Testerink, 2020). It is estimated that high salinity affects 20% of total cultivated land and 33% of irrigated agricultural land worldwide, which is responsible for producing around a third of the global crop supply (Athar & Ashraf, 2009; Rengasamy, 2010). The estimated economic impact of soil salinity on irrigated

land has been extrapolated to exceed 27 billion US$ per year (Qadir et al., 2014). By the year 2050, it is estimated that more than 50% of the arable land worldwide will be salinized (Jamil et al., 2011). As most crop plants are salt-sensitive glycophytes, improving plant salt tolerance is extremely important for ensuring food security. Even moderate salinity (EC 4-8 $dS.m^{-1}$) can reduce crop yields by 50-80% depending on the species (Panta et al., 2014). Progress in breeding for salt-tolerant crops has been hindered by a lack of understanding of the molecular basis of salt tolerance. Therefore, investigating how salinity affects plant growth and development, and how plants respond to salinity at a molecular level, is the first step in producing more salt-tolerant crop plants (Chinnusamy, Jagendorf & Zhu, 2005).

1.2. The impact of salinity on plant growth and development

Broadly speaking, salinity inhibits plant growth in two main phases: quickly during an ion-independent phase when the salt concentration begins to build up in the soil surrounding the plant root, and later during an ion-dependent phase once NaCl has accumulated to toxic levels within the plant shoot.

During the ion-independent phase, an osmotic stress occurs when a build-up of sodium ions (Na^+) in the environment results in the osmotic strength of the soil being greater than that inside the root cell. Almost immediately, this osmotic gradient drives water out of the cytosol of the plant cells (Shabala & Cuin, 2008). Water loss from the cytosol hinders normal cellular metabolism. To prevent this, water is moved from the vacuole into the cytosol, resulting in a reduction in cell turgor and decreased root and shoot elongation. Additionally, the osmotic potential of the plant is decreased and therefore water uptake is inhibited, thereby also reducing the uptake of important growth-limiting nutrients (Thompson et al., 1997; Shabala & Cuin, 2008). To prevent further water loss, plants rapidly close their stomata, resulting in a loss of photosynthetic activity and an increase in reactive oxygen species (ROS) due to over-reduction of the electron transport chain (Munns & Termaat, 1986; Yang & Guo, 2018). As a result of these changes, there is a rapid reduction in the shoot growth rate as there is a reduction in the rate at which growing leaves expand and new leaves emerge (figure 1.1-A). This has been recorded in numerous plants, including rice (Yeo et al., 1991), maize, (Cramer & Bowman, 1991) and wheat and barley (Passioura & Munns, 2000). The same changes occur when plants are exposed to polyethylene glycol (PEG), mannitol or KCl, illustrating that this

phase is not salt-specific (Yeo et al., 1991; Chazen, Hartung & Neumann, 1995). In roots, there are also rapid and transient reductions in primary and lateral root growth rates after NaCl exposure that are similar to those seen with KCl and mannitol, indicating that in roots these effects are also due to sudden changes in water potential (Frensch & Hsiao, 1994; Julkowska et al., 2017; Rodríguez et al., 1997). Therefore, this osmotic stress imposed by salt is not specific to salinity stress as similar osmotic stress is imposed by other abiotic and biotic stresses, such as drought and temperature stress. However, during this ion-independent phase there are also rapid responses to salinity stress which are salt-specific, involving Na^+ sensing and signalling before Na^+ has accumulated to toxic levels. Research has shown that during this phase, Ca^{2+} and ROS waves trigger downstream cascades to elicit systemic molecular responses in target organs, and may contribute to whole-plant stress tolerance (Choi et al., 2014; Al-shareef & Tester, 2019).

Once osmotic homeostasis is restored, usually after no longer than a day (Passioura & Munns, 2000; Munns, 2002), growth is resumed at a lower rate (figure 1.1-B) with root growth recovering significantly better than shoot growth.

When growth resumes, plants will resume water uptake and thus Na^+ and Cl^- ions will be taken up by the cell (Munns, 1993). This second growth reduction phase, which is ion-dependent, takes place after several days or weeks (depending on the type of plant) of continued salt exposure once Na^+ and Cl^- ions have entered the transpiration stream. In salt-sensitive plants, this results in a further reduction in the shoot growth rate (figure 1.1-C), primarily due to Na^+ accumulation. This is because of the physiochemical similarity between Na^+ and the essential element K^+, with Na^+ competing with K^+ for binding sites on proteins involved in key metabolic processes such as protein synthesis, ribosome functions, and enzymatic reactions (Marschner, 1995). There are over 50 cytoplasmic enzymes that require K^+ as a co-factor and can be inhibited by Na^+, making Na^+ accumulation detrimental (Marschner, 1995). Additionally, Na^+ competitively inhibits K^+ uptake, further decreasing cytosolic K^+ levels (Assaha et al., 2017). Furthermore, increased ROS levels, due to stomatal closure, enhances K^+ efflux through ROS-activated non-selective cation channels (NSCCs) (Wu, 2018). Overall, the decrease in K^+, along with increased cellular Na^+, results in reduced K^+/Na^+ ratios during this ion-dependent salinity stress – interrupting many metabolic processes. If Na^+ continues to be taken up, and eventually reaches toxic levels, this leads to senescence, primarily in older

leaves which are no longer expanding and diluting the ions to non-toxic levels like younger growing leaves do (Munns & Tester, 2008). If older leaves are dying faster than new leaves emerge, the whole plant will not have enough photosynthetic capacity to maintain carbohydrate levels necessary for the new leaves to grow and the plant will eventually die (Munns & Tester, 2008; Roy, Negrão & Tester, 2014).

More salt-tolerant plants are better able to respond to this ion-dependent phase of salinity stress and are better able to maintain shoot growth under saline conditions (figure 1.1-D).

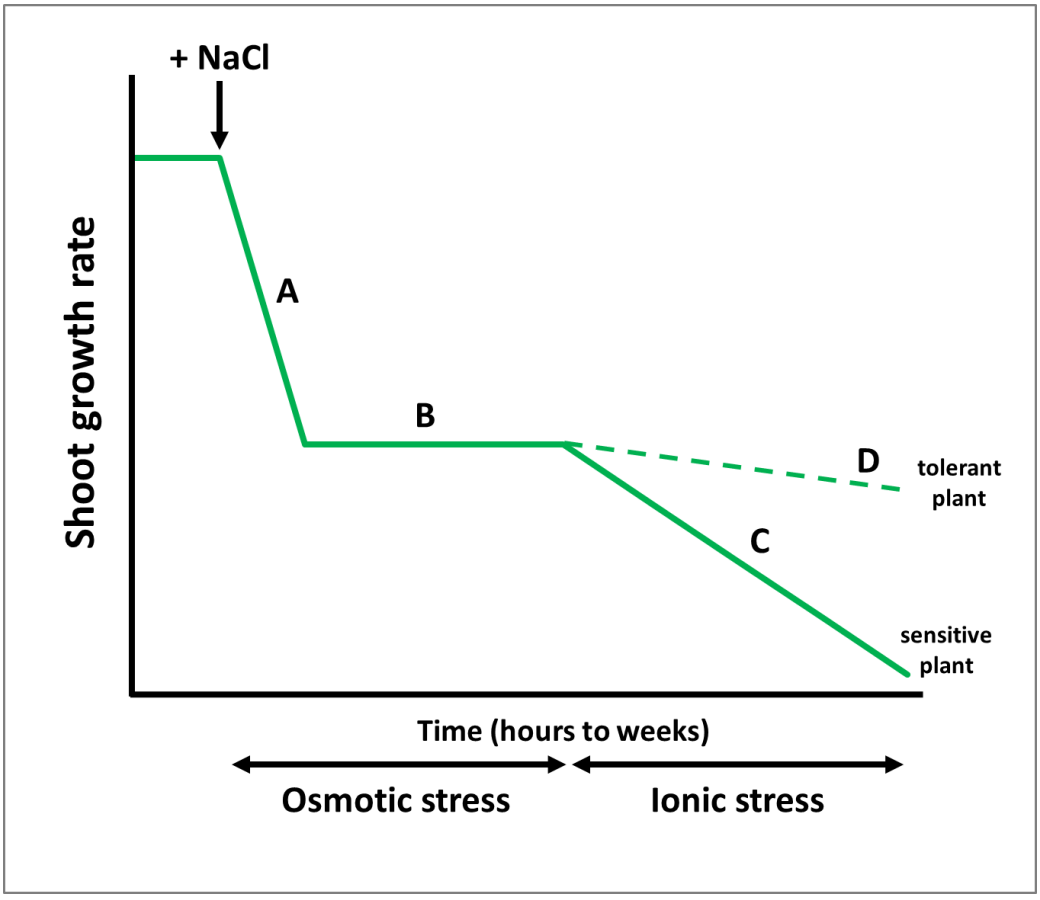

Figure 1.1: Reduction in plant shoot growth rate under saline conditions

A schematic showing the two phases of plant shoot growth reduction caused by salinity stress. During the first phase, shoot growth is rapidly reduced because of the osmotic stress caused by the saline solution outside of the plant roots (**A**). Once osmotic homeostasis is regained via osmotolerance mechanisms, growth resumes at a reduced rate (**B**). During the second shoot growth reduction phase, a more gradual decrease in shoot growth is observed when Na^+ and Cl^- ions have accumulated to toxic levels in the leaves which imposes an ionic stress in salt-sensitive plants (**C**). Salt-tolerant plants are better able to maintain growth during this second phase (**D**). Adapted from Munns (2005).

1.3. Plant responses to salinity stress

Plant responses to accumulation of Na^+ in the soil initiate within seconds (Julkowska & Testerink, 2015). In order to recover plant growth, plants employ three main strategies: 1) osmotolerance, 2) sodium ion exclusion, and 3) tissue tolerance mechanisms. Osmotolerance is a response to the ion-independent osmotic stress imposed by salinity whilst tissue tolerance mechanisms only occur during the ion-dependent phase of salinity and sodium ion exclusion likely occurs throughout the salinity stress period (Munns & Tester, 2008). These three mechanisms of salinity tolerance can be employed simultaneously by different species, depending on many factors such as the duration of stress, salt concentration and plant growth stage (Roy, Negrão & Tester, 2014). Osmotolerance will be discussed briefly below, whilst the latter two responses which are salt-specific will be discussed in section 1.4.

1.3.1. Osmotolerance

Osmotolerant plants are better able to maintain shoot and root growth under saline conditions whilst also maintaining stomatal conductance (Alqahtani et al., 2019). There are several osmotolerance mechanisms that plants employ, including 1) accumulation of compatible osmolytes, 2) regulation of ROS levels , 3) membrane rearrangement to maintain cell membrane integrity and correct for the loss of turgor induced by osmotic stress, and 4) hormonal regulation of growth and development.

Compatible osmolytes are low molecular weight organic compounds that lower the osmotic potential in the cytoplasm, whilst not impacting metabolic reactions, in order to balance the osmotic potential inside and outside of the cell to prevent water loss and enhance turgor pressure and cell expansion (Park, Kim & Yun, 2016). Examples of osmolytes include the nitrogen-containing solutes proline and glycine betaine, simple sugars such as sucrose and raffinose, complex sugars (e.g. trehalose), and sugar alcohols (e.g. sorbitol and mannitol) (Al-shareef & Tester, 2019). During salinity stress these osmolytes can also function as protein osmoprotectants, signalling molecules, and as antioxidants to reduce oxidative stress under saline conditions (Cheong & Yun, 2007). Several enzymes involved in controlling the rate of compatible osmolyte production have been shown to alter salinity tolerance. For example, overexpressing the *Δ-pyrroline-5-carboxylate synthetase* (*P5CS*) gene, the rate-limiting enzyme involved in plant proline biosynthesis, increases salinity tolerance in Arabidopsis

(Chen et al., 2013). However, synthesis of compatible osmolytes is energetically costly to plants, often resulting in decreased plant growth (Munns & Tester, 2008; Al-shareef & Tester, 2019).

In order to reduce ROS accumulation following stomatal closure, plants implement several antioxidant mechanisms including enzymatic ROS-scavengers such as superoxide dismutase (which coordinates the transfer of electrons to oxygen acceptors other than water), catalase and various peroxidases, as well as the production of non-enzymatic ROS-scavenging compounds (e.g. ascorbic acid) (Apel & Hirt, 2004; Park, Kim & Yun, 2016). As ROS waves also function in stress signalling, maintaining the correct balance of ROS is important in the plant response to salinity stress.

Osmotic stress perception results in production of second messengers such as Ca^{2+} (Knight, Trewavas & Knight, 1997). Increased cytosolic Ca^{2+} activates many phosphoprotein cascades involved in downstream signalling. One of these cascades results in the accumulation of abscisic acid (ABA), a hormone involved in osmotic stress responses including the regulation of guard cells to close stomata to prevent further water loss, and cellular dehydration tolerance by upregulating expression of genes encoding dehydration tolerance proteins (Zhu, 2002). Osmotic stress triggers activation of SNF1-related protein kinase 2s (SnRK2s) in both ABA-dependent and -independent manners. The aforementioned osmotic stress-induced accumulation of ABA activates subclass III SnRK2 kinases, while subclass I SnRK2s are activated in an ABA-independent pathway under osmotic stress. These SnRK2s play an important role in ABA signal transduction and in regulating downstream gene expression responses by activating ABA-responsive element binding factor (AREB/ABF) transcription factors in the nucleus to induce expression of stress-responsive genes (Zhao et al., 2020).

Additionally, to conserve water and decrease Na^{+} uptake, plants increase their root to shoot biomass ratio as a reduction in leaf growth relative to root growth lowers plant water use efficiency (WUE) (Munns & Tester, 2008).

While osmotic stress responses are important to investigate, the above only touches briefly on osmotic stress sensing and responses (refer to Zhao et al., (2020) and van Zelm et al. (2020) for detailed reviews). The work in our lab group focusses on investigating salt-specific plant responses to salinity stress and these will be discussed in more detail.

1.4. Salt-specific responses to salinity stress

1.4.1. Na^+ transport

Despite decades of research, the mechanisms whereby Na^+ enters roots and is transported throughout plants is still not well understood (Isayenkov & Maathuis, 2019). It is thought that Na^+ enters the root epidermal cells through either plasma membrane (PM) transporters/channels, or through "leakage" into the root from the apoplast (Essah, Davenport & Tester, 2003). Once inside the root epidermis, the Na^+ ions are transported radially through the concentric layers of root tissue (epidermis, cortex and endodermis) before being loaded into the xylem for transport to the shoot (Barberon & Geldner, 2014). Ion movement through these layers can occur via three different pathways: 1) through cellular connections (symplastic), 2) through the cell wall (apoplastic), and 3) cell-to-cell through transcellular pathways (Chinnusamy, Jagendorf & Zhu, 2005). The deposition of an apoplastic barrier, such as the Casparian strip, limits apoplastic Na^+ transfer across root cells into the xylem, thereby ensuring a higher selectivity for ion movement both into and out of the stele (Apse & Blumwald, 2007).

Many different PM channels/transporters are thought to play a role in Na^+ uptake and transport, as well as during plant salinity stress response mechanisms. Examples of these include the aforementioned non-selective cation channels (NSCCs), as well as high-affinity K^+ channels (HKTs), voltage-independent channels (VIC), intracellular Na^+/H^+ exchangers (NHXs), low-affinity K^+ channels, and aquaporins (Essah, Davenport & Tester, 2003; Assaha et al., 2017; Yang & Guo, 2018). Although the role of each transporter and the pattern of transporter gene expression can vary within species under different growth environments, these different transporters are thought to work in conjunction to mediate Na^+ uptake and transport (Apse & Blumwald, 2007). Figure 1.2 shows a simplified schematic of the location of the main plant Na^+ transporters identified to date, and in which direction they transport Na^+ ions, with further information about each family of transporters described thereafter.

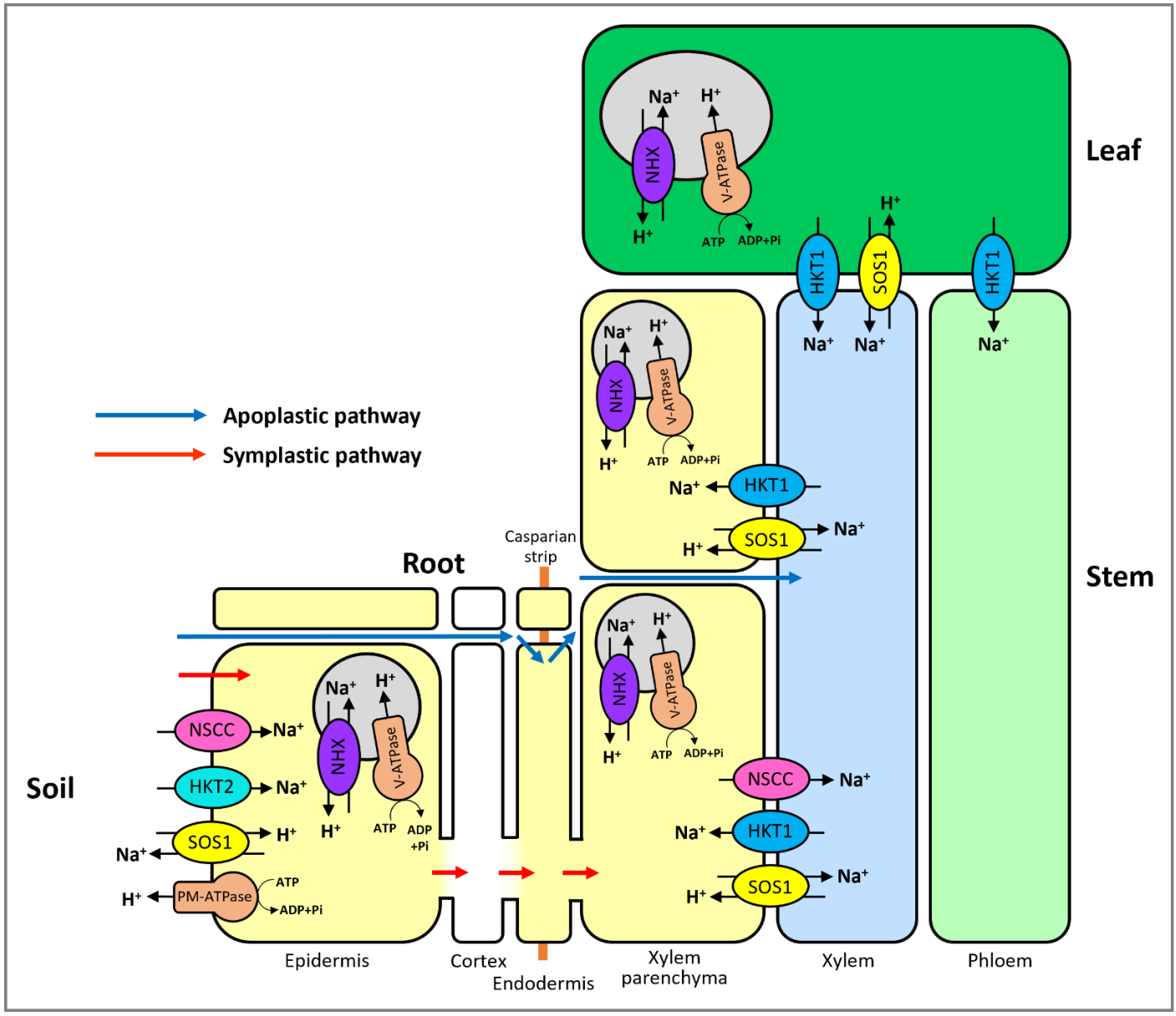

Figure 1.2: A schematic showing possible Na^+ transport routes in plants

Sodium (Na^+) is taken up and moved through the root via transporters including NSCCs, SOS1 (an NHX family member) and HKTs, loaded into the xylem and moved up the transpiration stream into the shoot. The Na^+ ions which reach the shoot tissue are either compartmentalised into vacuoles (grey) via tonoplast-based Na^+/H^+ exchangers from the NHX family, or transported back to the root via transporters such as HKT1. In the root, Na^+ is either compartmentalised into vacuoles or excreted back into the soil via transporters such as SOS1. The NHX family of transporters are fuelled by the plasma membrane ATPase (PM-ATPase) and vacuolar ATPase (V-ATPase) that actively pump H^+ in the opposite direction. Black arrows show the direction of Na^+ (or K^+ or H^+) movement through transporters. Blue arrows represent Na^+ entry sites and routes through cell walls (apoplastic pathway). Red arrows represent Na^+ entry sites and cytoplasmic routes through plasma-membranes (symplastic pathway). Adapted from Feki et al. (2015), Isayenkov & Maathuis (2019) and van Zelm et al. (2020).

1.4.1.1. Non-selective cation channels (NSCCs)

Generally, NSCCs, which include cyclic nucleotide-gated channels (CNGCs) and glutamate receptor-like channels (GLRs) (Demidchik, Essah & Tester, 2004), are thought to be the main transporters of Na^+ into plant roots under high soil salinity conditions (Tester & Davenport, 2003; Horie & Schroeder, 2004). These NSCCs are regulated by different salt-induced signals (such as Ca^{2+}, 3',5'-cyclic guanosine monophosphate (cGMP), and ROS), and are permeable to mono- and divalent cations, such as Na^+, K^+ and Ca^{2+} (Wang et al., 2013). The selectivity of CNGCs for Na^+ and K^+ is variable, with some more selective for one over the other, and some equally permeable to both (Apse & Blumwald, 2007).

1.4.1.2. High affinity K^+ transporters (HKTs)

In plants, two roles for HKTs exist; as Na^+-selective uniporters (HKT1 subfamily), and as Na^+/K^+ symporters (HKT2 subfamily) (Horie & Schroeder, 2004). Members of the HKT family have been shown to play important roles in plant salinity tolerance mechanisms. For example, the most studied member of subfamily 1, Arabidopsis AtHKT1;1 (the only member of the HKT family in Arabidopsis), has been shown to play various roles in shoot Na^+ exclusion. Several lines of evidence exist which show that AtHKT1;1 is involved in long-distance Na^+ transport; by facilitating shoot-to-root transport of Na^+ by loading Na^+ into the phloem stream and by unloading Na^+ from the xylem into xylem parenchymal cells (Sunarpi et al., 2005). Berthomieu et al. (2003) reported that an *athkt1;1* mutant showed decreased Na^+ concentration in the phloem sap, increased Na^+ in the aerial organs, and decreased Na^+ in the roots compared to WT plants, implying that AtHKT1;1 might play a role in Na^+ recirculation from shoots to roots by loading shoot Na^+ into the phloem and unloading it into the roots. Another study demonstrated, via immunoelectron microscopy using anti-AtHKT1;1 antibodies and an *AtHKT1;1-GUS* reporter line, that AtHKT1;1 is targeted to the plasma membrane in xylem parenchyma cells (in leaves). This study also showed that three *athkt1;1* loss-of-function mutants had higher Na^+ content in the xylem sap, indicating that AtHKT1;1 is important in the process of removing excess Na^+ from the xylem (Sunarpi et al., 2005). Transgenic Arabidopsis plants overexpressing *AtHKT1;1* in the root cells surrounding the xylem showed a significant reduction in shoot Na^+ and increased salinity tolerance (Møller et al., 2009). However, when this gene is constitutively expressed it results in detrimental effects, implying that AtHKT1;1 might have another function in Arabidopsis (Rus et al., 2001). This same study showed that

two *athkt1;1* mutants displayed reduced Na^+ accumulation compared to WT plants, implying that AtHKT1;1 might also play a role in Na^+ uptake from the soil (Rus et al., 2001). A more recent study supports this idea, showing that AtHKT1;1 mediates low-affinity Na^+ uptake in Arabidopsis under external conditions of 2.5 mM K^+ (Wang et al., 2015). While there is still contention over this role of AtHKT1;1 in Na^+ uptake, it is clear that AtHKT1;1 is crucial for the regulation of Na^+ homeostasis under saline conditions. Orthologues of AtHKT1;1 have been identified in many crop plants including rice (OsHKT1;5), wheat (TmHKT1;5-A and TaHKT1;5-D), and maize (ZmHKT1;2), where similar functions in shoot Na^+ exclusion are observed (Ren et al., 2005; Byrt et al., 2014; Zhang et al., 2023). This indicates that this is a widely used salt tolerance mechanism in monocot plants that has been conserved across evolution. Moreover, HKT1;5 has actually been identified as a salt tolerance determinant by quantitative trait locus (QTL) analysis in rice (Ren et al. 2005), wheat (Byrt et al., 2007), and barley (Hazzouri et al., 2018). Field trials have also shown that transferring *TmHKT1;5-A* into bread wheat reduced leaf Na^+ accumulation by 30%, further showing the importance of this HKT1 subfamily in Na^+ exclusion mechanisms of salinity tolerance (James et al., 2011).

In terms of Na^+ uptake from the soil, it is more widely accepted that only HKT2 subfamily members, also present in many monocots, are involved in mediating Na^+ uptake. For example, rice OSHKT2;1, which is localised to the PM of the root epidermis, mediates Na^+ uptake in low K^+, low Na^+ (<2 mM) conditions and down-regulation of this gene was shown to improve the tolerance of rice to salinity (Horie et al., 2007).

1.4.1.3. Intracellular Na^+/H^+ exchangers (NHXs)

The main role of NHXs is in exchanging Na^+ (or K^+) for H^+ across the tonoplast or plasma membrane in roots and shoots to improve salinity tolerance (Bassil et al., 2011). These transporters are driven by the proton electrochemical gradient generated by H^+-ATPases and pyrophosphatases (H^+-PPases), meaning that this mechanism of salinity tolerance is energetically expensive and comes at a cost to other plant processes (Munns et al., 2020). These NHXs are often located on vacuolar membranes and are thought to compartmentalise Na^+ (which will be discussed in more detail later). The Arabidopsis NHX antiporter *AtNHX1* was the first plant NHX homolog to be cloned and characterised in vacuolar Na^+ sequestration (Gaxiola et al., 1999). In Arabidopsis, overexpression of *AtNHX1* increases salt tolerance and

Na^+ accumulation in shoot tissue under saline conditions (Apse et al., 1999). Heterologous expression of *AtNHX1-5* in yeast mutants lacking endosomal vacuolar antiporters was able to rescue the salt sensitivity of the yeast mutant, thus indicating that these NHXs play a role in vacuolar transport of Na^+ to improve salinity tolerance (Aharon et al., 2003). Furthermore, tobacco plants overexpressing the cotton *GhNHX1* gene show enhanced salinity tolerance (Wu et al., 2004). Despite the earlier belief that NHXs were only involved in Na^+/H^+ exchange, evidence has emerged that NHX1 and NHX2 proteins may also operate as K^+/H^+ exchangers, playing a role in vacuolar potassium homeostasis because of their equal affinity for K^+ (Jiang, Leidi & Pardo, 2010; Maathuis, Ahmad & Patishtan, 2014). A study showed that Arabidopsis *nhx1 nhx2* double mutants had decreased vacuolar K^+ content, impaired osmoregulation, and compromised turgor generation for cell expansion compared to WT plants under saline conditions (Barragán et al., 2012). Additionally, Bassil et al. (2011) took a reverse genetics approach in Arabidopsis to show that AtNHX1 and AtNHX2 maintain vacuolar K^+ and, in the process, regulate the vacuolar pH and facilitate cell expansion. Another study showed that overexpression of the tomato *LeNHX2* enhanced salt tolerance by improving vacuolar K^+ compartmentalisation, resulting in a higher K^+/Na^+ ratio and thereby decreasing Na^+ toxicity (Rodríguez-Rosales et al., 2008). Taken together, these data show that the tonoplast localised NHXs seem to be important for intracellular Na^+ and K^+ transport in various plant species.

Another NHX protein that has been well characterised is Salt-Overly-Sensitive-1 (SOS1)/NHX7, a Na^+/H^+ exchanger shown in SOS1::GFP transgenic Arabidopsis to localise to the PM rather than the tonoplast (Shi et al., 2002). SOS1 was identified in a mutant screen for Arabidopsis lines unable to maintain root growth under saline conditions, where the *sos1* mutant was found to be over 20 times more sensitive to Na^+ compared to WT plants (Ding & Zhu, 1997). This NHX is important for Na^+ ion exclusion, discussed in more detail in section 1.4.2.1 (Ji et al., 2013).

1.4.2. Salinity response mechanisms

In most plant species, Na^+ appears to reach a toxic concentration before Cl^- does, and so the main plant responses to this ion-dependent salinity stress are Na^+ exclusion back into the soil, compartmentalisation of Na^+ into the vacuole, and K^+ retention in the cytosol. Additionally, leaf morphology is altered as leaves become thicker, with a smaller surface area, in order to

increase nitrogen and chlorophyll concentration per unit area to improve photosynthesis (James et al., 2002).

1.4.2.1. Na^+ ion exclusion

In order to reduce Na^+ levels, plants employ ion exclusion mechanisms which include: 1) minimising Na^+ uptake from the soil into root cells, 2) maximising Na^+ efflux from root cells into the soil, 3) reducing Na^+ loading into the root xylem, 4) increasing Na^+ retrieval from the xylem into root cells, and 5) transport of Na^+ away from the shoot tissue back to the root by maximising phloem loading.

The Salt-Overly-Sensitive (SOS) pathway, involving the SOS1 plasma membrane Na^+/H^+ exchanger mentioned previously, plays an important role in mediating many of these processes. In this pathway, high extracellular Na^+ leads to elevated Ca^{2+} (Knight, Trewavas & Knight, 1997) which is sensed by the SOS3 Ca^{2+}-binding protein. The SOS3 protein undergoes a conformational change upon Ca^{2+} binding which leads to it interacting with and activating SOS2, a serine/threonine protein kinase (Ji et al., 2013). This SOS3-SOS2 complex promotes recruitment of SOS2 to the PM, leading to SOS2-mediated phosphorylation of SOS1 (Zhu, 2002). Once phosphorylated, SOS1 is activated and increases Na^+ extrusion from root epidermal cells at the root-soil interface (figure 1.2), thereby reducing the net Na^+ uptake (Qiu et al., 2003). Therefore SOS1 , which has been shown to localise to the root epidermis using SOS1::GUS reporter lines, offers the first line of resistance to Na^+ accumulation, by extruding Na^+ back into the soil (Shi et al., 2002). This importance is evident when comparing Arabidopsis (a glycophyte) and its salt-resistant relative *Thellugiella salsuginea* (a halophyte), where the salt-resistant *T. salsuginea* has enhanced expression of *SOS1* in both leaves and roots compared to Arabidopsis. When *ThSOS1* is knocked-out, *T. salsuginea* is as susceptible as Arabidopsis to high salinity, with high accumulation of Na^+ in the shoot tissue (Oh et al., 2009). This also highlights the evolutionary conservation of this salt tolerance mechanism. Additionally, under severe salt stress, SOS1 is proposed to function in unloading Na^+ from shoot tissue into the root xylem to reduce Na^+ accumulation and damage in leaves that might be caused by exceeding the capacity of Na^+ sequestration in leaf cell vacuoles (Shi et al., 2002). This study showed that a *sos1* mutant had decreased Na^+ accumulation in the shoot under mild NaCl conditions (25 mM) compared to WT plants. Conversely, under high NaCl conditions

(100 mM), the *sos1* mutant had increased Na^+ content in the shoot compared to WT, while also displaying increased Na^+ content in the xylem sap compared to WT. Taken together, these results led the researchers to propose a mechanism whereby, under mild salinity, SOS1 functions in the PM to load Na^+ into the xylem in roots for its transfer and storage in leaf mesophyll vacuoles, and to extrude Na^+ from the shoot by loading it into the xylem, whilst under high salinity it functions to retrieve Na^+ from the xylem to extrude back into the soil (Shi et al., 2002).

Additionally, the aforementioned Casparian strip can play a role in restricting Na^+ transport from the cortical cells into the stele (Apse & Blumwald, 2007). Casparian strips can be formed in both the endo- and exodermis (Kreszies, Schreiber & Ranathunge, 2018). Importantly, Arabidopsis lacks the ability to form an exodermis, meaning that it only has the endodermal Casparian strip to act as a barrier against Na^+ (Nawrath et al., 2013).

1.4.2.2. Ionic tissue tolerance

Despite ion exclusion mechanisms, continued exposure to Na^+ will eventually mean that Na^+ will start accumulating in the cytosol of plant cells. To reduce cytosolic Na^+ and ensure adequate K^+/Na^+ ratios for correct enzyme functioning, plants compartmentalise Na^+ within vacuoles (known as ionic tissue tolerance) (Munns & Tester, 2008). This is mainly achieved by activation of the tonoplast NHXs (Apse et al., 1999; Blumwald, 2000), energised by the vacuolar H^+-ATPase (V-ATPase) and pyrophosphatase (V-PPase) (Fukuda et al., 2004). The SOS signalling pathway, discussed previously, is thought to play an indirect role in this process. A study using Arabidopsis tonoplast vesicles in ion transport assays showed that Na^+/H^+ exchange via AtNHX1 were greatly reduced in a *sos2* mutant, whilst addition of constitutively active recombinant SOS2 protein to these vehicles was able to promote Na^+/H^+ exchange (Qiu et al., 2004). Evidently, control of the SOS pathway is important in enabling plants to prevent Na^+ toxicity by both limiting Na^+ accumulation in shoot tissue, and compartmentalising Na^+ into vacuoles.

1.4.2.3. K^+ retention in the cytosol

As mentioned previously, K^+ is an essential macronutrient in plants, important in many enzymatic reactions. Additionally, K^+ plays an important role in osmotic adjustment and

turgor generation, regulation of membrane electric potential, and cytoplasmic pH homeostasis. It is the most abundant inorganic cation in plants, making up almost 10% of their dry weight (White & Karley, 2010). As Na^+ is physiochemically very similar to K^+, controlling the K^+/Na^+ ratio is important for salt tolerance. In addition to shuttling Na^+ away from the cytosol using the mechanisms described previously, plants also respond to salt stress by employing strategies to retain K^+ in the cytosol. Studies have shown that barley and wheat cultivars that are able to retain or increase cytoplasmic K^+ in their mesophyll cells are more salt tolerant (Wu et al., 2013). In fact, the ability to maintain K^+/Na^+ ratios is one of the distinguishing factors between salt tolerant and salt sensitive genotypes (Wu et al., 2015).

Retention of optimal cytosolic K^+ levels during salt stress can be achieved by increasing root K^+ uptake, increased loading of K^+ into the xylem for transport to the shoot, and inhibition of cytosolic K^+ efflux (Assaha et al., 2017). At the root-soil interface, K^+ uptake is mediated by high affinity K^+ uptake (HAK) or low affinity K^+ uptake (LAT). Here, HAK is modulated by the KT/HAK/KUP family of K^+ transporters, and LAT is mediated by members of the shaker family of K^+ channels (e.g. AKT1) (Gierth & Mäser, 2007). When conditions become saline, this causes Na^+-induced membrane depolarisation which prevents KT/HAK/KUP and AKT1 channels from moving K^+ into the cell. In order to prevent this, PM Na^+/H^+ exchangers (e.g., SOS1) maintain a stable membrane potential to improve K^+ uptake (Assaha et al., 2017). Additionally, other NHXs such as NHX1 and NHX2 maintain adequate K^+/Na^+ ratios by maintaining vacuolar K^+ content as described previously. The PM H^+-ATPase also plays a role in cytosolic K^+ retention, which will be discussed further in section 1.7.3.

1.4.2.4. Cl^- tolerance

Although not as widely researched due to Cl^- ions reaching toxic levels after Na^+ in most plant species, plants do have mechanisms to tolerate increased Cl^- ion uptake under saline conditions. Despite Cl^- being an essential nutrient in plants, involved in regulating enzymatic activity, turgor, and pH levels; Cl^- can also be toxic to plants if allowed to over-accumulate as Cl^- competes with major macronutrients such as nitrate (NO_3^-) for uptake from the soil, which is an important source of nitrogen for plants (Tyerman, 1992; Marschner, 1995; Xu et al., 1999; White & Broadley, 2001). As with Na^+, key aspects of Cl^- tolerance include reducing net Cl^- xylem loading, intracellular Cl^- compartmentalisation, and greater efflux of Cl^- from roots

back into the soil (Teakle & Tyerman, 2010). A network of predicted Cl^- transporters exists that could play a role in these processes; including cation-chloride cotransporters (CCCs), chloride channels (CLCs), aluminium-activated malate transporters (ALMTs) and nitrate excretion transporters (NAXTs) (Teakle & Tyerman, 2010). The rate-limiting step in Cl^- accumulation, the transfer of Cl^- from the root symplast to the xylem apoplast (which antagonises NO_3^- delivery to the shoots), is regulated under drought and saline conditions by abscisic acid (ABA), and is multigenic (Cubero-Font et al., 2016; Li et al., 2016).

1.5. Tools we use to study plant stress responses

The previous sections described the impact of salinity stress on plants and how the plant responds to both the ion-independent and ion-dependent components of salinity stress. The following section will describe some of the tools that are used by researchers in order to investigate how plants respond to stresses.

1.5.1. Arabidopsis as a model plant

Arabidopsis thaliana (Arabidopsis) is a small diploid plant in the Brassicaceae family and has been the model organism for research in plant science since the 1980s for a number of reasons (Meinke et al., 1998). Arabidopsis is easy to grow in petri dishes, in culture or in soil; is small in size, has a short life cycle, and the large amount of ±0.5 mm seeds produced allows for the rapid growth of many plants in a relatively small area (Meinke et al., 1998). It also undergoes self-fertilisation to produce multiple progeny and can easily be cross-fertilised by applying pollen to the stigma surface, allowing for easy generation of new genotypes. The Arabidopsis genome is organised in five chromosomes and was the first plant genome to be fully sequenced (The Arabidopsis Genome Initiative, 2000). Many different ecotypes (accessions) have been collected from natural populations distributed throughout Europe, Asia and North America, and are available for experimental analysis. A large multinational initiative, the *A. thaliana* 1001 Genomes Project, aims to sequence 1001 different Arabidopsis accessions (Weigel & Mott, 2009). As part of this project, many online tools are freely available for progressing Arabidopsis and plant research (https://1001genomes.org). Numerous optimised methods exist to easily mutagenize and transform Arabidopsis, allowing for efficient development of mutants, overexpressor and other genetically modified plant lines for functional characterisation of candidate genes *in planta.* Additionally, commercially

available mutants exist for almost all Arabidopsis genes (Alonso et al., 2003). Despite Arabidopsis itself not being an important crop plant, it has proven invaluable in the research of other economically important plants as there can be conservation of function of orthologues of Arabidopsis genes, meaning that often genes in crop plants have been identified, classified and characterised based on their sequence similarity and known function in Arabidopsis (Bolle, Schneider & Leister, 2016). For example, the Arabidopsis defence signalling gene *NONEXPRESSOR OF PR GENES 1 (AtNPR1)* was used to genetically engineer disease-resistance in tomato plants (Lin et al., 2004). Stephenson et al. (2019) also showed that by elucidating key regulators in Arabidopsis fruit patterning, they were able to translate this knowledge into oilseed rape (*Brassica napus*) to adjust the seed pod-opening process to significantly reduce seed loss, thereby increasing yield.

In terms of salt stress, Arabidopsis is a salt-sensitive glycophyte as it cannot complete its life cycle when exposed to constant conditions of 100 mM NaCl or more (Cackett et al., 2022). Compared to its salt-tolerant halophytic relative, *Thellungiella halophila*, there are very few genomic differences, indicating that salt tolerance is more likely as a result of changes in the transcriptome during growth under saline conditions (Kant et al., 2006). To this point, researchers showed that many genes known to be induced by abiotic stress in Arabidopsis exhibit higher levels of expression in *T. halophila* under unstressed conditions, suggesting that constitutive expression of conserved stress responsive genes forms a basis for the salt tolerance of *T. halophila* (Taji et al., 2004). Additionally, analysis of Arabidopsis and *T. halophila* transcript profiles has shown that 60% of stress-regulated genes are differentially regulated between the two species, with T*. halophila* transcript intensities suggesting stress-anticipatory preparedness in *T. halophila* (Gong et al., 2005). Thus, if we can determine how important salt tolerance genes are regulated in Arabidopsis, we might be able to engineer plants that anticipate and respond quicker to stress.

1.5.2. Transcriptome profiling

Transcriptomic profiling offers a snapshot into the genome-wide gene expression at a particular time point. The advantage of this is being able to determine which genes are being expressed, and to what level this occurs, offering insight into processes being carried out in the organism at the time of sampling. Microarrays are commonly used for quantitative

transcriptomic profiling as they are high-throughput, relatively cheap, and easy to perform (Baginsky et al., 2010). This technology involves binding an array of thousands to millions of known nucleic acid fragments to a solid surface which is then bathed with cDNA, synthesised from RNA isolated from a study sample (such as cells or tissue). Complementary base pairing between the sample and the chip-immobilized fragments produces light through fluorescence as the cDNAs are labelled with a fluorescent dye. This fluorescence is then detected using a specialized scanner (Bednar, 2000; Xiang & Chen, 2000). Microarrays manufactured by Affymetrix and Agilent are most commonly used in Arabidopsis (Redman et al., 2004; Busch & Lohmann, 2007). Another method that has become very popular for transcriptomic profiling is RNA sequencing (RNA-Seq), which was formerly more often used in non-model organisms, or for transcript discovery and genome annotation (Wang, Gerstein & Snyder, 2009; Baginsky et al., 2010). These methods are commonly used as an initial screen to identify interesting genes being differentially expressed.

1.6. Transcriptomic changes during the salt-specific, ion-dependent stress response

To date, few studies have differentiated between transcriptomic responses imposed by each of the ion-independent and ion-dependent components of salinity stress (Shavrukov, 2013), and typically, plants have been treated with high concentrations of NaCl, or with low NaCl concentrations but for very short periods of time (Abogadallah, 2010; Tang et al., 2011; Goyal et al., 2016; Li et al., 2019). As previously described, the salt-specific component of salinity stress (ion-dependent component) is only induced after a gradual accumulation of Na^+ ions within shoot tissue, days to weeks after exposure to NaCl. This means that these sorts of experiments would only have imposed an ion-independent osmotic stress (or even an osmotic shock resulting in plasmolysis) on the plants, failing to mimic natural exposure to salinity stress (Munns, 2002). Manipulation of genes identified in these analyses would not be specific to salinity stress and might detrimentally interfere with the plant response to other important stresses, such as drought or temperature stress (Shavrukov, 2013). For example, Tang et al. 2011 exposed Arabidopsis to 300 mM NaCl for only 30 minutes and looked at candidate gene expression. This type of stress would not occur naturally and is not physiologically relevant. In order to avoid inducing osmotic shock, whilst ensuring that both of the expected salt stress responses are induced, plants should either be exposed gradually to increasing NaCl concentrations over a period of days, or be exposed once-off to low concentrations of NaCl

(Shavrukov, 2013). Studies have been conducted using these techniques in various plants, such as rice (Wang et al., 2018), wheat (Luo et al., 2019), and Arabidopsis. One of these studies in Arabidopsis was conducted recently by our group (Cackett, 2019; Cackett et al., 2022).

In the study by Cackett et al. (2022), Arabidopsis seeds were sown onto media in petri dishes containing low, physiologically relevant concentrations of NaCl (0 mM, 50 mM, 75 mM, 100 mM and 125 mM NaCl) as well as iso-osmolar concentrations of sorbitol (0 mM, 100 mM, 150 mM, 200 mM and 250 mM sorbitol) and grown for two weeks (early development microarray). Microarray analysis was performed for transcriptome profiling, and genes differentially expressed in response to NaCl treatment, but not sorbitol, were classified as salt-specific; presumably responding to the ion-dependent component of salt stress. Overall, 2519 genes showed a salt-specific increase in expression, and 2272 genes showed a salt-specific decrease in expression. To determine what processes these salt-specific genes might be involved in, a gene ontology (GO) enrichment analysis was performed on genes differentially regulated by at least 2-fold. Interestingly, the GO term "response to auxin stimulus" was significantly enriched, with 25 genes annotated as such, including several *SMALL AUXIN-UPREGULATED RNA*s (*SAUR*s). Furthermore, a microarray was performed later in development on plants grown hydroponically for two weeks in untreated control conditions, and then grown for a further two weeks in 0, 50, 75 or 100 mM NaCl treatments (later development microarray) (Cackett, 2019). Again, genes differentially expressed under saline conditions were enriched in the "response to auxin stimulus" GO term (Cackett, 2019). The fact that this term was consistently enriched in the salt stress responsive transcriptome of Arabidopsis at different developmental stages suggests that auxin may be important in modulating salt-specific growth adaptations to salinity stress at different stages of growth and developmental (Cackett et al., 2022).

1.7. Auxin and its role in the plant response to salt stress

1.7.1. The role of auxin in plant growth

Despite being the first plant growth hormone to be identified some 100 years ago, auxin metabolism, biosynthesis and signalling are still not fully understood (Abel & Theologis, 2010). Indole-3-acetic acid (IAA), the most predominantly occurring auxin, plays an important role in many aspects of plant growth and development, including organogenesis, general plant

architecture, vascular development, senescence, and environmental and stress responses (Woodward & Bartel, 2005; Zhao, 2010). Accumulation of auxin plays a role in cell division and elongation through initiation of signal transduction pathways that result in altered levels and activation of proteins involved in plant growth, such as EXPANSINS which are cell wall-loosening proteins that promote cell elongation (Majda & Robert, 2018). Studies testing the effects of exogenous auxin on plant growth have shown that auxin has both growth promoting and inhibiting functions (Collett, Harberd & Leyser, 2000). Specifically, auxin promotes cell elongation in shoot tissue, initiates lateral root formation, increases gravitropism and phototropism, and promotes cell division in the cambium. Conversely, auxin inhibits the development of lateral buds and the elongation of primary roots (Collett, Harberd & Leyser, 2000). Evidently, the control and localisation of auxin accumulation is vital during plant development.

1.7.2. Auxin biosynthesis

Generally, plants have two different pathways for auxin biosynthesis, one that is tryptophan-dependent (TD), and one that is tryptophan independent (TI) (figure 1.3) (Woodward & Bartel, 2005). In the TI pathway, IAA is synthesised directly from indole, whereas in the TD pathway indole is first converted into L-tryptophan (L-Trp) (Normanly, Cohen & Fink, 1993). Both the TI and TD pathways are involved in maintaining auxin homeostasis (Di et al., 2016). Of the two, the TD pathway has been extensively studied and is known to contain four different pathways which result in IAA synthesis from L-Trp, named after the main intermediate in each pathway: the indole-3- acetamide (IAM) pathway, the indole-3-pyruvic acid (IPyA) pathway, the tryptamine (TAM) pathway, and the indole-3-acetaldoxime (IAOx) pathway (Woodward & Bartel, 2005). In the IAOx pathway, L-Trp is converted into IAOx, which is then converted either into IAM or indole-3-acetonitrile (IAN), both of which are then finally converted into IAA. Specifically, IAN is converted into IAA by the AtNIT1-3 family of enzymes (Bartling et al., 1992). These TD pathways, with the associated enzymes, are shown in figure 1.3.

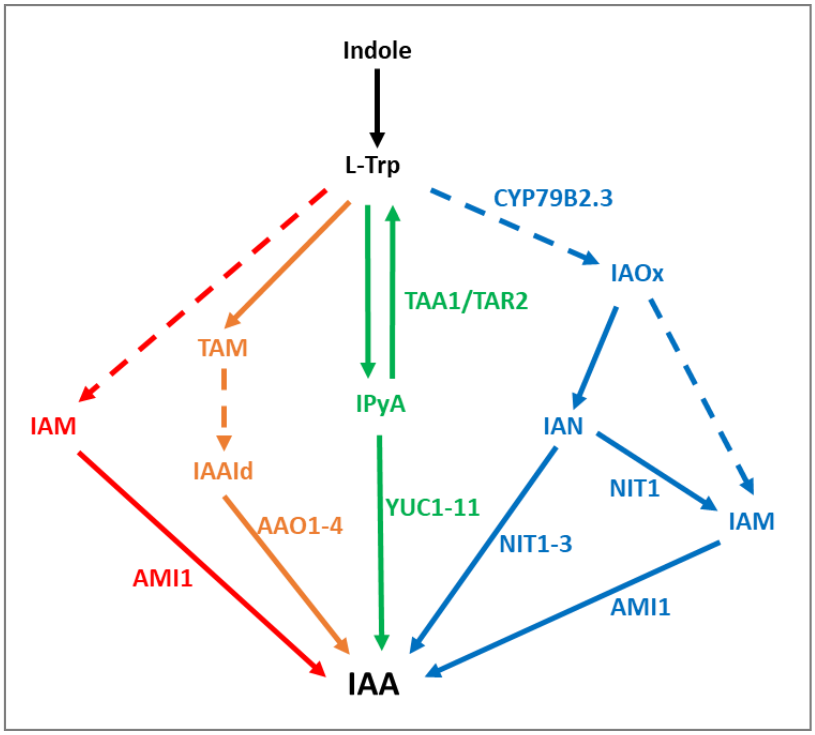

Figure 1.3: IAA biosynthesis from indole via the tryptophan-dependent (TD) pathway

The TD pathway of indole-3-acetic acid (**IAA**) biosynthesis has four routes named after their intermediates. These are the indole-3- acetamide (**IAM**) pathway, the tryptamine (**TAM**) pathway, the indole-3-pyruvic acid (**IPyA**) pathway, and the indole-3-acetaldoxime (**IAOx**) pathway, shown in red, orange, green and blue, respectively. Solid arrows refer to reactions with identified enzymes, and dashed arrows refer to unidentified/unconfirmed reactions. The enzymes involved are written next to the relevant arrow. **CYP79B2.3,** CYTOCHROME P450 FAMILY 79B2.3; **IAN**, indole-3-acetonitrile; **NIT1-3**, NITRILASE 1-3; **AMI1**, AMIDASE 1; **TAA1**, TRYPTOPHAN AMINOTRANSFERASE OF ARABIDOPSIS 1; **TAR2**, TRYPTOPHAN AMINOTRANSFERASE RELATED 2; **YUC1-11**, YUCCA 1-11; **IAAld**, indole-3-acetaldehyde; **AAO1-4**, ARABIDOPSIS ALDEHYDE OXIDASE 1-4. Adapted from Cackett et al. (2022).

1.7.3. Auxin-induced cell expansion via the acid growth mechanism

When exposed to auxin, plant cells pump protons into the apoplast at an enhanced rate, resulting in decreased apoplastic pH which activates cell wall-loosening processes that promote cell expansion – known as acid growth (Rayle & Cleland, 1992). This acid growth mechanism is initiated by the auxin-mediated activation of the PM H^+-ATPase, by promoting phosphorylation of the penultimate threonine residue (Thr^{947}) of the AHA2 H^+-ATPase isoform (Rudashevskaya et al., 2012; Takahashi, Hayashi & Kinoshita, 2012). Normally, a type 2C protein phosphatase (PP2C-D) interacts with the PM H^+-ATPase and dephosphorylates its

Thr^{947} residue, negatively regulating pump activity. The interaction of these two proteins was shown *in planta* in tobacco using a bi-molecular fluorescence complementation assay (BiFC), where AHA2 and PP2C-D were shown to interact with one another at the PM (Spartz et al., 2014). Additionally, these researchers isolated yeast PMs and subjected them to 14-3-3 far-western gel blot analysis and ATP hydrolysis assays. Using these methods, they showed a significant reduction in Thr^{947} phosphorylation in membranes prepared from cells coexpressing PP2C-D, as well as a reduction in vanadate-sensitive ATPase activity. Taken together, these results illustrated that PP2C-D is able to negatively regulate the AHA2 H^+-ATPase by dephosphorylating Thr^{947} (Spartz et al., 2014).

In response to elevated IAA levels, certain SAUR proteins accumulate and interact with the PP2C-D phosphatase, inhibiting its activity. Therefore, the PM H^+-ATPase remains phosphorylated at Thr^{947} and is active, pumping H^+ out of the cytoplasm into the apoplast, thereby lowering apoplastic pH (Spartz et al., 2014). This mechanism was largely elucidated by Spartz et al. (2014) where they showed, via immunoblot analysis with a α-Thr^{947P} antibody, that *SAUR19* overexpression increased the phosphorylation status of this Thr^{947} residue on the PM H^+-ATPase. They also showed that the PM H^+-ATPase activity increased in *SAUR19* overexpressing plants, by measuring the vanadate-sensitive ATP hydrolytic activity present in PM fractions prepared from the overexpressor (OE) line compared to WT, with the *SAUR19* OE displaying a 20-35 % increase in ATPase activity (Spartz et al., 2014). They also showed, via yeast two-hybrid analysis, that SAUR19 is able to directly interact with PP2C-D, and via *in vitro* phosphatase assays, that SAUR19 inhibits PP2C-D phosphatase activity. Additionally, they showed that SAUR9, SAUR40, and SAUR72 were also able to inhibit PP2C-D phosphatase activity (Spartz et al., 2014).

The auxin-induced decrease in apoplastic pH activates the aforementioned EXPANSINs (EXPs) (Rayle & Cleland, 1970; Cosgrove, 1993; Hager, 2003). The changes to the cell wall induced by EXPs promotes wall loosening, hydration and swelling which leads to cell expansion and growth (Majda & Robert, 2018). Additionally, the increased proton efflux into the apoplast creates a proton motive force (PMF) which increases solute uptake to increase turgor pressure, which also drives cell expansion and growth.

1.7.4. The link between auxin and salt stress

As previously discussed, salinity stress results in many changes in plant growth and physiology. It is therefore unsurprising that auxin has previously been linked to salt stress. Several studies have analysed IAA modulation of plant growth in response to NaCl. Jung & Park (2011) showed a possible role for auxin in ensuring seed germination only under favourable conditions, by demonstrating that addition of exogenous IAA suppressed germination rates of Arabidopsis seeds in saline environments, but not under normal growth conditions. However, in another study, priming seeds with IAA increased germination rates of both a salt-sensitive and salt-tolerant wheat variety under salt stress (Iqbal & Ashraf, 2007), indicating that there are possible differences in the role of auxin in germination under salt stress in different plant species.

The transcript levels of auxin biosynthetic genes and metabolite levels of IAA have also been measured following salt stress in different plant species. Jiang & Deyholos (2006) performed a microarray analysis on Arabidopsis roots following exposure to 150 mM NaCl, and found upregulation of two auxin biosynthetic genes, *AtNit1* and *AtNit2*. Additionally, an Arabidopsis line overexpressing another auxin biosynthetic gene, *AtYUC3,* showed reduced germination in high salt environments compared to WT plants, indicative of elevated auxin levels (Jung & Park, 2011). Treatment with NaCl has been shown to significantly reduce IAA concentration in rice leaves (Prakash & Prathapasenan, 1990). However, NaCl treatment has been reported to slightly increase IAA concentration in tomato shoots, but reduce IAA concentration in tomato roots (Dunlap & Binzel, 1996).

The involvement of auxin in altering tissue specific growth through the acid growth mechanism relies on auxin transport and redistribution throughout the plant. Interestingly, auxin transport has also been shown to change under saline conditions. Polar auxin transport, the main method by which auxin is transported through root tissue, is altered under saline conditions (Korver, Koevoets & Testerink, 2018). This is attributed to changes in activity of the PIN-FORMED (PIN) family of auxin efflux carriers. *PIN1*, *PIN3* and *PIN7* are down-regulated under saline conditions, thereby reducing auxin levels and causing a reduction in root meristem growth in Arabidopsis (Liu et al., 2015). This salt-mediated inhibition of root growth occurs as the root meristem size is reduced by nitric oxide (NO)-mediated modulation of auxin levels, involving the reduction in aforementioned *PIN* expression, as well as the stabilisation

of auxin-resistant 3 (AXR3)/indole-3-acetic acid 17 (IAA17), reducing auxin signalling (Liu et al., 2015). It has also been reported that short-term salt treatments cause changes in auxin distribution, oxidation of the cytosol and decrease in the number of root apical meristem cells (Jiang et al., 2016; Tognetti, Bielach & Hrtyan, 2017). Halotropism is another example of PIN-mediated changes in auxin levels that results in altered root growth under saline conditions. In this process, roots are able to actively redistribute auxin in the root tip by PIN2, allowing roots to bend in order to avoid high concentrations of salt in the growth medium and grow towards more favourable environments (Galvan-Ampudia et al., 2013).

1.7.4.1. Increased auxin biosynthesis via Nitrilase 2 in salt-stressed Arabidopsis

Interestingly, in our research group, IAA metabolite levels were measured by LC-MS/MS in Arabidopsis plants grown under the same conditions as described previously for the early development microarray analysis in section 1.6 (Cackett et al., 2022). This study showed that IAA levels are significantly elevated in plants grown under saline conditions, compared to plants grown in iso-osmolar sorbitol and untreated plants (Cackett et al., 2022). Additionally, the levels of three IAA intermediates, IAM, IPyA and IAN, were elevated in plants grown under saline conditions compared to the untreated controls. However, only the concentration pattern of IAN mirrored the observed changes in IAA levels in NaCl and sorbitol (Cackett et al., 2022).

Notably, the expression of three auxin biosynthetic genes, *Nitrilase 1* (*AtNit1*), *Nitrilase 2* (*AtNit2*), and *YUCCA4* (*AtYUC4*) increased in plants grown under saline conditions early in development, with significantly different expression patterns in plants grown on iso-osmolar sorbitol. The expression of *AtNit2* showed the greatest alteration in expression in plants grown under saline conditions compared to the other auxin biosynthetic genes, with an eight-fold induction under 125 mM NaCl conditions (Cackett et al., 2022). Furthermore, only *AtNit2* was significantly induced in shoot and root tissue in response to NaCl later in development, indicating that it may be involved in salt stress responses throughout development (Cackett, 2019). During auxin biosynthesis, AtNIT2 hydrolyses IAN into IAA (figure 1.3) (Normanly et al., 1997). Taken together, these results suggest that IAA biosynthesis is increased in response to NaCl at different developmental stages, via the hydrolysis of IAN to IAA by AtNIT2. Additionally, Arabidopsis lines overexpressing *AtNit2* (*35S::AtNit2*) showed enhanced survival

and plant growth in the presence of NaCl, but not iso-osmolar sorbitol. This *AtNit2* overexpressor also had increased IAA levels and decreased IAN compared to WT plants in response to salt stress; indicating elevated IAN turnover into IAA (Cackett et al., 2022). Overall, this data indicates that *AtNit2* is likely involved in the salt stress response through increasing IAA levels *in planta*, and this might be responsible for modulating growth in response to salt stress.

1.7.4.2. The disputed role of plant nitrilases

Nitrilase enzymes catalyse the hydrolysis of nitriles to the corresponding carboxylic acid and ammonia, and have been identified and characterised in plants, fungi, and bacteria (Howden & Preston, 2009). Plant nitrilases were first described in 1964 when a nitrilase enzyme was extracted from barley leaves, and found to convert IAN to IAA (Thimann & Mahadevan, 1964). In Arabidopsis, three nitrilase genes, *AtNit1-3*, are located next to each other on chromosome three, with another nitrilase gene, *AtNit4,* located on chromosome five. These four Arabidopsis nitrilase genes were identified by screening an Arabidopsis cDNA library (Bartling et al., 1992; Bartel & Fink, 1994). Phylogenetic analysis of the four Arabidopsis nitrilase sequences indicates that *AtNit1-3* are paralogs of one another as a result of gene duplication, with *AtNit1* and *AtNit2* arising from the most recent duplication event (appendix figure 6.1) (Abu-Zaitoon, 2014). These three nitrilase genes are therefore referred to as the *AtNit1* family, with the *AtNit4* gene forming its own branch separate from the *AtNit1* family (Janowitz, Trompetter & Piotrowski, 2009). Studies have shown that AtNIT4 has a high specificity for β-cyanoalanine, an intermediate in the cyanide detoxification pathway, and an extremely low specificity for IAN (Piotrowski, Schönfelder & Weiler, 2001).

As previously stated, the AtNIT1-3 enzymes hydrolyse IAN into IAA during the Trp-dependent auxin biosynthesis pathway (Bartling et al., 1992). However, there has been contention over this role, with some studies indicating that these enzymes are involved in cyanide detoxification and glucosinolate catabolism (Piotrowski, 2008). Vorwerk et al. (2001) measured the substrate specificity of recombinant *AtNit1, AtNit2,* and *AtNit3* using an assay based on the detection of ammonia released during the reaction. This study showed that all three Arabidopsis nitrilases do convert IAN to IAA, but with a lower velocity and affinity when compared to other substrates, including phenylpropionitrile which results from glucosinolate

breakdown (Vorwerk et al., 2001). Glucosinolates are amino acid-derived metabolites which act as defence compounds against pathogen and herbivore attack (Janowitz, Trompetter & Piotrowski, 2009). During glucosinolate catabolism, toxic compounds are produced; such as isothiocyanates and nitriles (Rask et al., 2000), with isothiocyanates being more predominant (Janowitz, Trompetter & Piotrowski, 2009). Pathogen attack and wounding, which would result in increased glucosinolate catabolism and thus nitriles, have been shown to induce *AtNit2* expression (Grsic-Rausch et al., 2000) – hence AtNIT2 could function to detoxify the nitriles produced during pathogen responses. The problem with the analysis by Vorwerk et al. (2001) is that it is based on recombinant enzyme activity in *in vitro* enzyme assays, meaning that some regulation or modification that might be important *in planta* might be missing.

Several studies have supported the role for AtNIT2 in auxin biosynthesis. Schmidt et al. (1996) showed that tobacco plants transformed with *AtNit2* were able to convert IAN into IAA, whilst untransformed plants were unable to catalyse this reaction. Shortly thereafter, a study showed that transgenic Arabidopsis overexpressing *AtNit2* had increased turnover of exogenous IAN, and sensitivity to the auxin effects of IAN (i.e., altered auxin-related growth phenotypes including root and hypocotyl elongation) (Normanly et al., 1997). Grsic et al. (1998) showed that *AtNit2* overexpressing plants had increased free IAA levels, whilst an antisense knock-down line had 75% less IAA compared to WT. Additionally, they showed that *AtNit2* expression increased by 21-fold following IAN application (Grsic et al., 1998). More recently, a study showed that a *nit2* RNA interference (RNAi) plant line had reduced responsiveness to IAA, increased tolerance to exogenous IAN, and a reduced total IAA pool, but no significant changes in free IAN or IAA (Lehmann et al., 2017). In agreement with this, Cackett et al. (2022) showed that *AtNit2* overexpressing lines produce more IAA, as mentioned previously.

As many other plant species have homologs of AtNIT4, some studies have stated that the primary role of plant nitrilases is in cyanide detoxification (Piotrowski, 2008). Additionally, some studies have stated that the IAOx pathway of auxin biosynthesis, involving IAN hydrolysis to IAA, is specific to the Brassicaceaes, as the NIT1-3 family of enzymes is only present in this family (Lehmann et al., 2017). However, other studies have indeed shown the presence of NIT1-3 homologs in different plant species and shown that these are involved in IAA biosynthesis. Two maize nitrilases have been identified, ZmNIT1 and ZmNIT2, and tested

to determine substrate specificity. While ZmNIT1 showed no specific turnover of the 18 nitriles tested, ZmNIT2 was able to hydrolyse a number of substrates, excluding β-cyanoalanine but including IAN (Park et al., 2003; Mukherjee et al., 2006), with its IAN turnover ten times higher in comparison with AtNIT1-3 (Vorwerk et al., 2001). Additionally, a study showed that *ZmNit2* is expressed in auxin-synthesising tissues such as maize kernels, and showed that ZmNIT2 hydrolyses IAN to IAA by demonstrating that *zmnit2* transposon insertion mutants could not convert exogenous IAN to IAA as in WT plants (Kriechbaumer et al., 2007). Additionally, they showed that *zmnit2* mutants had inhibited root growth in young seedlings, and accumulated less IAA conjugates in maize kernels and roots tips, suggesting a substantial contribution of ZmNIT2 to total IAA biosynthesis in maize (Kriechbaumer et al., 2007). Homologs of the AtNIT1-3 family have also been discovered in sorghum, with the SbNIT4A homolog forming a heterocomplex with SbNIT4B2 to hydrolyse IAN (Jenrich et al., 2007). This is important as it means that the model proposed by our group below in Arabidopsis (figure 1.4) might also be relevant in important crop plants such as maize and sorghum.

1.8. A model for the proposed salt-induced modulation of growth by auxin

Several studies have shown that when the activity of the PM H^+-ATPase is constitutively activated, plants are more salt tolerant (Gévaudant et al., 2007; Janicka-Russak et al., 2013; Wang et al., 2013; Bose et al., 2015), indicating that further work into investigating this could be fruitful in improving crop salt tolerance. It is proposed that this could be due to the increased PMF increasing K^+ retention in the cytosol via KT/HAK/KUP high affinity K^+ transporters, and by improving Na^+ extrusion via Na^+ antiporters such as SOS1 (Falhof et al., 2016; De Souza Miranda et al., 2017). Additionally, enhanced cell expansion could have a diluting effect on Na^+ ions accumulated in the cytoplasm.

Interestingly, multiple *SAUR* genes, including *AtSAUR9* (which has been shown to inhibit PP2C-D phosphatase activity – described earlier), were upregulated in a salt-specific manner in the Arabidopsis early and later development microarrays previously described, indicating that there may also be salt-induced changes in PM H^+-ATPase activity throughout development. Additionally, certain *EXP*s, such as *AtEXP11,* were also upregulated in a salt-specific manner, indicating that the acid growth mechanism is likely being activated in Arabidopsis to promote

expansion growth under saline conditions (Cackett et al., 2022). Furthermore, several *SAURs* and *EXPs* were differentially expressed in the *35S::AtNit2* line under saline conditions, but not in the WT (Cackett, 2019). Taking what is known from the literature about auxin-related mechanisms, combined with the changes in gene expression that we have observed, our research group has proposed a mechanism in Arabidopsis whereby salt-induced auxin accumulation modulates plant growth, as shown in figure 1.4. In this model; NaCl results in IAA accumulation (by increasing IAA synthesis from IAN, through induction of *AtNit2*). Elevated IAA results in upregulation of SAUR proteins, which in turn inhibit PP2C-D, allowing phosphorylation of Thr^{947} and thereby increasing PM H^+-ATPase pump activity, resulting in decreased apoplastic pH and increased turgor pressure. This activates EXPANSINS, increasing cell expansion and enhancing growth in saline conditions. Furthermore, the decreased apoplastic pH provides the PMF for the energy-dependent movement of Na^+ by transporters, such as SOS1, improving Na^+ exclusion and thereby preventing ion toxicity during salt stress. This PMF also enhances K^+ uptake into the cell, improving K^+/Na^+ ratios and improving salt tolerance.

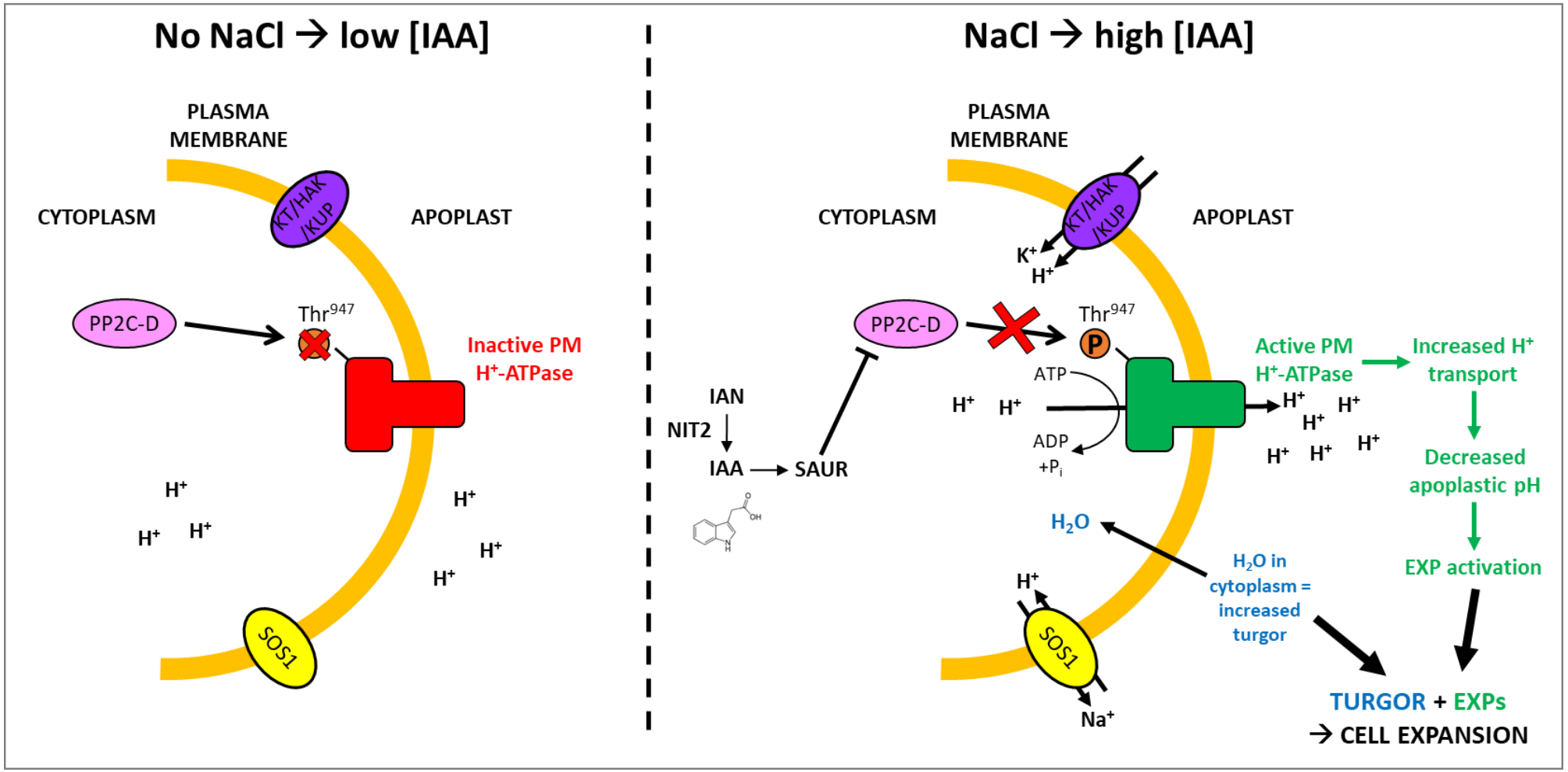

Figure 1.4. The proposed model for how salt-induced auxin accumulation could modulate plant growth under saline conditions

In the absence of NaCl, IAA biosynthesis is not induced, leaving PP2C-D free to dephosphorylate Thr^{947} on the PM H^+-ATPase, rendering the pump inactive and resulting in low extracellular [H^+]. NaCl exposure upregulates *AtNit2*, increasing IAA biosynthesis and IAA levels in the cytoplasm, inducing the expression of *SAURs*. SAUR proteins inhibit PP2C-D and thereforeThr^{947} remains phosphorylated and the PM H^+-ATPase pump is activated. This decreases the apoplastic pH, which activates EXP activity and results in overall cell expansion. Increased H^+ pumping into the apoplast also hyperpolarises the membrane which could affect the activity of voltage-dependent ion transporters and also provides increased H^+ availability for H^+ symporters and antiporters. Adapted from Cackett (2019)

1.9. *AtNit2* regulation

The basis for the whole salt response pathway hypothesised above starts with *AtNit2* upregulation. As *AtNit2* mRNA transcript levels are increased specifically under saline conditions (Cackett et al., 2022), it is likely that *AtNit2* gene expression is being regulated at the level of transcription. Currently, very little information about *AtNit2* regulation has been published in the literature. A few studies have previously linked *AtNit2* expression to other plant stress responses. For example, *AtNit2* has been shown to be upregulated under drought (Rasheed et al., 2016), sulphur deprivation (Kutz et al., 2002), and Clubroot biotrophic attack (Grsic-Rausch et al., 2000). Additionally, *AtNit2* has been reported be induced in response to exogenous application of the stress-related hormones abscisic acid (ABA) (Böhmer & Schroeder, 2011) and jasmonic acid (JA) (Sasaki-Sekimoto et al., 2005).

Despite being next to each other on chromosome 3, and performing the same function in IAN hydrolysis to produce IAA, the predicted promoter regions of the *AtNit1*, *AtNit2* and *AtNit3* genes are highly divergent in size and nucleotide sequence (Hillebrand, Bartling & Weiler, 1998). In a study conducted by Hillebrand, Bartling & Weiler (1998), 800 bp upstream of the *AtNit2* translation start site were analysed. They identified the elements of a putative minimal promoter for general transcription factor (GTF) binding in this region, including a CCAAAT box at -173 bp, and a TATA box either at -125 bp (TATTA) or at -142 bp (TATAAT).

Two studies have investigated regulation of *AtNit2* by a NAM/ATAF/CUC (NAC) family TF, AtATAF2. Huh et al. (2012) showed that 1) *AtATAF2* expression was induced by IAN treatment, 2) *AtNit2* induction by IAN treatment was reduced by 2-fold in an *atataf2* mutant, 3) *35S::AtATAF2* plants had abnormal developmental phenotypes, such as dwarfism, and had increased *AtNit2* expression compared to WT plants, 4) *atataf2* plants had 30% increased primary root elongation compared with WT plants, although this wasn't nearly as drastic as in *atnit1-3* mutants, and that the *atataf2* plants had 0.5-fold repression of *AtNit2* expression compared to WT. To show that these effects were as a result of direct binding of AtATAF2 to the *AtNit2* promoter, they conducted transient transactivation assays in Arabidopsis protoplasts and showed that AtATAF2 induced expression of the *AtNit2* promoter-driven *GUS* reporter gene. They confirmed this *in vitro* using an electrophoretic mobility shift assay (EMSA) which revealed binding of AtATAF2 to the *AtNit2* promoter at a position between -117 and -82. These authors concluded that AtATAF2 acts as a positive regulator of *AtNit2*

expression by binding directly to its promoter. However, in a more recent study, Nagahage et al. (2018) showed that AtATAF2 significantly repressed luciferase reporter gene expression driven by the same sized *AtNit2* promoter in Arabidopsis protoplasts, contradicting the finding by Huh et al. (2012). Other studies have shown that overexpression of *AtATAF2* both increases and decreases expression of certain pathogenesis-related genes under different conditions (Delessert et al., 2005; Wang, Goregaoker & Culver, 2009). Thus, it is possible that AtATAF2 both upregulates and downregulates the expression of some target genes (including *AtNit2*) in response to different environmental conditions. As *AtNit2* induction by IAN was not completely lost in the *ataf2* mutant line (Huh et al., 2012), this implies that other TFs must play a role in *AtNit2* regulation during auxin biosynthesis. However, no other TFs have been characterised for regulation of *AtNit2.*

1.10. Research objectives of this project

As the auxin biosynthetic gene, *AtNit2*, is upregulated specifically in response to NaCl, and *AtNit2* overexpressing Arabidopsis plants show improved growth and K^+/Na^+ ratios under saline conditions that are not seen in response to osmotic stress alone, we propose that this gene is a candidate for improving plant growth under saline conditions to improve plant salt tolerance (Cackett et al., 2022). Whilst the downstream effects of *AtNit2*-induced IAA accumulation on modulating plant growth are being uncovered by others in our group, it is important to also have a thorough understanding of its transcriptional regulation. Therefore, the main aim of this research project was to investigate the regulation of *AtNit2* by identifying TFs (other than AtATAF2) that are able to regulate its expression. To understand gene regulatory pathways, many different methods need to be used in combination. With this in mind, this project had four objectives to uncover potential *AtNit2* regulation: 1) to analyse the *AtNit2* promoter to identify potential TF binding sites which might indicate what family/families of TFs regulate the expression of this gene, 2) to identify salt-responsive TFs within these families and determine whether altered expression of these TFs results in changes in *AtNit2* expression and/or salt tolerance, 3) to use yeast-one-hybrid analysis to identify TFs that are able to bind to the *AtNit2* promoter, and 4) to validate any such TF-DNA interactions *in planta.* The first two of these objectives are covered in chapter 2, with the latter two objectives investigated in chapter 3.

Another aim of this study was to determine whether this work being conducted in Arabidopsis with regards to *AtNit2* and its potential role in the plant salt stress response is relevant to an economically important crop plant, maize. In chapter 4, a preliminary analysis of the maize NIT2 homolog was conducted in order to investigate this.

CHAPTER 2: FUNCTIONAL CHARACTERISATION OF ATMYB30 AND ATMYB2 IN THE REGULATION OF *NITRILASE 2*

2.1. INTRODUCTION

2.1.1. Regulation of gene transcription

Gene regulation is the process used to control the timing, location and degree to which genes are expressed. The overall activity of a gene is determined by transcription, mRNA processing, mRNA transport from the nucleus to the cytoplasm, translation, and sometimes also post-translational modifications of the protein. A variety of mechanisms can play a role in altering gene transcription, including chemical modification of DNA, and regulatory proteins. As previously mentioned, Arabidopsis has very little genomic differences compared to its salt-tolerant relative, *Thellungiella halophila*, and genes involved in the salt response in Arabidopsis are highly expressed in *T. halophila* in unstressed conditions, indicating that salt tolerance is more likely as a result of changes in the transcriptome (Kant et al., 2006). This means that it is vital that we understand how genes involved in salt tolerance are regulated in order for us to engineer more salt tolerant crop plants.

2.1.1.1. Chromatin-related regulatory proteins

The basic state for transcription in eukaryotes is restrictive, as a result of the packing of the DNA into chromatin, blocking the recognition of the promoter DNA by the basic transcription machinery (Kornberg, 1999). Therefore, chromatin remodelling/modification is necessary for transcription, and plays a role in the way that transcription factors are able to interact with promoter DNA (Riechmann, 2002). Chromatin-related regulatory proteins fall into two main classes. The first includes proteins that covalently modify histones, such as histone acetylases and deacetylases. Generally, histone acetylation is associated with transcribed chromatin, whereas deacetylation is associated with repression (Riechmann, 2002). The second class contains chromatin remodelling protein complexes that hydrolyse ATP to either move, eject or restructure nucleosomes. For example, the Switch/Sucrose Non-Fermentable (SWI/SNF) complex remodels chromatin structure by destabilising histone-DNA interactions, allowing easier access to the chromatin (Clapier et al., 2017). Thereafter, transcription factors are able to access the DNA in order to alter transcription levels.

2.1.1.2. Transcription factors

Transcription factors (TFs) are proteins which control the rate of transcription by binding to promoter DNA upstream of the gene's translation start site, at specific sites called transcription factor binding sites (TFBSs)/*cis*-regulatory motifs. Genes are regulated by TFs to ensure that they are expressed in the desired cells, at the correct time, and to the appropriate degree. They can work alone, or in a complex with other TFs to promote (as an activator) or block (as a repressor) the recruitment of RNA Polymerase II (RNA Pol II) to the promoter, the enzyme responsible for transcribing DNA into mRNA.

2.1.1.2.1. General transcription factors

The general transcription machinery is comprised of general transcription factors (GTFs) that recognise the promoter sequence and recruit RNA Pol II, a multi-subunit enzyme that initiates transcription (Cramer, Bushnell & Kornberg, 2001). These GTFs include transcription factor IIA (TFIIA), TFIIB, TFIID, TFIIE, TFIIF, and TFIIH. These GTFs carry out various functions, including positioning RNA Pol II on the promoter (TFIIB) and unwinding the DNA (TFIIH). The TFIID multi-subunit complex contains the TATA-box binding protein (TBP) and several TBP-associated factors (TAFs) required for promoter recognition (Green, 2000). These GTFs bind to the core promoter sequence, a region of about 70 bp flanking the transcription start site (TSS), containing the TATA box which is a T/A-rich sequence usually located 25-35 bp upstream of the TSS (Molina & Grotewold, 2005).

2.1.1.2.2. Activators and repressors

The main class of proteins associated with changes in gene transcription levels are sequence-specific DNA-binding TFs that act either as 1) activators of transcription, thereby increasing gene expression, or 2) repressors of transcription, thereby decreasing gene expression. These TFs are responsible for the selectivity in gene regulation, and are often themselves expressed in a temporal, tissue- or cell-type specific, or stimulus-dependent manner. However, this is not always the case as TF activity can also be regulated by other means such as post-translational modifications (PTMs) (Riechmann, 2002). TFs are modular proteins comprised of distinct, functionally separable domains such as DNA-binding domains (DBD) which provide DNA sequence specificity, and activation domains (AD) with contain binding sites for other proteins such as transcriptional coregulators. Most known TFs are grouped into families based

on their DNA binding domain (Luscombe et al., 2000). In order to alter RNA Pol II activity, and thus the rate of transcription, TFs can interact directly with different components of the general transcription machinery and with coactivators/corepressors, affecting complex formation, as well as with chromatin remodelling complexes to alter accessibility of DNA (Riechmann, 2002).

2.1.1.3. Investigating specific TF-gene regulatory relationships

Determining which TFs are responsible for regulation of a particular gene of interest (GOI) is a complex process. Many computational tools are available to assist with inferring gene regulatory networks in various organisms, including Arabidopsis (reviewed in Mercatelli et al., 2020). To identify specific TF-gene regulatory relationships, a variety of analyses need to be conducted.

Co-expression analyses take data from diverse experimental conditions and determine if one gene is regulated with the same pattern as another, therefore inferring some functional relationship (Zhang & Horvath, 2005). However, since correlation does not imply direct causation, this method is only useful as a preliminary approach in obtaining an initial list of candidate TFs. For example, if a particular GOI is co-expressed with a TF then it may be that the TF regulates that GOI, but further investigations are required. Additionally, as mentioned previously, TF activity might not be transcriptionally regulated.

Another method useful in narrowing down potential regulators of a GOI is by analysing its promoter sequence since specificity of TF binding is based on the interaction between the TF DBD and specific TFBSs present in promoter DNA. In Arabidopsis, there is on average one gene per 4.5 kb of DNA with the gene length (exons plus introns) being approximately 2 kb and the other ~2.5 kb containing the intergenic region. Genome-wide, transposons account for ~20% of intergenic DNA in Arabidopsis, resulting in an average of 2 kb of DNA encompassing both the 5’ and 3’ regions of a particular gene (The Arabidopsis Genome Initiative, 2000). Additionally, in Arabidopsis, TFBSs are enriched in the 200 bp upstream of the TSS of stress-responsive genes (Zou et al., 2011). As such, analysing the first 1 kb upstream of the GOI in Arabidopsis is usually sufficient to identify the TFBSs important in gene regulation (Riechmann, 2002). In eukaryotes, TFBSs are usually 5 to 15 bp long (Riechmann, 2002; Yu, Lin & Li, 2016). As TF families are grouped based on their DNA binding domain, this also means

that TFs within a particular family bind to similar TFBSs. This means that if a TFBS, known to be a target of a certain family of TFs, is present in the promoter of the GOI, one can infer that one or more TFs from that family may bind to regulate expression of that gene . However, many large TF families exist and many/all TFs from certain families may bind the same consensus motif, so identifying a particular TFBS doesn't provide information on exactly which TF binds in that promoter region. For example, evidence has shown that multiple TFs belonging to the WRKY family bind to a section of DNA called the W-box, that has a consensus sequence of TTGAC(C/T) (Eulgem et al., 2000). If a promoter of a GOI contains a W-box element, this indicates that one or more WRKY TFs may be able to bind to and regulate its expression, however exactly which ones, and under what circumstances, would take further investigation. By analysing the promoter sequence of a GOI, one can identify TFBSs that are known targets of certain TF families, thereby narrowing down potential regulators. However, specific TFBS for most TFs are still unknown, posing a significant limitation to this method. Additionally, as this method relies on predictions, it is more useful to identify direct TF-promoter interactions, which can also lead to the identification of new TFBS.

Many different methods exist to identify direct TF-DNA interactions. These assays are generally either DNA-driven, where the specific DNA sequence is probed with multiple proteins, or protein-driven where a specific TF is probed with multiple DNA sequences to determine what DNA sequences can be bound by that TF. Examples of assays that identify TF-DNA interactions include yeast one-hybrid (Y1H) assays (which will be discussed further in chapter 3) which are the main method used to identify TF binding to a known DNA sequence *in vivo*, EMSAs that are used *in vitro* to narrow down specific TFBSs, and chromatin immunoprecipitation (ChIP) assays that are used to identify different genes that a particular TF is able to bind to *in planta*. When the TF-DNA interaction is not discovered *in planta,* it is important to do a second validation step to confirm the interaction occurs *in planta* and to uncover how that TF regulates transcription of that specific GOI. This can be very difficult as TFs may need to be present in a complex to alter transcription, or, as mentioned, may only be active in certain cell- or tissue types, or under certain environmental conditions (Mercatelli et al., 2020). The same TF could even form part of different complexes to have different effects on promoter activity under different conditions.

Another method to uncover TF-gene regulatory relationships is by analysing gene expression following alteration of TF activity (e.g., by knocking out or overexpressing the TF). This can infer genes which may be regulated by that TF, although changes in gene expression could be due to direct or indirect mechanisms. Evidently, a combination of different approaches is necessary in investigating gene regulation at the level of transcription.

2.1.2. Chapter aims

The aim of this chapter was to functionally characterise two putative *AtNit2* regulators by analysing whether knock-out and overexpression of these TFs results in changes in *AtNit2* expression and/or salt tolerance.

2.2. MATERIALS AND METHODS

2.2.1. Chemical and stock solutions

The TRIzol® Reagent (#15596018), SuperScript™ III Reverse Transcriptase (#18080093), Gateway™ BP Clonase™ II Enzyme Mix (#11789020), Gateway™ LR Clonase™ II Enzyme Mix (# 11791020), GeneRuler 1 kb Plus DNA Ladder (#M1331) and GeneRuler Low Range DNA Ladder (#SM1193) were all purchased from Thermo Fisher Scientific (Massachusetts, USA). The RNeasy® Mini Kit (# 74104) and RNase-Free DNase set (#79254) were purchased from Qiagen (Hilden, Germany). The KAPA SYBR® FAST Universal qPCR Kit (# SFUKB) and KAPA Taq ReadyMix PCR kit (#KK1006) were purchased from Merck (Darmstadt, Germany) and the KAPA HiFi HotStart ReadyMix PCR kit (#7958927001) was purchased from Roche (Basel, Switzerland). Super-Therm DNA Polymerase PCR kit (#JMR-801) was obtained from Separation Scientific SA (Pty) Ltd (Johannesburg, South Africa). The 1 kb (#NO468S) and 100 bp (#NO467S) Quick-Load® DNA ladders were purchased from New England Biolabs (Massachusetts, USA). The Wizard® SV Gel and PCR Clean-Up System (#A9281) was purchased from Promega (Wisconsin, USA). The Zyppy™ Plasmid Miniprep Kit (catalogue no. D4036) was from Zymo Research (California, USA). Phyto agar (product no. P1003.100) was purchased from Duchefa Biochemie B.V. (Haarlem, Netherlands). All plant nutrient (PN) media components, most antibiotics and the glufosinate ammonium (catalogue no. 45520) were obtained from Merck (Darmstadt, Germany).

2.2.2. Arabidopsis seed stocks

Two different *atmyb30* T-DNA knock-out lines were obtained. The GABI-KAT 022F04 line (*atmyb30*-1/*myb30-1*) was obtained from Dr Susana Rivas at the French National Centre for Scientific Research (Rosso et al., 2003; Raffaele, Rivas & Roby, 2006) and the SALK_027644C line (*atmyb30-2*/*myb30-2*) was obtained from Dr Yanhai Yin at Iowa State University (Li et al., 2009). The Arabidopsis wild type Col-0 ecotype was used as the background to generate the 35S::*AtMYB30*, 35S::*AtMYB2* and 35S empty vector (EV) lines described in this chapter. The Col-0 seeds were obtained from A/Prof Robert Ingle (University of Cape Town, South Africa). All Arabidopsis seeds were stored at 4˚C.

2.2.3. Arabidopsis growth in soil

Arabidopsis seeds were vernalised for at least 48 hours at 4˚C before being grown on soil made up of a 1:1 mixture of peat (Jiffy Products, International AS, Norway) and vermiculite. The soil mixture was used to fill Arabaskets which were placed inside Aratrays on top of Araflats (Arasystems, Ghent, Belgium). Plastic wrap was used to cover the newly sown seeds for one week to ensure optimal humidity for germination and seedling establishment. Seedlings were fertilised with Phostrogen® All Purpose Plant Food (Bayer CropScience Group, Hertfordshire, UK) on the day that the plastic wrap was removed, one week after sowing. Thereafter the plants were watered, as required, from the bottom by adding water to the Araflats. Once plants grown in soil for seed bulking purposes had bolted, they were covered with Aracons consisting of Arabases and Aratubes (Arasystems, Ghent, Belgium) to prevent cross fertilisation. Watering ceased after seeds had been set and siliques had started drying. Seeds were harvested from individual plants once the entire plant was completely dry.

2.2.4. Arabidopsis growth on media

2.2.4.1. Arabidopsis seed sterilization

Arabidopsis seeds were surface sterilised by shaking for 5 min in 70% (v/v) EtOH. After the EtOH was aspirated off, the seeds were incubated in a bleach solution containing 10% (v/v) household bleach, 0.02% (v/v) Triton-X for 10 min with continuous shaking. Subsequently, the seeds were washed five times in sterile dH_2O with shaking during each wash step for at least

1 min. Lastly, the seeds were resuspended in 0.1% (w/v) phyto-agar and stored at 4˚C in the dark for vernalisation.

2.2.4.2. Plant nutrient (PN) media

Arabidopsis was grown in liquid or solid PN media, containing 5 mM KNO_3, 2 mM $MgSO_4.7H_2O$, 2 mM $Ca(NO_3)_2.4H_2O$, 0.5 mM FeNaEDTA and 1X micronutrients (70 µM H_3BO_3, 14 µM $MnSO_4.H_2O$, 0.5 µM $CuSO_4.5H_2O$, 1 µM $ZnSO_4.6H_2O$, 0.2 µM Na_2MoO_4, 10 µM NaCl and 0.01 µM $CoCl_2.6H_2O$). For solid media, 7% (w/v) phyto agar was added. After autoclaving, KPO_4 buffer (pH 5.5) was added to a final concentration of 2.5 mM (Haughn & Somerville, 1986).

2.2.5. Arabidopsis growth conditions

All Arabidopsis plant growth was carried out in a plant growth room under standard conditions (100 $\mu E.m^{-2}.s^{-1}$ light intensity, 16-hr light/8-hr dark, 22°C, 50-60% relative humidity).

2.2.6. Arabidopsis phenotyping in saline conditions

2.2.6.1. Early development in saline conditions

Seeds were sterilised and grown in 90 mm petri dishes on PN-agar (7% w/v) supplemented with 0, 50, 75, 100 or 125 mM NaCl or iso-osmolar concentrations of sorbitol (100, 150, 200 or 250 mM). For each plant line being analysed; four plates were set up per treatment, with 50 seeds sown onto each plate using a sterile glass Pasteur pipette. After 14 days, the number of surviving seedlings per plate was counted and the total mass of seedlings per plate was recorded by carefully removing all the surviving seedlings using forceps and weighing them on a mass balance. A seedling was deemed to have survived if it had developed true leaves and remained green. The mass per plant values (total mass of seedlings removed from plate divided by number of surviving seedlings) were calculated and analysed using Microsoft Excel.

2.2.6.2. Later development in saline conditions

The Araponics hydroponic growth system was used (Araponics, Liège, Belgium). Seeds were sterilised as in 2.2.4.1, sown onto seed holders filled with 0.7% agar, and placed into the Araponics high density support on top of the Araponics tray. The tray was filled with ¼

strength PN media and changed weekly for 3 weeks. During the first week, the seedlings were covered with a transparent lid to increase humidity for germination. After three weeks, the seedlings were transferred into low density supports on top of trays filled with ¼ strength PN supplemented with or without 75 mM NaCl for one week. Plants of the different lines being analysed were included in the same hydroponics box. Depending on the number of genotypes being analysed, this resulted in 4-6 seedlings per genotype per treatment combination. The root and shoot mass were recorded for each plant. The average shoot and root mass per plant per treatment for each genotype was calculated and analysed using Microsoft Excel.

2.2.7. Plasmid DNA purification

High quality plasmid DNA was isolated using the Zyppy™ Plasmid Miniprep Kit (Zymo Research, USA) according to the manufacturer's instructions.

2.2.8. Arabidopsis genomic DNA extraction

Arabidopsis gDNA was extracted from leaf tissue from 4 week old (soil grown) plants or whole 14 day old seedlings (from petri dishes) based on the method of (Edwards, Johnstone & Thompson, 1991) with some minor alterations. A single seedling or leaf was homogenised in 250 µL extraction buffer (200 mM Tris HCl pH 7.5, 250 mM NaCl, 25 mM EDTA pH 8.0 and 0.5% (w/v) SDS) in a 1.5 mL microcentrifuge tube and heated at 60˚C for 10 min. The DNA was extracted by adding an equal volume of chloroform, mixing well and then centrifuging at 10 000 x *g* for 10 min. The aqueous phase was then transferred into a new microcentrifuge tube. The DNA was precipitated by adding 1/10 volume 3 M sodium acetate pH 5.6 and 2 x volume ice cold 100% (v/v) EtOH and incubating at -20˚C for at least 1 hour. The DNA was pelleted by centrifugation at 10 000 x *g* for 10 min after which the pellet was washed in 70% (v/v) EtOH and the centrifugation repeated. The EtOH was aspirated off and the pellet allowed to air dry before being resuspended in 50 µL TE buffer (10 mM Tris HCl pH 8.0 and 1 mM EDTA, pH 8.0). All DNA was stored at -20˚C.

2.2.9. RNA extraction and cDNA synthesis

2.2.9.1. RNA extraction

Total RNA was extracted from plant tissue using TRIzol® Reagent (Thermo Fisher Scientific, Massachusetts, USA). Plant tissue was harvested, and flash frozen immediately in liquid nitrogen. Following salt assays, whole surviving seedlings were pooled (to a mass of ~100 mg) in triplicate for each NaCl concentration for RNA extraction. For control and lower NaCl and sorbitol concentrations these samples would have come from three separate petri dishes, but for the higher NaCl and sorbitol concentrations seedlings were pooled across plates to get enough tissue. For assessing gene expression in transgenic lines, pools of 15-25 whole surviving seedlings from PN plates (to a total mass of ~100 mg), or three whole leaves from different plants grown in soil were used. The exact samples for each experiment are described in the results section (2.3). For each sample, approximately 100 mg of plant tissue was homogenised in 1 mL TRIzol in a 1.5 mL microcentrifuge tube using miniature steel balls (Bearing Man Group, Cape Town, South Africa) and a paint shaker (SO-10m shaker, Fluid Management, USA) for four minutes. Following homogenisation, total RNA was extracted according to the manufacturer's guidelines (Thermo Fisher Scientific, Massachusetts, USA). The extracted RNA was resuspended in 87.5 µL nuclease-free H_2O and incubated in a heating block for 10-15 min at 60°C until fully resuspended. All RNA was stored at -80˚C.

2.2.9.2. DNase treatment and RNA clean up

Extracted RNA was DNase-treated using the RNase-Free DNase set (Qiagen, Germany) according to the manufacturer's instructions. Subsequently, a clean-up was performed using the RNeasy® Mini Kit (Qiagen, Germany) according to the manufacturer's instructions. Following RNA binding and subsequent washing of the column membrane, the column was placed into a clean 1.5 mL microcentrifuge tube and 30 µL of RNase-free H_2O was added directly to the spin column membrane followed by centrifugation for 1 min at 8000 x *g* to elute the RNA. The elution step was repeated into the same microcentrifuge tube with another 30 µL of RNase-free H_2O to ensure complete elution of the RNA from the spin column membrane.

2.2.9.3. Determining RNA quantity and quality

The RNA quantity and quality were analysed using a NanoDrop™ ND-1000 spectrophotometer (Thermo Fisher Scientific, Massachusetts, USA). The concentration was determined by measuring the optical density of the samples using a wavelength of 260 nm, where an OD_{260} of 1 equates to 40 µg.mL^{-1} for RNA. To assess the quality of the RNA, the ratio of the OD_{260}/OD_{280} was analysed where an absorbance ratio of ≥1.8 was considered high enough quality to use for downstream applications. The RNA quality was further assessed by analysing the rRNA bands after gel electrophoresis. For this, 1 µg RNA was run on a 1% (w/v) agarose gel as described in 2.2.13. If clear rRNA bands were seen with no smearing, the RNA was considered high enough quality for downstream applications.

2.2.9.4. cDNA synthesis

For samples determined to have adequate quantity and quality, 1 µg RNA was reverse transcribed into first-strand cDNA using the SuperScript™ III Reverse Transcriptase kit (Thermo Fisher Scientific, Massachusetts, USA) according to the manufacturer's instructions. Briefly, 1 µg of RNA was denatured at 65℃ for 5 min together with 500 ng oligo(dT) primers and 2 mM dNTPs (Kapa Biosystems, Cape Town, South Africa) in a total volume of 13 µL. After denaturing, samples were snap cooled at 4℃ for at least 1 min. To each sample, 1X First-Strand buffer, 5 mM dithiothreitol (DTT) and 200 U SuperScript™ III reverse transcriptase enzyme was added and mixed by pipetting. Samples were then incubated at 25℃ for 5 min, 60℃ for 1 hour and then 70℃ for 15 min. All heating/cooling steps were performed in a Gene Amp PCR system 2700 (Applied Biosystems™, Foster City, USA) or the SimpliAmp™ Thermal Cycler (Applied Biosystems™, Foster City, USA).

2.2.10. Primer design

Primers were designed and evaluated using NCBI Primer-BLAST software (https://www.ncbi.nlm.nih.gov/tools/primer-blast/) and DNAMAN software (version 4.1.2.1, Lynnon BioSoft, USA). Where possible, primers for qPCR were designed such that at least one of the primers spanned an exon-exon junction so that amplification would only be possible from cDNA templates to avoid detecting any genomic DNA contamination. Primers for Gateway® cloning were designed based off recommendations in the Gateway® Technology

manual (publication no. MAN0000282, Invitrogen™ by Life Technologies™, Thermo Fisher Scientific, Massachusetts, USA).

2.2.11. DNA and cDNA amplification by Polymerase Chain Reaction (PCR)

All PCRs were performed in the Gene Amp PCR system 2700 (Applied Biosystems™, Foster City, USA) or in the SimpliAmp™ Thermal Cycler (Applied Biosystems™, Foster City, USA). Three different Taq polymerases were used, depending on the primers and purpose of the PCR. These were the Super-Therm Taq Polymerase kit, the KAPA Taq ReadyMix PCR kit, and the KAPA HiFi HotStart ReadyMix PCR kit. The primers used are listed in Table 2.1 along with the specific Taq used, the annealing temperature (T_a) and the amplicon sizes. The PCR amplifications were performed in 20 µL reaction volumes. For all PCRs using plasmid DNA, 10 ng of template was used. For all colony PCRs, a small amount of a single bacterial colony was added using a sterile 10 µL pipette tip. When Arabidopsis DNA was being amplified, 1 µL was used as template.

2.2.11.1. Super-Therm Taq Polymerase kit

The Super-Therm Taq Polymerase kit (Separation Scientific (Pty) Ltd, Johannesburg, South Africa) was used for general PCRs (including genotyping, primer optimisation, etc.). Typically, the reaction consisted of 1 x reaction buffer, 2 mM $MgCl_2$, 250 µM dNTPs and 400 nM of each primer. Amplification conditions included an initial DNA denaturation step at 94℃ for 5 min, followed by 30-40 cycles of denaturation at 94℃ for 15 sec, primer annealing at T_a for 30 sec and elongation at 72℃ (allowing 30 sec per 1 kb amplified). A final elongation step was included at 72℃ for 10 min.

2.2.11.2. KAPA Taq ReadyMix PCR kit

The KAPA Taq ReadyMix PCR kit (Merck, Germany) was used for general PCRs (including genotyping, primer optimisation, etc.). Typically, the reaction consisted of 1 x KAPA Taq ReadyMix (with $MgCl_2$ at 1.5 mM) and 400 nM of each primer. Amplification conditions included an initial DNA denaturation step at 95℃ for 3 min, followed by 30-40 cycles of denaturation at 95℃ for 30 sec, primer annealing at T_a for 30 sec and elongation at 72℃, allowing 1 min per 1 kb amplified. A final elongation step was included at 72℃ for 2 min.

2.2.11.3. KAPA HiFi HotStart ReadyMix PCR kit

The KAPA HiFi HotStart ReadyMix PCR kit (Roche, Switzerland) was used for PCRs to generate products with a low error rate for downstream applications including cloning and sequencing. Typically, the reaction consisted of 1 x KAPA HiFi HotStart ReadyMix (with $MgCl_2$ at 2.5 mM) and 300 nM of each primer. Amplification conditions included an initial DNA denaturation step at 95℃ for 3 min, followed by 30-40 cycles of denaturation at 98℃ for 20 sec, primer annealing at T_a for 15 sec and elongation at 72℃, allowing 30 sec per 1 kb amplified. A final elongation step was included at 72℃ for 2 min.

2.2.12. Gene expression analysis by RT-qPCR

For all RT-qPCR experiments, the KAPA SYBR® FAST Universal qPCR kit (Merck, Germany) was used according to the manufacturer's guidelines, without the addition of 50 x ROX High/Low. Experiments were conducted using a Corbett Rotor-Gene 6000 HRM Real Time PCR machine (Qiagen, Germany) using the following parameters: one cycle at 95℃ for 3 min followed by 40 cycles of 95℃ for 3 sec, 60℃ for 20 sec and 72℃ for 1 sec. A final elongation step was included at 72℃ for 90 sec. Three technical replicates of each of the three biological replicates were performed for all the RT-qPCR experiments. Quality control and analyses were performed using the Rotor-Gene 6000 Series Software Version 1.7. Runs were deemed successful if a single peak was observed in the melt curve, indicating a single product was being amplified. A standard curve made using serially diluted cDNA (comprising off all the samples in a particular experiment), with an efficiency between 0.9 and 1.1 and an R^2 value greater than 0.97 was considered sufficient for further analyses. The RT-qPCR data was exported to Microsoft Excel for analysis whereby the calculated concentrations/expression values, extrapolated from the RT-qPCR standard curve, were normalized by dividing the calculated concentration of the gene of interest by the calculated concentration of the *A. thaliana* MONENSIN SENSITIVITY1 (*AtMON1*, AT2G28390) reference gene (Hong et al., 2010).

2.2.13. Visualisation of nucleic acids by gel electrophoresis

To visualise the results of an end-point PCR, DNA fragments were separated by agarose gel electrophoresis. The DNA samples in 1 x loading buffer (diluted from 6X stock solution: 0.25% (w/v) bromophenol blue, 40% (w/v) sucrose) were loaded onto 1-2% agarose gels (w/v) (1% for amplicons > 500 bp, 2% for amplicons < 500 bp) made up in 1X Tris-Acetate (TAE) buffer

(40 mM Tris, 20 mM acetic acid, 1 mM EDTA pH 8.0), containing 0.16 µg/mL ethidium bromide (EtBr) and electrophoresed in the same 1X TAE running buffer. A DNA ladder was included in each gel to determine the size of the amplicons. Electrophoresed DNA fragments were visualised and photographed on a short wavelength (310 nM) Gel Doc™ XR UV transilluminator (Bio Rad Laboratories, UK). For excision of DNA bands from an agarose gel, visualisation was performed with a long wavelength (365 nM) UV transilluminator.

2.2.14. DNA purification from PCR products

The PCR products or DNA fragments excised from an agarose gel were purified using the Wizard® SV Gel and PCR Clean-Up System (Promega, USA) according to the manufacturer's guidelines. DNA was eluted in 30 µL nuclease-free H_2O when purified from gel slices instead of 50 µL as recommended in the manual.

2.2.15. Determination of DNA quantity and quality

Purified plasmid DNA and DNA purified from PCR products and agarose gels was assessed for quantity and quality using a NanoDrop™ ND-1000 spectrophotometer (Thermo Fisher Scientific, Massachusetts, USA). The concentration of the DNA was determined by measuring the optical density of the samples using a wavelength of 260 nm where an OD_{260} of 1 equates to 50 $\mu g.mL^{-1}$ for double stranded DNA. To assess the quality of the DNA, the ratio of the OD_{260}/OD_{280} was analysed as the OD_{280} is indicative of protein contamination. An absorbance ratio of ≥1.8 was considered to be high enough quality to use for downstream applications.

2.2.16. DNA sequencing and analysis

DNA sequencing was performed on an ABI3730xl DNA analyser (Applied Biosystems™, Foster City, USA) at the Central Analytical Facility at Stellenbosch University, South Africa. The sequence data obtained was then analysed using Chromas (version 2.33, Technelysium Pty Ltd, Australia) and DNAMAN (version 4.1.2.1, Lynnon BioSoft, USA) software. The primers used for sequencing are listed in table 2.1.

2.2.17. Gateway Cloning Technology

2.2.17.1. Gateway vectors used

To generate an overexpression clone, two Gateway-compatible vectors were used. The pDONR™221 donor vector was obtained from Thermo Fisher Scientific (Massachusetts, USA) and the pB2GW7 destination vector (Karimi, Inzé & Depicker, 2002) was obtained from The Vlaams Instituut voor Biotechnologie (VIB) Centre for Plant Systems Biology affiliated with Ghent University (Ghent, Belgium).

2.2.17.2. BP recombination reactions

The coding sequences (CDS) of *AtMYB30* and *AtMYB2* were amplified using primers containing flanking *att*B sites (table 2.1) and purified. A BP recombination reaction was performed to transfer the *AtMYB30* or *AtMYB2* CDS respectively from the *att*B PCR product to the pDONR™221 donor vector (containing *att*P sites) to create a pDONR™221-*AtMYB30* and pDONR221™-*AtMYB2* entry clone. The BP recombination reaction was performed using the Gateway® BP Clonase II enzyme mix according to the manufacturer's instructions (Thermo Fisher Scientific, Massachusetts, USA). Specifically, 150 ng of pDONR221 and 50 fmol of PCR product were added. For *att*B1-*AtMYB2*-*att*B2 with a size of 883 bp, this equated to 29 ng of DNA, and for *att*B1-*AtMYB30*-*att*B2 with a size of 1033, this was 36 ng. After completion of the BP reaction, 2 µL of the reaction product was transformed into competent *E. coli* DH5α. The entry clones contained the *AtMYB30* or *AtMYB2* CDS respectively, flanked by *att*L sites and M13 primer binding sites. The M13 primers (found in table 2.1) were used for sequencing PCR-confirmed entry clones to ensure that the CDS was correctly amplified with no base changes, and that the *att*L sites were formed correctly on either side of the CDS.

2.2.17.3. LR recombination reactions

A LR recombination reaction was used to transfer the *AtMYB30* and *AtMYB2* CDS from a sequence-verified pDONR™221-*AtMYB30* and pDONR221™-*AtMYB2* entry clone respectively to the pB2GW7 destination vector (containing *att*R sites) to create the pB2GW7-*AtMYB30* and pB2GW7-*AtMYB2* expression clones. The LR recombination reaction was performed using the Gateway® LR Clonase II enzyme mix according to the manufacturer's instructions (Thermo Fisher Scientific, Massachusetts, USA). For each LR Clonase reaction, 150 ng of pB2GW7

plasmid DNA was added. For each entry vector, 1 µL of purified plasmid DNA was added, equal to 140 ng for the pDONR221-*AtMYB2* entry vector, and 110 ng for the pDONR221-*AtMYB30* entry vector. Subsequently, 2 µL of the resulting LR recombination reaction product was transformed into competent *E. coli* DH5α. The expression clones contained the *AtMYB30* or *AtMYB2* CDS respectively, downstream of the Cauliflower Mosaic Virus (CaMV) 35S promoter. The presence of the insert was confirmed by PCR analysis.

2.2.18. Bacterial work in *Escherichia coli*

2.2.18.1. *E. coli* growth

E. coli was cultured in Luria-Bertani (LB) medium (Sambrook, Fritsch & Maniatis, 1989) supplemented with appropriate antibiotics for plasmid selection. Solid media contained 1.5% (w/v) agar. The antibiotics used for selection include kanamycin (50 µg/mL), used for entry clone screening, and spectinomycin (100 µg/mL), used for expression clone screening. *E. coli* was cultured at 37˚C overnight without shaking for plates and with shaking at 80 rpm for liquid cultures.

2.2.18.2. Preparation of chemically competent *E. coli*

A 5 mL LB culture of *E. coli* DH5α was incubated at 37˚C with shaking overnight. The following day, 2 mL was sub-cultured into 250 mL LB media supplemented with 20 mM $MgSO_4$ and incubated at 37°C with shaking until reaching an OD_{600} of 0.4 to 0.6. Cells were pelleted by centrifugation at 5000 x *g* for 5 min at 4˚C, and then resuspended in 100 mL ice-cold transformation buffer 1 (TFB1) (30 mM potassium acetate, 100 mM RbCl, 10 mM $CaCl_2.2H_2O$, 50 mM $MnCl_2.4H_2O$, 15 % (v/v) glycerol, pH 5.8). The cells were incubated for 5 min in TFB1 before the centrifugation step was repeated. The pelleted cells were then resuspended in 10 mL ice-cold transformation buffer 2 (TFB2) (10 mM MOPS, 10 mM RbCl, 75 mM $CaCl_2.2H_2O$, 15% (v/v) glycerol, pH 6.8) and incubated on ice for 60 min. Cells were then divided into 100 µL aliquots in microcentrifuge tubes and immediately frozen in liquid nitrogen. The cells were stored at -80˚C.

2.2.18.3. Transformation of competent *E. coli*

In a microcentrifuge tube, 2 µL of BP or LR reaction sample, or 150 ng plasmid DNA of known concentration was mixed with 50 µL of competent *E. coli* cells and incubated on ice for 30 min. The cells were then heat shocked at 42˚C for 45 sec and immediately returned to ice for 2 min. Thereafter, 950 µL room temperate LB was pipetted into the mixture before it was incubated at 37˚C with shaking at 80 rpm for 90 min. The cells were then plated onto selective LB-agar media as described in 2.2.18.1 and grown overnight at 37˚C. Competent cells without the addition of plasmid DNA were used as a control for antibiotic selection. Transformants were screened by colony PCR (as described in 2.2.11) and overnight cultures were prepared, from which glycerol stocks of the positive transformants were generated by combining 500 µL of overnight bacterial culture with 500 µL 50% (v/v) glycerol. These were stored at -80˚C.

2.2.19. Bacterial work in *Agrobacterium tumefaciens*

2.2.19.1. Agrobacterium growth

The *A. tumefaciens* GV3101 strain (Holsters et al., 1980) was cultured in Luria-Bertani (LB) medium (Sambrook, Fritsch & Maniatis, 1989) supplemented with appropriate antibiotics for bacterial and plasmid selection. Solid media contained 1.5% (w/v) agar. The antibiotics used for selection included gentamycin (15 µg/mL) and rifampicin (150 µg/mL), used for selection of *A. tumefaciens* GV3101, as well as spectinomycin (100 µg/mL) for selection of the pB2GW7 expression clone. Unless otherwise stated, liquid Agrobacterium cultures were incubated for two days at 30˚C with shaking at 80 rpm, whereas cultures on LB-agar were incubated at 30˚C for 2-3 days without shaking.

2.2.19.2. Preparation of chemically competent Agrobacterium

A single colony of *A. tumefaciens* GV3101 was inoculated into 10 mL yeast extract peptone (YEP) media (1% w/v peptone, 1% w/v yeast extract, 0.5% w/v NaCl) supplemented with 100 µg/mL rifampicin and incubated overnight at 30˚C with shaking at 80 rpm. The following day, 2 mL was sub-cultured into 50 mL fresh YEP media with antibiotic selection. This was incubated at 30˚C with shaking until an OD_{600} of 0.5 to 1.0 was reached. The culture was then chilled on ice before the cells were pelleted by centrifugation at 3000 x *g* for 5 min at 4˚C. The supernatant was discarded before the cells were resuspended in 1 mL ice-cold 20 mM

$CaCl_2.2H_2O$. Cells were then divided into 100 µL aliquots in microcentrifuge tubes and immediately frozen in liquid nitrogen. The cells were stored at -80˚C.

2.2.19.3. Transformation of competent Agrobacterium

Plasmid DNA (25 µL = 4 µg for pB2GW7-*AtMYB2*, 3.7 µg for pB2GW7-*AtMYB30*, 5 µg for pB2GW7) was added to 100 µL of frozen competent *A. tumefaciens* cells. The mixture was then incubated in a water bath at 37˚C for 5 min to both thaw and heat shock the cells. Thereafter, 900 µL room temperature LB was pipetted into the mixture before incubation at 30˚C with shaking for 6 hours. The cells were then plated onto selective LB-agar media and incubated at 30˚C for 2-3 days until colonies appeared, as described in 2.2.19.1. Competent cells without the addition of plasmid DNA were used as a control for antibiotic selection. Transformants were screened by colony PCR (as described in 2.2.11) and overnight cultures were prepared, from which glycerol stocks of the positive transformants were generated. These were stored at -80˚C.

2.2.20. Floral-dip transformation of Arabidopsis plants

Agrobacterium-mediated stable transformation of Arabidopsis is based on the floral dip method described by Clough and Bent (1998). During this process, the region between the left and right border of the expression construct are transferred randomly into the Arabidopsis genome.

2.2.20.1. Plant preparation

For each construct to be dipped, 25 Arabidopsis Col-0 plants were grown on soil until the development of primary bolts, at about four weeks. These were clipped at the base of the rosette to promote secondary bolt development. The plants were then left until they displayed the maximum number of flowers with no siliques, which took approximately 10 more days.

2.2.20.2. Agrobacterium preparation

Successfully transformed *A. tumefaciens* (pB2GW7-*AtMYB2*/pB2GW7-*AtMYB30*) stored as a glycerol stock was streaked onto selective LB-agar and grown at 30˚C for 3 days. A single colony was then inoculated into 5 mL selective LB liquid media and incubated at 30˚C with

shaking at 80 rpm for 2 days. Thereafter, the entire 5 mL culture was used to inoculate a large-scale culture of 500 mL selective LB liquid media which was incubated overnight with shaking at 30˚C. Cells were harvested by centrifugation at 3500 x *g* for 15 min at room temperature and resuspended in 250 mL 5 % (w/v) sucrose containing 0.05% Silwet L-77 surfactant (Lehle Seeds, Round Rock, USA). The same procedure was followed for *A. tumefaciens* (pB2GW7) to create an empty vector control in the Arabidopsis Col-0 ecotype.

2.2.20.3. Floral dip

The aerial parts of the plants were submerged in the Agrobacterium cell-suspension for approximately 15 seconds. The dipped plants were then placed on their sides in trays lined with tissue paper, covered in plastic wrap, and left overnight in the growth room. The next day, the plants were uncovered and placed upright. Plants were watered from below, and covered with aracons, and allowed to set seed before drying down.

2.2.20.4. Isolation of transformed lines

The T1 seed was collected from the dipped T_0 plants, surface sterilised and plated on PN-agar (as described in 2.2.4) supplemented with 10 µg/mL glufosinate ammonium (GFSA). Using the floral-dip method, the expected transformation efficiency was 0.01, meaning that 1/100 T1 seeds were expected to be transgenic and be able to grow on GFSA. As such, 100 seeds were plated on PN media with 10 µg/mL GFSA for each T1 line, for each genotype. Transformed individuals, containing the Bialaphos acetyltransferase (*Bar*) gene from the pB2GW7 vector, are resistant to GFSA, the main active compound of the Basta herbicide. Seedlings on PN media served as a control to check germination efficiency. After 11-14 days, resistant individuals were identified and transplanted onto soil. When the plants were 4 weeks old, a leaf sample was taken for DNA extraction and PCR analysis to confirm the presence of the *Bar* gene. Confirmed transformants were allowed to grow to maturity and self-fertilise.

The T2 seed from the T1 plants was then collected and surface sterilised before screening on GFSA and PN (control) plates to determine the segregation ratios. Fifty seeds were plated on each type of media, in duplicate, for each line. After 11-14 days, four of the GFSA-resistant T2 seedlings, which could be heterozygous or homozygous transgenic, were transplanted onto soil. The screening was repeated in the subsequent T3 generation to identify homozygous

transgenic lines having 100% resistance to GFSA. For each identified potentially homozygous line, 20 seedlings were harvested randomly off the untreated PN plates, to confirm homozygosity by PCR. A line was determined to be homozygous if 1) the same number of seedlings survived on the PN plates and the GFSA plates by observation of the development of true leaves, as well as a lack of visual yellowing associated with GFSA-induced plant death, and 2) all 20 of the seedlings from untreated PN plates tested positive for a PCR product using the P35S forward and *AtMYB30* or *AtMYB2* reverse primers respectively or the *Bar* primer pair (in the case of the empty vector control lines) (table 2.1).

2.2.21. Analysis of early development microarray data

Previous transcriptomics data from our group was analysed for changes in expression of the genes of interest to this project. For this, data from a microarray experiment conducted by Dr Lara Donaldson at King Abdullah University of Science and Technology (KAUST) was obtained (Cackett et al., 2022). In this experiment, Arabidopsis Col-0 was grown for two weeks in petri dishes on PN-agar (6% w/v) supplemented with 0, 50, 75, 100 or 125 mM NaCl or iso-osmolar concentrations of sorbitol (0, 100, 150, 200 or 250 mM sorbitol). The experiment was conducted three times to get three independent biological replicates with each sample being a pool of approximately 50 seedlings. The RNA from these seedlings was extracted and submitted to the genomics facility at KAUST where they performed a microarray experiment using the Arabidopsis (V4) Gene Expression Microarray, 4x44k microarray chip by Agilent Technologies (California, USA). The microarray data was quantile normalised by Carlo Cannistraci. During this project, this dataset was used for candidate gene expression analysis using Microsoft Excel, whereby the average normalised counts and associated standard errors were calculated from the independent biological replicates for each treatment. This data was then used to plot graphs in Microsoft Excel.

2.2.22. Statistics

All statistical analyses were performed using TIBCO® Statistica™ version 13.5 software or Microsoft Excel. For most experiments, one-way analysis of variance (ANOVA) tests were performed in Statistica, and significantly different mean values identified by Fisher's least significant difference (LSD) post-hoc analysis. Letters were added to the relevant graphs to indicate significant differences as determined by ANOVA. When only two values were being

compared, two-tailed homoscedastic t-tests were performed in Microsoft Excel. Where linear relationships were observed and scatter plots were used, Microsoft Excel was used to test for significant differences in the regression slopes. For all analyses, p-values ≤ 0.05 were considered significant.

2.2.23. Bioinformatics

2.2.23.1. TFBS identification and visualisation

The Athena analysis suite (http://www.bioinformatics2.wsu.edu/Athena) (O'Connor, Dyreson & Wyrick, 2005), The Arabidopsis Gene Regulatory Information Server (AGRIS; https://agris-knowledgebase.org/AtcisDB/) (Davuluri et al., 2003) and the Plant Cis-acting regulatory Element database (PLACE) (https://www.dna.affrc.go.jp/PLACE/?action=newplace) (Higo et al., 1999) were used for identification and visualisation of *cis*-regulatory promoter elements, including TFBS, in the *Nitrilase 2* promoter.

2.2.23.2. Transcription factor identification from gene lists

The Plant Transcription factor & Protein Kinase Identifier and Classifier (iTAK; http://itak.feilab.net/cgi-bin/itak/online_itak.cgi) (Zheng et al., 2016) was used to identify transcription factors present in the list of genes upregulated ≥ 2-fold.

Table 2.1: The primers used in this chapter. F: forward primer, R: reverse primer

Primer name	Primer sequence (5'-3')	Reference (if applicable)	Amplicon size (bp)	Function	PCR kit	T_a
qAtNit2 F *qAtNit2* R	CTCCCGCCACTCTAGAAAAG AATAGCAGAAGCATGGTACTTGC	Cackett, 2019	185	RT-qPCR	SYBR® FAST	60˚C
qAtMYB30 F *qAtMYB30* R	CAGACAAGGCGATGGCGATA GCTTTCTCTCAAGGGTTTCTGGGT		201	RT-qPCR	SYBR® FAST	60˚C
qAtMYB2 F *qAtMYB2* R	CAATCCTAGTCAACTTCGTCTC AATCTTCGACCACCTATTGCC		209	RT-qPCR	SYBR® FAST	60˚C
AtMON1 F *AtMON1* R	CAGACAAGGCGATGGCGATA GCTTTCTCTCAAGGGTTTCTGGGT	Hong et al., 2010	244	RT-qPCR	SYBR® FAST	60˚C
				PCR	Super-Therm	55˚C
AtMYB30 FL F *AtMYB30* FL R	ATGGTGAGGCCTCCTTGT TCAGAAGAAATTAGTGTTTTCATCC		gDNA: 1414 cDNA: 972	PCR	Kapa RM	55˚C
*AtMYB30-att*B1 F *AtMYB30-att*B2 R	ggggacaagtttgtacaaaaaagcaggcttcATGGTGAGGCCTCCTTG* ggggaccactttgtacaagaaagctgggtcTCAGAAGAAATTAGTGTTTTCATCC*		1033	Cloning	Kapa HiFi	72˚C
					Kapa RM	55˚C
*AtMYB2-att*B1 F *AtMYB2-att*B2 R	ggggacaagtttgtacaaaaaagcaggcttcATGGAAGATTACGAGCG* ggggaccactttgtacaagaaagctgggtcTTAATTATACGAATACGATGTCG*		883	Cloning	Kapa HiFi	72˚C
					Kapa RM	50˚C
M13 F M13 R	GTAAAACGACGGCCAG CAGGAAACAGCTATGAC	Invitrogen	-	Sequencing	-	-
bar F *bar* R	AAGTCCAGCTGCCAGAAACC GAACTGACAGAACCGCAACG	Dr Lara Donaldson	733	Genotyping	Kapa RM	57˚C
P35S F *AtMYB30-att*B2 R	AATATCGGGAAACCTCCTCG ggggaccactttgtacaagaaagctgggtcTCAGAAGAAATTAGTGTTTTCATCC*	Dr Lara Donaldson /Designed	1450	Genotyping	Kapa RM	53˚C
P35S F *AtMYB2-att*B2 R	AATATCGGGAAACCTCCTCG ggggaccactttgtacaagaaagctgggtcTTAATTATACGAATACGATGTCG*	Dr Lara Donaldson /Designed	1300	Genotyping	Kapa RM	53˚C

***** attB sequences are shown in lowercase letters

2.3. RESULTS

2.3.1. Identification of candidate transcription factors

2.3.1.1. Identification of TFBS in the *Nitrilase 2* promoter

In order to determine what TFBS are contained within the *AtNit2* promoter, the putative promoter region, 1 kb upstream from the *AtNit2* translation start site, was analysed *in silico* using a combination of Athena (O'Connor, Dyreson & Wyrick, 2005) and PLACE (Higo et al., 1999). Table 2.2 shows that there were 12 predicted TFBS identified. Notably, five MYELOBLASTOSIS (MYB) TFBS were present in this region, and these are represented schematically in figure 2.1, and are shown in the promoter sequence in appendix figure 6.2. Additionally, the IBOXCORE motif is involved in binding of MYB factors of light-regulated genes in tomato (Czemmel et al., 2009) and may be an additional site at which MYB TFs can bind to the *AtNit2* promoter. Overall, this analysis suggests a potential role for one or more MYB TFs in *AtNit2* regulation.

Table 2.2: TFBS present in 1 kb upstream of *AtNit2*

Binding site name as per Athena/PLACE	Motif	Site in P*AtNit2*	# of sites in 1 kb upstream of *AtNit2*	Strand
MYB1AT	(A/T)AACCA	TAACCA	1	+
MYB2AT/MYB2CONSENSUSAT	(T/C)AAC(T/G)G	TAAC(T/G)G	2	+
MYB4 binding site	A(A/C)C(A/T)A(A/C)C	ACCAAAC	1	+
MYBCOREATCYCB1	AACGG	AACGG	1	+
GAREAT (GA-responsive element)	TAACAA(A/G)	TAACAAA	1	+
IBOXCORE	GATAA	GATAA	1	+
TATABOX2	TATAAAT	TATAAAT	1	+
TATABOX3	TATTAAT	TATTAAT	1	+
TATABOX5	TTATTT	TTATTT	1	+
GATABOX	TGATAA	TGATAA	1	+
WBOXNTERF3	TGAC(C/T)	TGAC(C/T)	2	-
Bellringer/replumless/ pennywise BS1 IN AG	AAATTAAA	AAATTAAA	2	+

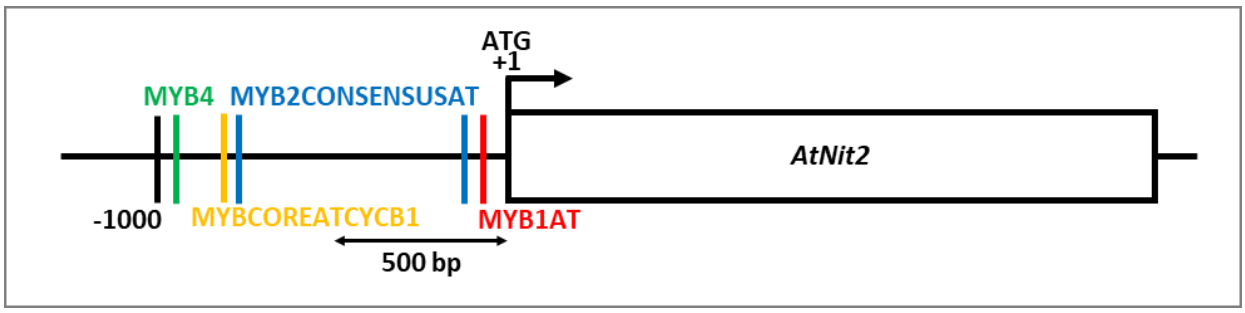

Figure 2.1: Schematic showing the presence of MYB binding sites in the *AtNit2* promoter

In this schematic, the *AtNit2* promoter positive strand is shown as a black line with the coding sequence indicated by a white box with a black outline. The translation start site (ATG) is labelled as +1 and all sites are labelled relative to this position. The MYB1AT binding site (red) is present at position -89 in the *AtNit2* promoter, with the MYB2CONSENSUSAT sites (blue), the MYBCOREATCYCB1 (yellow) site and the MYB4 binding site (green) present at positions -167, -733, -824 and -995 respectively.

2.3.1.2. Analysis of TFs upregulated in response to NaCl early in development

As the MYB TF superfamily is very large (198 genes) and functionally diverse (Yanhui et al., 2006; Dubos et al., 2010), it was important to narrow down a list of candidate MYB TFs for further characterisation. Although TFs can regulate gene expression in response to certain conditions and not themselves be transcriptionally regulated, an easy way of narrowing down candidate MYB TFs that might regulate *AtNit2* expression under saline conditions was to focus on TFs upregulated ≥ 2-fold in response to NaCl from the microarray. This list of genes was searched using iTAK (Zheng et al., 2016) for known TFs and the results can be seen in appendix table 6.1.

Of the 406 genes upregulated ≥ 2-fold in response to NaCl, 28 were identified to be TFs. Unsurprisingly, many of these TFs belong to families which are known to regulate genes in response to abiotic stress, such as the WRKY, bZIP, ERF/AP2 and MYB families. Notably, *AtATAF2* was not differentially regulated under saline conditions. Interestingly, only two MYB TFs were upregulated under saline conditions, *AtMYB2* (AT2G47190) and *AtMYB30* (AT3G28910). These TFs were selected for further analysis due to 1) AtMYB2 and AtMYB30 being able to potentially bind the MYB TFBS in the *AtNit2* promoter, 2) previous research showing that AtMYB2 regulates the expression of salt- and dehydration-responsive genes

(Yoo et al., 2005), and 3) previous research showing that *AtMYB30* is a direct target of BRI1-EMS-SUPPRESSOR 1 (BES1) and that together they regulate genes induced by brassinosteroids which cooperate with auxin to promote cell expansion and elongation (Nemhauser, Mockler & Chory, 2004; Walcher & Nemhauser, 2012). Specifically, AtMYB2 is able to bind to the 'MYB1AT' motif (TAACCA) (Yu et al., 2012) and 'MYB2AT' binding site (TAACTG) (Urao et al., 1993), both present in the promoter region of *AtNit2*. AtMYB30 has been shown to bind to multiple different variations of (C/T)A(A/C)C(T/C/A)A(C/A)C (Jinno et al., 2019), including A(A/C)CAAAC (Li et al., 2009; Liao, Zheng & Guo, 2017). Notably, the 'MYB1AT' motif (TAACCA) and the 'MYB4 binding site' motif (A(A/C)C(A/T)A(A/C)C) would conform to this and are both present in the promoter of *AtNit2.*

In order to validate the microarray showing that these TFs increase in expression in response to NaCl, Arabidopsis Col-0 was grown for two weeks in petri dishes on control PN-agar, or PN-agar supplemented with 50, 75, 100 or 125 mM NaCl, or iso-osmolar concentrations of sorbitol (100, 150, 200 or 250 mM sorbitol) to mimic the growth of the plants used in the microarray experiment (Cackett et al., 2022). After two weeks, RT-qPCR was used to analyse *AtMYB2, AtMYB30* and *AtNit2* gene expression using the qPCR primers listed in table 2.1.

Figure 2.2A shows that in the microarray experiment, *AtMYB2* expression was significantly higher in all NaCl treatments, and 150, 200 and 250 mM sorbitol, compared to the untreated control. Additionally, the expression of *AtMYB2* was higher in 125 mM NaCl than in the lower NaCl concentrations. Similarly, figure 2.2B shows that in the RT-qPCR experiment, *AtMYB2* expression was highest in the 125 mM NaCl treatment.

Figure 2.2C shows that *AtMYB30* expression was upregulated in the microarray experiment, specifically in response to increasing concentrations of NaCl, in a dose-dependent manner. The fold change induction of *AtMYB30* was significantly higher in all NaCl concentrations compared to the untreated control, and iso-osmolar sorbitol treatments. This result was not validated in the RT-qPCR experiment in figure 2.2D as there was no significant difference between any of the treatments and the control.

Because we were unable to confirm the salt specific expression of *AtMYB30*, RT-qPCR was also used to validate *AtNit2* expression in the same samples to ensure that the plants were responding in the same way to salt as in the original microarray. Figure 2.2E shows that *AtNit2*

gene expression was significantly upregulated in a dose-dependent manner in response to NaCl, but not sorbitol in the microarray, and figure 2.2F shows that this was validated by RT-qPCR. Overall, the microarray results suggest that *AtMYB2, AtMYB30* and *AtNit2* are upregulated in a dose-dependent manner under saline conditions. The RT-qPCR experiments were only able to validate that *AtNit2* expression, and that *AtMYB2* is upregulated in response to 125 mM NaCl. However, as *AtMYB30* is known to be an auxin response gene, the role of both *AtMYB2* and *AtMYB30* in the plant response to salt stress was further characterised using a functional genetics approach.

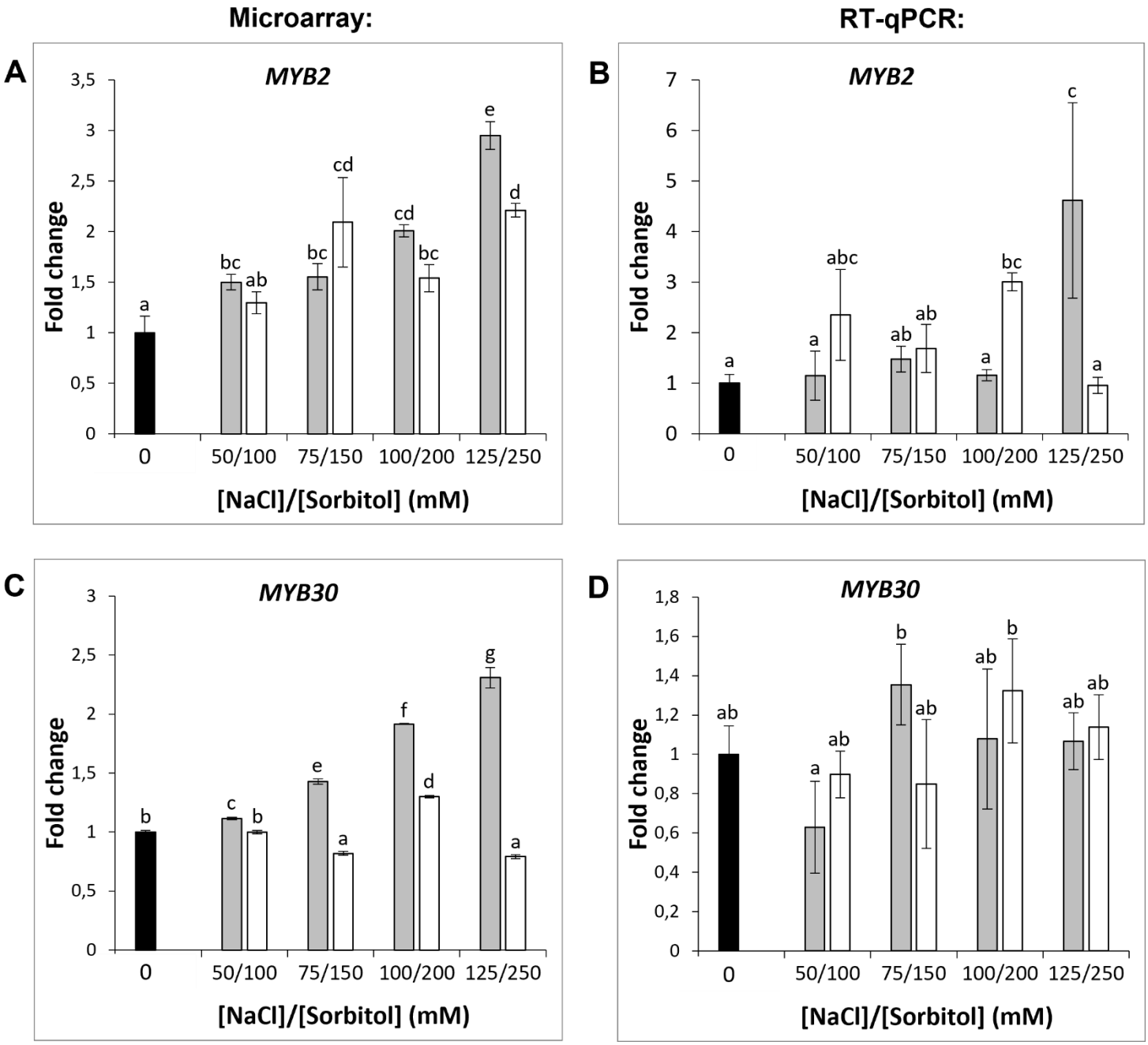

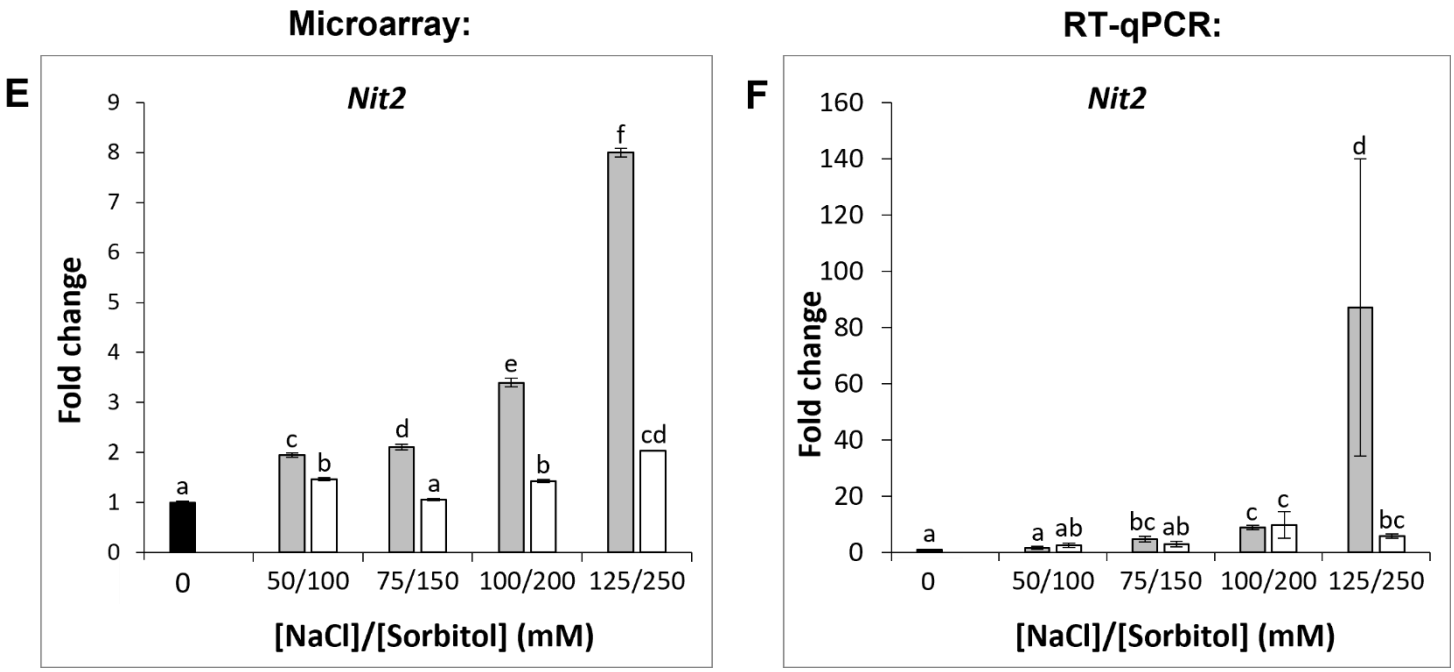

Figure 2.2: The expression of *AtMYB2, AtMYB30* and *AtNit2* in Arabidopsis Col-0 plants exposed to NaCl early in development

Gene expression was determined in Arabidopsis Col-0 seedlings grown in petri dishes on control PN-agar and PN supplemented with different concentrations of NaCl or iso-osmolar sorbitol for two weeks. Genes include: *AtMYB2* (**A** and **B**), *AtMYB30* (**C** and **D**), and *AtNit2* (**E** and **F**). The RT-qPCR experiments (**B**, **D** and **F)** were used to validate the results obtained from the microarray (**A**, **C** and **E**). All results are shown as an average fold change relative to the untreated control. The average was calculated from three independent biological samples. Different letters on the graphs indicate significant differences ($p \leq 0.05$) in mean fold change values as determined by Fisher LSD post-hoc analysis following a one-way ANOVA. Error bars indicate standard error. Black bar: untreated control, grey bars: NaCl treatments, white bars: sorbitol treatments. The RT-qPCR results for each gene were normalised to the *AtMON1* reference gene.

2.3.2. Generation of homozygous *AtMYB2* and *AtMYB30* overexpressing lines

2.3.2.1. The *AtMYB2* and *AtMYB30* overexpression constructs

Overexpression of *AtNit2* in Arabidopsis improves salt tolerance as its growth is less inhibited by saline conditions and it has improved ion homeostasis (Cackett et al., 2022). To determine whether an increase in *AtMYB2* or *AtMYB30* expression alters expression of *AtNit2*, and/or affects Arabidopsis salt tolerance, stably transformed Arabidopsis lines overexpressing each MYB transcription factor were generated.

Gateway Cloning Technology was used to clone each of the *AtMYB2* and *AtMYB30* coding sequences (CDS) into the pDONR™221 entry vector. After PCR confirmation and sequencing using the CDS flanking M13 primers (table 2.1), the *AtMYB2* and *AtMYB30* CDS was transferred into the pB2GW7 Arabidopsis expression vector, downstream of the constitutive Cauliflower Mosaic Virus 35S promoter, creating pB2GW7-*AtMYB2* (figure 2.3A) and pB2GW7-*AtMYB30* (figure 2.3B) respectively. These constructs were transformed into *E. coli* DH5α and colonies were screened from selection plates using colony PCR. Sequence-confirmed plasmid DNA was then transformed into Agrobacterium.

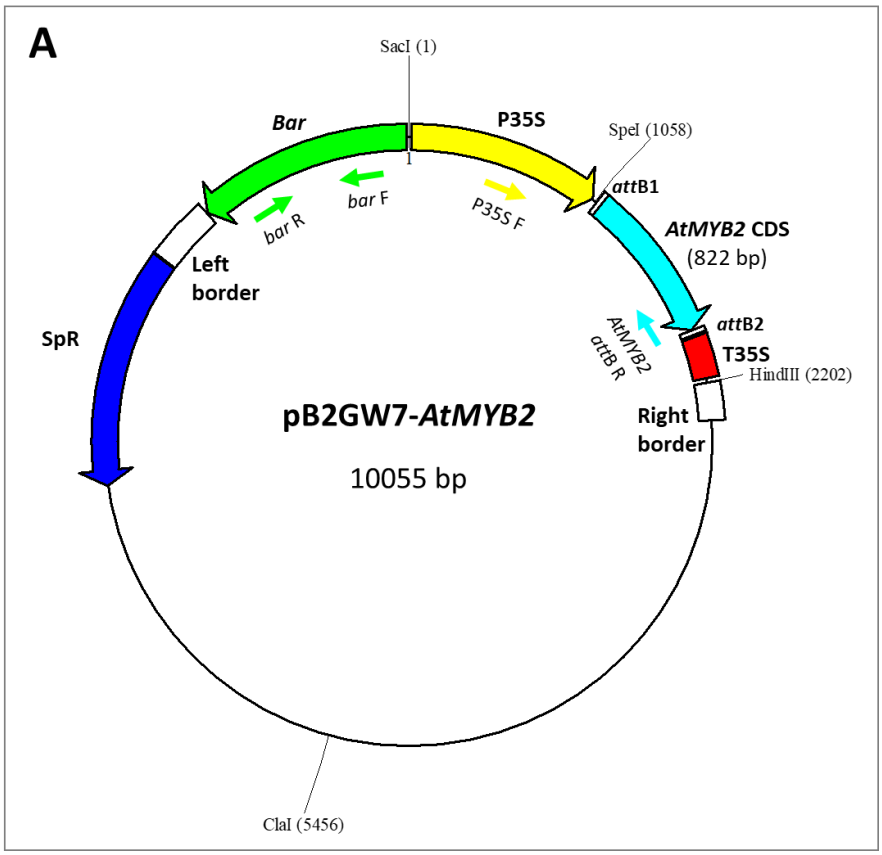

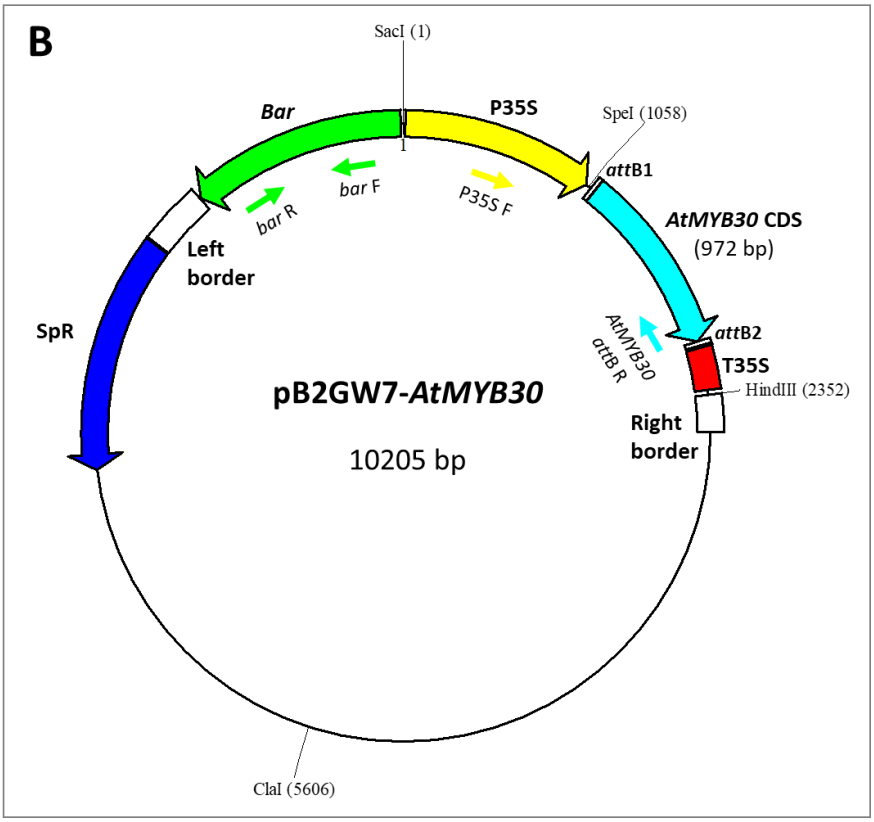

Figure 2.3: Map of pB2GW7-*AtMYB2* and pB2GW7-*AtMYB30* generated via Gateway cloning

Expression of the **A**) *AtMYB2* and **B**) *AtMYB30* coding sequence (**CDS**) is driven by the constitutive Cauliflower Mosaic Virus 35S promoter (**P35S**) and terminated by the 35S terminator sequence (**T35S**). Antibiotic selection of the plasmid in positive *E. coli* and *A. tumefaciens* transformants is made possible by the spectinomycin resistance gene (**SpR**). The bialaphos acetyltransferase gene (***Bar***) confers resistance to glufosinate ammonium which allows for selection of positive Arabidopsis transformants. The region between the **left border** and **right border** inserts randomly into the Arabidopsis genome via *Agrobacterium*-mediated floral-dip transformation. The primers used for selection of bacterial transformants and transgenic Arabidopsis lines are shown by arrows inside the vector and are described in Table 2.1.

2.3.2.2. Transformation of Arabidopsis with pB2GW7-*AtMYB2* and pB2GW7-*AtMYB30*

The pB2GW7-*AtMYB2* and pB2GW7-*AtMYB30* plasmids were transformed into Agrobacterium and a colony PCR was conducted on six colonies that grew on selective media using the 35S promoter forward primer and the *AtMYB2* or *AtMYB30 att*B2 reverse primer respectively (table 2.1, figure 2.3). Additionally, the pB2GW7 vector was transformed into

Agrobacterium as an empty vector (EV) control. A colony PCR was conducted on these colonies using the *Bar* primer pair.

Figure 2.4 shows that all Agrobacterium colonies and the positive control for each expression vector respectively had a single, defined amplicon at approximately the correct size of 1300 bp for *AtMYB2* (figure 2.4A) and 1450 bp for *AtMYB30* (figure 2.4B), confirming that these expression vectors had been successfully transformed into Agrobacterium. There were no bands seen in the H_2O no template controls, as expected. All Agrobacterium colonies transformed with EV DNA showed a band at the correct size for the *Bar* gene (figure 2.4C). The faint bands in some colonies could be due to not picking up enough bacterial sample to add to the PCR reaction tube. The presence of faint upper bands at approximately 1 kb and 1.5 kb could be caused amplification of Agrobacterium DNA by the *Bar* primer pair as these bands are not seen in the positive control which contains pB2GW7-*ZmNit2* plasmid DNA (chapter 4, section 4.4.3.1). A single Agrobacterium colony was selected for each (sample 1) to be used for Arabidopsis transformation.

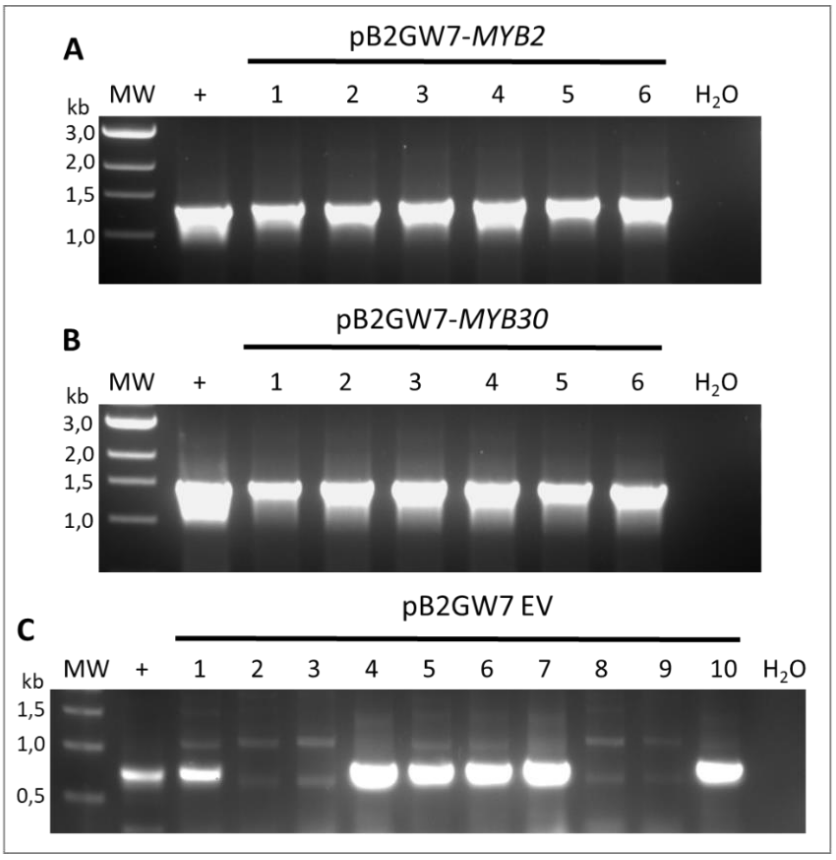

Figure 2.4: PCR confirmation of successful *Agrobacterium* transformations with pB2GW7-*AtMYB2,* pB2GW7-*AtMYB30* and pB2GW7 empty vector

A colony PCR was performed on colonies from *A. tumefaciens* transformed with **A:** pB2GW7-AtMYB2, using the P35S forward primer and *AtMYB2* attB2 R primer with an expected amplicon size of 1300 bp, **B:** pB2GW7-*AtMYB30,* using the P35S forward primer and *AtMYB30* attB2 R primer with an expected amplicon size of 1450 bp, and **C:** empty pB2GW7 vector, using the *Bar* primer pair with an expected amplicon size of 733 bp. A no template H_2O negative control PCR reaction was included in each case, with pB2GW7-*AtMYB2* #1*,* pB2GW7-*AtMYB30* #1 and pB2GW7 #1 plasmid DNA (sequence verified after cloning into *E. coli*) used as a template in each positive control (**+**) respectively. The MW marker included is the New England Biolabs Quick-Load® 1 kb DNA ladder.

After confirming positive Agrobacterium transformation with the expression clones, Agrobacterium-mediated floral-dip transformation of Arabidopsis Col-0 ecotype was performed. Glufosinate ammonium (GFSA) selection plates were used to isolate transgenic individuals from seeds collected from the transformed plants (T1 generation). Seedlings which were able to survive for 11 days on the selection plates (e.g., figure 2.5) were transferred onto soil.

Figure 2.5: Example of a T1 seedling selected for analysis off of a GFSA selection plate

Seeds collected from the first transgenic generation (T1) of the *35S::AtMYB2, 35S::AtMYB30* and *35S* EV lines were screened for survival on PN-agar supplemented with 10 µg/mL glufosinate ammonium (GFSA). Seedlings were grown for 11 days before any healthy, potentially transgenic, seedlings were identified and transferred to soil. The seedling circled in red is an example of a seedling that would be taken forward for analysis. The other seedlings on the selection plate which show visual bleaching and no true leaf development are indicative of the GFSA-induced plant death exhibited by wild-type seedlings which do not contain the *Bar* gene. From each transformed plant, 100 seeds were sown for selection.

Once the seedlings had established properly on soil, one leaf per line was harvested for DNA extraction and PCR analysis to confirm the presence of the transgene. Figures 2.6 and 2.7 show that several transgenic lines were isolated in the T1 generation for the *35S* EV, *35S::AtMYB2* and *35S::AtMYB30* Arabidopsis genotypes respectively.

Figure 2.6A shows that six transgenic *35S* EV (Col-0) lines were isolated as they contained a specific band amplified at the expected size, the same as the positive control, using the *Bar* primer pair. One line (#20) contained no amplicon, but the other six lines with *Bar* amplification were selected for further analysis.

Figures 2.6B and 2.7A show that five transgenic *35S::AtMYB2* lines were isolated that contained both the *Bar* gene (Fig 2.12B) and the *AtMYB2* coding sequence downstream of the 35S promoter (Fig 2.7A). Only one line (#5) produced an amplicon in the *Bar* PCR but not in the gene-specific PCR and thus was not taken forward; the other five produced a specific band at the expected size in both PCRs and were therefore selected for further analysis.

Figures 2.6C and 2.7B show that 10 transgenic *35S::AtMYB30* lines were isolated that contained both the *Bar* gene (Fig 2.6C) and the *AtMYB30* coding sequence downstream of the 35S promoter (Fig 2.7B). As all 10 seedlings had a specific band amplified at the expected size in both PCRs, all lines were selected for further analysis. All of the selected lines were then allowed to grow to maturity to self-fertilise and produce the next T2 generation.

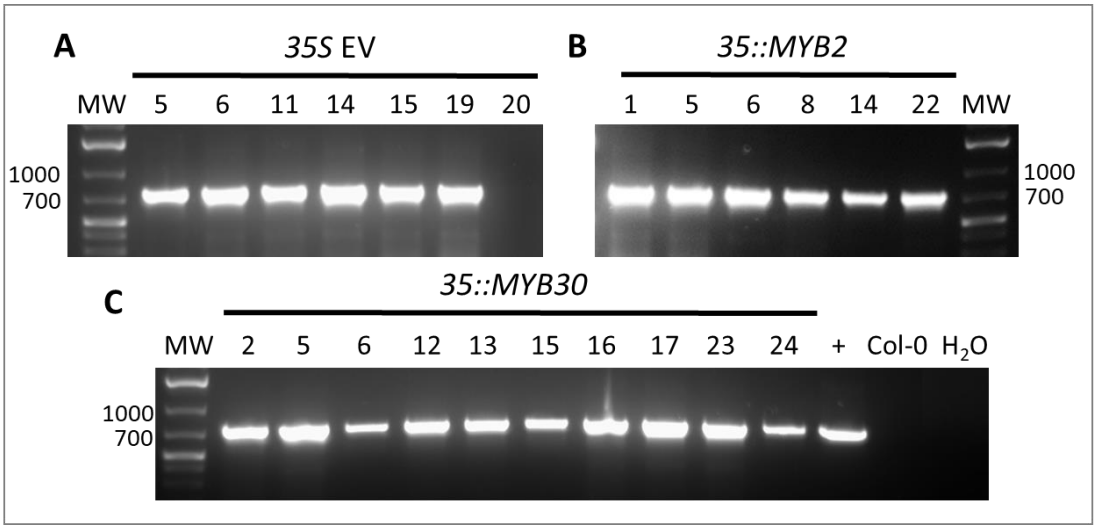

Figure 2.6: *Bar* PCR confirmation of EV, *35S::AtMYB2* and *35S::AtMYB30* Arabidopsis lines

A PCR was performed on DNA extracted from potentially transgenic Arabidopsis plants using the *Bar* primer pair with an expected amplicon of 733 bp. **A:** Seven potential *35S* EV lines. **B:** Six potential *35S::AtMYB2* lines. **C:** Ten potential *35S::AtMYB30* lines. No template (H_2O) and Col-0 negative control PCR reactions were included with sequence-verified pB2GW7-*AtMYB2* plasmid DNA used as a positive control (**+**). The MW marker included is the Thermo Scientific GeneRuler 1 kb Plus DNA Ladder.

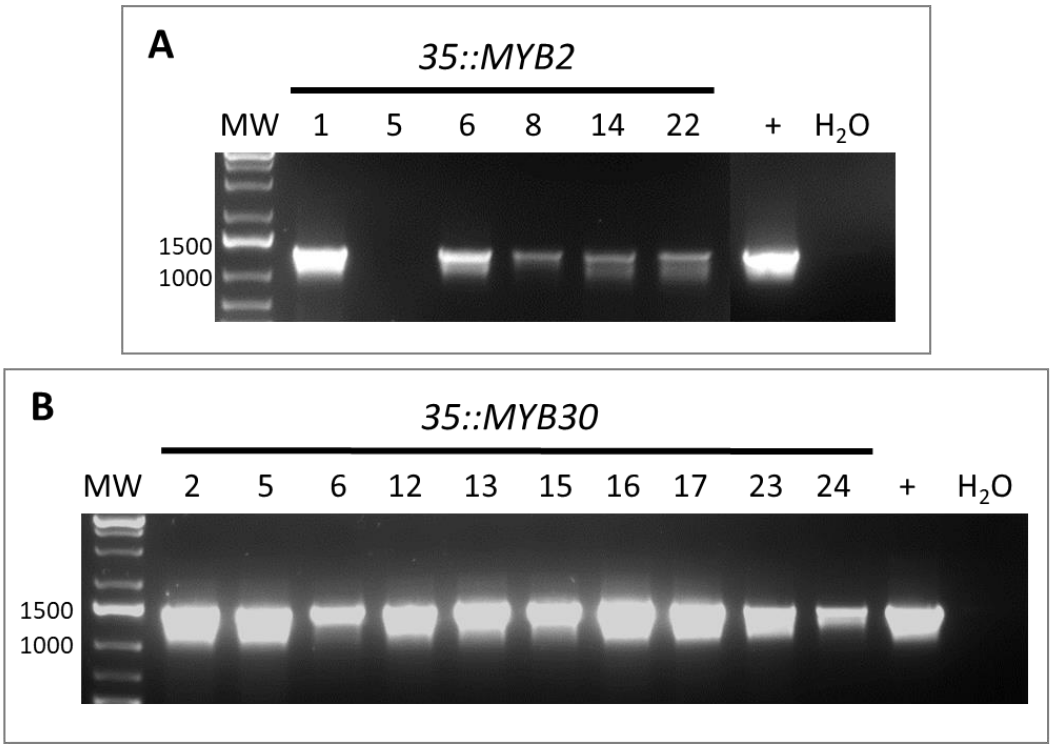

Figure 2.7: Gene-specific PCR confirmations of *35S::AtMYB2* and *35S::AtMYB30* Arabidopsis lines

A PCR was performed on DNA extracted from potentially transgenic Arabidopsis plants using the P35S forward primer and a gene-specific reverse primer. **A:** Six potential *35S::AtMYB2* lines were evaluated using the *AtMYB2* attB2 reverse primer with an expected amplicon size of 1300 bp. Sequence-verified pB2GW7-*AtMYB2* plasmid DNA was used as a positive control (**+**). **B:** Ten potential *35S::AtMYB30* lines were evaluated using the *AtMYB30* attB2 reverse primer with an expected amplicon size of 1450 bp. The pB2GW7-*AtMYB30* #1 plasmid DNA was used as a positive control (**+**). A no template H_2O negative control PCR reaction was included in both. The MW marker included is the Thermo Scientific GeneRuler 1 kb Plus DNA Ladder.

2.3.2.3. Confirmation of *AtMYB2* and *AtMYB30* overexpression

In the T2 generation, GFSA screening was used to identify lines which gave an approximate 3:1 ratio of transgenic (heterozygous or homozygous) to WT, which would indicate a single transgene insertion (appendix table 6.2). Several transgenic seedlings (which were either heterozygous or homozygous) per line were picked and transferred to soil. Another round of GFSA screening in the T3 generation led to identification of homozygous transgenic lines which were then transferred to soil for expression analysis, and to collect seed for future phenotyping experiments. For each of the homozygous *35S::AtMYB2, 35S::AtMYB30* and EV lines, six leaves (two leaves from three transferred plants per line) were pooled to form a single tissue sample for RNA extraction and subsequent cDNA synthesis. RT-qPCR was performed using the *AtMYB2, AtMYB30* and *AtMON1* reference gene qPCR primers listed in table 2.1. The *AtMYB2* and *AtMYB30* expression values were normalised to *AtMON1,* and the results are presented in figure 2.8A and B respectively.

Figure 2.8A and B show that *AtMYB2* and *AtMYB30* expression levels in the EV lines were comparable to Col-0 WT, therefore indicating that these EV lines are appropriate for downstream analyses. The EV lines 6.3 and 15.1 were selected for further analysis as they had the best germination frequencies and the most seeds available.

Additionally, figure 2.8A shows that all three *35S::AtMYB2* lines analysed showed higher *AtMYB2* levels than the EV lines, and that the expression varied between lines. This was expected due to the nature of Arabidopsis floral-dip transformation, where the transgene is

inserted randomly into the Arabidopsis genome. This means that the transgene DNA could have integrated near to or far from transcriptional activating elements or enhancers, or different regulatory elements or epigenetic markers, which would lead to variable expression levels. Two overexpressor lines were selected to be carried forward based on having the highest *AtMYB2* expression – lines 14.3 and 22.2.

Similarly, figure 2.8B shows that all four *35S::AtMYB30* lines analysed showed higher *AtMYB30* levels than the EV lines, with varying expression levels between lines. Lines 2.3, 16.2 and 23.2 were selected for further analysis. The reason for taking three lines forward in this genotype was due to line 2.3 having a visible dwarf phenotype in older seedlings (appendix figure 6.3) that we thought might interfere with subsequent assays. As this line had the highest *AtMYB30* expression, it was still carried forward for possible use in downstream phenotyping, however lines 16.2 and 23.2 were analysed first.

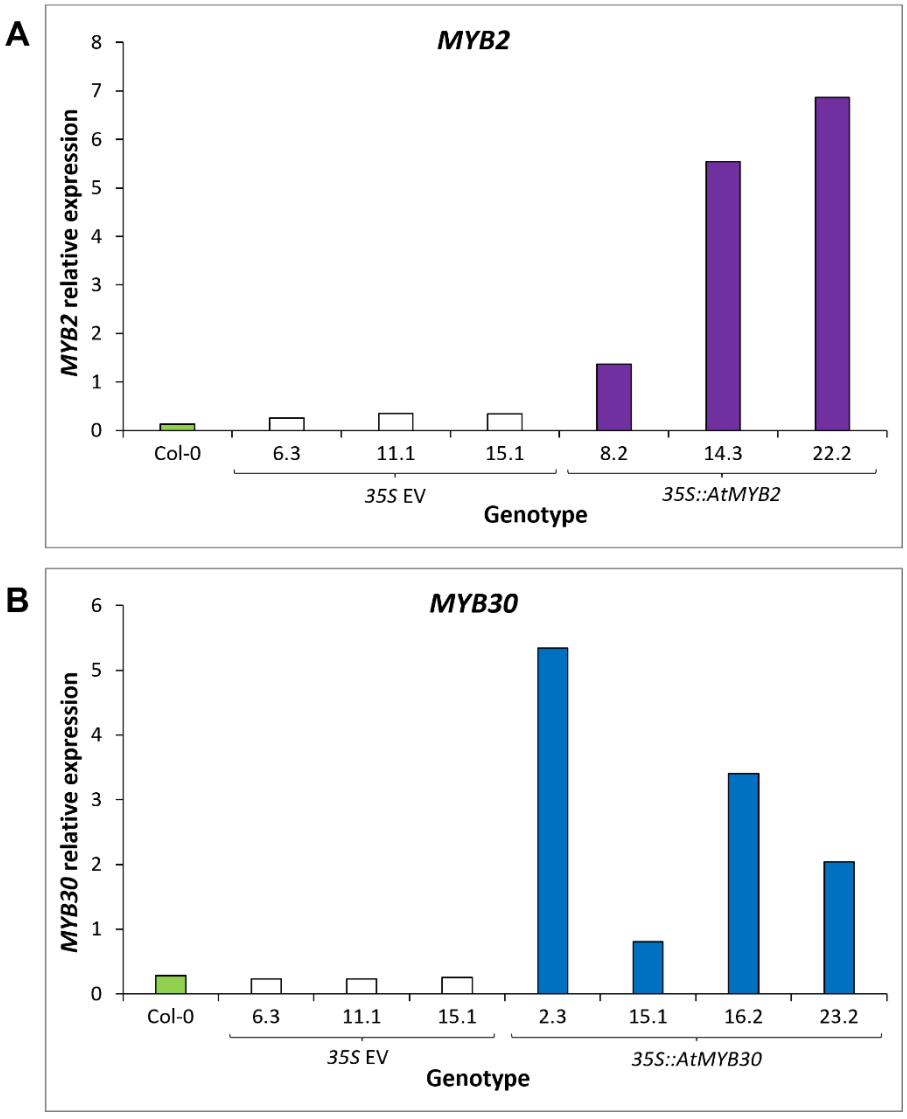

Figure 2.8: *AtMYB2* and *AtMYB30* gene expression in homozygous T3 plants

Arabidopsis plants were grown on PN-agar supplemented with 10 µg/mL GFSA for 11 days then transferred onto soil for two weeks. Tissue from two leaves of three plants were harvested and pooled for RNA extraction and cDNA was synthesised for RT-qPCR gene expression analysis. Expression of **A**: *AtMYB2* and **B**: *AtMYB30* are shown relative to the *AtMON1* reference gene. Col-0 WT Arabidopsis was included as a control.

For each of the selected lines, ten seedlings were harvested from PN-agar plates and used in DNA extractions and PCR to confirm homozygosity. For the *35S* EV lines, PCR was conducted using the *Bar* primer pair (figure 2.9A). For the *35S::AtMYB2* and *35S::AtMYB30* lines, PCR was conducted using the *35S* promoter forward primer and the gene-specific attB reverse primer respectively (figure 2.9B and C). All ten of the seedlings from each line for each genotype contained the specific transgene product and no amplicon was obtained in Col-0 WT or the H_2O negative controls. Along with the phenotype on selection plates (data not shown), this data indicates that these lines are all homozygous and therefore could be further analysed.

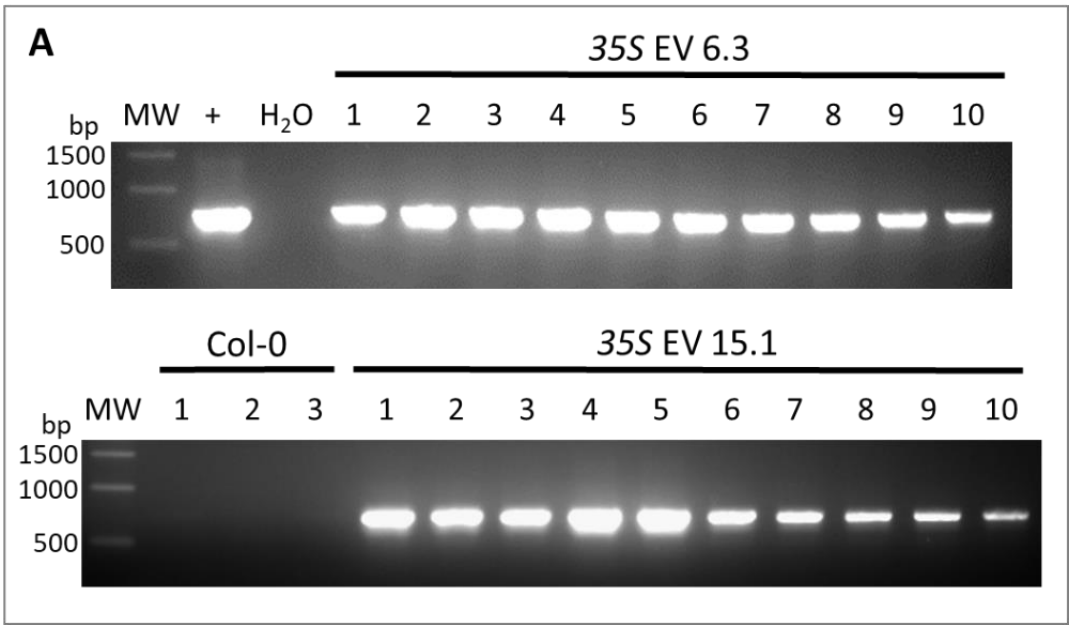

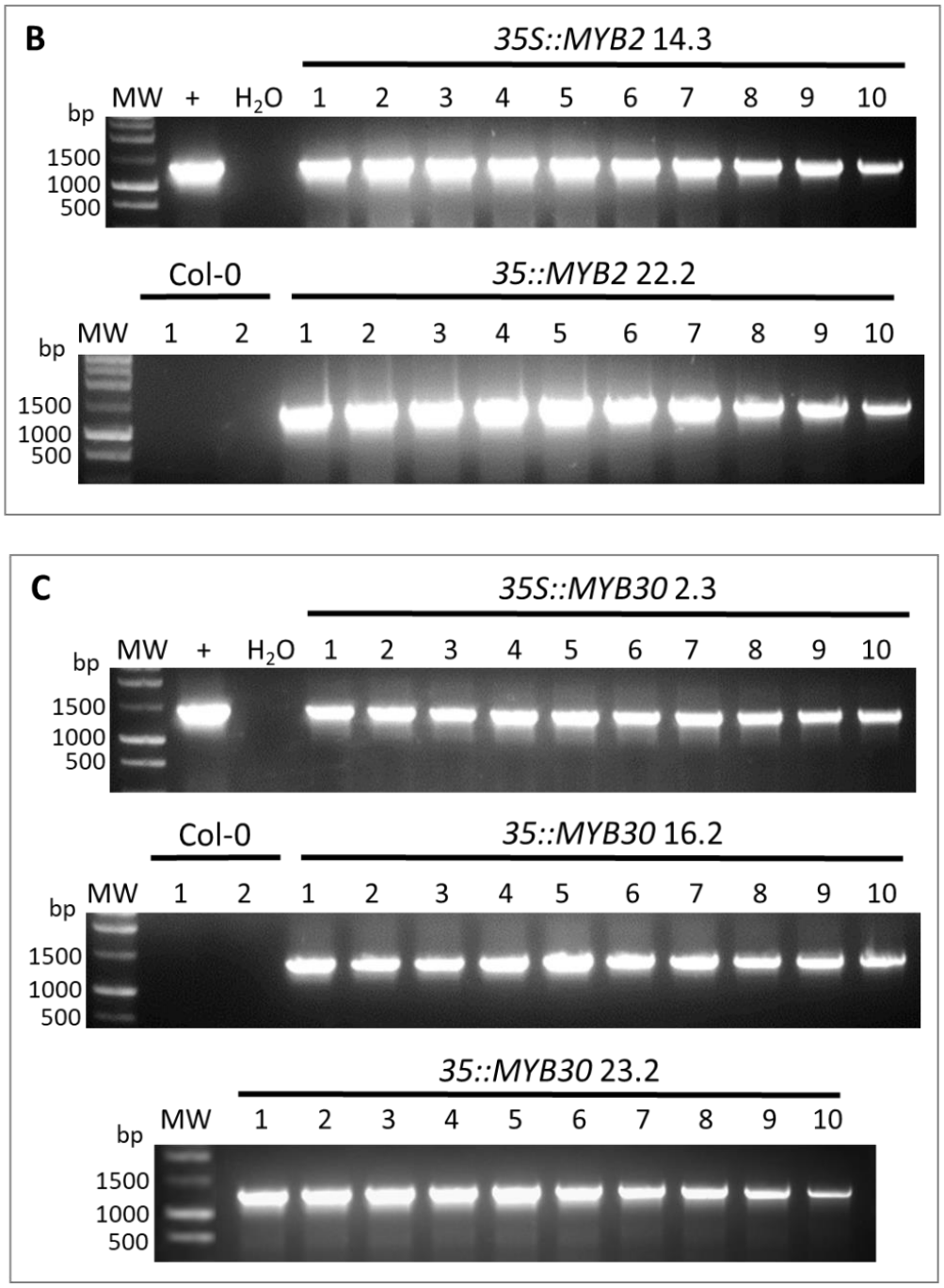

Figure 2.9: PCR confirmation of EV, *35S::AtMYB2* and *35S::AtMYB30* homozygosity in the T3 generation

A PCR was performed on DNA extracted from ten seedlings grown on PN plates used for screening T3 lines that were potentially homozygous for each genotype. **A:** The two EV lines were evaluated using the *Bar* primer pair with an expected amplicon size of 733 bp with pB2GW7-*AtMYB2* plasmid DNA as the positive control (+). **B:** The two *35S::AtMYB2* lines were evaluated using the P35S forward primer and *AtMYB2* attB2 reverse primer with an expected amplicon size of 1300 bp with pB2GW7-*AtMYB2* plasmid DNA as the positive control (+). **C:** The three *35S::AtMYB30* lines were evaluated using the P35S forward primer and *AtMYB30* attB2 reverse primer with an expected amplicon size of 1450 bp

with pB2GW7-*AtMYB30* plasmid DNA as the positive control (+). Col-0 WT DNA and a no template H_2O PCR reaction were used as negative controls in all PCRs. The MW marker included is the New England Biolabs Quick-Load® 1 kb DNA ladder.

To be sure that these lines were indeed homozygous, another set of T3 seeds were screened on GFSA selection plates as before, with the same results observed where none of the lines had any GFSA-induced bleaching or death (data not shown). Unfortunately, all seed of *35S::AtMYB30* line 2.3 had been lost and as a result, the homozygous sibling 2.1 was used for analysis. Ten seedlings were again harvested from a single PN control plate for PCR analysis with the same results observed as in figure 2.9 above. Additionally, the remaining tissue from each PN plate was pooled and harvested for RNA extraction and subsequent cDNA synthesis, and RT-qPCR gene expression analysis was performed to determine the variation in expression in each line. The calculated concentrations of *AtMYB2* and *AtMYB30* respectively were normalised to the *AtMON1* reference gene.

Figure 2.10A shows that there was no significant variation in expression of *AtMYB2* for each OE line, and that both of the *35S::AtMYB2* homozygous OE lines analysed showed significantly higher *AtMYB2* expression than the EV lines which had virtually no *AtMYB2* expression. This equated to around a 230-fold increase in both OE lines.

Figure 2.10B shows that there was significant variation between *35S::AtMYB30* lines 16.2 and 23.2 with the former having the significantly higher *AtMYB30* expression, and that both *35S::AtMYB30* lines had significantly higher *AtMYB30* expression than the EV lines. Line 16.2 showed a fold change of 4.6 while line 23.2 only had a 2.6-fold increase in *AtMYB30* expression compared to the EV lines. Figure 2.10C shows that expression of *AtMYB30* was even higher in the OE line 2.1, as expected according to figure 2.8B, with a fold change of expression of 8.7 compared to EV.

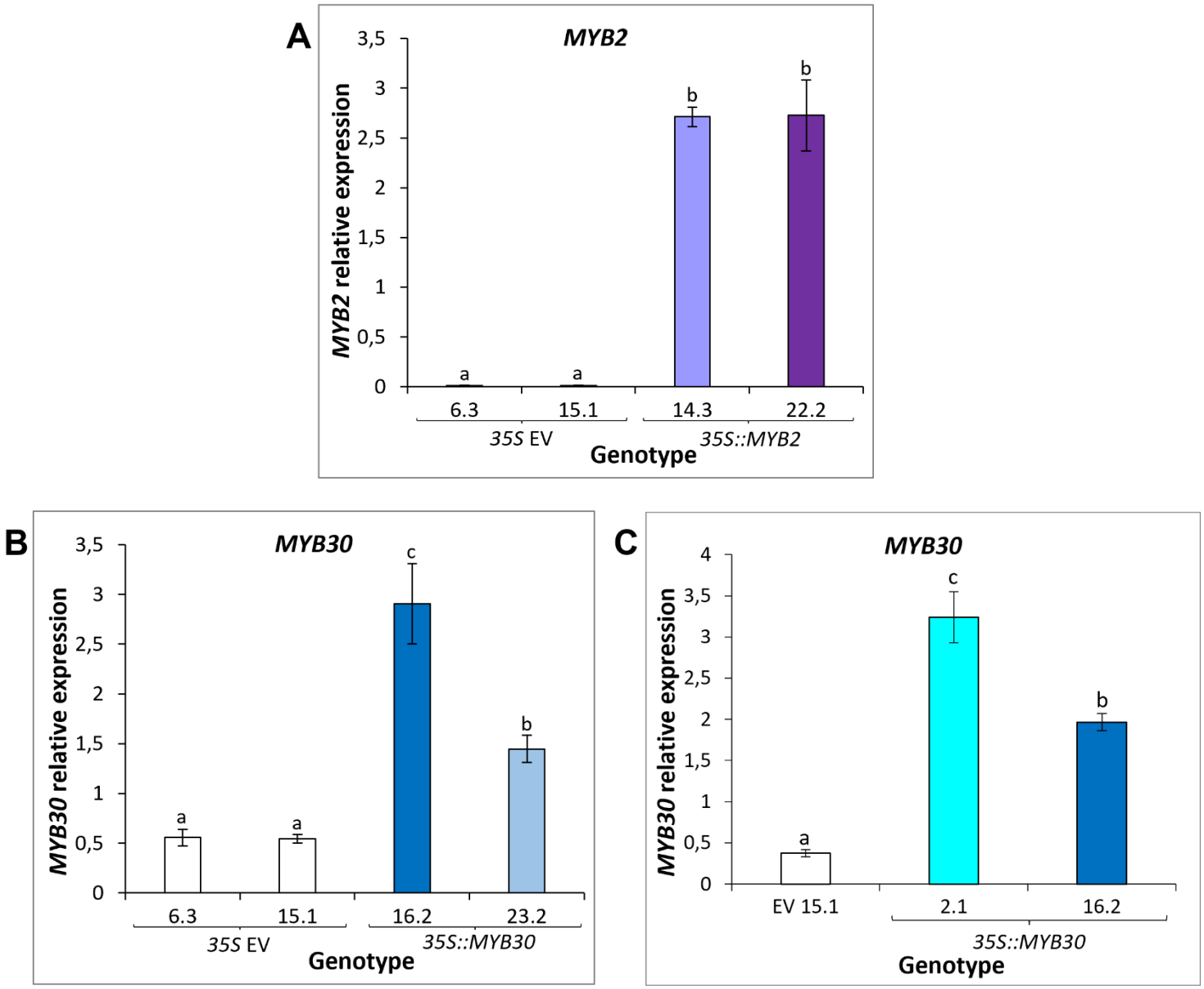

Figure 2.10: *AtMYB2* and *AtMYB30* gene expression in homozygous T3 seedlings

Arabidopsis seedlings were grown on PN-agar for 11 days. Tissue was harvested and pooled for RNA extraction and cDNA was synthesised for RT-qPCR gene expression analysis. The results are an average of three pools of tissue (n=3). Expression of *AtMYB2* (**A**) and *AtMYB30* (**B and C)** is shown relative to the *AtMON1* reference gene. Panels **B** and **C** show different *35S::AtMYB30* lines. Error bars indicate standard error. Different letters on the graphs indicate significant differences ($p \leq 0.05$) in mean values as determined by a one-way ANOVA with Fisher LSD post-hoc analysis.

2.3.3. Functional characterisation of *AtMYB30*

2.3.3.1. Validation of T-DNA insertion *atmyb30* mutant lines

The Salk Institute Genomic Analysis Laboratory (SIGnAL) T-DNA Express database (http://signal.salk.edu/cgi-bin/tdnaexpress) was used to identify lines with T-DNA insertions within the *AtMYB30* gene sequences. Plant lines GABI-KAT 022F04 (*atmyb30-1*/*myb30-1*) and SALK_027644C (*atmyb30-2*/*myb30-2*) were chosen for further analysis as they had both previously been characterised by other researchers who had confirmed their homozygosity and kindly provided them to us (Raffaele, Rivas & Roby, 2006; Li et al., 2009). The T-DNA insertion in the *atmyb30-1* line is located 10 bases into the second intron and for *atmyb30-2* it is in the 5' untranslated region (UTR) of *AtMYB30*, 10 bases upstream of the start codon (figure 2.11). These insertion sites have been confirmed using PCR analysis and sequencing (Raffaele, Rivas & Roby, 2006; Li et al., 2009).

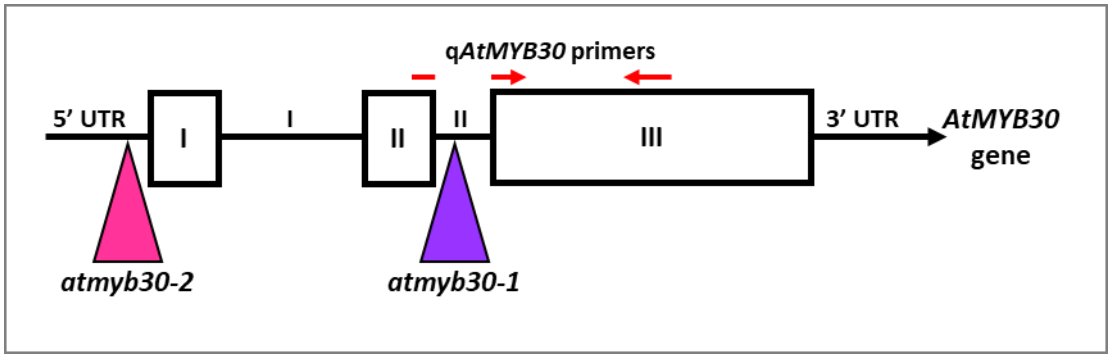

Figure 2.11: Sites of T-DNA insertion in the *atmyb30-1* and *atmyb30-2* lines

The T-DNA insertion for *atmyb30-1* (purple triangle) is 10 bp into the second intron. The T-DNA insertion for *atmyb30-2* (pink triangle) is 10 bp upstream of the *AtMYB30* start codon, in the 5' UTR. Exons, as annotated by TAIR, are depicted by black boxes, whereas UTR/introns are depicted as black lines. The red arrows represent the q*AtMYB30* primer set.

To confirm that the *atmyb30-1* and *atmyb30-2* lines obtained were indeed mutants with knocked-out expression of *AtMYB30*, two different methods were used. Firstly, 50 seeds from each line, as well as Col-0 as a control (as these lines were generated in the Col-0 background), were grown on PN-agar plates. After two weeks, seedlings from each plate were pooled for

RNA extraction and subsequent cDNA synthesis. An end-point PCR using primers which amplified the full-length *AtMYB30* coding sequence (*AtMYB30* FL F and R) was performed and showed no amplification in the *atmyb30-1* and *atmyb30-2* mutants (figure 2.12A) whereas there was amplification of the *AtMYB30* sequence in the Col-0 control, as expected. A PCR using the *AtMON1* reference gene primers was used to confirm the integrity of the cDNA and shows a band for each of the samples, confirming that the lack of a product in the *AtMYB30* PCR is not due to poor RNA quality or inadequate cDNA synthesis (figure 2.12B).

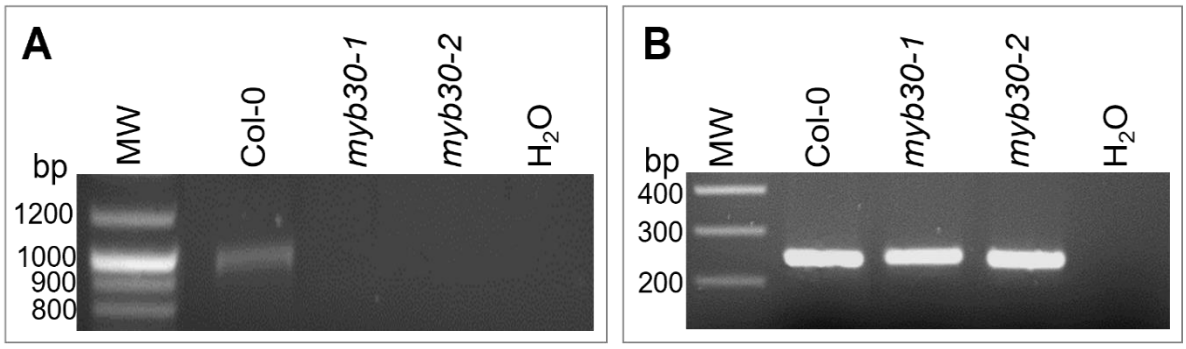

Figure 2.12: A PCR confirming that there is no full-length *AtMYB30* expression in the *atmyb30-1* and *atmyb30-2* lines

A: PCR was performed on cDNA from Col-0, *atmyb30-1* and *atmyb30-2* using *AtMYB30* full-length gene primers (*AtMYB30* FL F and R) with an expected amplicon size of 972 bp. **B:** PCR was performed on the same samples using the *AtMON1* reference gene primers, with an expected amplicon size of 244 bp, confirming integrity of the cDNA. H_2O was used as the template in the negative control reactions. The MW marker is the New England Biolabs Quick-Load® 100 bp DNA ladder.

A quantitative RT-qPCR experiment was also conducted using the q*AtMYB30* F and R primers to confirm that no *AtMYB30* mRNA was being produced in the two mutant lines. This forward primer spans across the end of exon 2 and the beginning of exon 3 and the reverse primer binds in exon 3 (figure 2.11). As can be seen in figure 2.13, there is a negligible amount of *AtMYB30* mRNA in both T-DNA mutant lines, as expected. These values calculated to a fold change reduction relative to Col-0 of 250- and 52.6-fold respectively for *atmyb30-1* and *atmyb30*-2, indicating that these lines are indeed null mutants. Therefore, both lines were taken forward for phenotypic characterization.

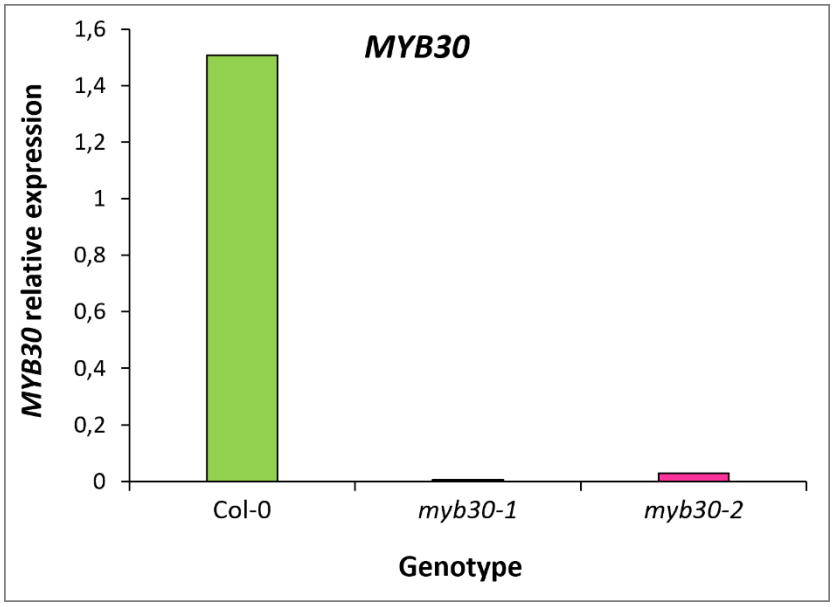

Figure 2.13: Analysis of *AtMYB30* expression in the *atmyb30-1* and *atmyb30-2* lines

Seeds from each Arabidopsis line were grown on PN-agar plates and after two weeks seedlings from each line were pooled for RNA extraction, cDNA synthesis and RT-qPCR analysis. qPCR was performed on the cDNA from Col-0, *atmyb30-1* and *atmyb30-2* pooled samples. These results show *AtMYB30* expression relative to the *AtMON1* reference gene. As there was only one pooled sample per genotype, no statistical analysis was performed.

2.3.3.2. Phenotypic characterisation of *35S::AtMYB30* and *atmyb30* lines

2.3.3.2.1. Growth of 35S::AtMYB30 plants exposed to saline conditions early in development

To determine whether overexpressing *AtMYB30* had an impact on plant growth in in saline conditions, *35S* EV and *35S::AtMYB30* plants were germinated and grown for two weeks on petri dishes containing PN-agar (control) and PN-agar supplemented with different concentrations of NaCl or iso-osmolar concentrations of sorbitol. Initially, the *35S::AtMYB30* lines 16.2 and 23.2 were used. The average mass per plant of the three lines was compared for each treatment to identify any phenotypic differences in their growth.

Figure 2.14A shows that the biomass production of all three plant lines decreased significantly in all NaCl and sorbitol treatments (except 50 mM NaCl), in a dose-dependent manner, compared to the untreated control for each line – as expected. Additionally, the

35S::AtMYB30 lines appeared to have significantly lower average plant mass than the EV line under untreated conditions and low concentrations of NaCl and sorbitol.

To account for the difference in the average plant mass between the lines in untreated conditions, the mass per plant was plotted relative to the untreated control for each line and the data is shown in figure 2.14B. Here, it is evident that the *AtMYB30* OE lines were significantly more tolerant of salinity stress as they both experienced a reduced loss in plant mass compared to the EV line. This can be clearly seen in figure 2.14C where under saline conditions the rate of biomass decrease is significantly less in both OE lines compared to the EV, as indicated by the gradient of the slope. There were no significant differences between the EV line and the OE lines under sorbitol conditions.

Additionally, *35::AtMYB30* line 2.1 was phenotyped only under saline conditions, and, as in figure 2.14B, no phenotype was observed for either OE line in sorbitol. Appendix figure 6.4 shows that the results were consistent with those seen in figure 2.14. Overall, this data indicates that higher levels of *AtMYB30* expression may correspond with an enhanced salinity tolerance due to less inhibition of growth under saline conditions.

A

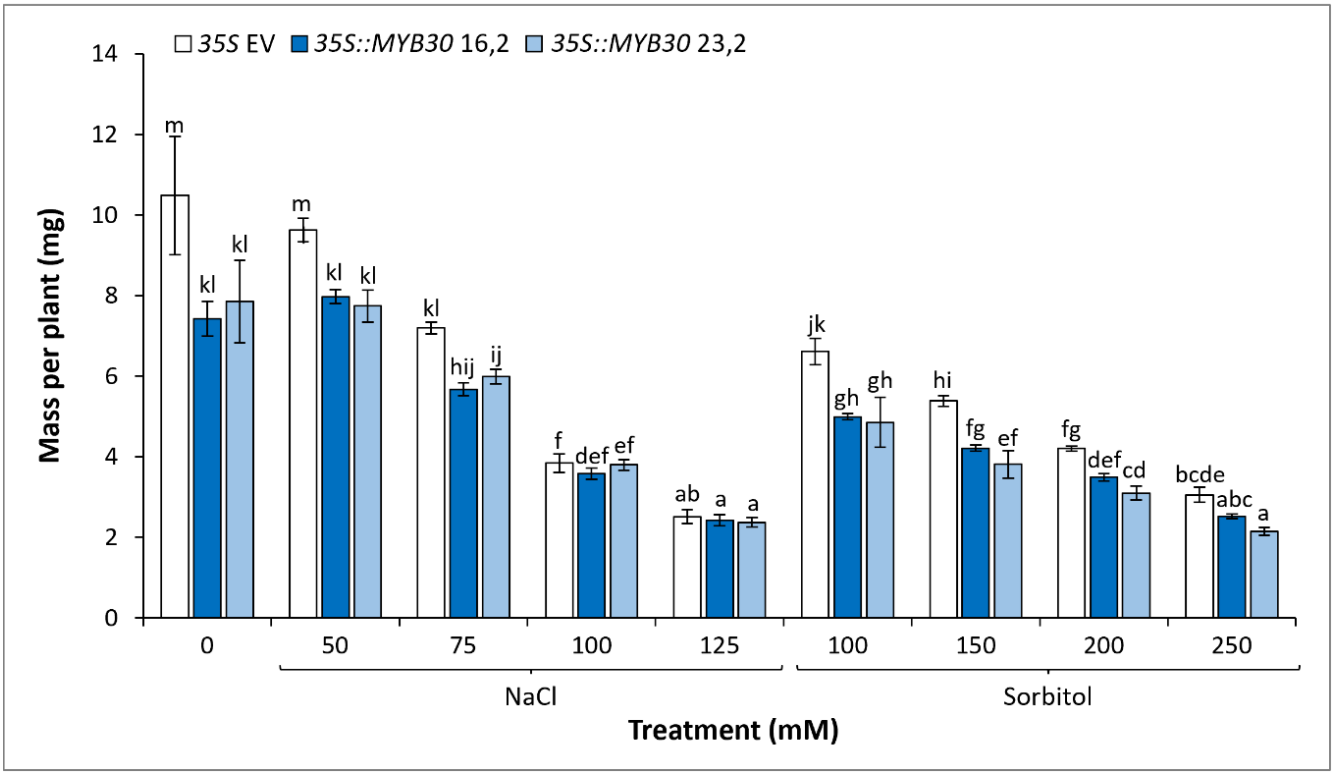

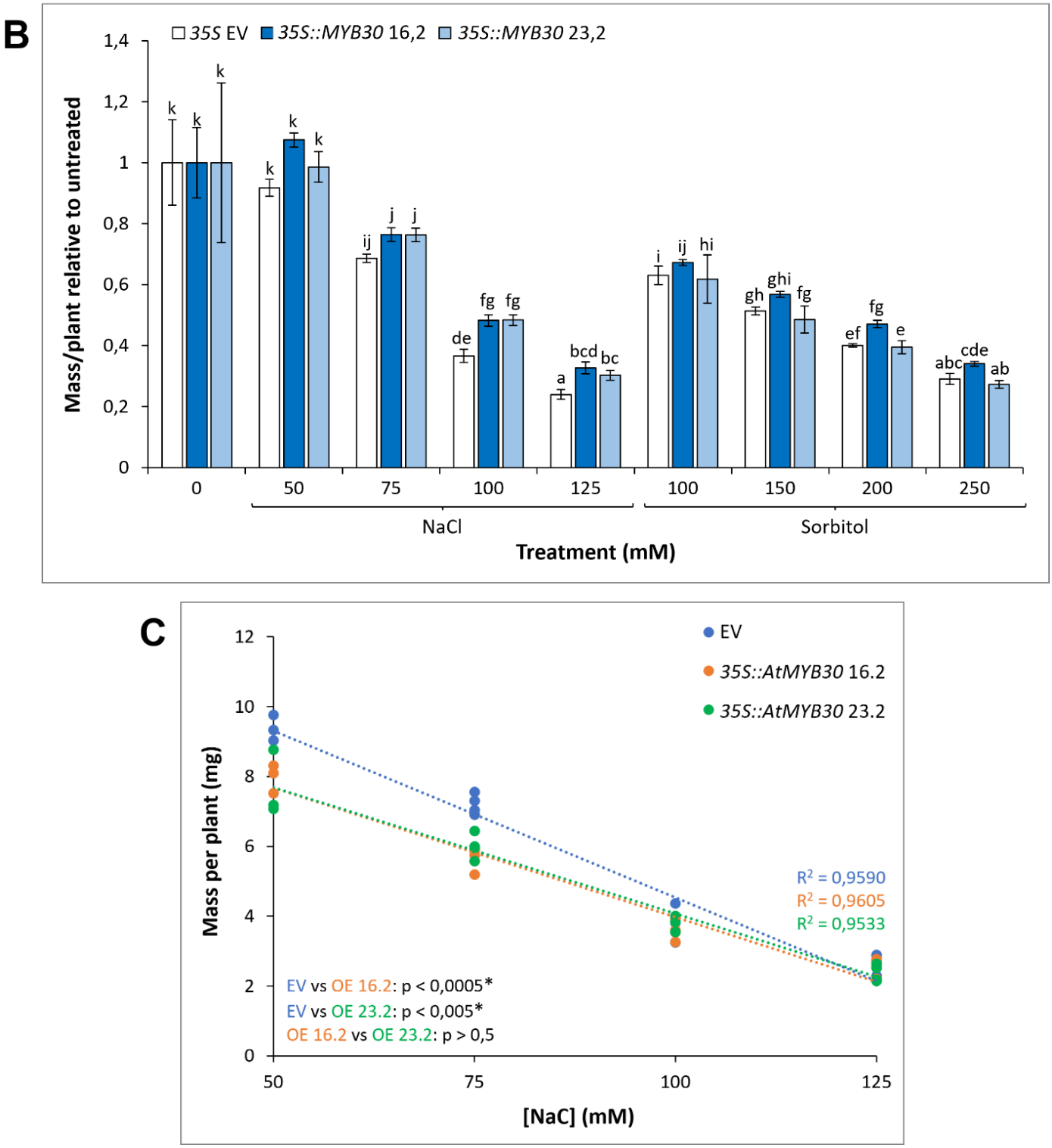

Figure 2.14: Growth of *35S::AtMYB30* plants exposed to saline conditions early in development

The EV and *35S::AtMYB30* plants were germinated and grown for two weeks on petri dishes containing untreated PN-agar (control) and PN-agar supplemented with the indicated concentrations of NaCl and sorbitol. **A:** The average mass per plant of each line. **B:** The average mass per plant plotted relative to the control (0 mM) for each line. Error bars indicate standard error. Different letters on the graphs

indicate significant differences ($p \leq 0.05$) in mean values as determined by a one-way ANOVA with Fisher LSD post-hoc analysis. **C:** The mass per plant is plotted as a regression analysis for NaCl conditions. The results show four replicates for each treatment with 50 seeds sown per plate (n=4). The experiment was repeated three times with comparable results. Each slope was compared statistically to one another to determine any significant differences and the results are shown in the bottom left corner with an asterisk indicating statistical significance.

2.3.3.2.2. Growth of *atmyb30* plants exposed to saline conditions early in development

To determine what impact knocking out *AtMYB30* has on salinity tolerance, Col-0 and the *atmyb30* mutant lines were phenotyped under saline conditions.

Figure 2.15A shows that the average mass per plant decreases significantly with each increasing NaCl or sorbitol treatment for each line respectively, indicating that both stresses impose a dose-dependent inhibition on plant growth, as expected. The average mass per plant of both *atmyb30* mutant lines was comparable under most treatment conditions and these mutant lines had significantly lower average plant mass than the WT Col-0 line under almost all treatment conditions.

When the differences in average plant mass in untreated conditions were considered by plotting each genotype relative to its untreated control (figure 2.15B), growth of the *atmyb30-2* mutant does appear to be more inhibited by salt as the average mass per plant is significantly lower than the WT lines in all NaCl concentrations. This is not specific to salt, however, as the average plant mass relative to untreated is also significantly lower in the *atmyb30-2* line in 150, 200 and 250 mM sorbitol treatments. The same is not true for *atmyb30-1* as there was no significant difference to WT.

Overall, the *atmyb30* lines showed that knock down of *AtMYB30* resulted in significantly smaller seedlings under all conditions, and a greater degree of growth inhibition under saline conditions than WT (only in *atmyb30-2*). Despite this being a weak phenotype, this data supports our hypothesis that *AtMYB30* might play a role in the plant response to salinity stress.

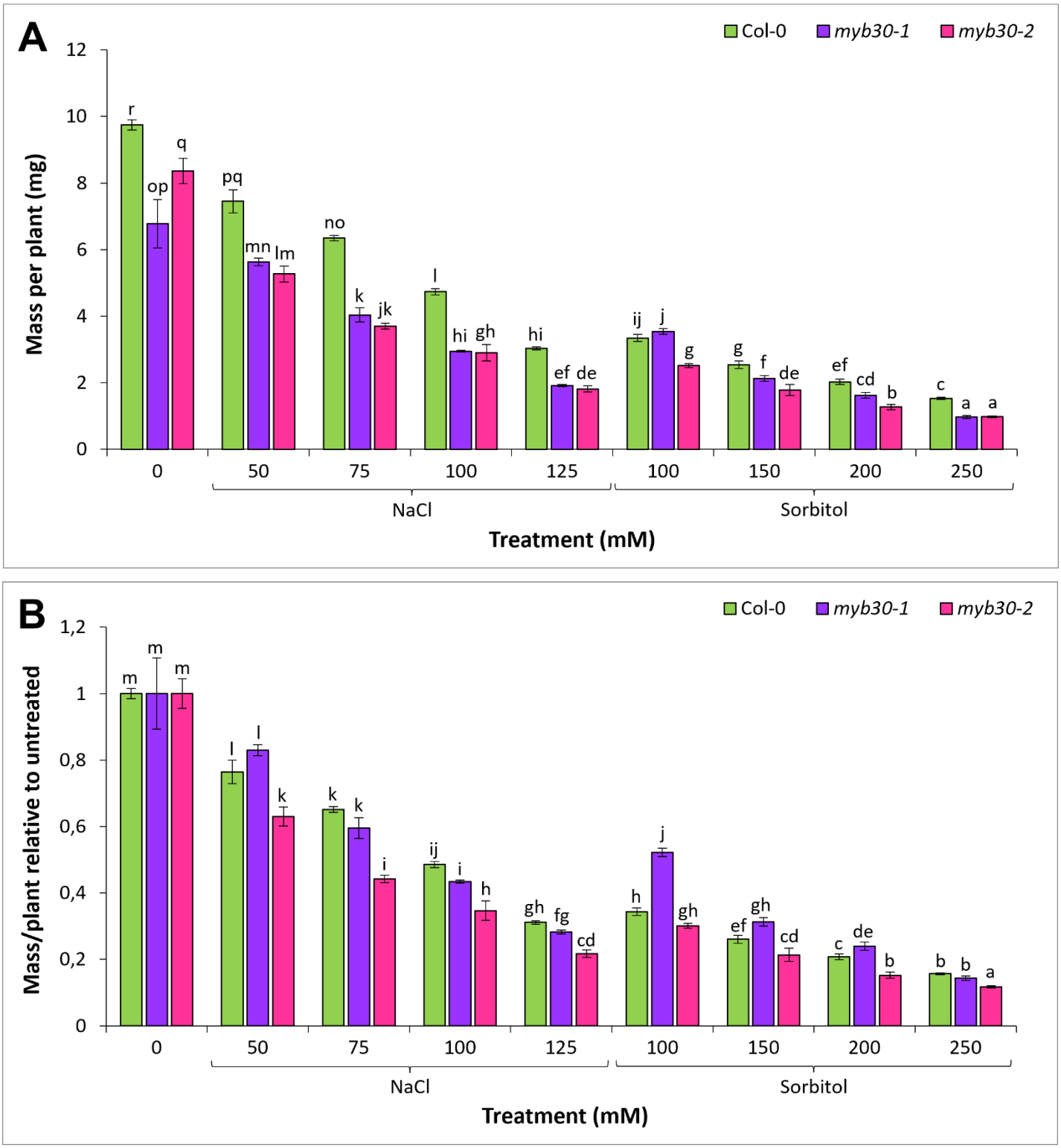

Figure 2.15: Growth of *atmyb30* plants exposed to saline conditions early in development

Arabidopsis seedlings were germinated and grown for two weeks on petri dishes containing untreated PN-agar (control) and PN-agar supplemented with the indicated concentrations of NaCl and sorbitol. **A:** The average mass per plant. **B:** The average mass per plant plotted relative to the control (0 mM) for each line. The results are an average of four replicates for each treatment with 50 seeds sown per plate (n=4). The experiment was repeated three times with comparable results. Error bars indicate

standard error. Different letters on the graphs indicate significant differences ($p \leq 0.05$) in mean values as determined by a one-way ANOVA with Fisher LSD post-hoc analysis.

2.3.3.2.3. Growth of 35S::AtMYB30 and atmyb30 plants exposed to saline conditions later in development

Since the plant response to salt is different at different developmental stages, *35S* EV 15.1, *35S::AtMYB30* 2.1, *35S::AtMYB30* 16.2 and *myb30-2* plants were phenotyped under saline conditions later in development in order to determine whether the altered salt tolerance seen in *AtMYB30* mis-expressing plants is developmental stage specific. Plants were grown hydroponically in ¼ strength PN media for three weeks, then transferred onto ¼ strength PN media supplemented with or without 75 mM NaCl for a further week. The *35S* EV line was used as the WT control for both the *35S::AtMYB30* and *atmyb30-2* lines. At the end of the experimental period, the shoot and root mass of each plant was recorded to determine the average per plant for each line in each treatment.

Figure 2.16A shows that the average shoot mass was significantly lower in all genotypes in 75 mM NaCl compared to untreated conditions, as expected. The only line that showed any significant difference was the *35S::AtMYB30* 2.1 line which had a significantly lower average shoot mass than the other genotypes in both the untreated and saline conditions. When plotting the average shoot mass relative to the untreated control for each genotype respectively (figure 2.16B), there was no significant difference between either OE line, *myb30-2,* and the EV control under saline conditions, indicating that mis-expression of *AtMYB30* does not have a significant impact on shoot salt tolerance of older plants grown in 75 mM NaCl.

Figure 2.16C shows that the average root mass was significantly lower in all genotypes in 75 mM NaCl compared to untreated conditions, as expected. Again, *35S::AtMYB30* line 2.1 had a significantly lower average root mass than the other genotypes in both the untreated and saline conditions. Considering the relative data, figure 2.16D shows that the only line with a change in salt-induced inhibition of root mass was *AtMYB30* OE line 16.2 as it had a significantly lower average root mass relative to untreated in 75 mM NaCl compared to the EV line.

Overall, there was no consistent effect of *AtMYB30* mis-expression on plant growth in saline conditions later in development. This contrasted with the data seen early in development (figures 2.14 and 2.15), indicating that *AtMYB30* might play different roles in salinity tolerance at different developmental stages in Arabidopsis.

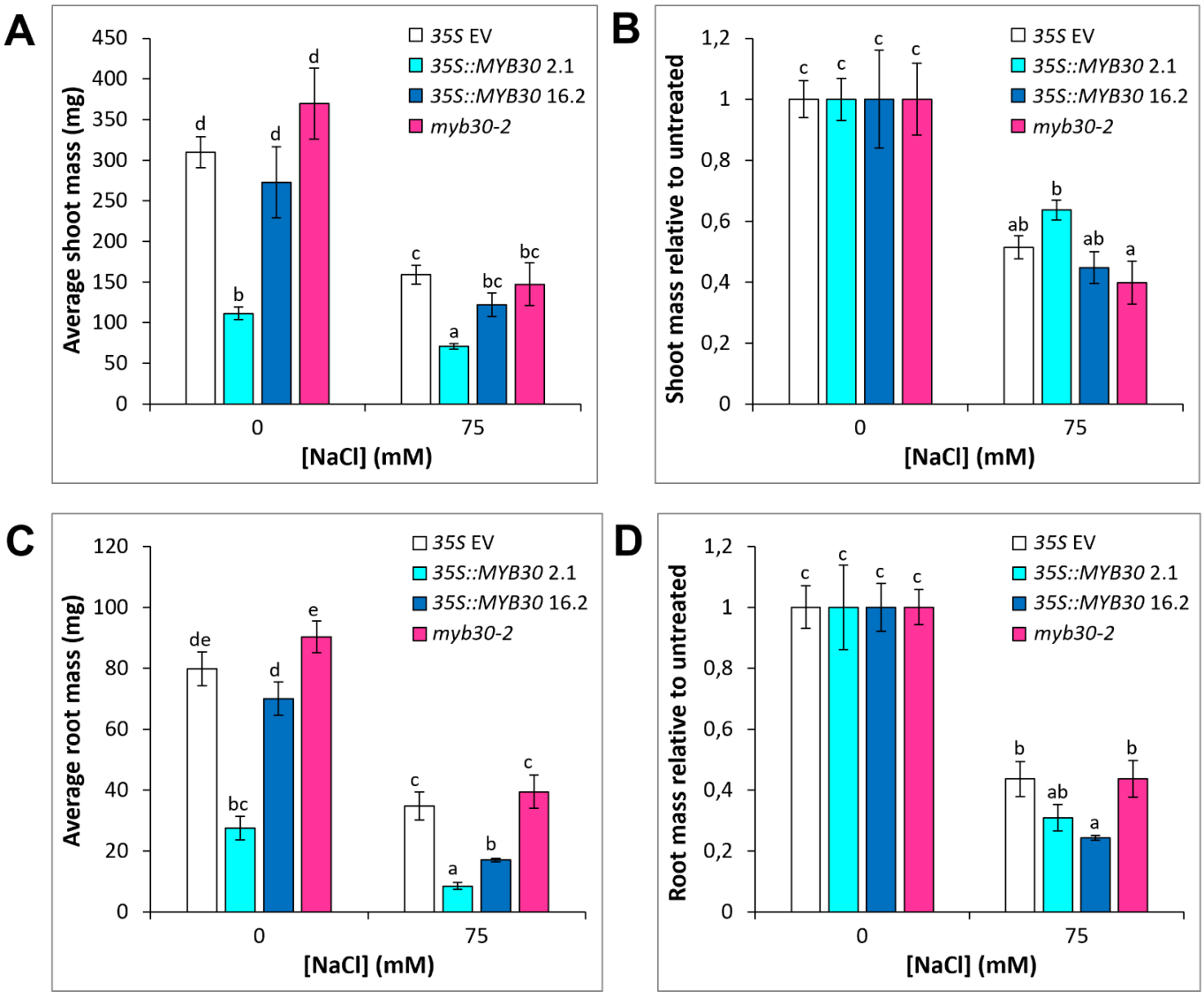

Figure 2.16: The average shoot and root mass of EV, *35S::AtMYB30* and *myb30-2* plants after one week of salt treatment later in development

The *35S* EV, *35S::AtMYB30* and *atmyb30* plants were grown hydroponically in ¼ strength PN media without salt stress for three weeks. Plants were then transferred onto PN media supplemented with 0 or 75 mM NaCl and grown under saline conditions for a further week. **A:** The average shoot mass per plant. **B:** The average shoot mass plotted relative to the control (0 mM) for each genotype. **C:** The average root mass per plant. **D:** The average root mass plotted relative to untreated for each

genotype. The results are an average of five plants for each treatment for the EV and *myb30-1* genotypes, and four plants/treatment for the *35S::AtMYB30* lines (n≥4). Error bars indicate standard error. Different letters on the graphs indicate significant differences ($p \leq 0.05$) in mean values as determined by a one-way ANOVA with Fisher LSD post-hoc analysis.

2.3.3.2.4. *AtNit2 g*ene expression analysis in *35S::AtMYB30* and *atmyb30* plants

To determine whether mis-expressing *AtMYB30* is accompanied with changes in *AtNit2* levels, tissue was collected from the 0 and 100 mM NaCl plates from the experiments reported previously (section 2.3.3.2.1 and 2.3.3.2.2) and RT-qPCR gene expression analysis was performed.

Figure 2.17A shows that *AtNit2* expression was significantly higher in all genotypes under saline conditions compared to untreated control conditions, as expected. Both of the *AtMYB30* OE lines had a significantly higher *AtNit2* expression in untreated conditions compared to EV. This was mimicked in saline conditions, although this difference was not significant for *AtMYB30* OE line 2.1.

Figure 2.17B shows that there was no significant differences in *AtNit2* expression between Col-0 and the *atmyb30* KO lines under control conditions, but both KO lines had significantly higher *AtNit2* expression under saline conditions compared to Col-0.

Overall, this data indicates that altering *AtMYB30* expression does lead to changes in *AtNit2* expression, although *AtMYB30* mis-expression does not directly correlate with these changes, indicating that *AtMYB30* alone is not responsible for regulating *AtNit2* gene expression.

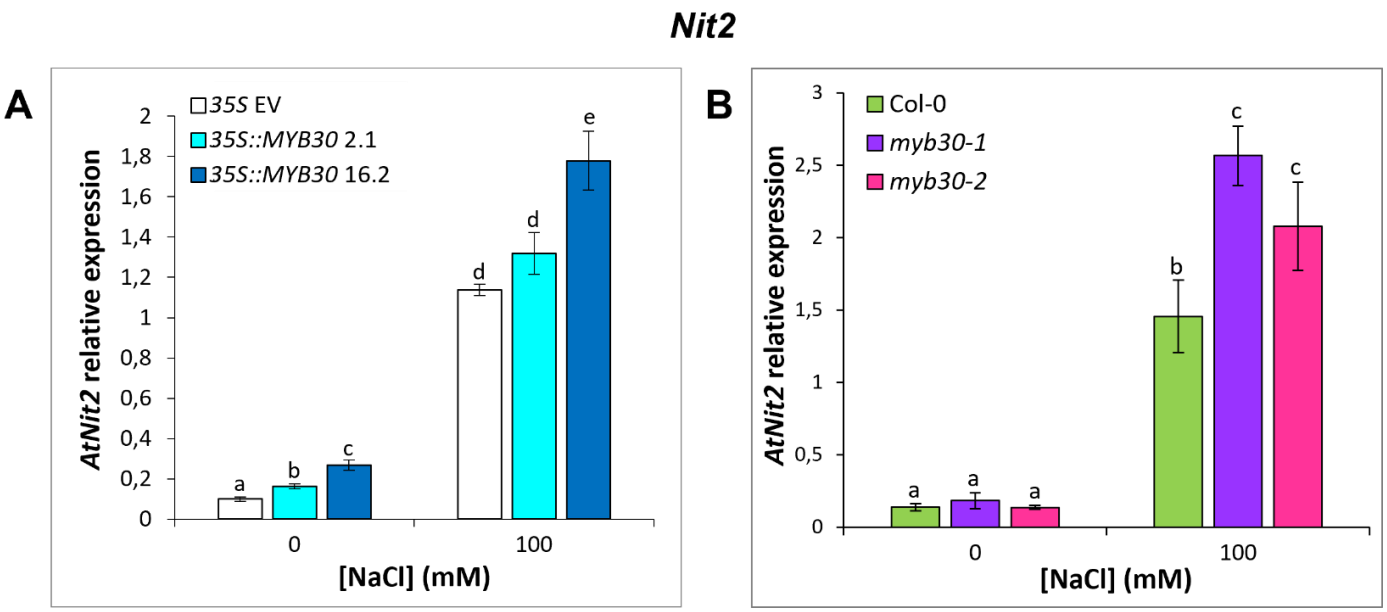

Figure 2.17: Expression of *AtNit2* in *35S::AtMYB30* and *atmyb30* lines under saline conditions

Arabidopsis seedlings were grown on PN-agar or PN-agar supplemented with 100 mM NaCl for two weeks. Tissue was harvested and pooled for RNA extraction and cDNA was synthesised for RT-qPCR gene expression analysis. The results are an average of three pools of tissue (n=3) for the **A:** *35S::AtMYB30* lines, and **B:** *atmyb30* lines. Expression of *AtNit2* is shown relative to the *AtMON1* reference gene. Error bars indicate standard error. Different letters on the graphs indicate significant differences ($p \leq 0.05$) in mean values as determined by a one-way ANOVA with Fisher LSD post-hoc analysis.

2.3.4. Functional characterisation of *AtMYB2*

2.3.4.1. Growth of *35S::AtMYB30* plants early in development under saline conditions

To determine whether overexpressing *AtMYB2* had an impact on plant growth in salt early in development, *35S* EV and *35S::AtMYB2* plants were germinated and grown for two weeks on petri dishes containing untreated PN-agar (control) and PN-agar supplemented with differing concentrations of NaCl or iso-osmolar concentrations of sorbitol. The average mass/plant of the EV and two *AtMYB2* OE lines was compared for each treatment to identify any phenotypic differences in their growth.

Figure 2.18 shows that increasing NaCl and sorbitol concentrations inhibits plant growth, as expected. However, there are no significant differences observed between the average plant

mass in any treatments between the genotypes, except in 50 mM NaCl where *35S::AtMYB2* line 14.3 has a significantly lower average mass/plant than EV. This experiment was repeated three times, with comparable results, showing no significant differences in average plant mass between the genotypes. This indicates that overexpressing *AtMYB2* in Arabidopsis does not lead to any biomass changes early in development in response to saline conditions.

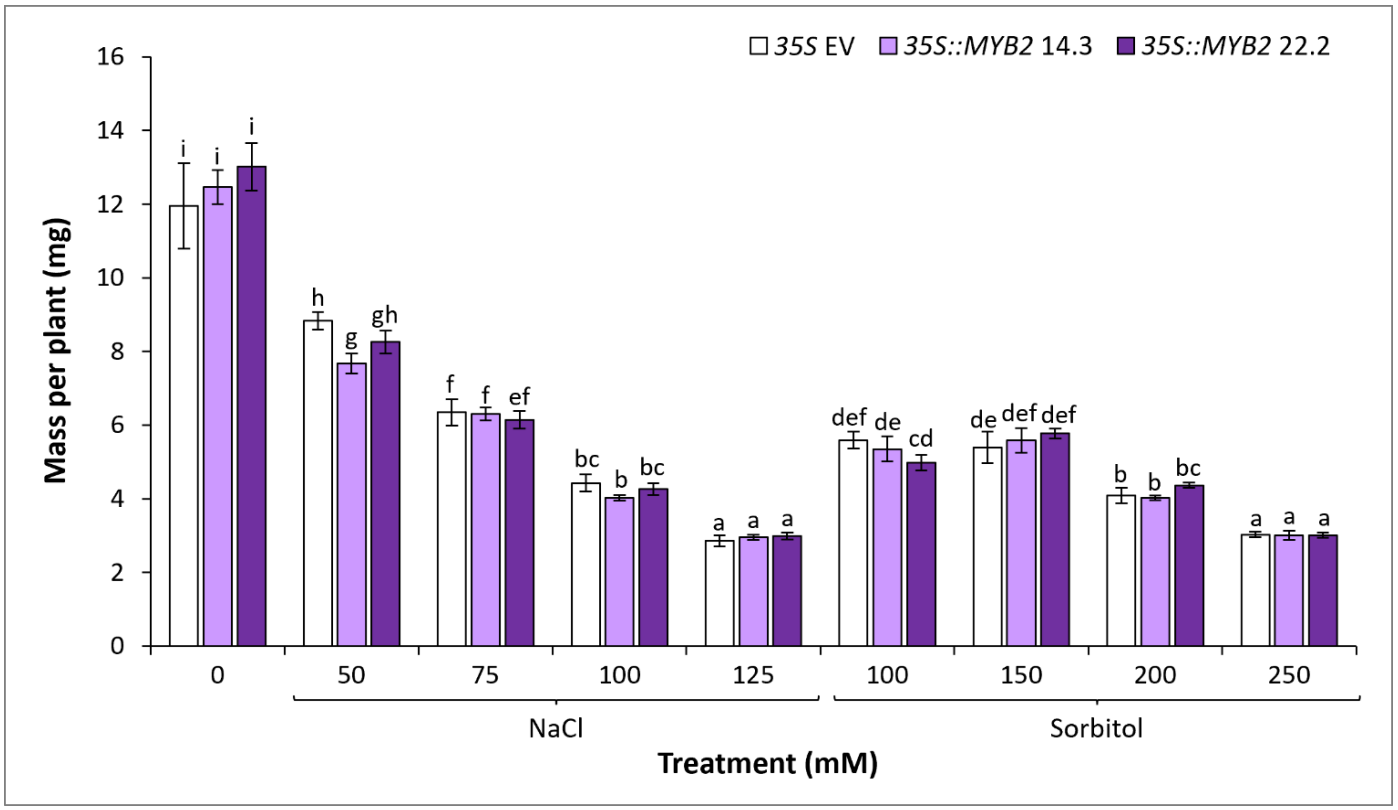

Figure 2.18: Growth of *35S::AtMYB2* plants exposed to saline conditions early in development

The EV and *35S::AtMYB2* plants were germinated and grown for two weeks in petri dishes containing untreated PN-agar (control) and PN-agar supplemented with the indicated concentrations of NaCl and sorbitol. The average mass per plant of the *35S* EV line and *35S::AtMYB2* lines 14.3 and 22.2 are plotted as an average of four replicates for each treatment with 50 seeds sown per plate (n=4). The experiment was repeated three times with comparable results. Error bars indicate standard error. Different letters on the graphs indicate significant differences ($p \leq 0.05$) in mean values as determined by a one-way ANOVA with Fisher LSD post-hoc analysis.

2.3.4.2. *AtNit2 g*ene expression analysis in *35S::AtMYB2* plants

To determine whether overexpressing *AtMYB2* resulted in any change in *AtNit2* gene expression in untreated conditions, RT-qPCR gene expression analysis was conducted. As can be seen in figure 2.19, there was no significant differences between either of the *35S::AtMYB2* lines and EV.

As no change in *AtNit2* gene expression was observed in *AtMYB2* OE lines, and no growth phenotype was observed when exposed to saline conditions early in development. These lines were not further characterised. Additionally, no *atmyb2* KO lines were phenotyped in this project for the same reasons.

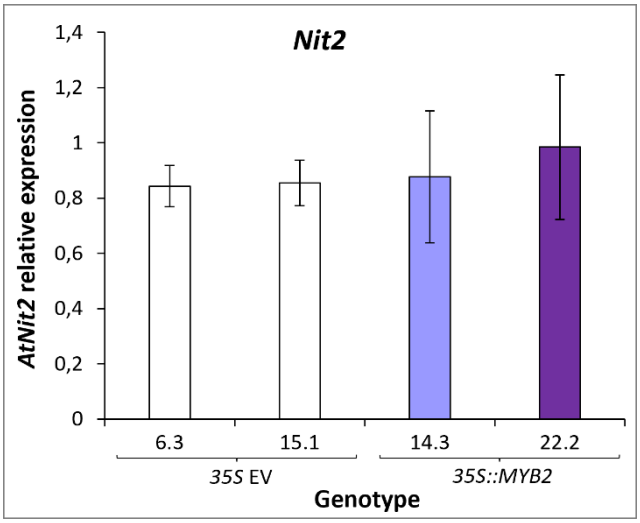

Figure 2.19: *AtNit2* gene expression in homozygous *35S::AtMYB2* lines

Arabidopsis seedlings were grown on PN-agar for 11 days. Tissue was harvested and pooled for RNA extraction and cDNA was synthesised for RT-qPCR gene expression analysis. The results are an average of three pools of tissue (n=3). Expression of *AtNit2* is shown relative to the *AtMON1* reference gene. Error bars indicate standard error. Different letters on the graphs indicate significant differences ($p \leq 0.05$) in mean values as determined by a one-way ANOVA with Fisher LSD post-hoc analysis.

2.4. DISCUSSION

2.4.1. AtMYB2 and AtMYB30 were identified as transcription factor candidates

As a first approach to identify candidate TFs that could be involved in regulating auxin biosynthesis via *AtNit2*, bioinformatics analyses identified TFBS present in the 1 kb upstream of the *AtNit2* ATG translation start site (table 2.2). Interestingly, five of the TFBS identified were MYB binding sites (figure 2.1 , appendix figure 6.2). When looking at the list of TFs upregulated ≥ 2-fold under saline conditions alongside *AtNit2* in the early development microarray (appendix table 6.1), two MYB TFs were identified, *AtMYB2* and *AtMYB30.* Additionally, *AtMYB30* was included in the list of salt-specific genes with the enriched GO term "response to auxin stimulus" in the microarray (Cackett et al., 2022). The microarray data for these TFs in figure 2.2 shows that they were induced in response to NaCl. Unfortunately, only *AtMYB2* expression in 125 mM NaCl was validated by qPCR (figure 2.2B). As this data came from two different experimental set ups (i.e., not the same RNA), this could be due to a number of reasons such as differences in the conditions that the plants were grown under (different lights, different growth chambers, etc), differences in the Col-0 seed stocks, and different times of day that the tissue was harvested.

Both *AtMYB2* and *AtMYB30* have previously been found to play a role in abiotic stress responses. Urao et al. (1993) showed that *AtMYB2* expression was induced by short-term treatment of 250 mM NaCl over a 24 hour period. Furthermore, MYB2 has been shown to regulate expression of salt- and dehydration-responsive genes in Arabidopsis, such as the proline biosynthetic enzyme *P5CS1* (Δ^1-pyrroline-5-carboxylate synthase 1), which confers salt tolerance by facilitating proline accumulation (Yoo et al., 2005). *AtMYB2* has also been shown to play an important role in ABA-dependent gene expression under drought and salt stress by activating transcription of RESPONSIVE TO DESICCATION 22 (*RD22*), an important dehydration-responsive gene (Abe et al., 2003). Recently, MYB30 has been shown to participate in salt tolerance in Arabidopsis following SUMOylation by the small ubiquitin-like modifier E3 ligase SIZ1. These researchers determined that once SUMOlyated, MYB30 is able to bind to the promoter of *AOX1a* (*alternative oxidase 1a*; involved in alternative respiration and cellular redox homeostasis) and upregulate its expression in response to salt stress (Gong et al., 2020). Furthermore, AtMYB30 has been previously linked to auxin in plants. Li et al. (2009) showed that MYB30 can directly interact with BES1 and increase induction of *SAUR15*

expression (one of the “response to auxin” genes from the early development microarray analysis) and other genes induced by brassinosteroids, plant hormones which work together with auxin to promote cell expansion and elongation (Nemhauser, Mockler & Chory, 2004; Walcher & Nemhauser, 2012). Altogether, these results led us to select MYB2 and MYB30 for characterisation under saline conditions, using a functional genetics approach.

2.4.2. Phenotypic analysis of *atmyb30* and *35S::AtMYB30* plants

2.4.2.1. Altering expression of *AtMYB30* affects plant growth early in development

Overexpression of *AtNit2* in Arabidopsis improves salt tolerance as its growth is less inhibited by saline conditions and it has improved ion homeostasis (Cackett et al., 2022). To determine whether altered *AtMYB30* levels effects *AtNit2* expression and/or salt tolerance, *35S::AtMYB30* and *atmyb30* T-DNA mutant lines were phenotyped. An important factor to consider however is that both the *AtMYB30* KO and OE lines were in the Col-0 background as was the original microarray, but the *AtNit2* OE was in the No-0 background. Different Arabidopsis ecotypes have different salinity tolerances, with Col-0 known to be more salt tolerant than No-0 (Cackett, 2019). This indicates that the salt response in both ecotypes might be slightly different.

An opposite phenotype was observed between the OE lines and a single KO line (*atmyb30-2*) under saline conditions early in development, as would be expected. Figure 2.15 shows that knocked out expression of *AtMYB30* resulted in significantly smaller seedlings under all conditions, which were less salt tolerant – as observed by a greater degree of growth inhibition under saline conditions than WT. However, this phenotype was only observed in the *atmyb30-2* line and not in *atmyb30-1* (figure 2.15B). The reason for the difference in the degree of inhibition between the two KO lines is unlikely to be because of differences in *AtMYB30* expression, as both were validated to be knock-outs (figure 2.13). Therefore, this could be due to one of the lines having an additional T-DNA insertion, possibly causing disruption to another gene and therefore giving a different phenotype. It is known that in the Arabidopsis T-DNA insertion mutant collection, the true number of inserts per line is unknown (O’Malley, Barragan & Ecker, 2015). Therefore, a third *atmyb30* mutant line should be characterised to confirm the salt sensitivity phenotype. Previously, Gong et al. (2020) screened a pool of T-DNA insertion mutants for lines that displayed altered seedling growth

on 125 mM NaCl and identified an *atmyb30* mutant as being salt-sensitive. In this experiment, seeds were germinated and grown in petri dishes on media with or without 125 mM NaCl for 10 days. The *atmyb30* mutant line displayed smaller seedlings with a significantly repressed rate of cotyledon greening by saline conditions compared to WT Col-0. Additionally, they showed that shoot and root growth of the *atmyb30* line was significantly suppressed under saline conditions compared with WT (Gong et al., 2020). This *atmyb30* mutant has a T-DNA insertion within exon one, different to the two mutants used in our analyses, and could therefore be obtained for analysis using our experimental set up.

The *35S::AtMYB30* lines displayed a significantly reduced degree of growth inhibition (i.e., maintained growth better) under saline conditions compared to the EV control (figure 2.14), indicating that they were more salt tolerant and that AtMYB30 could play a role in maintaining plant growth in response to salt stress. Interestingly, the *AtMYB30* OE lines displayed a significantly lower average plant mass compared to the EV under untreated conditions, indicating that overexpression of *AtMYB30* had a detrimental impact on plant growth in untreated environments, but a beneficial role in response to high concentrations of NaCl (figure 2.14). There is precedent for this as there have been numerous examples showing that constitutive expression of genes encoding transcription factors, ion transporters or biosynthetic proteins can lead to undesirable phenotypes, especially under non-stressed conditions (Karakas et al., 1997; Sheveleva et al., 1997; Kasuga et al., 1999; Cortina & Culiáñez-Macià, 2005; Hmida-Sayari et al., 2005; Suárez, Calderón & Iturriaga, 2009), however this was not seen for the *AtNit2* OE in the early development salt assays (Cackett et al., 2022). As AtMYB30 is proposed to be a positive regulator of programmed cell death associated with plant disease resistance, by modulating salicylic acid (SA) levels and SA-associated gene expression, (Vailleau et al., 2002; Raffaele, Rivas & Roby, 2006) it is also possible that in the absence of salt stress, the overexpression of AtMYB30 might lead to accelerated cell death, as seen by Raffaele et al. (2006). In future, it would be interesting to test whether driving overexpression of *AtMYB30* expression under the control of a stress-inducible promoter, or multiple copies of its own promoter, would lead to a more desirable phenotype where there is less of a penalty under untreated conditions and salt tolerance is improved (Zhu et al., 1998; Kasuga et al., 1999; Garg et al., 2002; Su & Wu, 2004; Vendruscolo et al., 2007). To investigate whether the role AtMYB30 plays in the salt response early in development is due to changes

in auxin levels, assays looking at auxin-related growth phenotypes such as root and hypocotyl elongation could be conducted using the OE and KO lines under control and saline conditions.

To investigate whether the altered growth phenotypes in the *AtMYB30* OE and KO lines was developmental stage specific, the same lines were tested later in development. Figure 2.15A and C show that there was again a growth penalty observed for overexpressing *AtMYB30* under untreated conditions, however this difference was only significant for *AtMYB30* OE line 2.1. No significant differences in average shoot or root mass were seen between the EV line and *atmyb30-2* KO line under untreated and saline conditions, indicating that knocking out *AtMYB30* does not influence plant growth under this experimental set up. Overall, the degree of inhibition of shoot and root growth were not altered in the *AtMYB30* OE or KO lines compared to the EV control, indicating that *AtMYB30* might not play a role in the response to salinity stress later in development. Differences between the two developmental stages could be due to differences in the role that AtMYB30 plays in the salt stress response at different stages of development as it has been shown that the Arabidopsis salt stress transcriptome is different at different developmental stages (Cackett, 2019), or could be due to other factors present in the different experimental set ups (e.g., less transpiration occurring in plate assays compared to hydroponics). Additionally, this early development salt assay is confounded by germination. Under unfavourable environmental conditions, ABA accumulates and results in seed dormancy and inhibits seeds from germinating (Okamoto et al., 2006). As many ABA mutants escape germination under stress without being truly stress tolerant, we should conduct germination assays on ABA to confirm that we are not looking at ABA mutants. Ideally, growth in salt should be measured for the same plants over multiple time points (e.g., using advanced phenomics to look dynamically at growth under saline conditions) to account for differences in growth rate, as measuring at a single time point may mean that we have assumed plants that are growing slower are more sensitive to salinity.

Overall, these results indicate that AtMYB30 plays a role in the salt stress response early in development, as *35S::AtMYB30* lines are more salt tolerant and the *atmyb30-2* KO line is less salt tolerant at this developmental stage.

2.4.2.2. Altered *AtMYB30* expression leads to changes in *AtNit2* expression

Based on the finding that the *atmyb30-2* KO and *AtMYB30* OE lines had opposite phenotypes in terms of salt tolerance, we would expect that if AtMYB30 is involved in *AtNit2* regulation, we would see opposite changes in *AtNit2* levels between the OE and KO lines, compared to WT. It is evident from the *35S::AtMYB30* lines that increasing expression of *AtMYB30* leads to modest increases in expression of *AtNit2* in untreated plants, which persists under saline conditions (figure 2.17A). However, this difference is small compared to the salt-induced upregulation of *AtNit2* expression. It is important to note, however, that the *AtMYB30* OE lines phenotyped did not have very high overexpression of *AtMYB30* which could be why no drastic change in phenotype or *AtNit2* expression was seen. This could be because of selection against high *AtMYB30* expression given the dwarf phenotype seen in the line with the highest *AtMYB30* expression (appendix figure 6.3).

Meanwhile, both *atmyb30* KO lines showed a modest increase in *AtNit2* expression under saline conditions, but not in untreated (figure 2.17B). Overall, this data indicates that *AtNit2* induction under saline conditions is maintained irrespective of whether *AtMYB30* is overexpressed or knocked out. This result was unexpected as it has previously been shown that when *AtNit2* is overexpressed in Arabidopsis, it is associated with improved plant growth in saline conditions (Cackett et al., 2022). Thus, we had hypothesised that the *atmyb30-2* line which showed more growth inhibition in saline conditions, might have lower *AtNit2* expression. The result seen in figure 2.17B could be due to the redundancy in the MYB transcription factor family and could mean that knocking out *AtMYB30* alone is not sufficient to prevent the salt-induced upregulation of *AtNit2*. It is still unclear whether any R2R3-type *MYB* genes are completely unique and functional redundancy is thought to mask the effects of mutations in *MYB* genes (Stracke, Werber & Weisshaar, 2001). Additionally, if AtMYB30 plays a role in *AtNit2* induction under saline conditions, there may be mechanisms in place to alter expression/activity of other TFs to induce *AtNit2* expression which may be more efficient and result in higher *AtNit2* levels compared to WT. This result also indicates that small increases in *AtNit2* expression (such as that seen between Col-0 and the *atmyb30* lines in 100 mM NaCl) are not sufficient to improve salt tolerance, as these lines were significantly smaller than Col-0 under saline conditions (figure 2.15). However, it is also possible that knocking out *AtMYB30* expression could negatively alter expression of other genes important in the plant

salt stress response, therefore outweighing any gain in increased *AtNit2* expression. As previously mentioned, Gong et al. (2020) showed that AtMYB30 positively regulates *AtAOX1a* expression under saline conditions to maintain redox homeostasis. When *AtMYB30* expression was knocked out, *AtAOX1a* expression was decreased and plants were more sensitive to salt stress (Gong et al., 2020). Looking at the *atmyb30-2* line alone, we could conclude that the decrease in salinity tolerance could be as a result of knocking out this *AtAOX21a* pathway, and that plants lacking this might upregulate *AtNit2* under saline conditions in an attempt to improve salt tolerance. However, the fact that the *AtMYB30* OE lines were more salt tolerant and expressed elevated *AtNit2* levels under both untreated and saline conditions indicates that *AtMYB30* might play a role in regulating *AtNit2* independent of any role in *AtAOX1a* regulation.

2.4.3. *35S::AtMYB2* plants show no alteration of salt tolerance or *AtNit2* expression

35S::AtMYB2 plants were generated and showed no significant difference in average plant mass compared to the EV control line in our salt stress assay (figure 2.18). As previously mentioned, researchers have shown that AtMYB2 regulates expression of the proline-synthesising enzyme *P5CS1* which confers salt tolerance by facilitating accumulation of proline that acts as a compatible osmolyte to confer osmotolerance (Yoo et al., 2005). Additionally, the rice MYB2 homolog, OsMYB2, has been shown to play a role in tolerance to salt, cold, and dehydration stress (Yang, Dai & Zhang, 2012). In this study, *OsMYB2* OE plants were more salt tolerant and accumulated more soluble sugars and proline, and decreased levels of H_2O_2, compared to WT plants under saline conditions. Therefore, it is surprising that overexpressing *AtMYB2* in Arabidopsis did not lead to any changes in salt tolerance. However, this result does not necessarily mean that changing levels of *AtMYB2* does not lead to changes in Arabidopsis growth under saline conditions, as we only measured phenotypic changes after two weeks on specific concentrations of NaCl. Additionally, these assays were conducted in tissue culture which is an engineered environment with limitations including lack of humidity control and condensation from transpiration. Phenotyping on soil or in hydroponics under saline conditions could be performed to assess whether there are any salt-related phenotypes. Additionally, more subtle phenotypes can be investigated such as changes in root bending using halotropism plate assays. Proline levels should also be analysed in the *AtMYB2* OE lines in future.

Previous evidence has shown that AtMYB2 protein represses the formation of axillary meristems by inhibiting expression of *REGULATOR OF AXILLARY MERISTEMS 1* (*AtRAX1*) in response to environmental stresses (long-day, salt and dehydration) so that plants can undergo a shorter vegetative development stage under environmental stresses (Jia et al., 2020). As auxin is involved in apical dominance by suppression of axillary bud growth, low auxin levels are required at the shoot apex to enable axillary bud/meristem growth. It is therefore also possible that AtMYB2 could repress the formation of axillary meristems by increasing the accumulation of auxin through regulation of *AtNit2.* However, expression of *AtNit2* was not significantly altered by *AtMYB2* overexpression (figure 2.19), indicating that increasing *AtMYB2* expression alone is not able to cause changes in *AtNit2* expression. Nevertheless, *AtMYB2* might still play a role in regulating *AtNit2* under saline conditions and this can be measured in future. Additionally, overexpression of a negative regulator may not lead to any phenotypic changes as this could lead to stronger repression of the gene while mutant lines would lift repression and thus may reveal a phenotypic effect. Therefore, *atmyb2* mutant lines should be characterised to determine whether knocking out *AtMYB2* leads to any changes in *AtNit2* expression. This was not conducted during this project as *atmyb2* T-DNA insertion lines ordered from NASC (SALK_045455 and SALK_043075) were never received, and the seeds of the two *atmyb2* mutant lines described by Guo & Gan (2011) had lost their viability. Unfortunately, these T-DNA insertion lines came from the University of Wisconsin Arabidopsis Knockout Facility which no longer distribute seeds. As previously mentioned, the MYB TF family is large, therefore there is a risk of functional redundancy within the family so KO lines may not provide a phenotype.

2.4.4. Summary

The results from this chapter indicate that *AtMYB30* may play a positive role in regulation of *AtNit2* and the Arabidopsis salt stress response. Two Arabidopsis lines overexpressing *AtMYB30*, and one *atmyb30* knockout line, were less or more sensitive to salt stress early in development respectively, in accordance with the increased salt tolerance of the *AtNit2* OE. There was no change in average plant mass of *AtMYB2*-overexpressing lines compared to wild-type empty vector lines after two weeks on various concentrations of NaCl or sorbitol, indicating that increasing *AtMYB2* expression alone is not sufficient to improve salt tolerance under these conditions. There may be other MYB TFs which play a role in *AtNit2* regulation,

that aren't transcriptionally regulated under saline conditions, that can be characterised in future. However, this family is large and narrowing down other MYB candidates is difficult. Therefore, it was necessary to use another method to identify other TFs that might play a role in *AtNit2* regulation.

CHAPTER 3: IDENTIFICATION OF POTENTIAL *NITRILASE 2* REGULATORS

3.1. INTRODUCTION

The current knowledge of *AtNit2* regulation is limited. Whilst the previous chapter took a targeted approach to identify potential regulators, here we report on a method of investigating *AtNit2* regulation based on an unbiased approach. To do this, we wanted to identify all Arabidopsis transcription factors (TFs) with the ability to bind to the *AtNit2* promoter that could potentially act as regulators of *AtNit2* to alter its expression under saline conditions, or indeed under any conditions.

3.1.1. The yeast one-hybrid (Y1H) assay

Generally, TFs are composed of at least two domains: an activation domain (AD) and a DNA-binding domain (DBD). Binding of TFs to specific sites/motifs in gene promoters occurs via their DBD, while the AD mediates RNA polymerase II recruitment (Lee & Young, 2000). Many properties of transcriptional regulation, such as the modular nature of the DBD and AD, were first demonstrated with the yeast GAL4 protein (Ma & Ptashne, 1987). The observations that the AD of the GAL4 TF is separable from its DBD, and that these functional domains can be fused to heterologous proteins, forms the basis of the Y1H assay (Sadowski & Ptashne, 1989), one of the most popular methods of investigating protein-DNA interactions (PDI) *in vivo.*

The Y1H assay is based on two main components, shown in figure 3.1. These are, 1) an expression construct that encodes a fusion between a TF of interest and a yeast transcription AD (such as the GAL4 AD), and 2) a reporter construct containing DNA of interest upstream of a minimal promoter for the AD (e.g., the *GAL4* minimal promoter) and an easily detectable reporter gene (Reece-Hoyes & Marian Walhout, 2012). The hybrid protein is commonly referred to as the “prey”, while the DNA of interest is called the “bait”. Both constructs are transformed into suitable yeast strains and if the TF binds the DNA in the milieu of the yeast nucleus, the AD induces reporter gene expression. One of the main limitations of this assay is that the yeast AD activates reporter activity regardless of whether the TF is an activator or repressor, therefore the Y1H assay only reports on the physical PDI (Reece-Hoyes & Marian Walhout, 2012). Additionally, “sticky” proteins with promiscuous DBD often give false positive results. Importantly, there may be a constraint on bait size that is linked to the distance over

which a prey can activate reporter expression, most commonly thought to be about 400 bp (Ouwerkerk & Meijer, 2011).

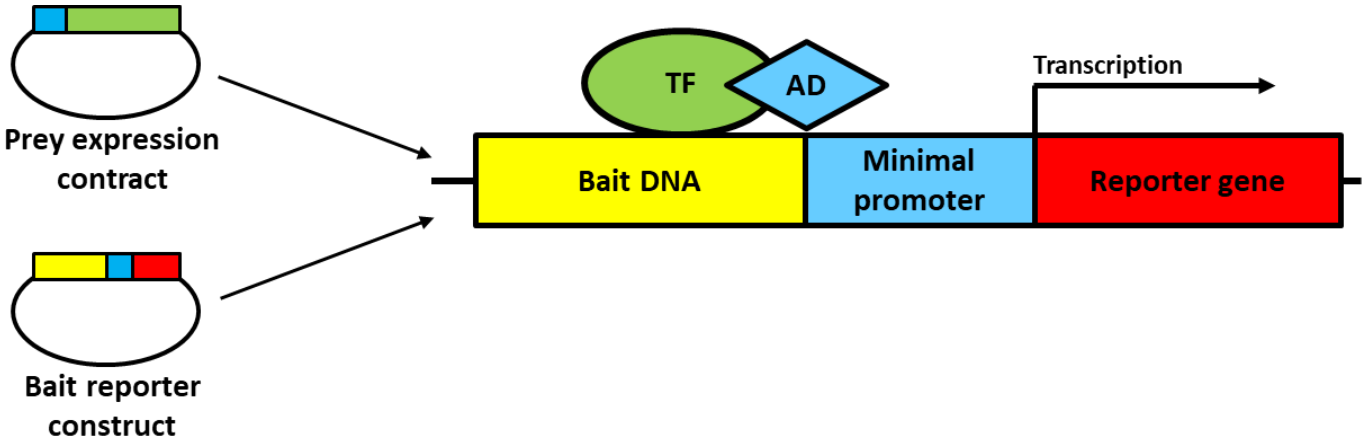

Figure 3.1: A schematic of the basic components of the Y1H assay

A prey expression construct includes an activation domain (AD) fused to a TF of interest. The bait reporter construct contains the bait DNA (usually a promoter fragment) cloned upstream of a minimal promoter and a reporter gene. If the TF is able to interact with the bait DNA, the AD is brought into proximity of the minimal promoter and reporter gene activity is activated.

Two of the most common reporter assays in the Y1H system make use of auxotrophic yeast mutants or colorimetric markers (e.g. the *LacZ* reporter gene) (Reece-Hoyes & Marian Walhout, 2012). A gene enabling amino acid production can be used as a reporter gene in a relevant auxotrophic yeast strain, and one of the most common genes used for this purpose is *HIS3,* the product of which, imidazoleglycerol-phosphate dehydratase, is the enzyme which catalyses the sixth step of histidine production (Glynn et al., 2005). For high-throughput screening, the use of auxotrophic yeast mutants is advantageous as many transformants can be screened simultaneously and only those with reporter activity (indicating PDI) will grow on media lacking that amino acid. Importantly, the activity of *HIS3* can be inhibited by adding 3-amino-1,2,4-triazole (3AT) to the growth media, a competitive inhibitor of the HIS3 gene product which therefore decreases histidine production (Joung, Ramm & Pabo, 2000). This also enables us to distinguish 'strong' and 'weak' PDI phenotypes based on how much 3AT the PDI can withstand. Advances have been made in developing high-throughput methods of

Y1H screening using either TF-centered assays, where a library of bait reporter constructs is screened, or DNA-centered, where a prey library is screened against a DNA bait (Reece-Hoyes & Marian Walhout, 2012). In Arabidopsis specifically, a comprehensive prey TF library has been developed combining the TFs predicted from four independent databases (PlnTFDB: http://plntfdb.bio.unipotsdam.de, DATF: http://datf.cbi.pku.edu.cn, DBD: http://www.transcriptionfactor.org, and REGIA Consortium: http://www.jicgenome-lab.co.uk) (Pruneda-paz et al., 2014).

3.1.2. Transient reporter gene assays in Arabidopsis mesophyll protoplasts

As the Y1H system is unable to provide information on 1) whether PDI occurs *in planta*, 2) the *in vivo* conditions under which these TFs may bind, and 3) the type of regulatory effect (activation or repression), other methods are necessary for investigating this following the Y1H assay. Commonly, transient reporter transactivation/transrepression assays in plant cells are used, which test the ability of individual TFs to alter promoter activity (either positively or negatively) by measuring reporter gene activity. This transient gene expression system is a powerful tool for rapid gene functional analysis (Abel & Theologis, 1994). This is a low-throughput assay which relies on the identification of candidate TFs from previous data. In this assay, plant cells are transfected with three vectors; 1) containing a reporter gene under the control of the promoter DNA of interest, 2) containing the candidate TF under the control of a constitutive promoter, and 3) containing a different reporter that can be used for normalisation of transfection efficiency (Reece-Hoyes & Marian Walhout, 2012). Once normalised, the reporter activity controlled by the promoter of interest can be compared across samples transfected with different candidate TFs and control vector to determine whether the TF is able to alter the promoter activity.

Arabidopsis mesophyll protoplasts are a common system for transient reporter assays *in planta* as DNA, RNA and protein delivery into the cell is relatively simple (Yoo, Cho & Sheen, 2007). Protoplasts are plant cells that have had their cell walls removed by mechanical, chemical or enzymatic means. Agrobacterium-mediated gene delivery, particle bombardment and treatment of protoplast-plasmid mixtures with polyethylene glycol or electroporation are most commonly used to transfect protoplasts (Davey et al., 2005). One of the main advantages of this system is that the plant protoplasts maintain many of the same

physiological responses and cellular activities as intact plants and therefore it is possible to investigate conserved aspects of plant signalling mechanisms (Sheen, 2011). Therefore, this system is a popular method for validating Y1H interactions and determining whether identified TFs are able to activate or repress reporter (and therefore promoter) activity.

Luciferase is one of the most widely used reporters, and various forms exist; including firefly luciferase (LucF) from *Photinus pyralis*, and renilla luciferase (LucR) from the sea pansy *Renilla reniformis* (Matthews, Hori & Cormier, 1977; De Wet et al., 1985). Although both LucF and LucR are bioluminescent reporters, they possess different enzyme structures and substrate requirements, making it possible to selectively distinguish between the luminescent reactions for each enzyme (Sherf et al., 1996; McNabb, Reed & Marciniak, 2005). This forms the basis for the Dual-Luciferase® Reporter Assay System (Promega, USA) which is commonly used in transactivation assays in protoplasts. In this assay system, *LucF* is coupled to the candidate promoter and *LucR* is driven by a constitutive promoter on another (control) vector. LucF activity therefore reports on promoter activity and LucR activity is used to normalise LucF activity, to account for transfection efficiency. This relies on two assumptions, 1) that if the LucR vector has been successfully transfected into a cell then the LucF vector has also been (McNabb, Reed & Marciniak, 2005), and 2) that the expression of LucR is unaffected by co-transfected vectors or experimental treatments (Ho & Strauss, 2004).

3.1.3. Chapter aims

The aim of this chapter was to identify Arabidopsis transcription factors which are capable of binding directly to the *AtNit2* promoter using Y1H analysis, and to validate a selection of these using transient reporter assays in Arabidopsis protoplasts. Thereafter, the aim was to characterise the selected transcription factors by analysing whether knock-out of these TFs affects plant growth in saline conditions, and expression of *Nit2.*

3.2. MATERIALS AND METHODS

3.2.1. Chemical and stock solutions

All yeast strains and most media components were obtained from Clontech, a division of Takara Bio (California, USA). The yeast nitrogen base without amino acids and 3-amino-1,2,4-triazole (3AT) were obtained from Merck (Darmstadt, Germany). Zymolyase was obtained from Zymo Research (California, USA). The Dual-Luciferase® Reporter Assay System (E1910), PureYield™ Plasmid Midiprep System (A2492) and 1 kb DNA ladder (G5711) were obtained from Promega (Wisconsin, USA). The Cellulase R10 and Macerozyme R10 were obtained from Yakult Pharmaceutical Industry Co., Ltd. (Tokyo, Japan). The Bioline BioMix™ Red Polymerase Mix (BIO-25006) and Bioline 1kb HyperLadder™ (BIO-33053) were obtained from Meridian Bioscience (Ohio, USA).

3.2.2. Yeast one-hybrid screening

The Y1H experiment was performed in Professor Katherine Denby's lab at the University of York, according to the screening protocol described by Hickman et al. (2013).

3.2.2.1 Generating "bait" yeast

Four overlapping *AtNit2* promoter fragments of approximately 400 bp (figure 3.3, appendix figure 6.2) were amplified by PCR to add *att*B sites using the primers in table 3.1 as described in chapter 2, section 2.2.11.3. These fragments were then transferred via BP recombination into pDONR™/Zeo (Invitrogen) as described in chapter 2, section 2.2.17.2. Following PCR confirmation and sequencing using the M13 primers, the promoter fragments were transferred into the Gateway converted pHISLeu2GW vector (Hickman et al., 2013) via LR recombination reaction as in chapter 2, section 2.2.17.3. The resulting constructs each contained the respective promoter fragment upstream of the *GAL4* minimal promoter and the *HIS3* reporter gene and allow for Leu-selection of yeast growth. Yeast strain Y8930 (*MATα*) (Clontech) was transformed with the pHISLeu2GW-promoter clones to generate bait strains.

3.2.2.2. The "prey" TF library

The prey library consisted of 1956 Arabidopsis TFs fused to an N-terminal GAL4 activation domain (GAL4_AD) in pDEST™22 (Invitrogen), and has been described previously (Pruneda-paz et al., 2014). This vector allows for Trp-selection of yeast growth. This library was

previously transformed into yeast strain Y8800 (*MATα*) (Clontech) and stored in 96-well format as glycerol stocks at -80˚C with each well containing yeast transformed with a different TF.

3.2.2.3. Yeast growth

Saccharomyces cerevisiae yeast was grown either on complete yeast extract peptone dextrose (YPDA) media (1% (w/v) yeast extract, 2% (w/v) bacto peptone, 2% (w/v) glucose, 65 mM adenine) or synthetic defined (SD) media (2% (w/v) glucose, 0.5% (w/v) $(NH_4)_2SO_4$, 0.34% (w/v) yeast nitrogen base) supplemented with specific amino acid dropout (DO) mixes as below:

SD-Leu:	0.69 g/L amino acid DO-Leu
SD-Trp:	0.74 g/L amino acid DO-Trp
SD-Leu/-Trp:	0.64 g/L amino acid DO-Leu/-Trp
SD-Leu/-Trp/-His:	0.62 g/L amino acid DO-Leu/-Trp/-His

For solid yeast media in petri dishes, 2% (w/v) agar was included. Yeast cultures were incubated at 30˚C. Liquid cultures were incubated with shaking on an orbital shaker at 200 rpm.

3.2.2.4. Yeast transformation

A small-scale transformation protocol was followed to transform yeast strain Y8930 with the pHISLeu2GW-promoter constructs. A 10 mL overnight yeast culture was grown in YPDA. The following day, 1 mL of culture was centrifuged at 250 x *g* for 5 minutes, and the supernatant was removed. The cells were resuspended in 1 mL 0.1 M LiAc. The cells were again pelleted by centrifugation and resuspended in fresh 1 mL 0.1 M LiAc. The cells were then incubated in a 30˚C water bath for 1 hour. During this time, a DNA mix was prepared containing 3 µL of purified plasmid DNA, 4 µL of 2mg/ml salmon sperm carrier DNA (sigma D1626) (that had been boiled for 10 minutes and then put on ice for 5 minutes), and 290 µL 50% PEG 3350. This DNA/PEG mix was pre-heated to 30˚C. Once the yeast cells had finished incubating, 100 µL of cell suspension was added to the DNA/PEG mix and this was incubated for a further 50 min in the water bath at 30˚C. Thereafter, the cells were heat shocked at 45˚C for 15 min in another water bath. The cells were then pelleted at 550 x *g* for 15 min. The supernatant was carefully removed and the cells were resuspended in 200 µL sterile H_2O. The cell suspension

was then spread on SD-Leu (SD media supplemented with all amino acids except leucine) selection plates and these were incubated until positive transformants appeared.

3.2.2.5. Library screening for interactors with pooled bait strains

Working cultures of the bait strains were prepared by inoculating a small amount of pHISLeu2GW (hereafter referred to as just pHISLeu2) yeast into 5 mL of SD-Leu media in 50 mL centrifuge tubes. Simultaneously, working cultures of the Y1H library were prepared by inoculating 5 µL of the frozen glycerol stock into 200 µL of SD-Trp media (SD media supplemented with all amino acids except tryptophan) in a round-bottom 96-well plate. These cultures were incubated overnight at 30˚C, with shaking at 75 rpm on an orbital shaker, until an OD_{600} of 0.4 – 0.9 was reached (mid-log phase). Thereafter, the yeast strains were mated on YPDA media. This was done by pipetting 3 µL spots of the library yeast onto YPDA media in a 150 mm diameter petri dish, using an 8-channel pipette in the same layout as the library plate. After the spots were dry, 3 µL of the bait strain yeast was pipetted on top of each spot and allowed to dry. For the initial library screening, the four bait strains containing the four different promoter fragments were pooled together in order to save time. Each bait strain yeast was also spotted individually on the media to ensure all four were growing correctly. A positive control was included (Harvey et al., 2020). The plates were incubated overnight at 30˚C. The following day, if all spots had grown correctly, the yeast was replicated by pressing the plate onto sterile velvet cloth thereby transferring the yeast in the same configuration as on the plate. Next, the selection plates were pressed onto the yeast print, starting with the most stringent selection plate (usually SD-Leu/-Trp/-His + 1 mM 3AT) and then followed by the least stringent plate (SD-Leu/-Trp). These selection plates were included as media lacking leucine and tryptophan would only allow successfully mated diploid yeast to grow, thereby validating that all the TF library yeast were mated with the bait yeast. On the media additionally lacking histidine, only yeast with interaction between the TF and promoter would have grown as the *HIS3* reporter gene had been activated by bringing the GAL4_AD into proximity of its minimal promoter. The addition of 3AT in these selection plates was to control leaky expression of the *HIS3* gene by acting as a competitive inhibitor of the *HIS3* gene product. These selection plates were then incubated overnight at 30˚C. The next day, the selection plates were cleaned by pressing them to individual sterile velvets in order to remove any spots of dead yeast that may interfere with the results. Thereafter, the selection plates

were incubated at 30˚C for 2-5 days, until clear growth of the positive control was seen. Each plate was then photographed and TFs with positive yeast growth were recorded.

3.2.2.6. Rescreening of interactors with individual bait strains

Once all the library plates had been successfully screened, the identified TFs that showed growth (indicating interaction) in the initial screening were rescreened against each individual promoter fragment bait strain, as well as an empty vector control in order to determine which interactions were real, and with which promoter fragment each TF was interacting. In this pairwise screening, a selection plate -Leu/-Trp/-His + 10 mM 3AT was also included. This pairwise screening was repeated three times. These plates were photographed and the growth for each TF was then scored as either:

- \- no growth
- \+ little growth (a few spots)
- ++ medium growth
- +++ strong growth.

3.2.2.7. Identification of interacting TFs

Although each well location (i.e., row letter A-H, column number 1-12, e.g., D5) for each library 96-well plate (numbered 1-21) in the TF library has been mapped to a specific TF, the identity of each interacting TF was validated to ensure no contamination or mixing of yeast had occurred. To do this, a small aliquot of yeast cells was harvested from the -Leu/-Trp/-His + 3AT selection plates (thereby ensuring the interacting TF is present in the sample) and resuspended in 15 µL lysis buffer (0.1 M $NaPO_4$, pH 7.4, 1U zymolyase). The samples were then incubated for 15 min at 37˚C followed by 5 min at 95˚C in a thermocycler. The samples were then cooled to 10˚C and 50 µL sterile H_2O was added to each. The yeast lysate was then centrifuged at 1000 x *g* for 10 minutes to pellet the yeast cell debris. For each sample, 2 µL of the yeast lysate was used in a PCR reaction with the pDEST22 F and R primers that bind in the pDEST22 vector on either side of the TF (table 3.1). These PCRs were conducted using the Bioline BioMix™ Red Polymerase Mix. Amplification conditions included an initial DNA denaturation step at 95˚C for 5 min, followed by 35 cycles of denaturation at 95˚C for 30 sec, primer annealing at 55˚C for 30 sec and elongation at 72˚C for 2 min. A final elongation step was included at 72˚C for 5 min. The resulting products were electrophoresed and visualised

on 1% TAE agarose gels using EtBr. The amplicon sizes were compared to those predicted for the TFs, and the gel-excised PCR products (as in chapter 2, section 2.2.14) were sequenced (as in chapter 2, section 2.2.15) using the pDEST22 primers to confirm the TF identity.

3.2.2.8. Isolation of pDEST22 vector DNA containing the interacting TFs

In order to isolate the pDEST22 vectors containing the relevant TFs for downstream use, plasmid DNA was extracted from the *E. coli* version of the TF library. To do this, 5 µL of the *E. coli* library glycerol stock for each TF was inoculated into 5 mL LB + 100 µg/mL ampicillin and incubated overnight with shaking at 37˚C. Thereafter, plasmid purification was performed using the NucleoSpin® Plasmid Miniprep Kit (Macherey-Nagel, USA), according to the manufacturer's instructions. The resulting plasmid DNA was amplified using the pDEST22 primers to confirm the amplicon sizes (as in section 3.2.2.7) and sequencing was conducted, as before, to confirm the identity of the TFs.

3.2.3. Analysis of microarray data

Data from two microarray experiments was obtained from Dr Lee Cackett and Dr Lara Donaldson (Cackett, 2019; Cackett et al., 2022). These datasets were used to analyse expression of the identified TFs from the Y1H assay under saline conditions using Microsoft Excel, whereby the average normalised counts and associated standard errors were calculated from the independent biological replicates for each treatment/tissue type/genotype. This data was then used to plot graphs in Microsoft Excel. One-way analysis of variance (ANOVA) tests were performed in Statistica as described in chapter 2, section 2.2.22.

3.2.3.1. Arabidopsis early development salinity microarray

The early development microarray is described in chapter 2, section 2.2.21.

3.2.3.2. Arabidopsis later development salinity microarray

Previous transcriptomics data from our group was analysed for changes in expression of the genes of interest to this project. Data from a second microarray experiment was obtained from Dr Lee Cackett. For this later development microarray experiment, Arabidopsis Col-0 was grown hydroponically in untreated ¼ strength PN for two weeks after which the plants

were transferred onto ¼ strength PN media supplemented with 0, 50, 75 or 100 mM NaCl for two weeks (Cackett, 2019). The experiment was repeated three times to obtain three biological replicates. Each shoot sample was a pool of 3-6 leaves from three different plants, while root samples were comprised of the entire root system from 2-3 plants pooled together. RNA was extracted from the root and shoot tissue respectively and sent to the University of York where Dr Lee Cackett performed the microarray experiment using SurePrint G3 Custom GE 8x60K (Agilent, Santa Clara, USA) microarray slides designed by the Vicki Buchanan-Wollaston group at the University of Warwick based on target transcripts from TAIR10. The microarray data was normalised by Stuart Meier using the quantile between arrays normalisation method from the Limma R package (Ritchie et al., 2015; Cackett, 2019). During this project, this dataset was used for candidate gene expression analysis using Microsoft Excel, whereby the average normalised counts and associated standard errors were calculated from the independent biological replicates for each treatment. This data was then used to plot graphs in Microsoft Excel.

3.2.4. Transient reporter assays in Arabidopsis protoplasts

3.2.4.1. Reporter assay vector preparation

The promoter-reporter vector: The full length of DNA upstream of the *AtNit2* translation start site encompassing the four fragments used in the Y1H screening (1368 bp) was amplified to add *att*B primers and transferred into pDONR221 via BP recombination reaction as in chapter 2, section 2.2.17.2. Sequence-verified promoter DNA was then transferred into pGWL7 via LR recombination as in chapter 2, section 2.2.17.3. In this vector, the *AtNit2* promoter is upstream of the firefly luciferase gene, *LucF.* It contains an ampicillin resistance gene for selection in *E. coli.* This vector will be hereafter referred to as P*AtNit2::LucF* (figure 3.2A).

The TF effector vectors: The *AtHMGB9* and *AtSPL7* coding sequences (CDS) were transferred from the pDEST22 vectors into a modified pUC19 vector, pUC19-35S-Rfa-35S-sGFP (Li et al., 2012), using Gateway Cloning Technology (see chapter 2, section 2.2.17). Briefly, the TF was transferred from the pDEST22 vector via BP recombination into pDONR221. Following PCR and sequence verification, the TF was transferred into the pUC19 vector via LR recombination.

Constitutive transcription of the TF cloned into the Reading Frame Cassette A (Rfa) as well as sGFP are driven by independent CaMV 35S promoters. The vector contains an ampicillin resistance gene for selection in *E. coli*. The vector was donated by Professor Steven Hussey (University of Pretoria). These vectors will be hereafter referred to as pUC19-*HMGB9* and pUC19-*SPL7* respectively (figure 3.2B).

Empty vector control: pUC19-35S-NOS-35S-sGFP (abbreviated as pUC19-EV; figure 3.2C) was created by removing the Rfa sequence of the pUC19-35S-Rfa-35S-sGFP through LR recombination with a self-ligated pCR8®/GW/TOPO® vector. A CaMV 35S promoter constitutively expresses sGFP. This vector was also donated by Professor Steven Hussey.

Renilla Luc transfection control vector: The pBS-35S-Ala-LucR vector (abbreviated as pLucR; figure 3.2D) constitutively expresses LucR from the Renilla luciferase gene *LucR* which is driven by the CaMV 35S promoter. It contains an ampicillin resistance gene for selection in *E. coli*. This was used as a control vector for transfection efficiency. This vector was donated by Professor Albrecht von Arnim (University of Tennessee).

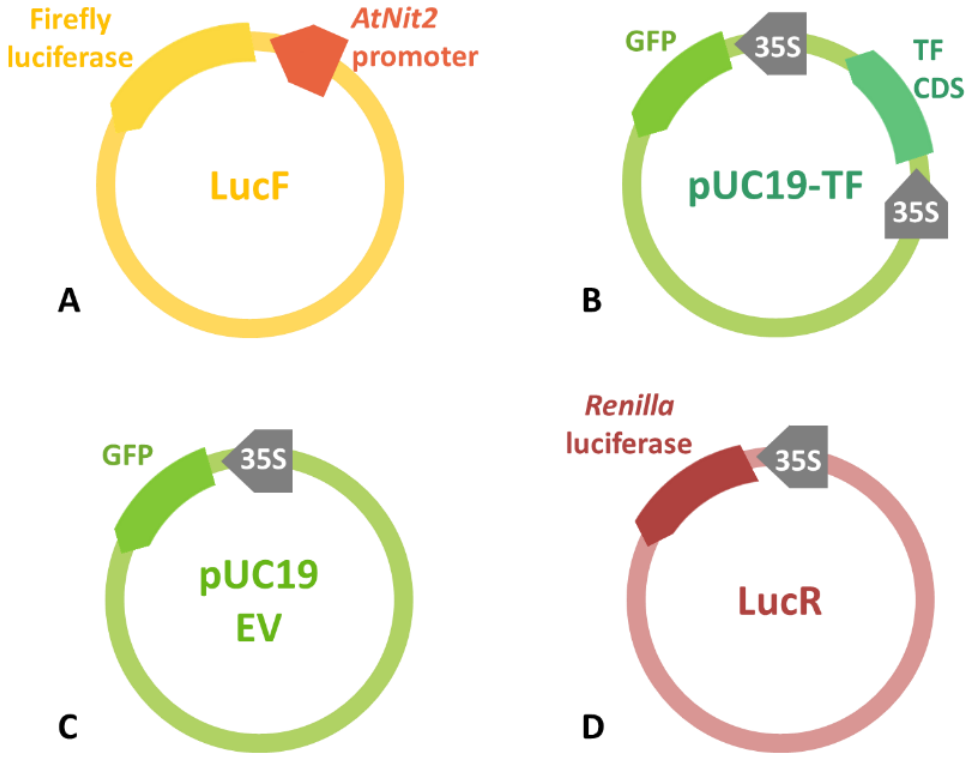

Figure 3.2: Schematic representation of the four vectors used in the transfection of Arabidopsis protoplasts

A: Reporter vector containing the *AtNit2* promoter upstream of *LucF*. **B:** Vector which constitutively expresses both GFP and the relevant candidate TF, *AtHMGB9* or *AtSPL7*. **C:** An "empty vector" which constitutively expresses GFP but lacks any TF. **D:** Vector which constitutively expresses *LucR*. "35S" indicates the position of the constitutive CaMV 35S promoter.

3.2.4.2. Bulk plasmid DNA extractions

High quality plasmid DNA was isolated using the PureYield Plasmid Midiprep System (Promega, USA) according to the manufacturer's instructions. The extracted plasmid DNA was concentrated using a Savant™ Speedvac® Plus to ensure a high enough concentration for transfection (~2 μg/μL).

3.2.4.3. Arabidopsis mesophyll protoplast isolation

Arabidopsis mesophyll protoplasts were isolated and transformed according to a published protocol (Yoo, Cho & Sheen, 2007), with a few amendments. Briefly, Arabidopsis Col-0 was grown for 3-4 weeks in a plant growth room under short photoperiod, low light conditions (50-75 $\mu E.m^{-2}.s^{-1}$ light intensity, 12-hr light/12-hr dark, 22°C, 50-60% relative humidity). Twenty well-expanded, healthy leaves (true leaf numbers five, six or seven) were removed and cut into 0.5-1 mm strips using a sharp scalpel blade and submerged in 10 μL enzyme solution (20 mM MES (pH 5.7), 0.4 M mannitol, 20 mM KCl, 10 mM $CaCl_2$, 0.1% (w/v)BSA, 1.5% (w/v) cellulase R10, 0.4% (w/v) macerozyme R10) in a petri dish. The enzyme solution was infiltrated into the leaf strips using a vacuum for six minutes, twice. Digestion was continued in the dark at room temperature for three hours, without shaking. The rest of the protocol was followed without any amendments.

3.2.4.4. Protoplast transfection

A DNA-PEG-calcium transfection was performed according to the protocol by Yoo, Cho & Sheen (2007). For each experiment, ten transfections were performed. Each vector combination below was transfected in triplicate, with one "No DNA" control included. The

vectors were added in the ratio 5:4:1 of TF effector : promoter reporter : pLucR transfection control.

The vector combinations included:

- pUC19-EV + P*AtNit2::LucF* + pLucR
- pUC19-*HMGB9* + P*AtNit2::LucF* + pLucR
- pUC19-*SPL7* + P*AtNit2::LucF* + pLucR

The transfections were performed for 15 minutes and stopped by dilution with 400 µL W5 solution (2 mM MES (pH 5.7), 154 mM NaCl, 125mM $CaCl_2$, 5 mM KCl). The protoplast mixture was then centrifuged at 100 x *g* for 2 min and the supernatant was removed. Thereafter the transfected protoplasts were incubated for 21 hours (based on a time trial conducted by Jessica Proctor (2020)) in 1 mL W5 solution in six-well plates coated with 5% (v/v) foetal calf serum.

3.2.4.5. Microscopy

Fluorescent microscopy was used to evaluate protoplast viability and confirm transfection had occurred, using a Nikon Ti-E Inverted fluorescent microscope and NIS Elements Software (Nikon Instruments Inc., Tokyo, Japan). The TexasRed filter was used to visualise chlorophyll autofluorescence, and the FITC filter was used to visualise GFP fluorescence. Protoplast concentration was determined using a MultiCount10™ disposable counting slide (#MC100, Immune Systems Ltd., UK) under an Olympus CH20 compound microscope (model #CH20BIMF200).

3.2.4.6. Dual-luciferase reporter (DLR) assays

Reporter assays were performed using the Promega Dual-Luciferase Reporter Assay System according to the manufacturer's instructions. Briefly, the protoplasts were harvested by centrifugation at 100 x *g* for 2 min in round-bottom 2 mL microcentrifuge tubes. The harvested protoplasts were then lysed in 150 µL passive lysis buffer (PLB) according to the protocol provided, and the resulting lysate was used in the DLR assay to measure LucF and LucR activity. A GloMax® Explorer Multimode Microplate Reader (Promega, USA) with dual injectors was used to perform the DLR assay, using the standard DLR assay parameters recommended by the manufacturer. The resulting LucF readings were normalised to the LucR readings to account for transfection efficiency. Microsoft Excel was used to analyse the data

and two-tailed homoscedastic t-tests were performed to determine any statistical differences ($p \leq 0.05$).

3.2.5. Characterisation of T-DNA insert lines

3.2.5.1. Homozygous T-DNA mutant lines

An *athmgb9* T-DNA insertion line (SALK_076225C) was obtained from the Nottingham Arabidopsis Stock Centre (NASC). A homozygous *atspl7* T-DNA insertion line (SALK_125385C) was kindly provided by Toshiharu Shikanai (Kyoto University, Japan) (Yamasaki et al., 2009). Both of these T-DNA lines were created in the Col-0 background. The *athmgb9* was verified as being homozygous by randomly extracting DNA from 14 seedlings and performing two different PCR analyses as designed using the Salk Institute Genomic Analysis Laboratory (SIGnAL) T-DNA Primer Design tool (http://signal.salk.edu/tdnaprimers.2.html). The first PCR was performed using a gene-specific primer pair flanking the T-DNA insertion site and the second was performed using the gene-specific forward primer with a SALK T-DNA specific reverse primer contained with the T-DNA insertion (table 3.2). Thereafter, RNA extraction and cDNA synthesis were performed according to chapter 2, section 2.2.9, and the lack of full length mRNA product was confirmed by PCR using the full length (FL) gene primers in table 3.2, according to chapter 2, section 2.2.11.2. To confirm that the cDNA was viable, a PCR was also conducted using the *Actin 2* (*AtAct2,* AT3G18780) primer pair.

3.2.5.2. Phenotyping in saline conditions

Mutant lines were phenotyped early in development in saline conditions following the same method as in chapter 2, section 2.2.6.1, however only with NaCl and not sorbitol as a preliminary analysis. Tissue was harvested from the untreated and 100 mM NaCl plates and RNA extraction and cDNA synthesis were performed according to chapter 2, section 2.2.9. Gene expression analysis was then conducted by RT-qPCR as in chapter 2, section 2.2.12, using the *AtHMGB9, AtSPL7* and *AtNit2* qPCR primers listed in table 3.2. The *AtMON1* reference gene was used (Hong et al., 2010).

Table 3.1: The primers used for the Y1H and DLR assays. F: forward primer, R: reverse primer

Primer name	Primer sequence (5'-3')	Reference (if applicable)	Amplicon size (bp)	Function	PCR kit	T_a
M13 F M13 R	GTAAAACGACGGCCAG CAGGAAACAGCTATGAC	Invitrogen	-	Sequencing	-	-
pDEST22 F pDEST22 R	TATAACGCGTTTGGAATCACT AGCCGACAACCTTGATTGGAGAC	Invitrogen	-	PCR	BioMix Red	55˚C
P*AtNit2/1-att*B1 F P*AtNit2/1-att*B2 R	ggggacaagtttgtacaaaaaagcaggcttcAATCTCACGGTTTACCGCAG* ggggaccactttgtacaagaaagctgggtcTTTTTCTGTTTTAACTTGAGCTTTAG*		433	Cloning	Kapa HiFi	55˚C
P*AtNit2/2-att*B1 F P*AtNit2/2-att*B2 R	ggggacaagtttgtacaaaaaagcaggcttcGGTAGAACGAGTTTGGGTCG* ggggaccactttgtacaagaaagctgggtcTTAATCTGCGATACACCGTG*		458	Cloning	Kapa HiFi	55˚C
P*AtNit2/3-att*B1 F P*AtNit2/3-att*B2 R	ggggacaagtttgtacaaaaaagcaggcttcCTTTTAAATTGATTGGAATTATAAATC* ggggaccactttgtacaagaaagctgggtcTTCATCCGTGGTATACCAT*		460	Cloning	Kapa HiFi	55˚C
P*AtNit2/4-att*B1 F P*AtNit2/4-att*B2 R	ggggacaagtttgtacaaaaaagcaggcttcCAGCCATTTTACCAAATAAATACTCAAG* ggggaccactttgtacaagaaagctgggtcCGTCTTACCATCTAATCTAGTTTGGT*		460	Cloning	Kapa HiFi	55˚C
pHISLeu2GW F	GATGTGCTGCAAGGCGATTAA	Hickman et al.,2013				
P*AtNit2* int F *Luc* R	AATCTCACGGTTTACCGCAG GTCGCTTCCGGATTGTTTA		±1600	PCR	Supertherm	54˚C
P35S F *AtHMGBP* FL R	AATATCGGGAAACCTCCTCG CTAAAAAGCCTTGCCGTTTGTC	Dr Lara Donaldson	±1400	PCR	Kapa RM	53˚C
P35S F *AtSPL7* FL R	AATATCGGGAAACCTCCTCG TCAAATTTTGTGTACCAATCTCATTCGG	Dr Lara Donaldson	±2800	PCR	Kapa RM	53˚C
AtHMGBP FL F *GFP* R	ATGTCATCGGACAACGAATCG GTCCTCCTTGAAGTCGATGC		±3200	PCR	Kapa RM	55˚C
AtSPL7 FL F *GFP* R	ATGTCTTCTCTGTCGCAATCG GTCCTCCTTGAAGTCGATGC		±4600	PCR	Kapa RM	55˚C

***** *att*B sequences are shown in lowercase letters

Table 3.2: The primers used for *athmgb9* and *atspl7* Arabidopsis mutant characterisation. F: forward primer, R: reverse primer

Primer name	Primer sequence (5'-3')	Reference (if applicable)	Amplicon size (bp)	Function	PCR kit	T_a
gAtHMGB9 F *gAtHMGB9* R	AAGCAAGACAGTCCGATTTTTAG AACACTCCTCCAACTTCCCTC	SIGnAL	1088	Genotyping	Kapa RM	55˚C
gAtHMGB9 F SALK T-DNA BP	AAGCAAGACAGTCCGATTTTTAG GCGTGGACCGCTTGCTGCAACT	SIGnAL	±700	Genotyping	Kapa RM	55˚C
AtHMGB9 FL F *AtHMGB9* FL R	ATGTCATCGGACAACGAATCG CTAAAAAGCCTTGCCGTTTGTC		1017	PCR	Kapa RM	55˚C
AtSPL7 FL F *AtSPL7* FL R	ATGTCTTCTCTGTCGCAATCG TCAAATTTTGTGTACCAATCTCATTCGG		2406	PCR	Kapa RM	55˚C
qAtHMGB9 F *qAtHMGB9* R	TCACGAGGAGGGGAGGTTAC TGTGAAACTCGACGAACCTTGA		305	RT-qPCR	SYBR® FAST	60˚C
qAtSPL7 F *qAtSPL7* R	TGCCAGAGATTATGTGGGCG AAAAGACACGAGAAACCGGC		293	RT-qPCR	SYBR® FAST	60˚C
qAtNit2 F *qAtNit2* R	CTCCCGCCACTCTAGAAAAG AATAGCAGAAGCATGGTACTTGC	Cackett et al., 2022	185	RT-qPCR	SYBR® FAST	60˚C
AtMON1 F *AtMON1* R	CAGACAAGGCGATGGCGATA GCTTTCTCTCAAGGGTTTCTGGGT	Hong et al., 2010	244	RT-qPCR	SYBR® FAST	60˚C
AtAct2 F *AtAct2* R	AGTGGTCGTACAACCGGTATTGT CATGAGGTAATCAGTAAGGTCACGT	Ingle et al., 2015	138	PCR	Kapa RM	55˚C

3.3. RESULTS

3.3.1. Y1H screening to identify TFs that bind to the *AtNit2* promoter

3.3.1.1. Preparation of promoter fragment vectors for Y1H analysis

Four overlapping *AtNit2* promoter fragments (figure 3.3, appendix figure 6.2) were amplified and cloned into pHISLeu2GW using Gateway Cloning Technology. Hereafter the vectors containing the fragments will be designated as pHISLeu2-P*AtNit2*/X, where X is the number of the promoter fragment.

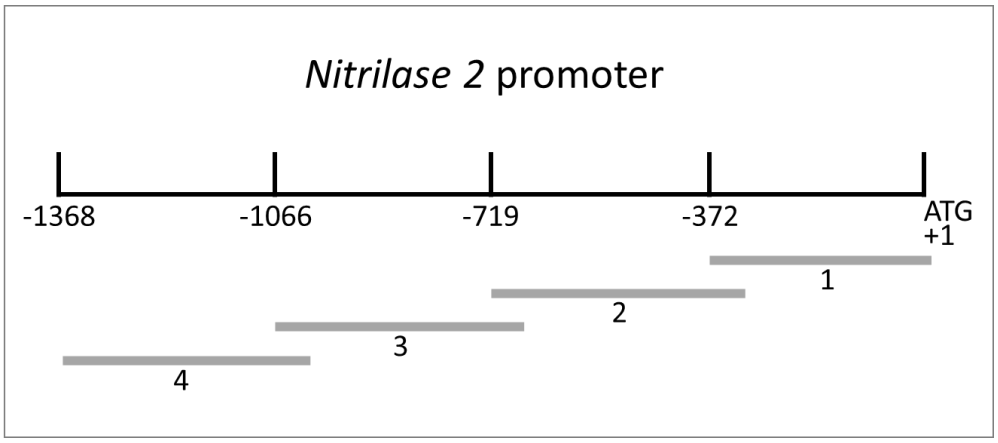

Figure 3.3: A schematic showing the four overlapping *AtNit2* promoter fragments used in the Y1H assay

The four promoter fragments (grey) are labelled as 1-4 with fragment 1 being closest to the translation start site (ATG). In this schematic, the *AtNit2* promoter is shown as a black line with the coding sequence indicated by a white box with a black outline.

The generated pHISLeu2 vectors containing the various promoter fragments were transformed into *E. coli* and colony PCRs were performed using the pHISLeu2 forward primer and the relevant promoter *att*B2 reverse primer (table 3.1) to confirm transformation with the correct promoter fragment. Figure 3.4 shows the results of each colony PCR where it is evident that all four tested colonies for each fragment contain an amplicon of the correct size (± 500 bp as vector F primer binds upstream of the *att* site), with no amplification seen in the H_2O no template controls. Plasmid DNA was extracted, sequenced, and sent to the University of York where I completed the Y1H experiments. Here, each plasmid was transformed into *S. cerevisiae* yeast Y8930 (*MAT*α).

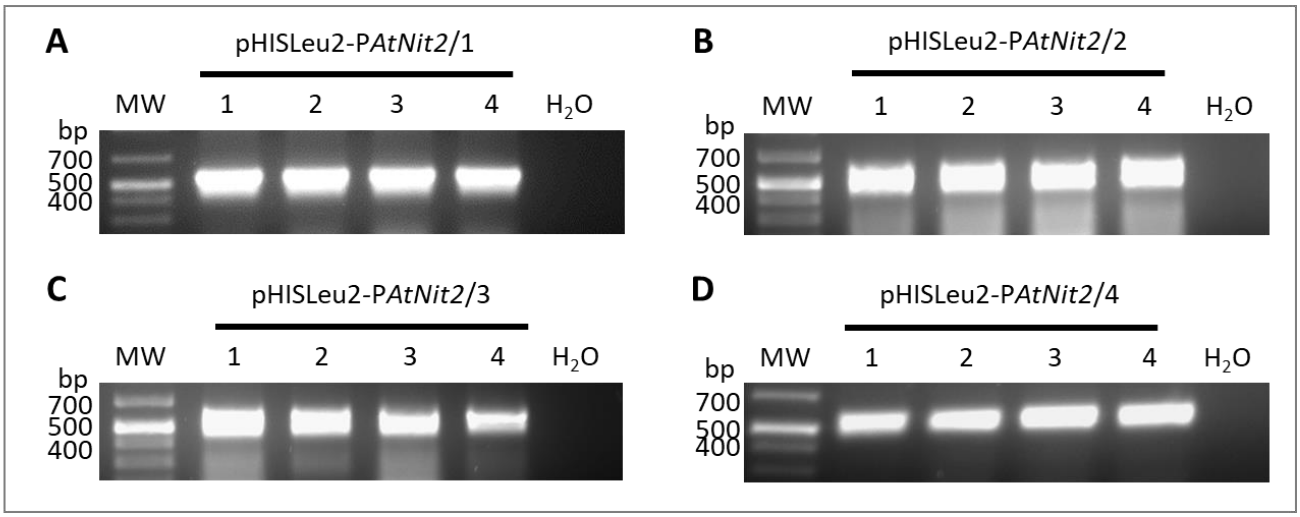

Figure 3.4: PCR confirmation of successful generation of pHISLeu2-promoter vectors

A colony PCR was performed on colonies from *E. coli* transformed with **A**: pHISLeu2-P*AtNit2*/1, **B**: pHISLeu2-P*AtNit2*/2, **C**: pHISLeu2-P*AtNit2*/3, and **D**: pHISLeu2-P*AtNit2*/4. The pHISLeu2 forward primer was used, with the fragment-specific *att*B2 reverse primer, with expected amplicon sizes of ± 500 bp. A no template H_2O negative control PCR reaction was included in each case. The MW marker included is the New England Biolabs Quick-Load® 100 bp DNA ladder.

3.3.1.2. Test to confirm no autoinduction by promoter fragment constructs

To determine whether the pHISLeu2-P*AtNit2* constructs capable of autoinduction, each "bait" yeast was tested with "prey" yeast transformed with pDEST22 empty vector and five random TFs from the library plate 7. Figure 3.5A shows that on YPDA complete media, each yeast strain was able to grow individually, but on SD-Leu/-Trp plates no yeast could grow as expected, validating that the amino acid selection was working.

Figure 3.5B shows the results from the autoinduction test, where the "bait" and "prey" yeast were spotted on top of each other on YPDA and then replicated onto selective media. It is evident from the results on SD-Leu/-Trp media that mating had occurred between all yeast tested as growth was observed. The yeast transformed with the transcription factor from plate 7, well G9, mated with all of the "bait" yeast strains became pink in colour, indicating that this yeast strain had picked up a mutation and had become auxotrophic for adenine (Weng & Nickoloff, 1997), but this colour change was not relevant to our experiment. On the SD-Leu/-Trp/-His + 1 mM 3AT plates, no induction of the *HIS3* reporter gene was observed with pDEST22 EV or any of the TFs tested, indicating that there was no autoinduction of the

HIS3 gene, and that these "bait" promoter yeast strains could be used in a TF library screening. Yeast from a previous yeast two-hybrid (Y2H) experiment (Harvey et al., 2020) were included as a positive control. This study showed that the 'TPL' binding domain (BD) was able to interact with activation domain (AD) '21', and when these yeast strains are mated it results in growth on SD-Leu/-Trp/-His + 3AT. As growth was seen in this positive control on the selection plate, it indicates that the media was correctly made and that the negative results seen with my promoter fragments were valid.

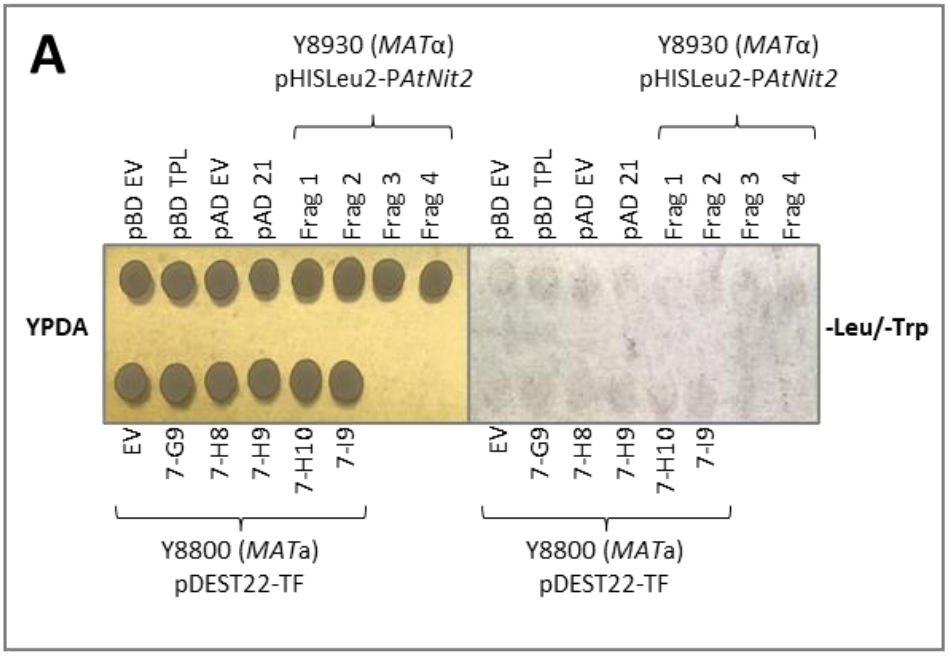

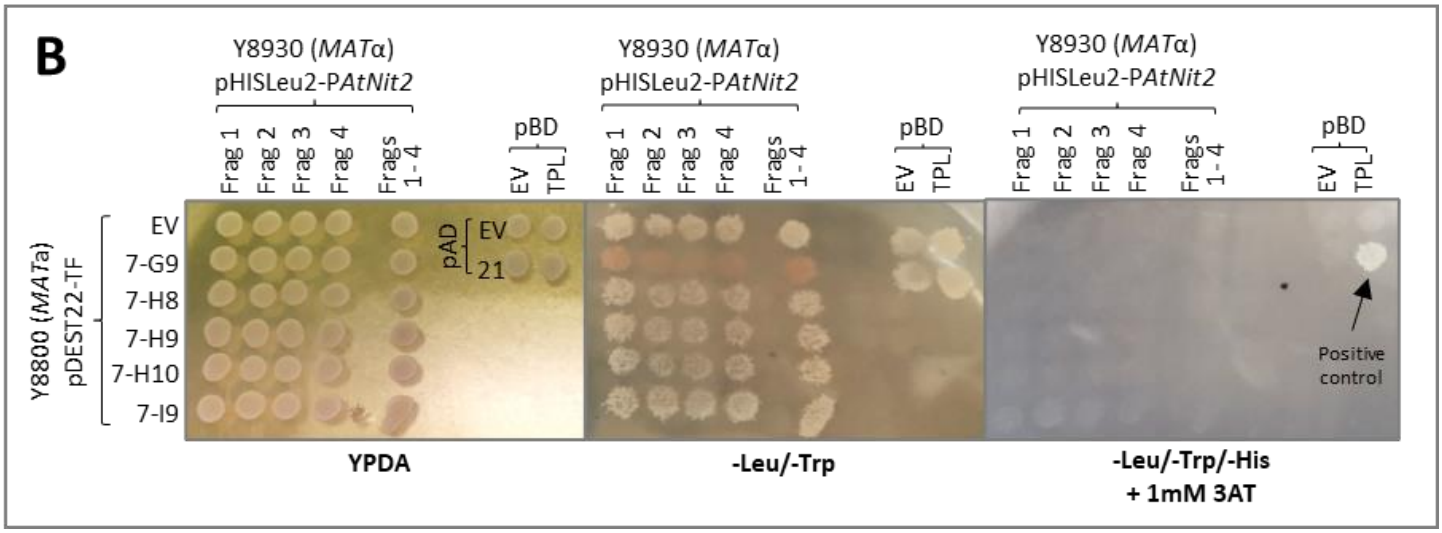

Figure 3.5: Test for autoinduction of *HIS3* gene in promoter "bait" yeast

A: Y8930 (mating type α) yeast transformed with the pHISLeu2-P*AtNit2*/1-4 vectors ("bait") and Y8800 (mating type a) yeast transformed with pDEST22 containing different TFs from the library ("prey") were grown on YPDA complete media overnight. The following day, they were replicated onto SD-Leu/-Trp and incubated for four days to confirm that all yeast was viable and not able to grow on selective media without being mated. **B:** The "bait" and "prey" yeast strains were mated on YPDA media and grown overnight. Thereafter, the yeast was replicated onto selective media and allowed to grow for four days (with cleaning of the plate the day after replication to remove any dead transferred yeast). SD-Leu/-Trp was used to test for mating, and SD-Leu/-Trp/-His + 1 mM 3AT media was used to test for *HIS3* induction. pBD-TPL x pAD-21 was included as the positive control for *HIS3* induction.

3.3.1.3. Y1H library screening using pooled promoter "bait" strains

The "bait" yeast strains transformed with each of the four pHISLeu2-*AtNit2* promoter fragments were cultured and pooled for the initial screening of the 21 library "prey" yeast 96-well plates. The results showing the screening of library plate 7 are shown in figure 3.6 as a representation of what the library screening looked like.

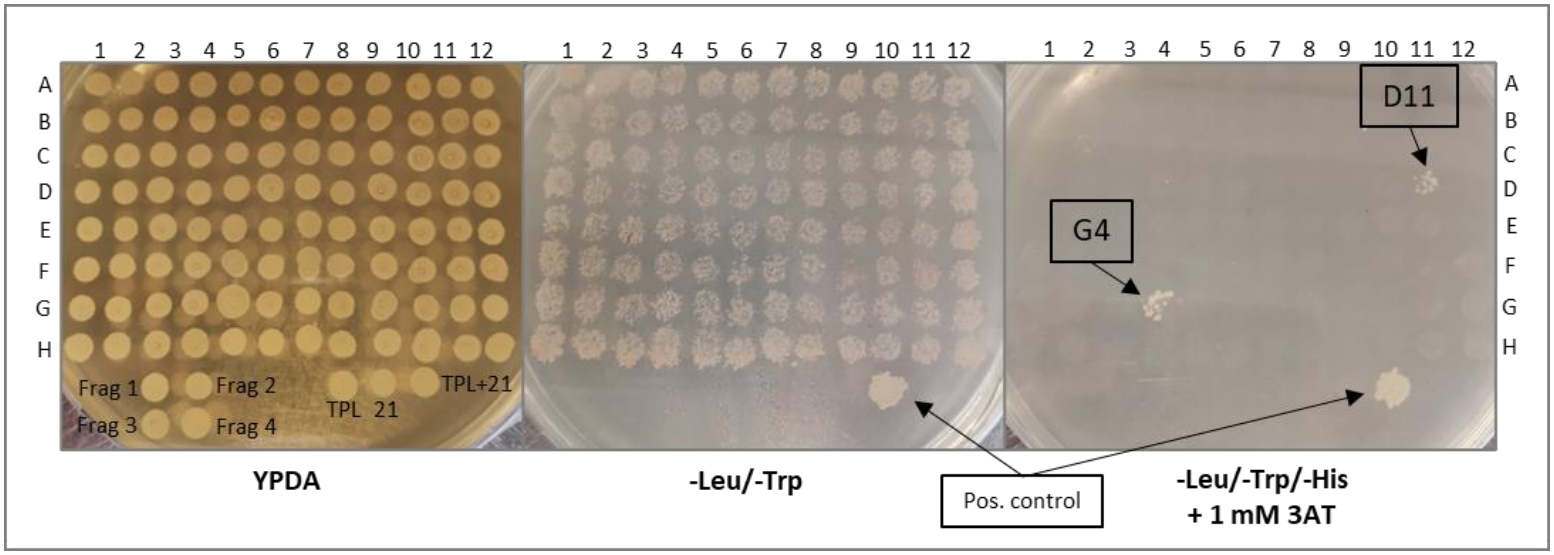

Figure 3.6: Y1H screening of library plate 7

The Y8930 (mating type α) yeast transformed with the pHISLeu2-P*AtNit2*/1-4 vectors ("bait") was pooled and spotted on top of Y8800 (mating type a) yeast transformed with pDEST22 containing different TFs from the library ("prey") plate 7 and were grown on YPDA complete media overnight. The following day, the yeast was replicated onto SD-Leu/-Trp and SD-Leu/-Trp/-His + 1 mM 3AT and

incubated for four days at 30˚C until clear growth of the positive control (TPL+21) was seen. Two "prey" yeast strains from plate 7, wells G4 and D11, were able to mate with the *AtNit2* promoter "bait" yeast and grow on selective media, indicating that the TFs these yeasts contain are able to interact with one or more of the promoter fragments. pBD-TPL x pAD-21 was included as the positive control for *HIS3* induction.

Eleven TFs were identified as potential interactors of one or more of the *AtNit2* promoter fragments from the screening of the 21 library plates. These TFs are listed in table 3.3. Notably, neither of the MYB TFs characterised in chapter 2, nor AtATAF2, showed any binding to the *AtNit2* promoter fragments tested in the Y1H experiment, despite the fact that the predicted TFBS fall within the 1368 bp promoter region tested. Additionally, no other TFs matched up to the predicted TFBS in table 2.2.

Table 3.3: The identity of the 11 TFs able to bind to the *AtNit2* promoter fragments

Gene name/description	Gene accession number	Clone location (plate-well)	TF family
GeBP, GL1 Enhancer Binding Protein, STKR1, Storekeeper Related 1	AT4G00270	07-D11	GeBP
HB34, Homeobox protein 34, ZHD9, Zinc Finger Homeodomain 9	AT3G28920	07-G04	ZF-HD
HB24, Homeobox protein 24, ZHD6, Zinc Finger Homeodomain 6	AT2G18350	08-G05	ZF-HD
HB28, Homeobox protein 28, ZHD7, Zinc Finger Homeodomain 7	AT3G50890	10-A01	ZF-HD
DNA-binding storekeeper protein-related transcriptional regulator (**DbSPR1**)	AT4G00390	10-H07	GeBP
HMGB9, High mobility group box protein with ARID/BRIGHT DNA-binding domain-containing protein	AT1G76110	12-E03	ARID
DNA-binding storekeeper protein-related transcriptional regulator (**DbSPR2**)	AT4G25210	12-F07	GeBP
TCP20, Teosinte Branched 1, Cycloidea, PCF (TCP)-domain Family Protein 20	AT3G27010	15-G05	TCP
TCP3, Teosinte Branched 1, Cycloidea and PCF Transcription Factor 3	AT1G53230	16-A03	TCP
GL2, Glabra 2	AT1G79840	19-G09	HB
SPL7, Squamosa Promoter Binding Protein-like 7	AT5G18830	19-G10	SBP

Information on the "gene name/description" associated with each gene accession number is reported according to TAIR (https://www.arabidopsis.org/). Information on the TF families were obtained from http://plntfdb.bio.uni-potsdam.de. **GeBP**: glabrous-enhancer-binding protein, **ZF-HD**: zinc-finger homeodomain, **ARID**: AT-rich interaction domain, **TCP**: teosinte branched1/cincinnata/proliferating cell factor, **HB**: homeobox, **SBP**: SQUAMOSA promoter-binding protein.

3.3.1.4. Pairwise screening of *AtNit2* promoter fragments with each interacting TF

In order to ensure that these interactions observed in the library plate screenings were specific to the *AtNit2* promoter, and to determine to which promoter fragment the TF is able to bind, a pairwise screening approach was taken whereby each of the TFs (and the pDEST22 EV control) was tested with each of the promoter fragments individually, as well as the pHISLeu2 empty vector. This was repeated three times with comparable results, with the results from one of the pairwise screenings shown in figure 3.7 and summarised in appendix table 6.3.

Figure 3.7A shows that all yeast transformants were viable and able to grow on complete YPDA media. Each yeast strain was spotted individually (labelled as -) to ensure that the growth seen was not from only one of the two yeast strains spotted on each coordinate. All mating occurred successfully, as indicated by growth of all mated yeast on SD-Leu/-Trp (figure 3.7B).

The results in figure 3.7C illustrate the importance of adding 3AT to the SD-Leu/-Trp/-His media to reduce leaky *HIS3* expression, as all pDEST22-TF yeast mated with pHisLeu2 EV were able to mate and grow when 3AT was not added. Therefore, only the results from yeast on selective media containing 3AT were considered.

Figure 3.7D shows that the interaction between two of the TFs, DbSPR1 and TCP3, was not observed in the pairwise screening. This was not necessarily unexpected as these TFs had shown very little growth in the initial library screening and were included to confirm whether this interaction was real. Additionally, the interactions with three of the TFs, GeBP, DbSPR2 and TCP20 were seen to be non-specific, as these TFs were also able to cause *HIS3* induction of the pHISLeu2 EV. The other six TFs showed specific interactions with one or more of the *AtNit2* promoter fragments.

Overall, no TFs were found that interacted with the first *AtNit2* promoter fragment 1, closest to the ATG translation start site. The HB34 TF bound to *AtNit2* promoter fragment 3, and HB24 was able to bind to fragments 2-4, indicating that there must be at least two TFBS at which this TF can bind within the promoter, although binding was strongest with fragments 3 and 4. It appears as though HB28 bound most strongly to *AtNit2* promoter fragment 4, with some binding in fragments 2 and 3. Additionally, HMGB9 was able to bind strongly to promoter fragment 2, with some binding with fragments 3 and 4 as well. Both GL2 and SPL7 bound specifically to *AtNit2* promoter fragment 4. The results for these TFs which bound specifically to the *AtNit2* promoter are summarised in table 3.4.

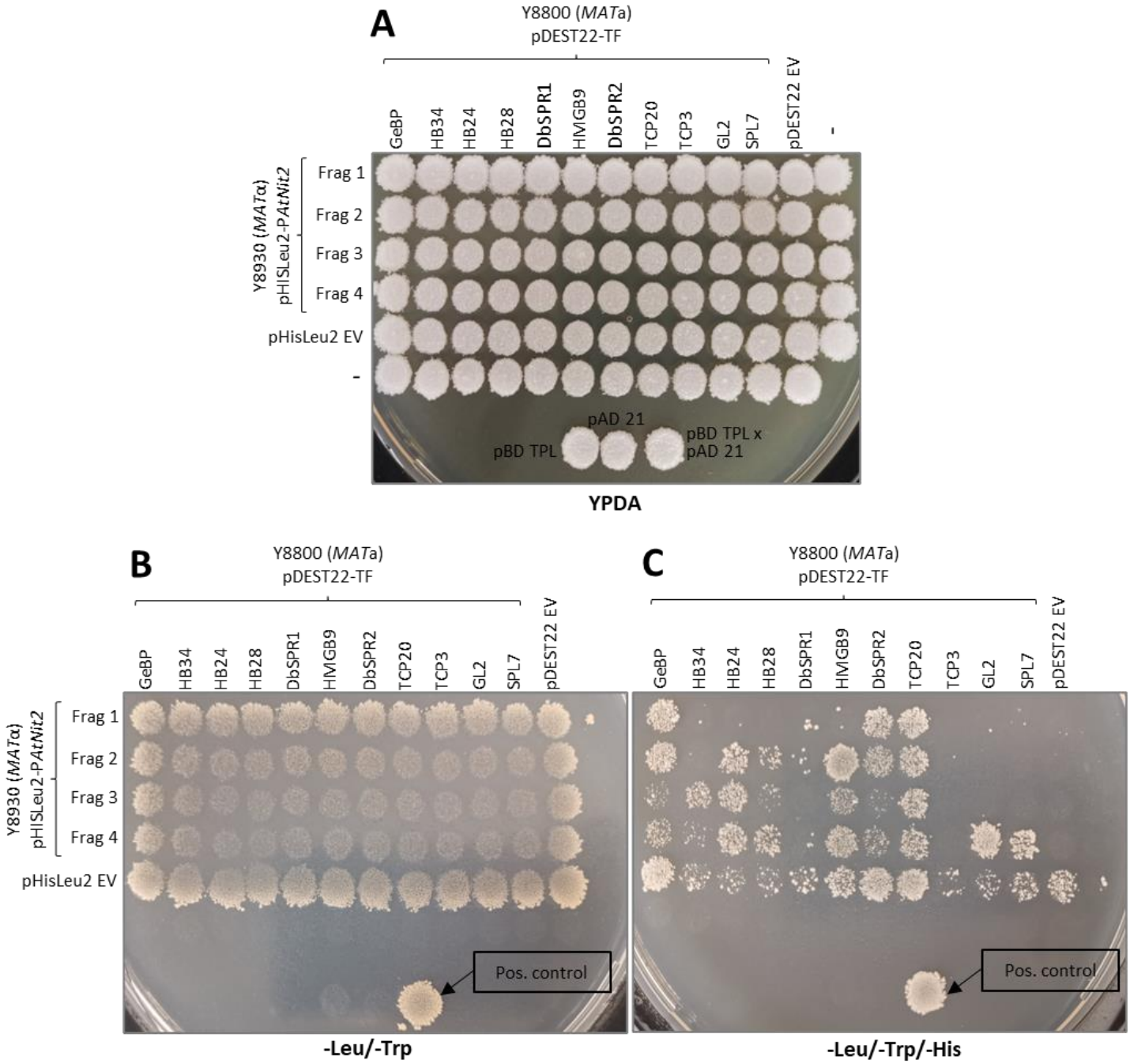

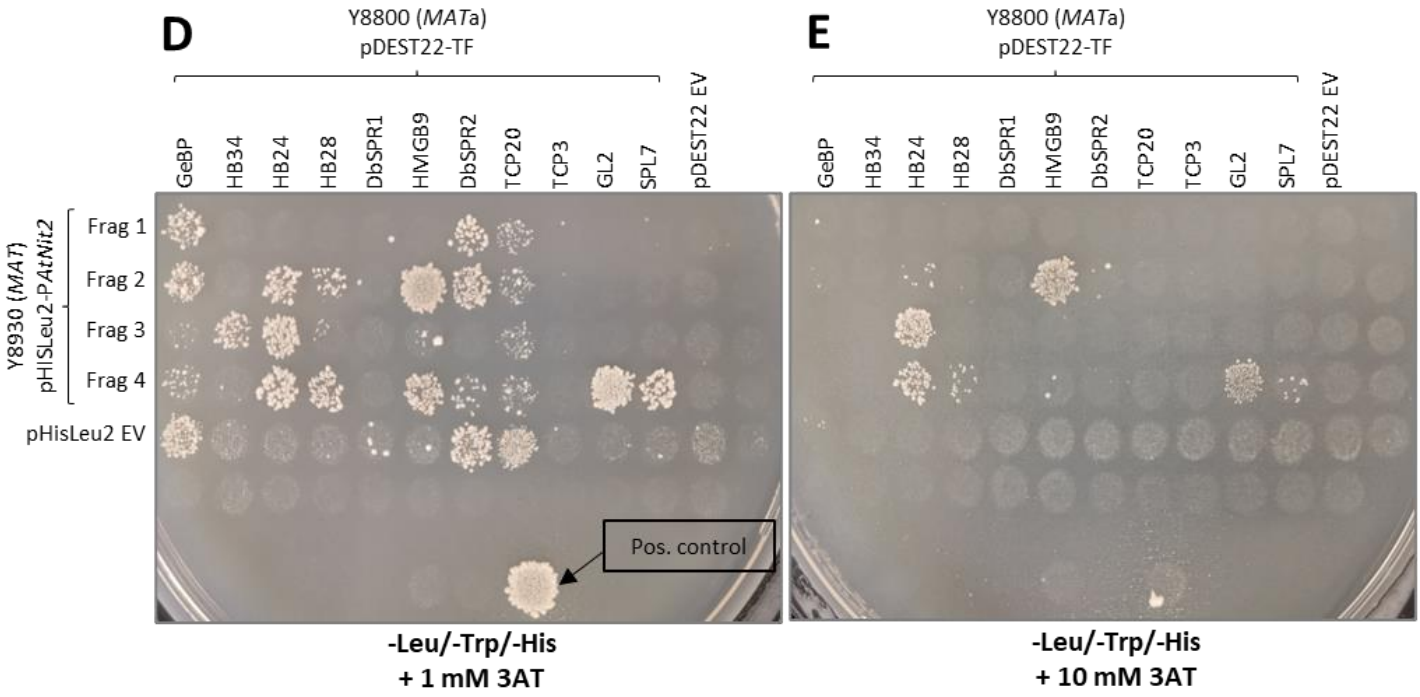

Figure 3.7: Results of the pairwise screening of interacting TFs with each *AtNit2* promoter fragment

Interactions between the TFs identified in the Y1H library screen and the *AtNit2* promoter fragments were tested in a pairwise Y1H screen. All yeast grew on non-selective YPDA media (**A**) and controls were included showing that each yeast strain could grow individually (labelled as -). All yeast spots where "bait" and "prey" yeast strains were spotted on top of each other grew on SD-Leu/-Trp media (**B**) indicating mating had occurred successfully. Binding was assessed by yeast growth on selective SD-Leu/-Trp/-His media (**C**) with the addition of 1 mM (**D**) or 10 mM 3AT (**E**). pBD-TPL x pAD-21 was included as the positive control for *HIS3* induction. The full TF names are listed in table 3.3.

Table 3.4: TFs that bound specifically to the *AtNit2* promoter in the Y1H pairwise screening

Gene name	Gene accession number	TF family	Coding sequence (bp)	Promoter fragment bound
HB34	AT3G28920	ZF-HD	939	3
HB24	AT2G18350	ZF-HD	789	2, 3 & 4
HB28	AT3G50890	ZF-HD	750	2, 3 & 4

HMGB9	AT1G76110	ARID	1017	2 & 4
GL2	AT1G79840	HB	2244	4
SPL7	AT5G18830.1	SBP	2406	4

Where more than one promoter fragments were bound, the fragment with the most growth (indicating highest reporter gene activity) is labelled in red. **ZF-HD**: zinc-finger homeodomain, **ARID**: AT-rich interaction domain, **TCP**: teosinte branched1/cincinnata/proliferating cell factor, **HB**: homeobox, **SBP**: SQUAMOSA promoter-binding protein.

To confirm the identity of the interacting TFs, yeast was harvested from the selection plates and cell lysate was used in a PCR with the pDEST22 F and R primers (table 3.1), which bind on either side of the TF insertion and the results are shown in figure 3.8A. As can be seen, the amplicons were all ± 400 bp larger than the predicted size of each TF CDS listed in table 3.4, as expected based on where the primers bind on either size of the insertion. In the EV, the band size is based on the size of the chloramphenicol resistance (Cm^R) gene and *ccd*B suicide gene present in between the *att*R sites in the vector. The second band present in the HB34 sample was not present when the PCR was repeated (appendix figure 6.5).

The pDEST22-TF plasmids were extracted from the *E. coli* version of the TF library and PCR was performed again to confirm the TF identities. Figure 3.8B shows that the results were comparable to the band sizes seen in the yeast lysate samples (figure 3.8A), indicating that the correct plasmid DNA had been extracted from the *E. coli* library. These PCR products were sequenced and confirmed the TF identities.

Overall, the Y1H experiment identified six TFs that have not previously been shown to bind to the *AtNit2* promoter or be involved in *AtNit2* regulation. These are HB34, HB24, HB28, HMGB9, GL2, and SPL7.

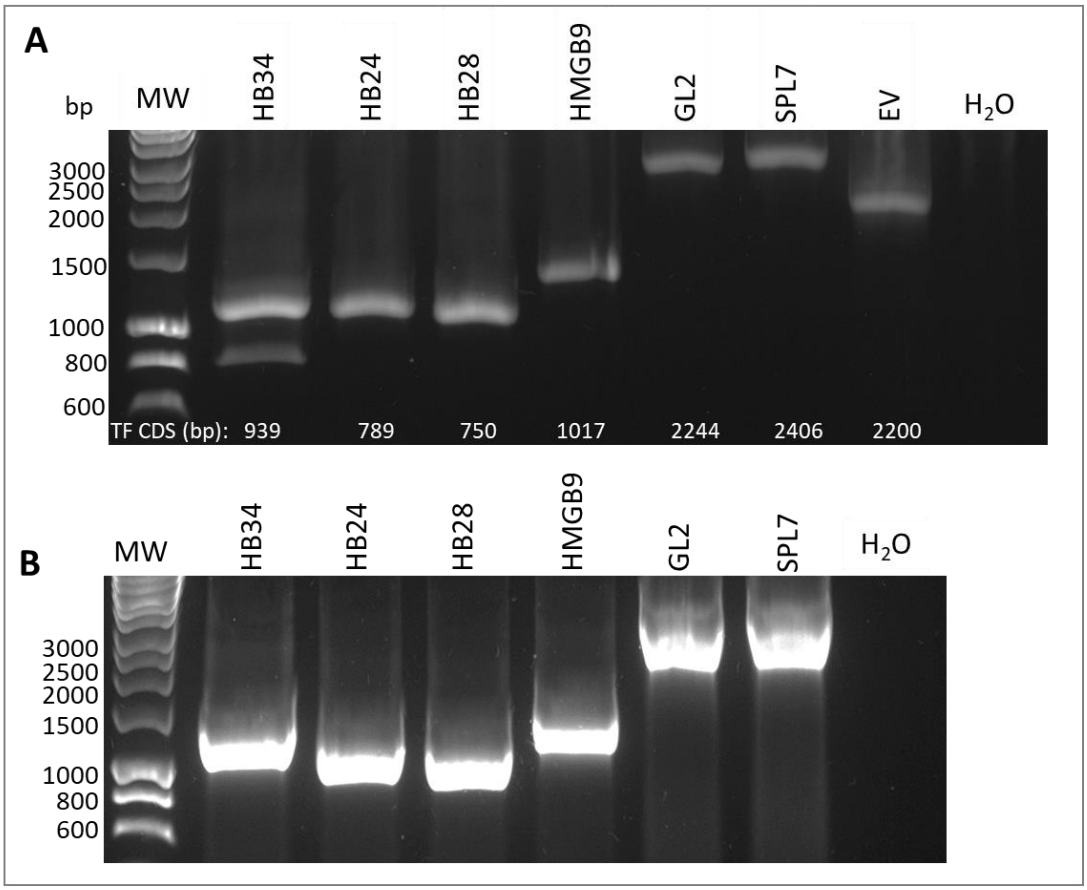

Figure 3.8: PCR confirmation of the TFs present in the interacting yeast "prey" strains and *E. coli* version of the TF library

A PCR was performed using the pDEST22 primer pair on **A:** yeast lysate samples from the interacting yeast on selective media, **B:** plasmid DNA extracted from the *E. coli* version of the TF library. The amplicons in both PCRs were expected to be ± 400 bp larger than the size of the relevant TF CDS which are listed at the bottom of the top gel image. A no template H_2O negative control was included in both PCRs. The MW marker included is the Bioline 1kb HyperLadder™.

3.3.2. Gene expression analysis of the interacting TFs under saline conditions

To investigate whether any of these TFs that are able to bind to the *AtNit2* promoter are salt-responsive, their expression was analysed under saline conditions using the available microarray data (Cackett, 2019; Cackett et al., 2022). This was also done to see how the expression of these TFs corresponds to *AtNit2* expression in the same datasets, where *AtNit2* was significantly upregulated in a dose-response manner in response to saline conditions early in development (figure 2.2E) and later in development primarily in shoot tissue (Cackett,

2019). To allow easy comparison, the *AtNit2* expression in the later development microarray is plotted in appendix figure 6.6.

Figure 3.9A shows that *AtHB34* is salt-responsive as *AtHB34* expression was significantly higher under saline conditions than untreated. Later in development, it appears as though *AtHB34* expression is predominantly expressed in shoot tissue and decreases slightly in response to 100 mM NaCl (figure 3.9B). Overall, *AtHB34* does appear to be slightly salt responsive, but its function may depend on developmental stage.

Figure 3.9C shows that *AtHB24* expression was slightly decreased in response to all NaCl concentrations except 125 mM NaCl early in development. Similar to *AtHB34, AtHB24* was also predominantly expressed in shoot tissue later in development and decreased slightly in response to 100 mM NaCl (figure 3.9D). This indicates that *AtHB24* expression is marginally salt-responsive.

Figure 3.9E shows that *AtHB28* displays a small dose-dependent increase in expression under saline conditions early in development. However, later in development *AtHB28* expression decreased in shoot tissue (where it was more predominantly expressed) under high salinity (100 mM NaCl) (figure 3.9F) and remained the same in root tissue. This indicates that *AtHB28* might play a different role in response to salinity at different developmental stages.

Figure 3.9G shows a pronounced negative relationship between *AtHMBG9* expression and salinity early in development as *AtHMGB9* expression decreases in a dose-dependent manner in response to NaCl, opposite to that seen with *AtNit2*. The same trend was not seen with sorbitol, indicating that this change in *AtHMGB9* expression was specific to the ionic component of salinity stress. Later in development, *AtHMGB9* was predominantly expressed in shoot tissue where it was downregulated in response to 100 mM NaCl figure 3.9H).

Similarly, *AtGL2* expression showed a strong negative relationship specifically under NaCl conditions early in development (figure 3.9I), opposite to that seen with *AtNit2.* However, no change in *AtGL2* expression in either root or shoot tissue was seen later in development (figure 3.9J). This indicates that *AtGL2* may only play a role in the response to salinity early in development.

Figures 3.9K and L show that neither salinity nor osmotic stress significantly alter *AtSPL7* expression early or later in development.

Although some of these TFs were salt-responsive and some weren't, this does not necessarily mean that they are more or less important in *AtNit2* regulation, as a TF is able to regulate gene expression under certain conditions without itself being differentially regulated. However, this data does seem to hint at a possible role of *AtHMGB9* and *AtGL2* in the plant response to salt stress.

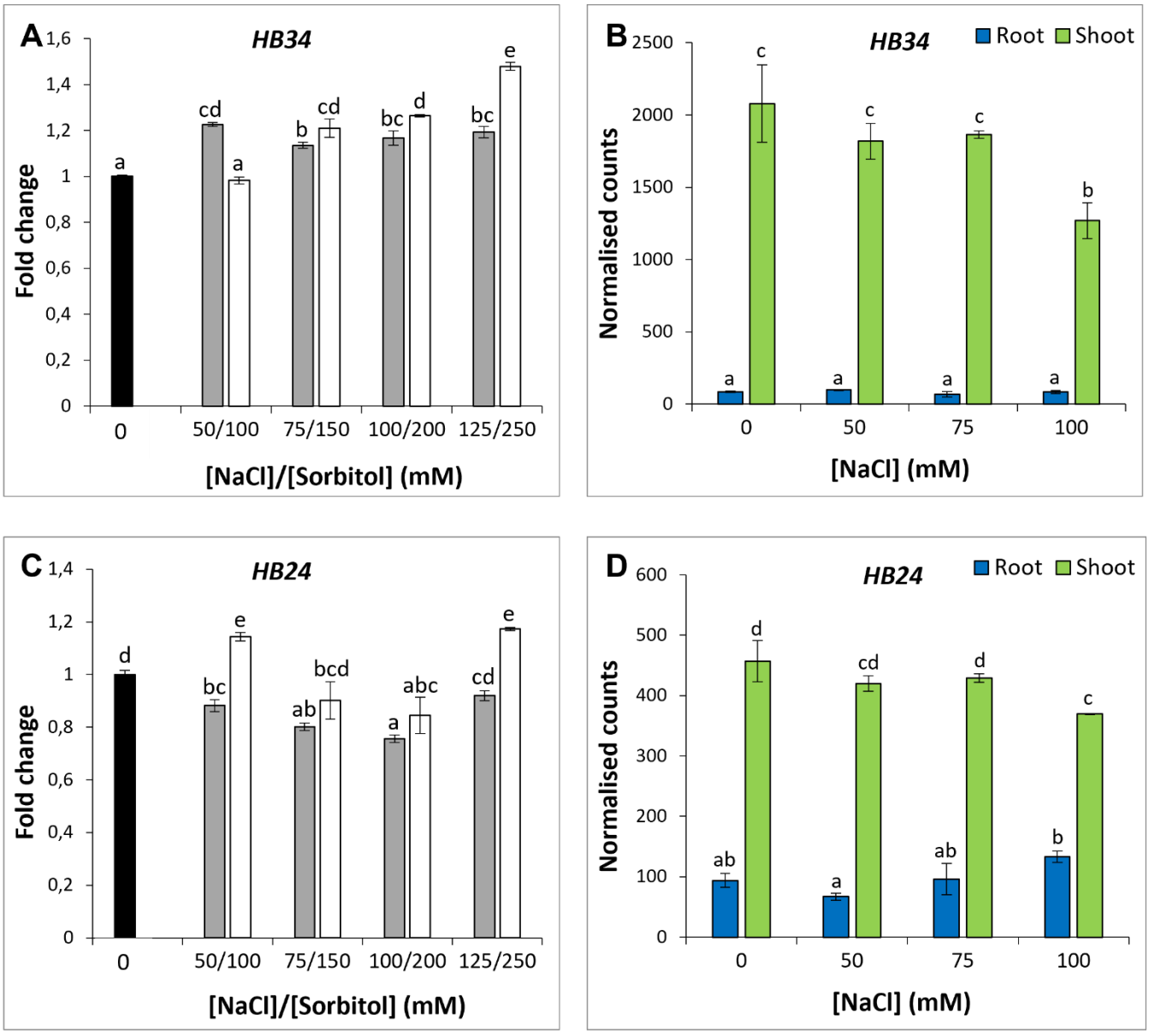

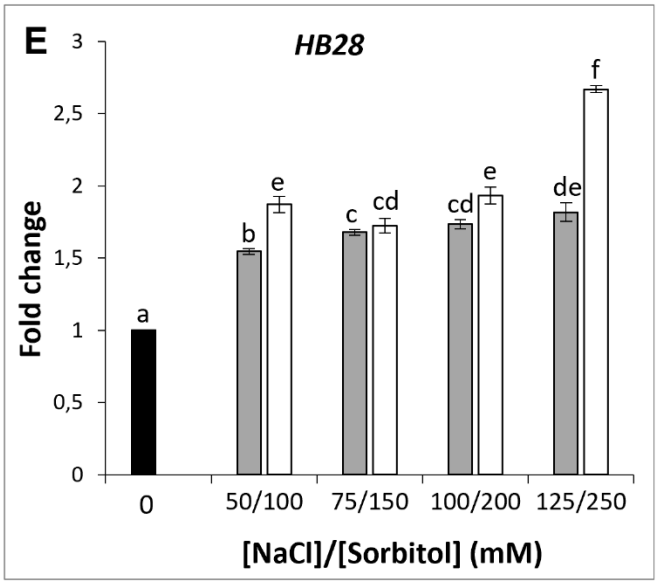
E
HB28
Fold change
3
2,5
2
1,5
1
0,5
0
a
b
e
c
cd
cd
e
de
f
0
50/100
75/150
100/200
125/250
[NaCl]/[Sorbitol] (mM)

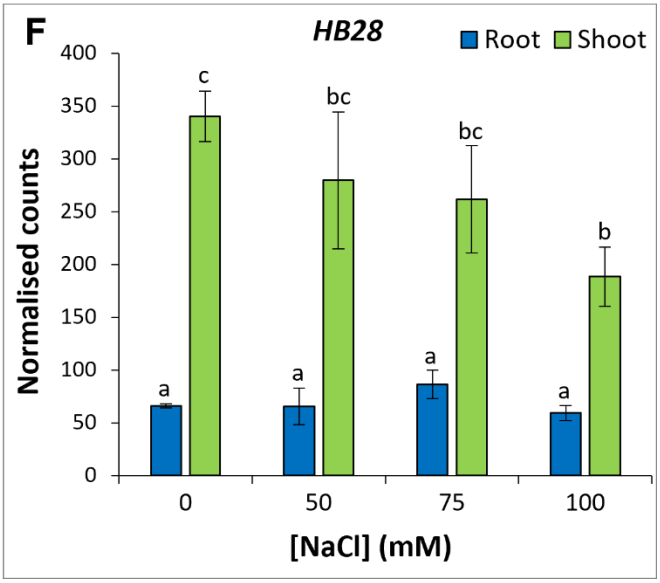
F
HB28
Root
Shoot
Normalised counts
400
350
300
250
200
150
100
50
0
a
c
a
bc
a
bc
a
b
0
50
75
100
[NaCl] (mM)

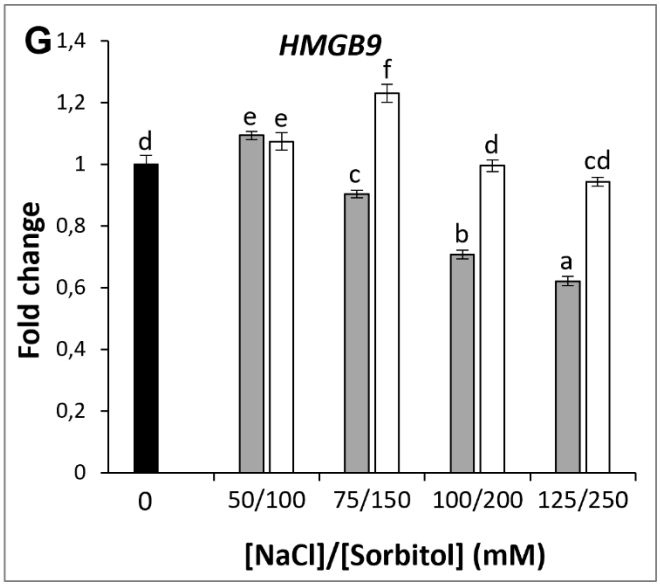
G
HMGB9
Fold change
1,4
1,2
1
0,8
0,6
0,4
0,2
0
d
e
e
c
f
b
d
a
cd
0
50/100
75/150
100/200
125/250
[NaCl]/[Sorbitol] (mM)

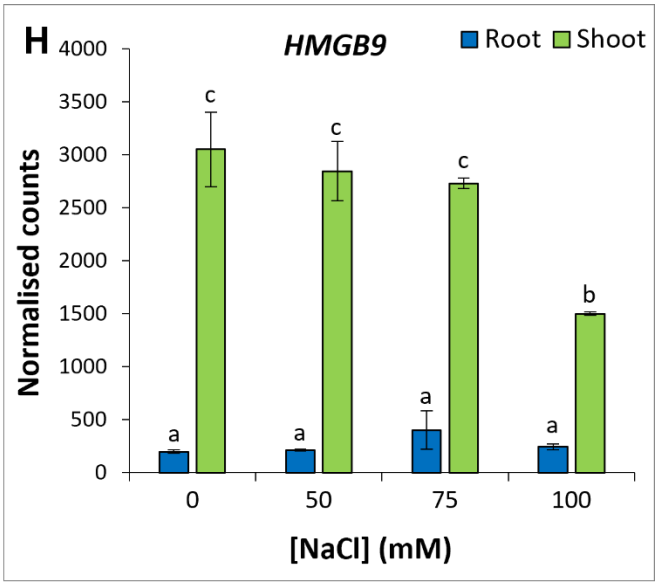
H
HMGB9
Root
Shoot
Normalised counts
4000
3500
3000
2500
2000
1500
1000
500
0
a
c
a
c
a
c
a
b
0
50
75
100
[NaCl] (mM)

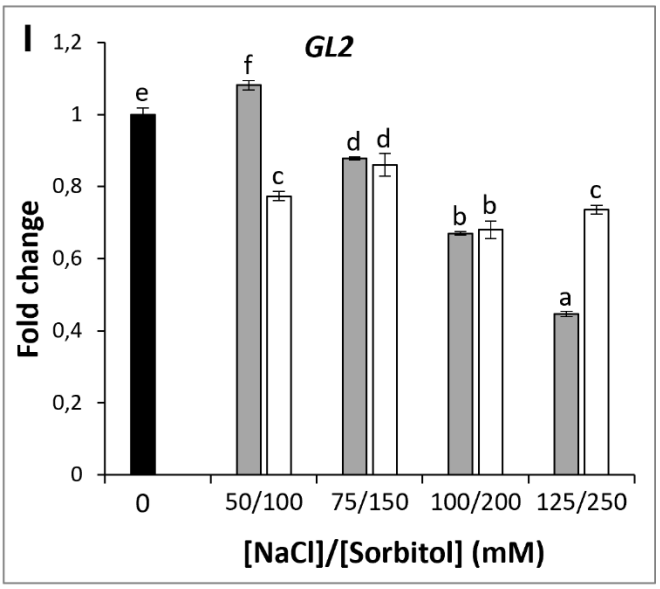
I
GL2
Fold change
1,2
1
0,8
0,6
0,4
0,2
0
e
f
c
d
d
b
b
a
c
0
50/100
75/150
100/200
125/250
[NaCl]/[Sorbitol] (mM)

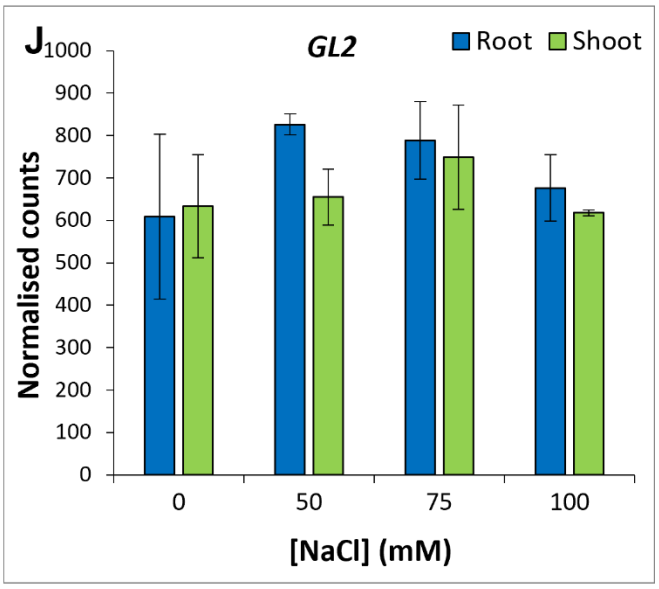
J
GL2
Root
Shoot
Normalised counts
1000
900
800
700
600
500
400
300
200
100
0
0
50
75
100
[NaCl] (mM)

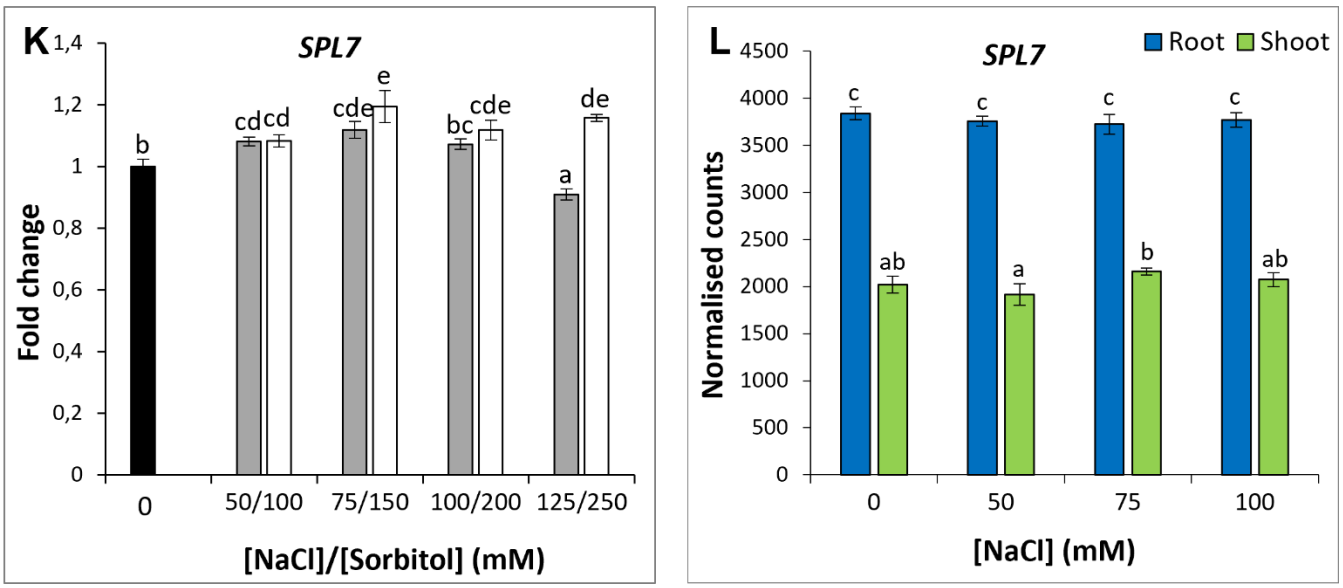

Figure 3.9: Microarray expression of the six potential *AtNit2* regulators from the Y1H screen

In the early development microarray (**A, C, E, G, I** and **K**), gene expression was determined in Arabidopsis Col-0 seedlings grown in petri dishes on control PN-agar and PN supplemented with different concentrations of NaCl or iso-osmolar sorbitol for two weeks (black bar: untreated control, grey bars: NaCl treatments, white bars: sorbitol treatments). The results are shown as an average fold change relative to the untreated control. The later development microarray (**B, D, F, H, J** and **L**) was performed on Arabidopsis Col-0 seedlings grown hydroponically for two weeks in untreated control conditions then transferred to media containing the indicated concentrations of NaCl for a further two weeks (blue bars: root, green bars: shoot). Genes include: *AtHB34* (**A** and **B**), *AtHB24* (**C** and **D**), *AtHB28* (**E** and **F**), *AtHMGB9* (**G** and **H**), *AtGL2* (**I** and **J**), and *AtSPL7* (**K** and **L**). Error bars indicate standard error. Different letters on the graphs indicate significant differences ($p \leq 0.05$) in mean fold change values as determined by Fisher LSD post-hoc analysis following a one-way ANOVA.

3.3.3. Validation of interactions identified in the Y1H assay

Two TFs were selected for validation in two different ways: first, using transient reporter assays in Arabidopsis mesophyll protoplasts to determine whether the TF can bind to and alter the activity of the *AtNit2* promoter *in planta*, and second through characterisation of T-DNA insertion mutants for changes in growth under saline conditions and alteration of *AtNit2* expression. For this, *AtHMGB9* and *AtSPL7* were selected. The former was selected based on its expression in the two microarray experiments (figures 3.9G and H), and the latter was selected as *atspl7* T-DNA mutants had previously been characterised by other

researchers who were able to supply them to us as confirmed homozygous lines (Yamasaki et al., 2009).

3.3.3.1. Transient reporter assays in Arabidopsis mesophyll protoplasts

The full length *AtNit2* promoter that spanned the four fragments used in the Y1H experiment was cloned into the pGWL7 reporter vector, upstream of the firefly luciferase gene, *LucF*. After transformation into *E. coli,* a colony PCR showed amplification of the correct size product in all four colonies using the P*AtNit2* internal forward primer and the Luc reverse primer (appendix figure 6.7A). Each of the TFs were cloned into a modified pUC19 vector to form pUC19-*HMGB9* and pUC19-*SPL7* which were thereafter transformed into *E. coli.* Colony PCR was conducted using the 35S forward primer and the *AtHMGB9* or *AtSPL7* full length reverse primer respectively and showed amplicons of the expected sizes (appendix figure 6.7B and C).

Following plasmid DNA midiprep, these PCRs were repeated on the purified plasmid DNA to ensure the correct plasmid DNA was present in the samples to be used for protoplast transfection.

Lane 1 of figure 3.10 shows the correct size PCR product (1.6 kb) from pGWL7-P*AtNit2* amplified with the P*AtNit2* internal forward primer and the Luc reverse primer, confirming that the *AtNit2* promoter is in this vector, upstream of *LucF.*

Figure 3.10 lanes 2 and 3 show the results of PCR amplification of the pUC19-*HMGB9* and pUC19-*SPL7* vectors using the 35S forward primer and *AtHMGB9* or *AtSPL7* full length reverse primer respectively. The correct sized amplicons were seen, 1.4 kb for *AtHMGB9* and 2.8 kb for *AtSPL7.* This confirms that these TFs are present in the plasmid DNA downstream of the 35S promoter. Additionally, to confirm that GFP is present in these vectors to be used as a method of verifying protoplast transfection using fluorescent microscopy, PCRs were conducted on these two vectors using the appropriate *AtHMGB9* or *AtSPL7* full length forward primer with the GFP reverse primer. The results in figure 3.10 lanes 4 and 5 show amplification of the correct size products, 3.2 kb for *AtHMBG9* and 4.6 kb for *AtSPL7.* These results confirmed correct plasmid DNA preparation.

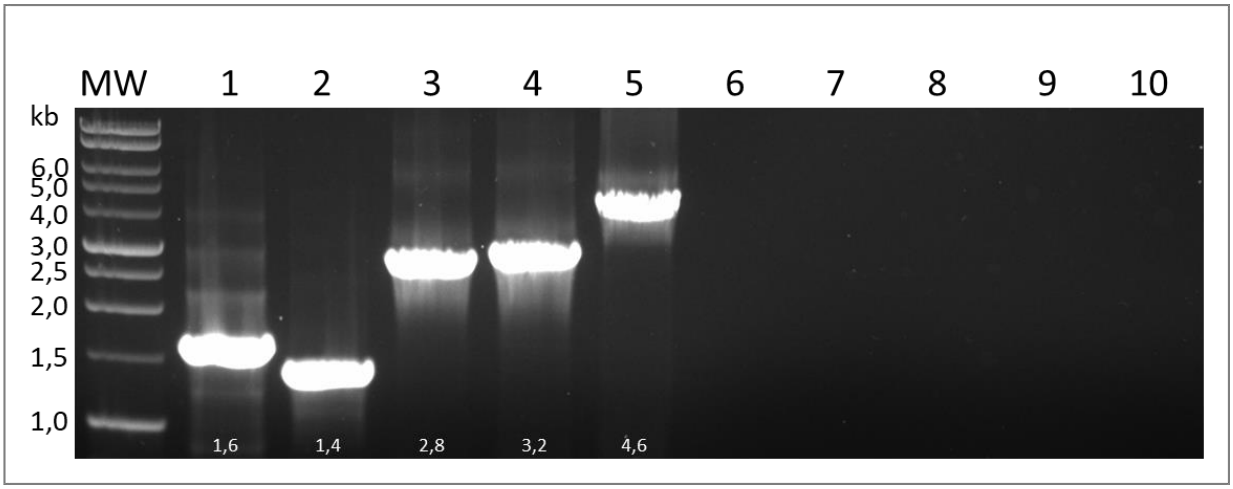

Figure 3.10: PCR confirmation of purified pGWL7-P*AtNit2*, pUC19-*AtHMGB9* and pUC19-*AtSPL7* vectors

PCRs were performed on purified midi-prepped plasmid DNA as follows; **lane 1:** pGWL7-P*AtNit2*, using the P*AtNit2* internal forward primer and the *Luc* reverse primer with an expected amplicon size of 1.6 kb, **lane 2:** pUC19-*AtHMG9,* using the P35S forward primer and *AtHMGB9* FL reverse primer with an expected amplicon size of 1.4 kb, **lane 3:** pUC19-*AtSPL7,* using the P35S forward primer and *AtSPL7* FL reverse primer with an expected amplicon size of 2.8 kb, **lane 4:** pUC19-*AtHMG9,* using the *AtHMGB9* FL forward primer and *GFP* reverse primer with an expected amplicon size of 3.2 kb, and **lane 5:** pUC19-*AtSPL7,* using the *AtSPL7* FL forward primer and *GFP* reverse primer with an expected amplicon size of 4.6 kb. A no template H_2O negative control PCR reaction was included in each case and are shown in wells 6-10. The expected amplicon sizes are shown in white at the bottom of the gel image. The MW marker included is the Promega 1 kb DNA ladder.

Arabidopsis mesophyll protoplasts were isolated and viewed under a microscope to verify that the protoplasts were intact and of the correct size of ± 50 µm. Appendix figure 6.8 confirms this. After the protoplasts were diluted to the correct working concentration, transfection was performed. Figure 3.11 shows a representation of Arabidopsis protoplasts of the correct size, expressing GFP from the pUC19 empty vector seen under a fluorescent microscope, confirming successful transfection.

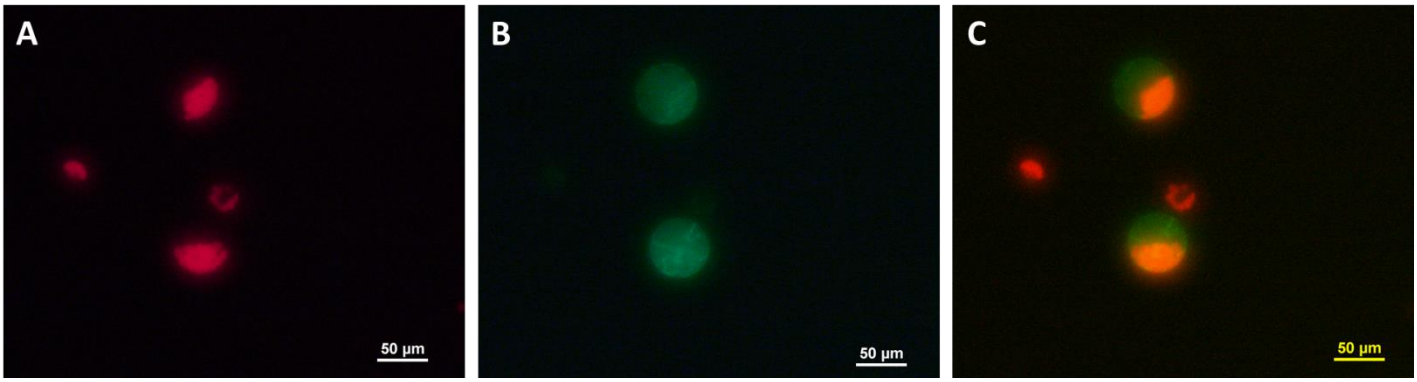

Figure 3.11: Arabidopsis protoplasts expressing GFP

Representative images of successfully transfected protoplasts. **A:** Chlorophyll autofluorescence, seen using the TexasRed filter, **B:** Cells expressing GFP from the effector vector, seen using the FITC filter, and **C:** Overlay of images A and B.

Once transfected, the protoplasts were incubated for 21 hours to allow time for expression of the TF, binding of the TF to the *AtNit2* promoter and Luc reporter activity. Protoplasts were then lysed and used in a dual luciferase reporter assay to measure LucF and LucR activity simultaneously. The LucF activity was then normalised to the constitutively produced LucR activity to account for transfection efficiency. The whole process of isolating protoplasts, transfection and the DLR assay was repeated twice with near identical results. The results from both assays are combined and shown in figure 3.12.

It is evident that *AtHMGB9* expression significantly reduces LucF activity from the *AtNit2* promoter reporter compared to the EV control, indicating that AtHMB9 is a negative regulator of *AtNit2* promoter activity and thus *AtNit2* expression. This also confirms the Y1H result that *AtHMGB9* is able to bind directly to the *AtNit2* promoter DNA. There was no significant difference in *AtNit2* promoter activity when protoplasts were transfected with pUC19 EV or pUC19-*AtSPL7*, indicating that AtSPL7 is not able to alter *AtNit2* promoter activity in this experimental set up.

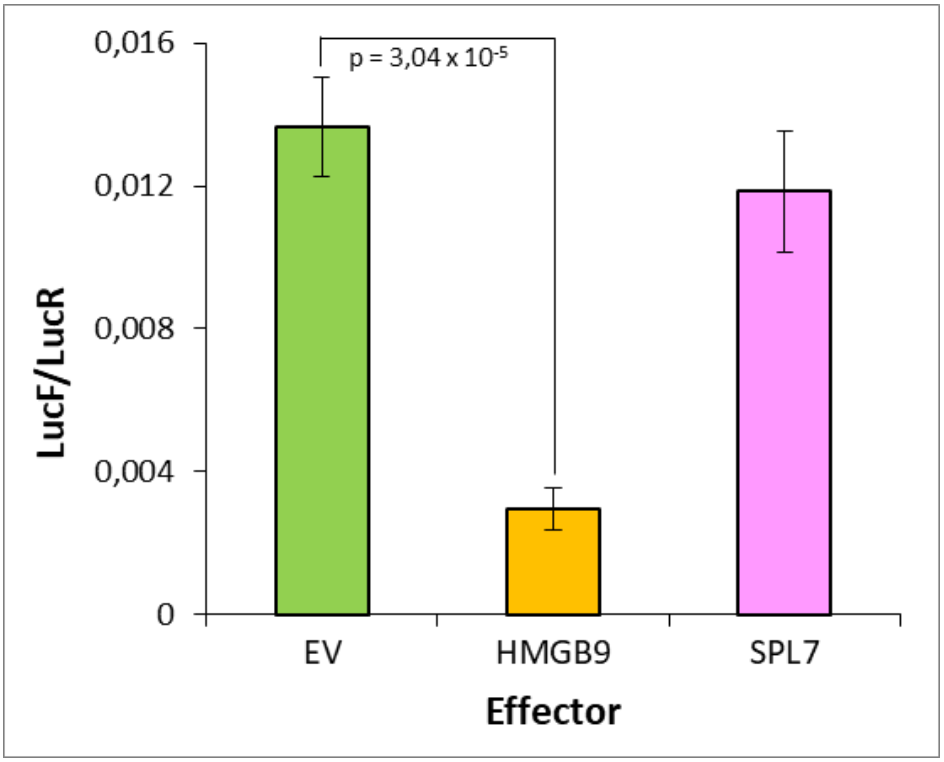

Figure 3.12: *AtNit2* reporter assay to investigate regulation by AtHMBG9 and AtSPL7

Arabidopsis mesophyll protoplasts were isolated and co-transfected with three vectors: a P*AtNit2*::*LucF* reporter vector, a vector constitutively expressing *LucR*, and an effector vector which constitutively expresses both *GFP* and *AtHMGB9*/*AtSPL7* or an "empty vector" which expresses *GFP* but lacks an effector gene. LucF activity was measured 21 hours after transfection and normalised to the LucR activity for each transfection. Values shown are mean values ± standard error from six biological repeats (two experiments performed in triplicate) (n=6). The p-value shown is from a two-tailed homoscedastic t-test.

3.3.3.2. Characterisation of *athmgb9* mutants

3.3.3.2.1. Isolation of a homozygous *athmgb9* mutant line

An *athmgb9* T-DNA insertion line (SALK_076225C) was obtained from NASC. The T-DNA insertion site was predicted to be in the promoter region of *AtHMGB9*, the location of which is shown in figure 3.13. Initially the seeds were planted on soil and allowed to self-fertilise to bulk up the seed. This generated 14 parental plant lines from which DNA was extracted to screen for homozygous T-DNA mutants. A PCR-based method was used for screening whereby primers were designed to distinguish between wild type (WT) and mutant alleles. Gene-specific primers (shown in blue in figure 3.13), that lie on either side of the predicted T-DNA

insertion site, would only amplify the WT allele. Due to the T-DNA insertion being approximately 6000 bp, the region is too large to PCR amplify when a mutant allele is present. Mutant alleles are identified by a separate PCR in which a T-DNA specific reverse primer (orange in figure 3.13) and the gene specific forward primer was used. The two separate PCRs were performed on DNA from the 14 parental plants. All 14 plants showed no product in the PCR for the WT allele (figure 3.14A) but did show an amplicon of the expected size in the PCR for the mutant allele (figure 3.14B), indicating that all plants tested were homozygous for the T-DNA insertion in *AtHMGB9*. Additionally, one of the PCR products from the PCR for the mutant allele was sequenced and confirmed the site of the T-DNA insertion, 165 bp upstream of the *AtHMGB9* translation start site.

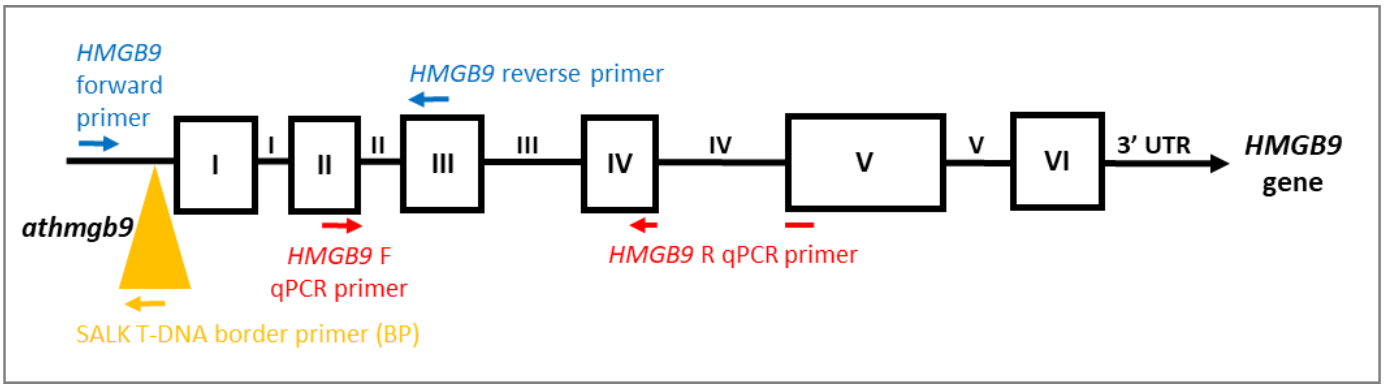

Figure 3.13: Site of T-DNA insertion in the *athmgb9* line

The T-DNA insertion for *athmgb9* (orange triangle) is in the *AtHMBG9* promoter. Exons, as annotated by TAIR, are depicted by white boxes, whereas introns are depicted as black lines. The red arrows represent the *AtHMGB9* qPCR primer set. The gene-specific primers for genotyping PCRs are shown in blue, and the SALK T-DNA border primer (BP) is shown in orange.

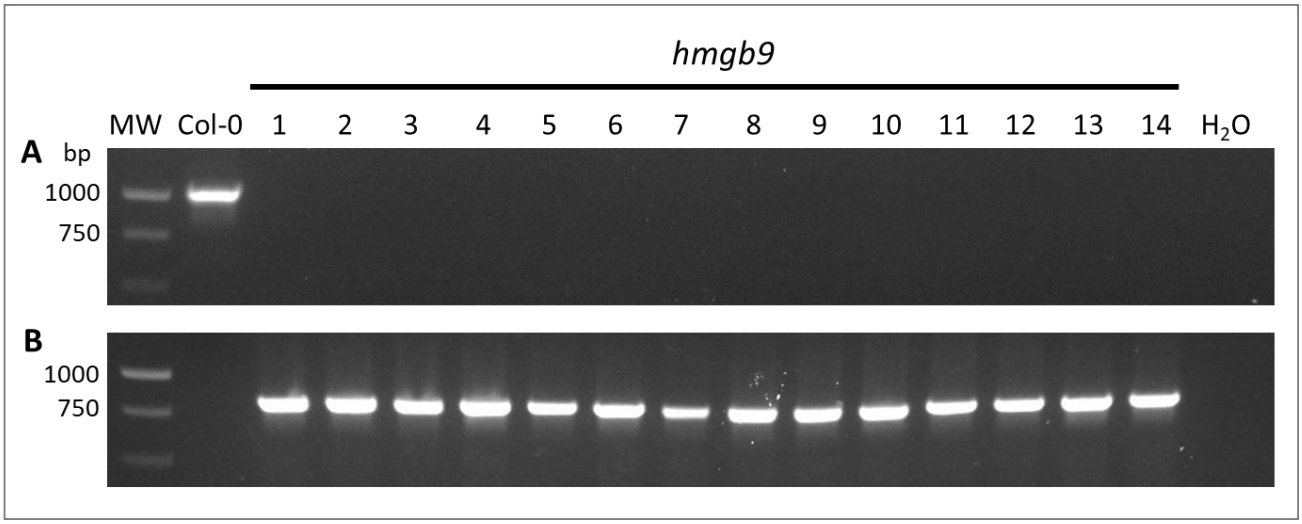

Figure 3.14: PCR confirmation of *athmgb9* homozygosity

Fourteen *athmgb9* plants were screened by PCR to confirm homozygosity. **A:** There was no product from any of the *athmgb9* plants using the *AtHMGB9* gene-specific primer set that had an expected amplicon size of 1088 bp. **B:** The *AtHMGB9* forward primer and SALK T-DNA reverse primer reported the presence of the T-DNA insertion in all 14 mutant plants (expected amplicon size: 529 - 829 bp), confirming that the plants were all homozygous. Col-0 DNA was included as a positive and negative control for the respective PCRs. The MW marker included is the Promega 1 kb DNA ladder.

To confirm that there was no full length *AtHMGB9* mRNA being produced, RT-PCR was used. Leaves were harvested from three different *athmgb9* plants, as well as Col-0 as a control (as these lines were generated in the Col-0 background), and RNA extraction and subsequent cDNA synthesis were performed. A PCR using primers which amplified the full-length *AtHMGB9* coding sequence (*AtHMGB9* FL F and R) was performed and showed reduced amplification in the mutants compared to Col-0. However, there was a small amount of *AtHMGB9* expression present in the mutants, indicating that this T-DNA line is a knock-down mutant rather than a null mutant (figure 3.15A). A PCR using the *AtAct2* reference gene primers was used to confirm the integrity of the cDNA and shows a band for each of the samples (figure 3.15B), confirming that the lighter product in the *AtHMGB9* PCR is not due to poor RNA quality or inadequate cDNA synthesis. Overall, this indicates that this *athmgb9* line has knocked-down expression of *AtHMGB9.*

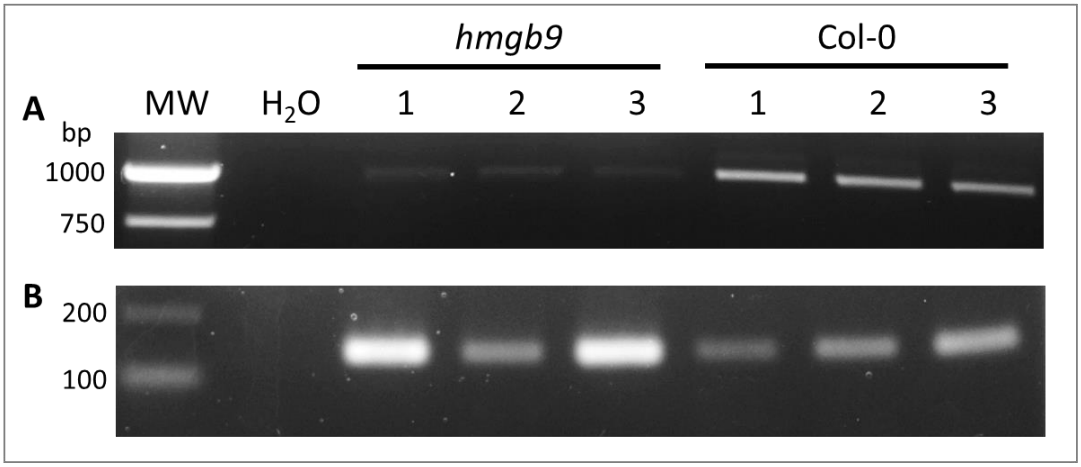

Figure 3.15: PCR to evaluate *AtHMGB9* expression in the *athmgb9* T-DNA mutant line

A: PCR was performed on cDNA from three mutant and Col-0 plants using *AtHMGB9* full-length gene primers (*AtHMGB9* FL F and R) with an expected amplicon size of 1017 bp. **B:** PCR was performed on the same samples using the *AtAct2* reference gene primers, with an expected amplicon size of 138 bp, confirming integrity of the cDNA. H_2O was used as the template in the negative control reactions. The MW marker included is the Promega 1 kb DNA ladder.

3.3.3.2.2. Growth of *athmgb9* plants exposed to salinity early in development

To determine whether knock-down of *AtHMGB9* expression has an impact on plant growth in in saline conditions, Col-0 and *athmgb9* plants were germinated and grown for two weeks on petri dishes containing PN-agar (control) and PN-agar supplemented with 100 mM NaCl. The average mass/plant of the two lines was compared for each treatment to identify any phenotypic differences in their growth. This experiment was repeated three times, with four technical replicates each, and the results were consistent.

Figure 3.16A shows that the biomass of the *athmgb9* mutant was significantly lower than WT Col-0 under both untreated and saline conditions, and that biomass was significantly reduced in both genotypes under saline conditions. To account for the difference in the average plant mass between the lines in untreated conditions, the mass per plant was plotted relative to the untreated control for each line and the data is shown in figure 3.16B. Here, it is evident that the *athmgb9* line shows a significantly lower average plant mass relative to Col-0 under saline conditions, indicating that this line has decreased salt tolerance compared with Col-0.

This experiment was repeated once with the full range of NaCl concentrations and the same trend was seen (appendix figure 6.9).

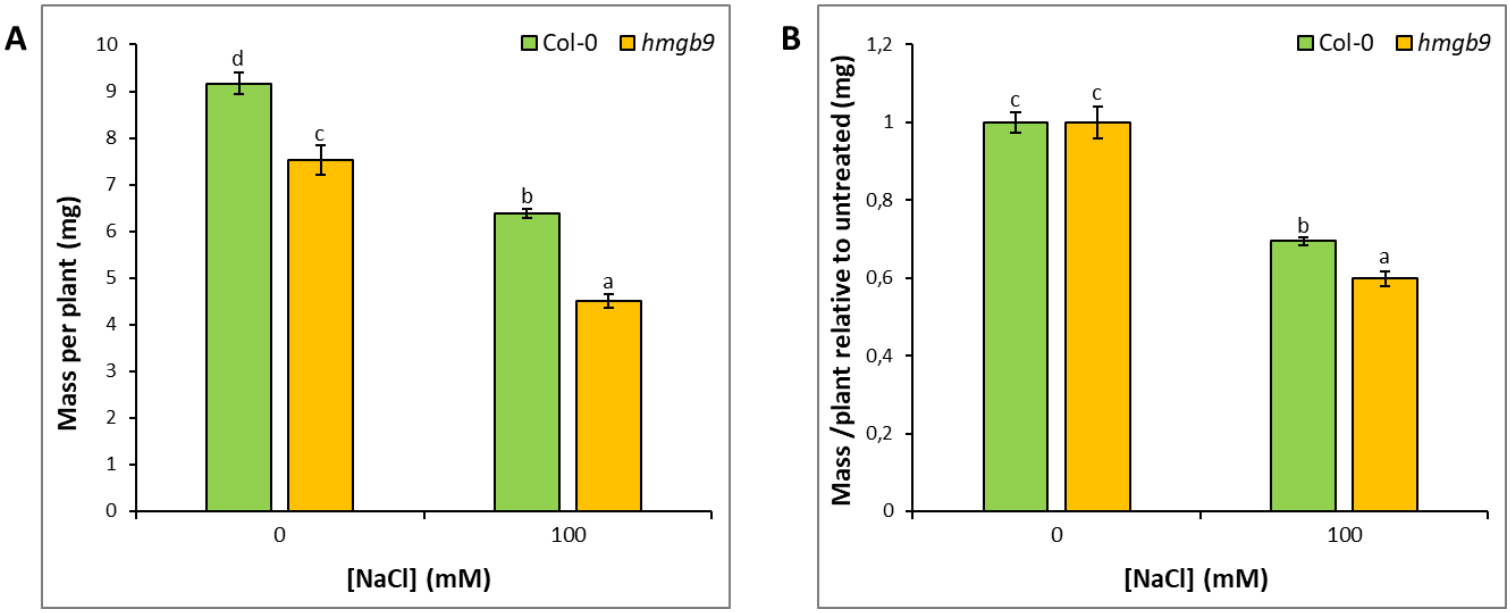

Figure 3.16: Growth of *athmgb9* plants exposed to salinity early in development

Col-0 and *athmgb9* plants were germinated and grown for two weeks on petri dishes containing untreated PN-agar (control) and PN-agar supplemented with the indicated concentrations of NaCl. **A:** The average mass per plant of each line. **B:** The average mass per plant plotted relative to the control (0 mM) for each line. Error bars indicate standard error. For each treatment, the results show four replicates combined from three independent experiments with 50 seeds sown per plate (n=12). Different letters on the graphs indicate significant differences ($p \leq 0.05$) in mean values as determined by a one-way ANOVA with Fisher LSD post-hoc analysis.

3.3.3.2.3. Gene expression in the *athmgb9* mutant line

To determine whether knocking down *AtHMGB9* expression is accompanied by changes in *AtNit2* mRNA levels, tissue was collected from Col-0 and *athmgb9* plants that had been germinated and grown for two weeks on petri dishes containing PN-agar (control) and PN-agar supplemented with 100 mM NaCl.

Figure 3.17A firstly confirms that *AtHMGB9* expression is decreased under saline conditions in WT Col-0, as previous seen in the microarray data (figure 3.9G). Additionally, it can be seen

that *AtHMGB9* expression is indeed knocked down under both control and saline conditions in the *athmgb9* mutant line compared with Col-0.

Figure 3.17B shows that *AtNit2* expression is not significantly different under control conditions between WT Col-0 and the *athmgb9* mutant, however *AtNit2* expression is slightly but significantly higher in the *athmgb9* mutant than Col-0 in 100 mM NaCl. Overall, this data indicates that AtHMGB9 might be partially regulating *AtNit2* under saline conditions.

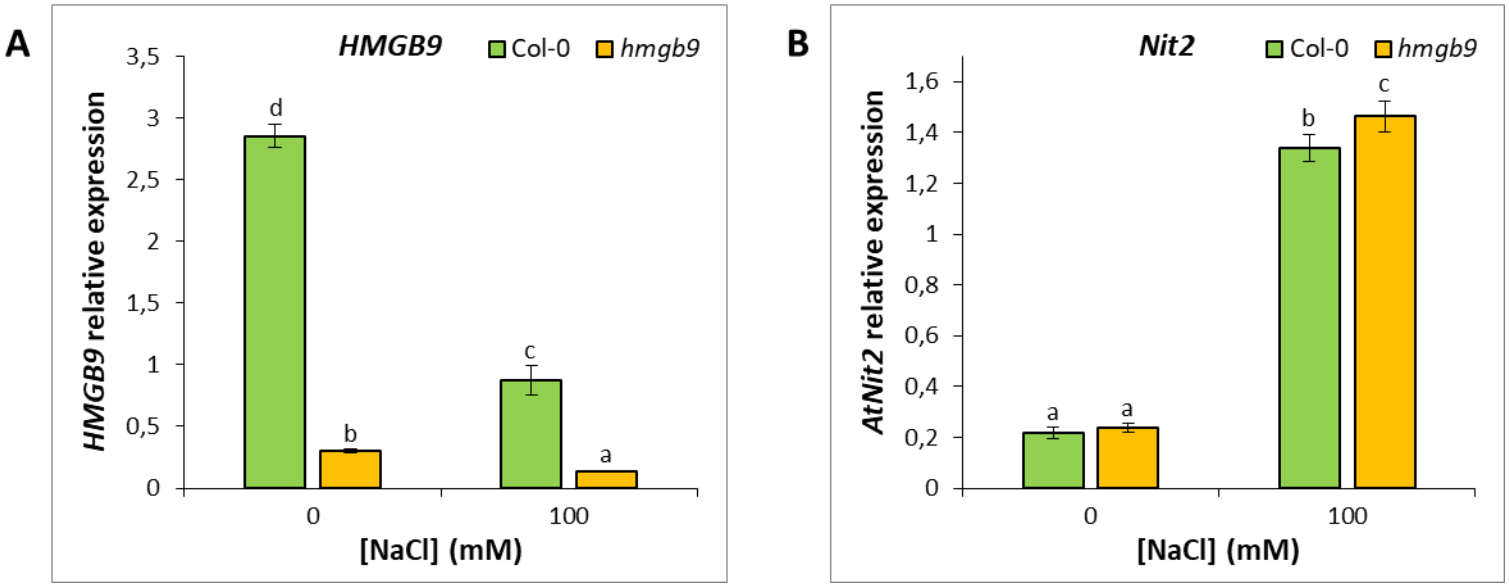

Figure 3.17: Expression of *AtNit2* and *AtHMGB9* in Col-0 and *athmgb9* lines under saline conditions

Arabidopsis seedlings were grown on PN-agar (control) or PN-agar supplemented with 100 mM NaCl for two weeks. Tissue was harvested and pooled for RNA extraction and cDNA was synthesised for RT-qPCR gene expression analysis. **A:** *AtHMGB9* expression. **B:** *AtNit2* expression. The results are an average of three pools of tissue (n=3). Expression of each gene is shown relative to the *AtMON1* reference gene. Error bars indicate standard error. Different letters on the graphs indicate significant differences ($p \leq 0.05$) in mean values as determined by a one-way ANOVA with Fisher LSD post-hoc analysis.

3.3.3.3. Characterisation of *atspl7* mutants

3.3.3.3.1. Identification of a homozygous *atspl7* mutant line

A homozygous *atspl7* T-DNA insertion line (SALK_125385C) was kindly provided by Toshiharu Shikanai (Kyoto University, Japan) (Yamasaki et al., 2009). These researchers showed that this line was homozygous for the T-DNA insertion, and that the T-DNA insertion site was in the fifth intron, as shown in figure 3.18.

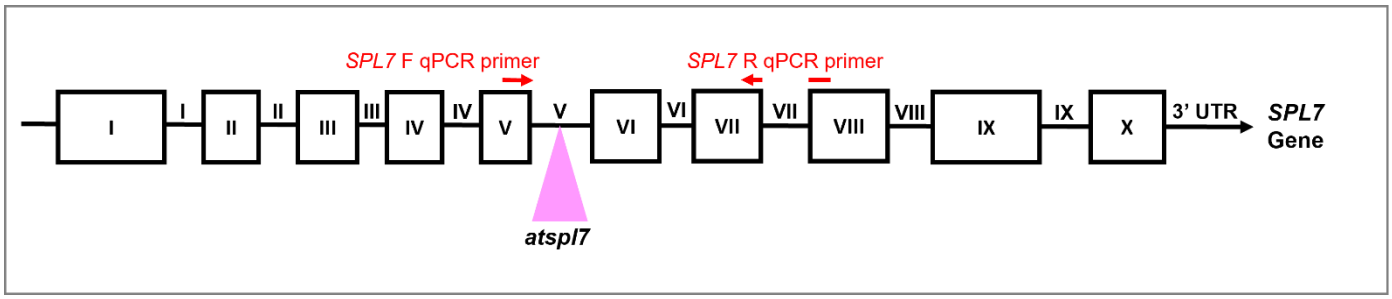

Figure 3.18: Site of the T-DNA insertion in the *atspl7* line

The T-DNA insertion for *atspl7* (blue triangle) is in the fifth intron in the *AtSPL7* gene. Exons, as annotated by TAIR, are depicted by black boxes, whereas introns are depicted as black lines. The red arrows represent the *AtSPL7* qPCR primer set.

To confirm that there was no full length *AtSPL7* mRNA being produced, RT-PCR was used. Leaves were harvested from three different *atspl7* plants, as well as Col-0 plants as a control (as these lines were generated in the Col-0 background), and RNA extraction and subsequent cDNA synthesis were performed. An end-point PCR using primers which amplified the full-length *AtSPL7* coding sequence (*AtSPL7* FL F and R) was performed and showed no amplification in the mutants (figure 3.19A) whereas there was amplification of the *AtSPL7* sequence in the Col-0 controls, as expected. A PCR using the *AtAct2* reference gene primers was used to confirm the integrity of the cDNA and shows a band for each of the samples (figure 3.19B), confirming that the lack of a product in the *AtSPL7* PCR is not due to poor RNA quality or inadequate cDNA synthesis. Overall, this indicates that this line has knocked-out expression of *AtSPL7.*

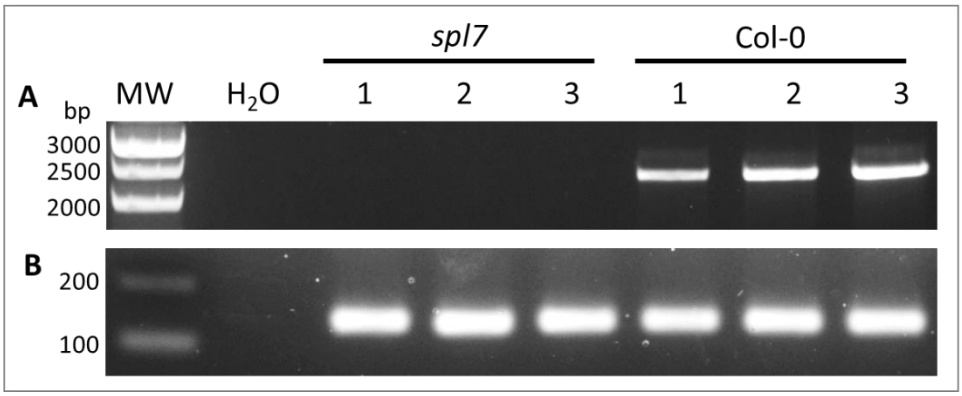

Figure 3.19: PCR confirming that there is no full-length *AtSPL7* expression in the *atspl7* T-DNA mutant line

A: PCR was performed on cDNA from three mutant and Col-0 plants using *AtSPL7* full-length gene primers (*AtSPL7* FL F and R) with an expected amplicon size of 2406 bp. **B:** PCR was performed on the same samples using the *AtAct2* reference gene primers, with an expected amplicon size of 138 bp, confirming integrity of the cDNA. H_2O was used as the template in the negative control reactions. The MW marker included is the Promega 1 kb DNA ladder.

3.3.3.3.2. Growth of *atspl7* plants exposed to salinity early in development

To determine whether knocking out *AtSPL7* expression has an impact on plant growth in saline conditions, Col-0 and *atpl7* plants were germinated and grown for two weeks as described previously. The average mass/plant of the two lines was compared for each treatment to identify any phenotypic differences in their growth. This experiment was repeated three times, with four technical replicates each, and the results were consistent.

Figure 3.20A shows that biomass was significantly reduced in both genotypes under saline conditions, as expected. It also shows that no significant differences were seen between the WT Col-0 and *atspl7* lines under untreated conditions, but that the *atspl7* plants were significantly smaller than Col-0 on 100 mM NaCl. However, when plotting the mass per plant relative to the untreated control for each line, it is evident that the Col-0 WT and *atspl7* line display the same degree of growth inhibition under 100 mM NaCl conditions (figure 3.20B). To determine whether different NaCl concentrations have any impact, this experiment was repeated once with various NaCl concentrations (figure 3.20C). Here, it is evident that only under high NaCl concentrations is there a significant difference between the salt tolerance of WT and *atspl7,* with the biomass of the mutant being more inhibited under 125 mM NaCl

than WT. Overall, this data indicates that the *atspl7* mutant does not show any pronounced differences in growth compared to WT under low NaCl conditions but might be more sensitive to salinity under high concentrations of NaCl (but this needs confirming).

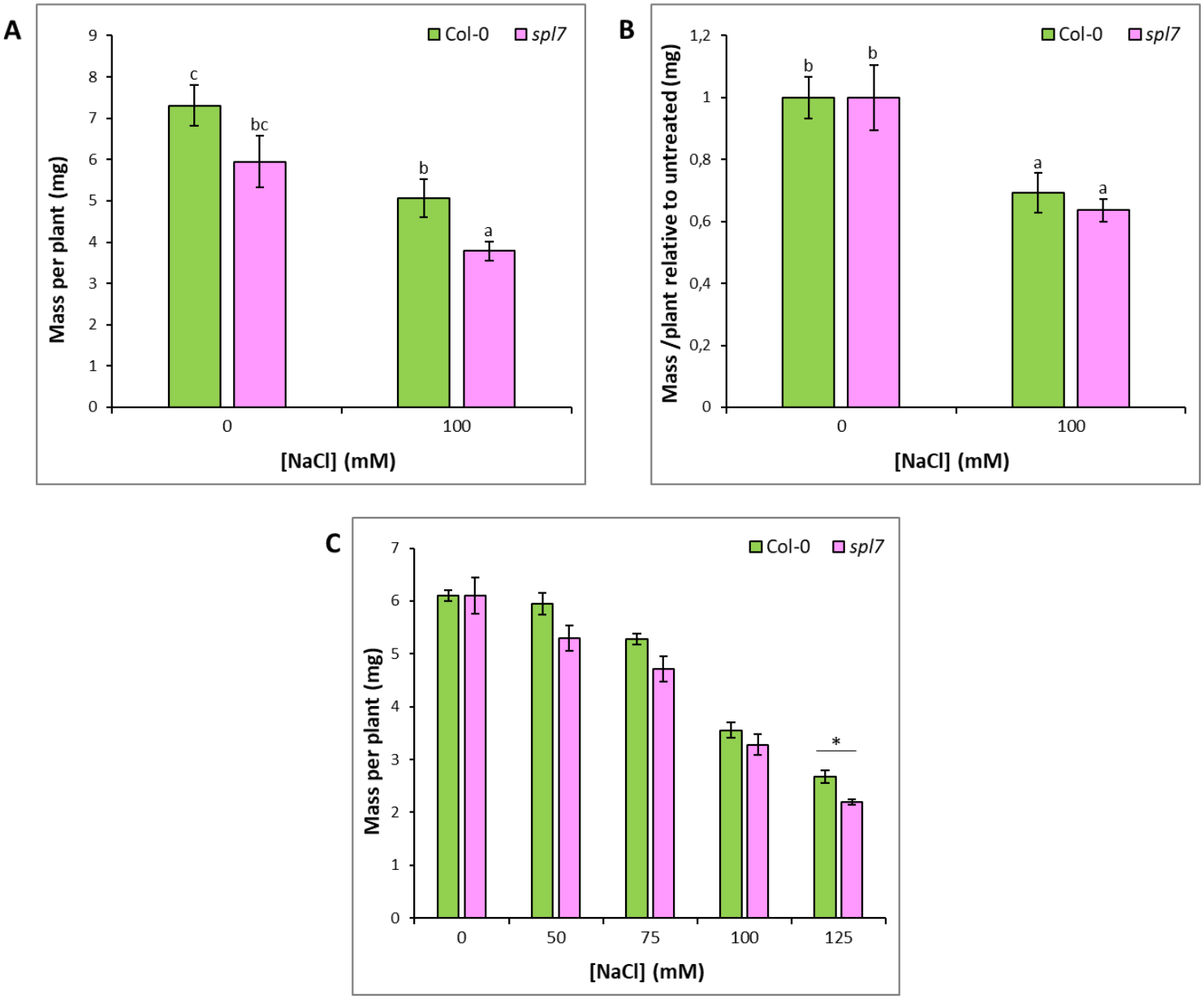

Figure 3.20: Growth of *atspl7* plants exposed to salinity early in development

Col-0 and *atspl7* plants were germinated and grown for two weeks on petri dishes containing untreated PN-agar (control) and PN-agar supplemented with the indicated concentrations of NaCl. The average mass per plant of each line is plotted, with the error bars indicating the standard error. **A:** The average mass per plant of each line. **B:** The average mass per plant plotted relative to the control (0 mM) for each line. For each treatment, the results show four replicates combined from

three independent experiments with 50 seeds sown per plate (n=12). Different letters on the graphs indicate significant differences ($p \leq 0.05$) in mean values as determined by a one-way ANOVA with Fisher LSD post-hoc analysis. **C:** The average mass per plant of each line on varying NaCl concentrations. The results show four replicates for each treatment with 50 seeds sown per plate (n=4). Asterisks represent statistical differences between the lines as determined from a two-tailed homoscedastic t-test ($p \leq 0.05$).

3.3.3.3.3. Gene expression in the *atspl7* mutant line

To determine whether knocking down *AtSPL7* expression is correlated with changes in *AtNit2* levels, tissue was collected from Col-0 and *atspl7* plants that had been germinated and grown for two weeks on petri dishes containing PN-agar (control) and PN-agar supplemented with 100 mM NaCl.

Figure 3.21A firstly confirms that *AtSPL7* is indeed knocked out under both control and saline conditions in the *atspl7* mutant line. This data also shows that *AtSPL7* is slightly upregulated in Col-0 under 100 mM NaCl compared to untreated conditions, as previously seen in the microarray (figure 3.9K).

Figure 3.21B shows that *AtNit2* expression is significantly upregulated in Col-0 in 100 mM NaCl compared to untreated conditions, as expected. Interestingly, *AtNit2* expression was significantly higher in the *atspl7* KO line in both untreated and saline conditions, compared to Col-0.

Overall, this data indicates that decreasing *AtSPL7* expression might lead to increased *AtNit2* expression, implying that *AtSPL7* might be negatively regulating *AtNit2* under both untreated and saline conditions. However, since AtSPL7 could not significantly transactivate or transrepress the *AtNit2* promoter in the protoplast transactivation assays (figure 3.12), this increased *AtNit2* expression is likely an indirect effect of long-term *AtSPL7* loss-of-function.

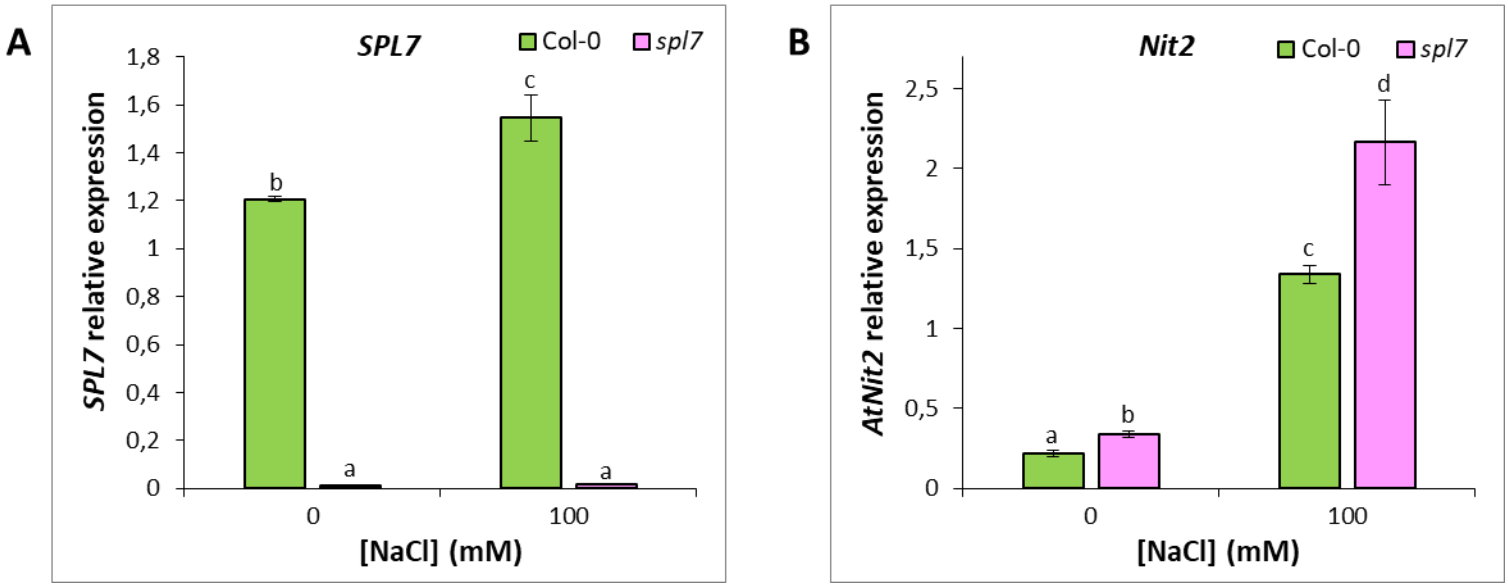

Figure 3.21: Expression of *AtNit2* and *AtSPL7* in Col-0 and *atspl7* lines under saline conditions

Arabidopsis seedlings were grown on PN-agar (control) or PN-agar supplemented with 100 mM NaCl for two weeks. Tissue was harvested and pooled for RNA extraction and cDNA was synthesised for RT-qPCR gene expression analysis. **A:** *AtSPL7* expression. **B:** *AtNit2* expression. The results are an average of three pools of tissue (n=3). Expression of each gene is shown relative to the *AtMON1* reference gene. Error bars indicate standard error. Different letters on the graphs indicate significant differences ($p \leq 0.05$) in mean values as determined by a one-way ANOVA with Fisher LSD post-hoc analysis.

3.4. DISCUSSION

3.4.1. Y1H analysis identified six TFs with the ability to bind the *AtNit2* promoter DNA

A yeast one-hybrid assay was used to screen a TF library (Pruneda-paz et al., 2014) to identify TFs that are able to bind directly to fragments of the *AtNit2* promoter (Col-0 ecotype). This method is useful as an unbiased, high-throughput screen for identifying protein/DNA binding but is unfortunately prone to false-negative results as many TFs may not be able to bind in isolation or may require binding at a fixed distance from the transcription start site (TSS) (Hickman et al., 2013). Additionally, TFs may require post-translational modifications (PTMs) to be active that do not occur in yeast (Fuxman Bass, Reece-Hoyes & Walhout, 2016). These are some of the disadvantages of using the Y1H to screen for interactions between plant TFs and promoters, as performing a reporter assay in yeast cells as opposed to plant cells may

decrease the likelihood that the results obtained mirror what happens *in planta*. For instance, no interaction was detected between AtATAF2 and the *AtNit2* promoter, but AtATAF2 has been shown to bind directly to the *AtNit2* promoter in a previous study where they used an electrophoretic mobility shift assay (EMSA) as well as in transient protoplast transactivation assays (Huh et al., 2012). This also means that the lack of interaction between AtMYB30 or AtMYB2 and the *AtNit2* promoter in the Y1H does not disprove the hypothesis that they may be regulators of *AtNit2,* especially seeing as though previous research has shown that AtMYB30 needs to be SUMOlyated by AtSIZ1 before it is able to bind to the *AtAOX1a* promoter and upregulate *AtAOX1a* gene expression in response to salt stress (Gong et al., 2020). Nevertheless, six TFs that had never previously been linked to *AtNit2* were identified that bound specifically to one or more of the *AtNit2* promoter fragments. These were AtHB34, AtHB24, AtHB28, AtHMGB9, AtGL2, and AtSPL7 (table 3.4).

3.4.2. The homeobox (HB)/zinc finger-homeodomain (ZF-HD) TFs

Three of the identified TFs, AtHB34, AtHB24, and AtHB28, belong to the homeobox (HB) TF family and contain a homeodomain (HD). The HD is a 60-amino acid DNA-binding domain (BD) found in many transcription factors (Tan & Irish, 2006). About 100 HD-encoding genes have been identified In Arabidopsis, belonging to a few different classes (Chan et al., 1998; Riechmann, 2002). Previous research has shown that the members of each class share both sequence similarity and play related roles *in planta*, although the role of the ZF-HD TFs has not been as extensively characterised as the other HD classes (Tan & Irish, 2006). The ZF-HD class is made up of 14 TFs, AtHB21-34. Tan & Irish (2006) showed through Y2H analysis that most of the members of the ZF-HD family heterodimerize with other members of the family and some are able to homodimerize. Each of the three ZF-HD proteins identified in our Y1H screen were shown to strongly interact with at least three other members of the TF family, however not with each other. They were also unable to homodimerize. The same researchers also showed through loss-of-function mutants that a subset of these genes have redundant functions, including AtHB34 which seems to be redundant with AtHB23 and AtHB30 (Tan & Irish, 2006). This data implies that even though AtHB24, AtHB28 and AtHB34 were the only ZF-HD TFs that directly interacted with the *AtNit2* promoter DNA in the Y1H analysis, there may be other members of this family that heterodimerize with these TFs for them to effect any change on transcriptional regulation. Additionally, there may be redundancy between the

three ZF-HD TFs that do bind to the *AtNit2* promoter, and therefore only one or two, but not all three may be necessary for appropriate *AtNit2* regulation.

The results of the pairwise Y1H experiment with each of the interacting TFs (figure 3.7) suggests that all three ZF-HD TFs are able to bind to *AtNit2* promoter fragment 3, suggesting that this fragment may contain a conserved ZF-HD binding site. As AtHB24 and AtHB28 are also able to bind fragments 2 and 4, it is likely that there are at least three ZF-HD motifs in the *AtNit2* promoter. The canonical binding site for most HD proteins is NNATTA (Fraenkel et al., 1998; Connolly, Augustine & Francklyn, 1999), with 34 sites conforming to this sequence across all four fragments of the *AtNit2* promoter. To explicitly map the binding sites of these TFs, EMSAs or ChIP-qPCR can be conducted in future. Surprisingly, DAP-seq data in the Plant Cistrome Database (http://neomorph.salk.edu/dap_web/pages/index.php; O'Malley et al., 2016) has shown binding of AtHB13 to the *AtNit2* promoter, but no other ZF-HD TFs (see appendix figure 6.9).

Interestingly, *AtHB34* and *AtHB28* were slightly upregulated under saline conditions early in development (figure 3.9A & E) but appeared to slightly decrease under saline conditions later in development (figure 3.9B & F), indicating that their function may depend on developmental stage. *AtHB24* expression appeared to follow the same trend later in development (figure 3.9D) but was slightly downregulated under saline conditions early in development (figure 3.9C). Overall, none of these ZF-HD TFs were particularly salt-responsive meaning that they may not play a role in the salt stress response, but could play a role under other conditions, or that PTMs may be responsible for altering their activity under certain conditions. These TFs were not selected for further analysis in this project due to the redundancy present in the family. Their ability to bind to the *AtNit2* promoter *in planta* should be assessed in future work.

3.4.3. GL2

Of the six TFs identified in the Y1H screening, AtGL2 is the best characterised. AtGL2 is part of the homeodomain-leucine zipper (HD-Zip) class of HD proteins, and is generally considered to be a negative regulator of root hair growth and development and has also been linked with controlling development of the seed coat and mucilage (Di Cristina et al., 1996; Masucci et al., 1996; Ohashi et al., 2002; Han et al., 2020). It has been shown to act as both a

transcriptional activator and repressor of various genes (Di Cristina et al., 1996; Ohashi et al., 2002; Tominaga-Wada et al., 2009). Salinity has been shown to decrease CG methylation of the GL2 gene body, associated with reduction in *AtGL2* expression (Beyrne, Iusem & González, 2019) – consistent with our findings that *AtGL2* showed a strong dose-dependent decrease in expression early in development under saline conditions (figure 3.9I), however no change in expression was seen later in development (figure 3.9J). This data suggests that if AtGL2 is involved in *AtNit2* regulation, it may be acting as a repressor early in development as its expression pattern is opposite to that of *AtNit2.*

The GL2-gene-specific recognition sites are known as L1 boxes, with a sequence of TAAATG(C/T)A (Abe, Takahashi & Komeda, 2001). The AtGL2 protein has been shown to bind to L1-box DNA through Y1H analysis (Tominaga-Wada et al., 2009). Notably, the only motif conforming to this L1-box is a TAAAATG motif on the negative strand of the *AtNit2* promoter fragment 4, which in the pairwise Y1H screening showed strong interaction with AtGL2. Future research can be conducted to test the interaction between AtGL2 and the *AtNit2* promoter *in planta* and determine whether AtGL2 is able to negatively or positively alter *AtNit2* promoter activity. Arabidopsis mutants with *AtGL2* KO and OE exist and would be interesting to characterise for their salt tolerance and *AtNit2* expression, but we have been unable to access these.

3.4.4. HMGB9

AtHMGB9 belongs to the group of Arabidopsis high mobility group B proteins which also includes AtHMGB10, AtHMGB11 and AtHMGB15. This subfamily is classified as ARID/HMG proteins due to containing two DNA binding domains: an N-terminal AT-rich interaction domain (ARID), and a C-terminal HMG-box domain. Hansen et al. (2008) showed that these ARID/HMG TFs are widely expressed in Arabidopsis and localise mainly in nuclei, and that AtHMGB9 binds specifically to A/T-rich DNA. Multiple studies have shown that *AtHMGB9* is more highly expressed in leaves, flowers, and seedlings compared to roots and seeds (Hansen et al., 2008; Roy et al., 2016), which is consistent with our findings that *AtHMGB9* is more highly expressed in shoot tissue than root tissue (figure 3.9H). AtHMGB9 shares a 43% amino acid sequence identity with AtHMGB15, a TF that plays an important role in regulating gene expression during pollen tube growth (Xia et al., 2014). However, until recently, this was the

only study to show a physiological role for any of these ARID/HMG proteins. Recently, the promoter region of *AtHMGB15* was analysed and a number of stress responsive *cis* regulator elements (CREs) were identified. The same study showed that expression of *AtHMGB9* was induced by cold stress, and that AtHMGB15 bound to the A(A/C)ATA(A/T)(A/T) motif in DNA binding and footprinting assays (Mallik et al., 2020). Notably, in the pairwise Y1H screening (figure 3.7), AtHMGB9 bound specifically to fragments 2 and 4 of the *AtNit2* promoter – two regions containing an AAATAAA motif. Moreover, fragment 2 which showed stronger interaction with AtHMGB9 (as indicated by growth in 10 mM 3AT) contains two of these motifs, whereas fragment 4 only contains one. Interestingly, The Plant Cistrome Database (http://neomorph.salk.edu/dap_web/pages/index.php; O'Malley et al., 2016), containing DAP-seq data from Arabidopsis seedlings, does not include a peak for AtHMGB9 upstream of *AtNit2* (see appendix figure 6.9). However, it does show that the top motif for AtHMGB9 is A(A/T)TTAAT, a region present multiple times in the *AtNit2* promoter tested. Therefore, there may have just not been binding of AtHMGB9 to the promoter under their conditions tested.

Our findings show that *AtHMGB9* expression decreased in a dose-dependent manner early in development under saline conditions (figure 3.9G) and later in development in shoot tissue (figure 3.9H). These results were opposite to those for *AtNit2,* suggesting that AtHMGB9 may act as a negative regulator of *AtNit2* expression. Figure 3.12 shows that AtHMGB9 transrepresses *AtNit2* promoter activity *in planta*, confirming this hypothesis that AtHMGB9 is able to repress *AtNit2* expression. However, *athmgb9* lines showed only a slight increase in *AtNit2* expression under saline conditions (figure 3.17B) which suggests that AtHMGB9 may only be partially regulating *AtNit2* under saline conditions. Additionally, *AtNit2* expression was not altered in the *athmgb9* mutant in control conditions, implying that AtHMGB9 might not regulate *AtNit2* expression under control conditions, or that another TF is responsible for maintaining *AtNit2* expression at a baseline level under control conditions, i.e., there could be another *AtNit2* repressor able to keep *AtNit2* expression stable in untreated conditions when *AtHMGB9* is knocked down, or an activator that ensures *AtNit2* is expressed irrespective of AtHMBG9. Interestingly, *athmgb9* knock-down lines showed slightly decreased salt tolerance (despite slightly higher *AtNit2* expression) (figure 3.16) implying that AtHMGB9 could be responsible for other important processes in the salt-stress response besides regulating *AtNit2* gene repression. These lines should be analysed later in development to

identify any changes in *AtNit2* expression or salt tolerance as *AtHMGB9* expression is decreased in response to 100 mM NaCl later in development (figure 3.9H) .

3.4.5. SPL7

Previous research has shown that AtSPL7 is a transcriptional activator of many genes involved in copper (Cu) homeostasis (e.g. copper transport proteins) in Arabidopsis (Yamasaki et al., 2009; Araki et al., 2018; Busoms et al., 2021), and it has been shown to be upregulated by abscisic acid (ABA) (Carrió-Seguí et al., 2016) and Cu-deficiency (Yamasaki et al., 2009). The role of AtSPL7 in copper deficiency has been extensively investigated, but no potential role in auxin biosynthesis via *AtNit2* has been investigated.

Yamasaki et al. (2009) showed that the SQUAMOSA promoter binding protein (SBP) domain of AtSPL7 binds to GTAC motifs in the *miR398* promoter *in vitro*. Interestingly, two GTAC motifs exist in the *AtNit2* promoter, however these are in fragments 1 and 2, whereas AtSPL7 interacted specifically with fragment 4 of the *AtNit2* promoter. More recently, a study showed that AtSPL7 can bind to various motifs with the only conserved nucleotides being a central TAC (Weirauch et al., 2014), of which there are 20 in the *AtNit2* promoter across all four fragments. Further research will need to be conducted if the exact binding site of AtSPL7 in the *AtNit2* promoter is to be determined.

Previous work has shown that *AtSPL7* mRNA accumulates mainly in roots (Yamasaki et al., 2009), consistent with our findings (figure 3.9L). Notably, *AtNit2* is more highly expressed in shoot tissue (Cackett, 2019). The analysis of *AtSPL7* expression from the microarray data shows that *AtSPL7* is not significantly altered under saline conditions early or later in development (figure 3.9K &L), besides for a slight decrease early in development in the highest NaCl concentration tested (125 mM). However, other data obtained showed that *AtSPL7* was slightly upregulated in response to 100 mM NaCl in Col-0 (figure 3.21B). Overall, it appears as though *AtSPL7* expression is not particularly salt responsive. However, this does not mean that AtSPL7 does not play a role in *AtNit2* regulation as the transcript level of *AtSPL7* may not need to be altered to affect its activity. Instead, post-transcriptional/translational modifications or processes may be occurring to activate this TF, and differential binding with other co-factors may be involved in modulating AtSPL7 activity under different conditions.

We showed that AtSPL7 did not alter *AtNit2* promoter activity in transient reporter assays *in vivo* (figure 3.12), indicating that AtSPL7 does not bind to the *AtNit2* promoter in Arabidopsis mesophyll protoplasts, or that binding of AtSPL7 alone is not sufficient to alter *AtNit2* promoter activity. This implies that AtSPL7 may only be able to alter *AtNit2* promoter activity under certain conditions, or in certain tissues/cell types, or with certain co-factors, as earlier predicted. Specifically, as *AtSPL7* is primarily expressed in root tissue (figure 3.9L), it may only be able to alter promoter activity in this tissue type. This protoplast reporter assay should also be repeated with different incubation times to determine if this makes any difference. Interestingly, *atspl7* KO plants showed increased *AtNit2* expression under both control and saline conditions early in development (figure 3.21B), but this was not associated with any consistent changes in salt tolerance (figure 3.20). The magnitude of *AtNit2* upregulation was less than 2-fold, and this therefore shows that small changes in *AtNit2* expression are not able to improve salt tolerance. This data does however imply that *AtSPL7* might be important in negatively regulating *AtNit2* expression, but not specifically under saline conditions. Further work should be conducted to investigate what conditions, co-factors or post-transcriptional/translational modifications may be necessary for AtSPL7 to regulate *AtNit2* activity.

3.4.6. Summary

The results presented here are the first to show that AtHB24, AtHB28, AtHB34, AtHMGB9, AtGL2 and AtSPL7 are able to bind directly to the *AtNit2* promoter in yeast. Furthermore, AtHMGB9 is able to bind to and negatively regulate *AtNit2* promoter activity *in planta,* implying that AtHMGB9 is a negative regulator of *AtNit2.* However, *athmgb9* mutant lines displayed only slightly increased *AtNit2* expression under saline conditions, and were slightly less salt tolerant, indicating that other regulators must exist to maintain *AtNit2* expression. When transiently overexpressed in Arabidopsis mesophyll protoplasts, AtSPL7 was unable to alter *AtNit2* promoter activity, but *atspl7* lines showed slightly increased *AtNit2* expression, indicating that AtSPL7 may play a role in negatively regulating *AtNit2* expression but may require other co-factors. This slight increase in *AtNit2* expression was not associated with any changes in salt tolerance, suggesting that *AtNit2* expression needs to be more highly upregulated to increase salinity tolerance. Overall, it seems as though multiple TFs may play roles in *AtNit2* regulation under different conditions.

CHAPTER 4: FUNCTIONAL CHARACTERISATION OF THE MAIZE *NITRILASE 2* HOMOLOG UNDER SALINE CONDITIONS IN ARABIDOPSIS

4.1. INTRODUCTION

4.1.1. Maize

Maize (*Zea mays*) is one of the most important crop plants globally and is grown under a wide spectrum of soil and climatic conditions. Based on tonnage, maize is the most produced staple crop worldwide, with 1162352997 tonnes produced in 2020 (http://www.fao.org/faostat). To put this into perspective, wheat was the second-most produced staple crop, with 35% less produced. The main reason for this is the versatility of maize, as it provides essential raw material for food, livestock feed, pharmaceuticals, and other industrial products. While significant advances have been made in improving maize since domestication, advancements in yield and stress tolerance are still needed in order to address the food demand from increasing population sizes under changing climates (Gong et al., 2015).

Although maize is categorised as being moderately sensitive to salt stress (Maas et al., 1983; Chinnusamy, Jagendorf & Zhu, 2005), there is a wide intraspecific genetic variation observed for salt tolerance (Mansour et al., 2005). This large genotypic variation for salt tolerance makes maize a good candidate for integrating tolerance characteristics through conventional breeding strategies in order to develop more salt tolerant plant lines, or through transgenic approaches which are much faster than conventional breeding and can be used to engineer more salt tolerant maize with less undesirable side effects, but rely on the identification of candidate genes (Gosal, Wani & Kang, 2010; Hoopes et al., 2019). Thus far, several countries have been receptive to advances in crop genetic engineering, including growing genetically modified (GM) maize. One example of GM maize is the commercially available DroughtGard™, produced by Monsanto, that has an insertion of the *Cold shock protein B* (*CspB*) gene from *Bacillus subtilis* that confers enhanced drought tolerance (Eisenstein, 2013). This GM maize line is currently being grown in several countries, including Nigeria, the United States of America, Canada and Japan ("GM Approval Database - MON-8746Ø-4", 2022), indicating that there is already precedent to accept GM maize.

In maize, salinity induces many different resistance mechanisms similar to those employed in Arabidopsis (Farooq et al., 2015). Of particular interest, more naturally salt tolerant maize varieties are thought to maintain growth under saline conditions according to the acid growth theory (Hager, 2003). In contrast to the salt-sensitive maize hybrid Pioneer 3906, the salt-resistant hybrid SR 03 maintained plasma membrane H^+ pumping and had reduced apoplastic pH in the presence of 100 mM NaCl (Pitann, Zörb & Mühling, 2009). This indicates that our hypothesis in Arabidopsis whereby *AtNit2* upregulation in saline conditions increases active auxin accumulation and auxin-mediated activation of the plasma membrane H^+-ATPase to improve salt tolerance, might also be relevant in maize.

4.1.2. Maize nitrilases

As previously introduced, nitrilase proteins are found throughout the plant kingdom and possession of nitrilase genes is thought to be the ancient state in higher plants (Piotrowski, 2008). There are two nitrilase genes in maize, *ZmNit1* and *ZmNit2*, which are co-orthologs of *AtNit1-4*. This is evident in the phylogenetic tree in appendix figure 6.1 which shows that *AtNit1-4* duplicated and diversified after the monocot-dicot split. However, ZmNIT2 has been shown to hydrolyse IAN to IAA, with an efficiency up to 20 times higher than AtNIT1/2/3 (Vorwerk et al., 2001; Park et al., 2003; Mukherjee et al., 2006). Furthermore, *ZmNit2* is expressed in maize tissues that show auxin-synthesising activity, such as kernels and primary root tips (Jensen & Bandurski, 1994). Additionally, *zmnit2* knockout mutants also accumulate significantly less IAA conjugates in kernels and primary root tips where nitrilase protein and IAN are present (Kriechbaumer et al., 2007). Conversely, ZmNIT1 has shown no specific turnover of IAN and instead has only been implicated in β-cyanoalanine hydrolysis during cyanide detoxification (Park et al., 2003; Mukherjee et al., 2006; Kriechbaumer et al., 2007) which makes it functionally homologous to AtNIT4. To date, *ZmNit2* has not be implicated in the maize response to salt stress.

4.1.3. Chapter aims

The overall objective of this chapter was to determine whether our work in Arabidopsis is relevant to maize. To this end, there were three main aims; 1) to determine the effect that salinity has on growth and development of a South African maize variety, Kalahari Early Pearl, and to determine whether the maize homolog of *AtNit2* is upregulated under saline

conditions, 2) to generate Arabidopsis lines overexpressing the maize *Nit2* homolog and determine whether it is able to phenocopy *AtNit2* by improving salt tolerance, and 3) to investigate whether the maize *Nit2* homolog may be regulated similarly to *AtNit2.*

4.2. MATERIALS AND METHODS

4.2.1. Maize seed stock

Zea mays L. commercial white maize variety Kalahari Early Pearl (KEP) seeds were obtained from Kirchhoffs (Johannesburg, South Africa).

4.2.2. Maize seed sterilisation

Maize seeds were surface sterilised by submerging in 100% (v/v) ethanol (EtOH) for 1 min, followed by shaking for 30 sec after which the EtOH was aspirated off. Thereafter, the seeds were submerged in 50% (v/v) commercial bleach, 0.1% (v/v) Triton-X 100 for 15 min followed by shaking for 1 minute before the bleach mixture was aspirated off. The sterilised seeds were then washed five times in sterile dH_2O with shaking for 30 sec between each wash. Following the last wash, the seeds were covered in sterile dH_2O and left for 1 hour after which the seeds were removed and allowed to dry overnight on sterile filter paper, in a petri dish sealed with parafilm.

4.2.3. Hoagland's complete nutrient solution

Maize was grown hydroponically using a modified Hoagland's solution containing 1 mM KH_2PO_4, 6 mM KNO_3, 4 mM $Ca(NO_3)_2.4H_2O$, 2 mM $MgSO_4.7H_2O$, 0.05 mM FeNaEDTA and micronutrients (46 µM H_3BO_3, 9.11 µM $MnSO_4.H_2O$, 0.77 µM $ZnSO_4.7H_2O$, 0.32 µM $CuSO_4.5H_2O$ and 0.103 µM $Na_2MoO_4.2H_2O$) (Hoagland & Arnon, 1950). All Hoagland's solution components were obtained from Merck (Darmstadt, Germany)

4.2.4. Maize phenotyping in saline conditions

Maize was grown hydroponically using a modified version of the Arabidopsis Araponics System described in section 2.2.6.2 (Araponics SA, Belgium). The system was modified in order to accommodate the size of the maize seeds and subsequent growth. A seed holder system was made consisting of 50 mL plastic conical-bottomed centrifuge tubes that were cut

in half at the 25 mL mark as well as at the base such that there was a hole large enough for the maize roots to grow through into the media. A small piece of rockwool was added to the bottom of each tube followed by 2 cm of vermiculite, onto which a sterilised maize seed was placed. The 1.8 L boxes were filled with Hoagland's solution and the homemade seed holder placed on top of the boxes, such that the bottom of the tubes containing the rockwool were submerged. Lids covered the system for four days to increase the humidity for germination. On the fifth day, five seedlings of the same size were randomly transferred onto fresh Hoagland's solution supplemented with 0, 75, 150, 225 or 300 mM NaCl. An air pump (Rena Air 300) was used to aerate the media from this point onwards. On day 14, after nine days of growth in control or saline conditions, root and shoot tissue was weighed. Additionally, tissue from the second leaf or from the root of three plants in each treatment were harvested and pooled for RNA extraction. Three independent biological experiments were conducted to obtain three biological replicates. All growth was carried out in a controlled growth room at 27°C, 50-60% relative humidity and a 12-hr light (200 $\mu mol.m^{-2}.s^{-1}$)/12-hr dark cycle.

4.2.5. Identification of maize gene homologs

The BLAST tool on the National Centre for Biotechnology Information (NCBI) website (https://blast.ncbi.nlm.nih.gov/Blast.cgi) was used to identify maize homologs of the two putative transcription factors characterised in the previous chapter, *AtHMGB9* and *AtSPL7.* A protein-protein BLAST (BLASTp) search was conducted to query the respective Arabidopsis protein sequence against the *Zea mays* non-redundant protein sequence database. Thereafter, a reciprocal BLASTp search was performed to query the protein sequence of the best match/top hit from maize against the Arabidopsis database.. The available literature was also consulted in order to determine the correct homologs.

4.2.6. Maize RNA extraction and cDNA synthesis

Shoot and root tissue from the hydroponically grown maize were harvested and frozen immediately in liquid nitrogen. The tissue was ground in liquid nitrogen using a mortar and pestle after which approximately 100 mg of ground tissue was added to 1 mL TRIzol reagent. Subsequent RNA extraction, DNase treatment, quality determination and cDNA synthesis were carried out as described in chapter 2, section 2.2.9.

4.2.7. Maize gene expression analysis by RT-qPCR

RT-qPCR was performed on the maize shoot and root cDNA as described in chapter 2, section 2.2.12, using the primers listed in table 4.1. The annealing temperature used for all primers was 60°C. Maize membrane protein PB1A10.07c (*ZmMEP*, GRMZM2G018103) was used as a reference gene (Manoli et al., 2012). The data generated was analysed using the Rotor-Gene software and Microsoft Excel, and statistical analyses were conducted in Statistica as described in chapter 2, section 2.2.22.

4.2.8. Arabidopsis seed stocks and growth

The Arabidopsis wild type No-0 ecotype was used as the background to generate the 35S::*ZmNit2* and 35S empty vector lines described in this chapter. The No-0 seeds were obtained from Bonnie Bartel (Rice University, Houston, Texas). All Arabidopsis seeds were stored at 4°C. All Arabidopsis plant growth was carried out in a plant growth room under standard conditions (100 $\mu mol.m^{-2}.s^{-1}$ light intensity, 16-hr light/8-hr dark, 22°C, 50-60% relative humidity).

4.2.9. Cloning of the *ZmNit2* overexpression vector

To generate a *ZmNit2* overexpression clone, Gateway Cloning Technology was used, following the same protocols and workflow as in chapter 2, section 2.2.17. The *ZmNit2* coding sequence was amplified from *Zea mays* B73 cDNA. In the BP recombination reaction, 150 ng of pDONR221 and 50 fmol (37.9 ng) of *att*B1-*ZmNit2*-*att*B2 PCR product were added. The resulting BP recombination reaction product was transformed into chemically competent *Escherichia coli* DH5α and the resulting entry clones were confirmed by PCR and sequencing. A LR recombination reaction was then used to transfer the *ZmNit2* CDS into the pB2GW7 destination vector to create a pB2GW7-*ZmNit2* expression clone containing the *ZmNit2* CDS downstream of the CaMV 35S promoter. The presence of the insert was confirmed by PCR analysis. The pB2GW7-*ZmNit2* vector was transformed into Agrobacterium as in chapter 2, section 2.2.19.3.

4.2.10. Transient *35S::ZmNit2* expression in tobacco

The pB2GW7-*ZmNit2* expression clone as well as EV were transiently expressed in *Nicotiana benthamiana* tobacco plants using the method as described by Regnard et al. (2010). Briefly,

Agrobacterium transformed with each vector were grown up overnight at 30˚C with shaking at 200 rpm in induction medium comprising selective LB and 10 mM MES 4-morpholineethane sulfonic acids (pH 5.6) supplemented with 20 µM acetosyringone. Cells were pelleted at 1000 x *g*, resuspended in infiltration medium (10 mM MES, 10 mM $MgCl_2$ (pH 5.6), 200 µM acetosyringone) and diluted in infiltration medium to an OD_{600} of 0.5. After incubation at 22˚C for two hours, cells were vacuum infiltrated into 4-week-old *N. benthamiana* plants grown in a plant growth room under standard conditions (60-80 $\mu mol.m^{-2}.s^{-1}$ light intensity, 16-hr light/8-hr dark, 22°C). After three days, tissue was collected for 1) RNA extraction and cDNA synthesis to validate transient expression by PCR, and 2) for leaf disc salt assays.

4.2.11. Leaf disc salt assays and chlorophyll analysis

A method was adapted from Sanan-Mishra et al. (2005) whereby leaf discs of 0.8 cm diameter were excised from plant leaves and floated in 3 mL solution of PN media (control) or PN supplemented with 100, 200 or 300 mM NaCl for three days. Thereafter, the leaf discs were transferred into 3 mL 80% (v/v) acetone and incubated at 4˚C in the dark for seven days for chlorophyll extraction. The chlorophyll *a* and *b* content were determined spectrophotometrically by taking absorbance readings of the extracted solutions at 663 nm and 646 nm and using the following calculations:

- Chl *a* = (12.21 x A663) – (2.81 x A646) for 1 ml 80% (v/v) acetone
- Chl *b* = (20.13 x A646) – (5.03 x A663) for 1 ml 80% (v/v) acetone

4.2.12. Transformation and isolation of *35S::ZmNit2* lines

The pB2GW7-*ZmNit2* expression vector, as well as EV (transformed into *A. tumefaciens* in chapter 2, section 2.2.19.3), were transformed into Arabidopsis (No-0 ecotype) using the Agrobacterium-mediated floral-dip transformation protocol as in chapter 2, section 2.2.20. Transformed lines were isolated on PN-agar supplemented with 10 µg/mL glufosinate ammonium (GFSA) as described in chapter 2, section 2.2.20.4. To confirm the presence of the transgene, PCR analysis was conducted as in chapter 2, section 2.2.11 and the resulting products were analysed using gel electrophoresis as in chapter 2, section 2.2.13. To confirm *ZmNit2* overexpression, Arabidopsis RNA extraction, DNase treatment, quality determination and cDNA synthesis were carried out as described in chapter 2, section 2.2.9. Thereafter, gene expression analysis was performed as in chapter 2, section 2.2.12. The data generated was

analysed using the Rotor-Gene software and Microsoft Excel, and statistical analyses were conducted as described in chapter 2, section 2.2.22.

4.2.13. Phenotyping *35S::ZmNit2* plant growth under saline conditions

Arabidopsis phenotyping under saline conditions was performed both early and later in development as in chapter 2, section 2.2.6. This was done in such a way to mimic the experiments done on *35S::AtNit2* plants as closely as possible.

4.2.14. Maize *Nit2* promoter analysis

PLACE (https://www.dna.affrc.go.jp/PLACE/?action=newplace) (Higo et al., 1999) was used for identification and visualisation of *cis*-regulatory promoter elements, including TFBS, in the *ZmNit2* promoter region 1kb upstream of the translation start site (ATG).

Table 4.1: The primers used for cloning, genotyping and gene expression analysis. F: forward primer, R: reverse primer

Primer name	Primer sequence (5'-3')	Reference (if applicable)	Amplicon size (bp)	Function	PCR kit	T_a
ZmMEP F *ZmMEP* R	TGTACTCGGCAATGCTCTTG TTTGATGCTCCAGGCTTACC	Manoli et al., 2012	203	RT-qPCR	SYBR® FAST	60˚C
ZmNit1 F *ZmNit1* R	GACGATGACTATGTGCAGACCTAA CAATCTCGTCCAATCCATGTATA	Park et al., 2003	204	RT-qPCR	SYBR® FAST	60˚C
ZmNit2 F *ZmNit2* R	CGCTGTATGGTAAAGGTATTGAG AGATGGAGAAATGATAACGCTG		239	RT-qPCR	SYBR® FAST	60˚C
ZmARID6 F *ZmARID6* R	GAGGTGTAGAGGATAAGGAGCGATA TGACAGCAGCATATCATCTTGGCT		170	RT-qPCR	SYBR® FAST	60˚C
ZmSBP11 F *ZmSBP11* R	AGGGGGAGGTTGGAAGATCA CCCTCCAAAGTCAGTGTTTTCAC		192	RT-qPCR	SYBR® FAST	60˚C
EF1α F *EF1α* R	TGGGCCTACTGGTCTTACTACTGA ACATACCCACGCTTCAGATCCT	Lin et al., 2014	135	PCR	Kapa RM	55˚C
*ZmNit2-att*B1 F *ZmNit2-att*B2 R	ggggacaagtttgtacaaaaaagcaggcttcATGGCTCTCGTGACCTCG* ggggaccactttgtacaagaaagctgggtcTCAGTAAGACTTAGTATCGATATCA*		1147	Cloning	Kapa HiFi	72˚C
				Genotyping	Super-Therm	55˚C
M13 F M13 R	GTAAAACGACGGCCAG CAGGAAACAGCTATGAC	Invitrogen	-	Sequencing	-	-
Bar F *Bar* R	AAGTCCAGCTGCCAGAAACC GAACTGACAGAACCGCAACG	Dr Lara Donaldson	733	Genotyping	Kapa RM	57˚C
P35S F *ZmNit2* int R	AATATCGGGAAACCTCCTCG GTCGGCTGTAATCAGTGCCT	Dr Lara Donaldson	1357	Genotyping	Kapa RM	53˚C
AtMON1 F *AtMON1* R	CAGACAAGGCGATGGCGATA GCTTTCTCTCAAGGGTTTCTGGGT	Hong et al., 2010	244	RT-qPCR	SYBR® FAST	60˚C
				PCR	Super-Therm	55˚C
AtEXP11 F *AtEXP11* R	TTGCGGTTGATGCGTTTAG GCCGAGTAAAGATCTCCGTAAC	Paul Ferrandi	118	RT-qPCR	SYBR® FAST	60˚C

***** *att*B sequences are shown in lowercase letters

4.3. RESULTS

4.3.1. Analysis of maize plant growth and gene expression under saline conditions

4.3.1.1. Maize growth and development are inhibited under saline conditions

To assess the impact of both the ion-independent and ion-dependent phases of NaCl stress on Kalahari early pearl (KEP) maize growth and development, a hydroponics-based assay was used. Figure 4.1 shows that plants grown under saline conditions for nine days have reduced number and size of leaves. Plants grown under control conditions on average have five leaves, whilst plants grown in 75 and 150 mM NaCl had four leaves and those in 225 and 300 mM NaCl had three leaves. This stalling of maize shoot development was associated with a change in the root architecture as there was a reduction in primary and seminal root length as the concentration of NaCl increased. Additionally, figure 4.1 also shows that, although maize growth was inhibited, the plants were able to survive and grow with no senescent tissue observed over the experimental period in all NaCl concentrations.

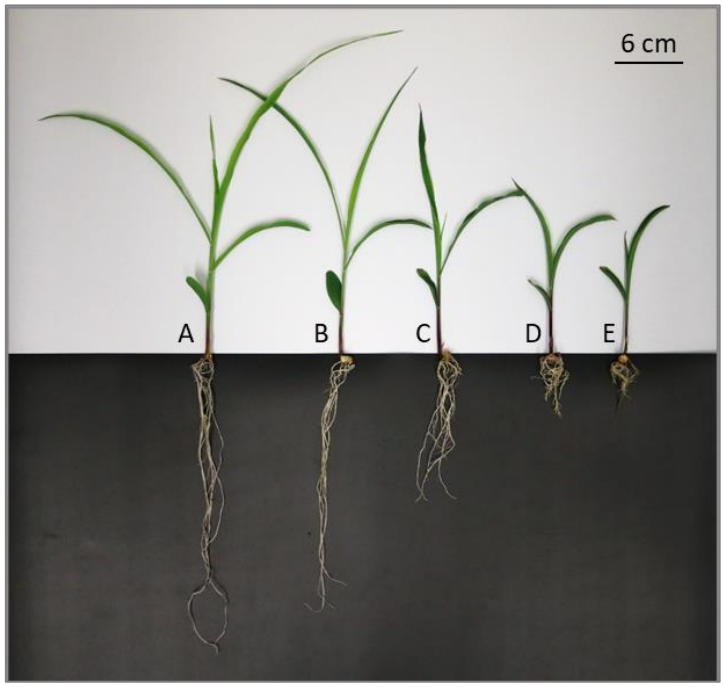

Figure 4.1: The impact of NaCl on maize growth and development

Maize plants were grown hydroponically in Hoagland's solution for five days then transferred onto fresh Hoagland's solution with or without NaCl for nine days. Letters on the plants refer to the concentration of the NaCl treatment; **A**: 0 mM (control), **B**: 75 mM, **C**: 150 mM, **D**: 225 mM and **E**: 300 mM with at least three plants analysed per treatment. The photo shows a single representative example and the whole experiment was repeated three times with consistent results.

Figure 4.2A and B show the effect of NaCl on KEP maize shoot and root mass. Both the shoot and root mass exhibited a dose-dependent reduction with increasing NaCl. At low doses, salt stress appears to be more inhibitory on shoot growth than on root growth. This translated into an increase in root:shoot ratio, as expected, however this was only significantly higher than the control in the 150 and 225 mM NaCl treatments (figure 4.2C). Overall, NaCl significantly reduced KEP maize shoot and root growth, as expected.

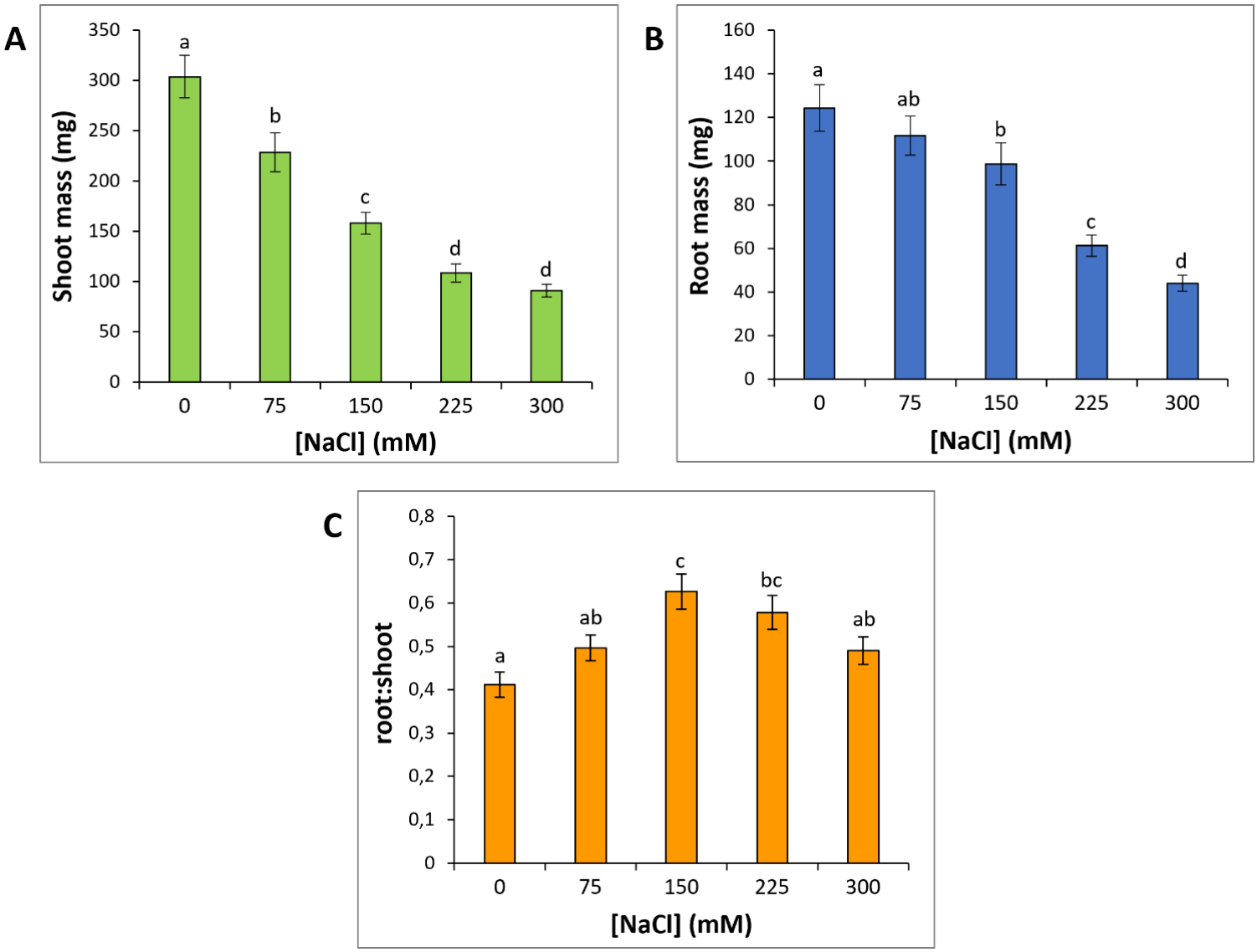

Figure 4.2: The impact of NaCl on maize root and shoot growth

Maize plants were grown hydroponically in Hoagland's complete nutrient solution for five days then transferred onto Hoagland's solution supplemented with the indicated concentrations of NaCl for nine days. Thereafter, shoot and root fresh biomass were measured for each plant. **A**: The average shoot

fresh mass. **B**: The average root fresh mass. **C**: The average root:shoot ratio. The results show data combined from three independent experiments with three plants measured for each treatment in each experiment (n=9). Error bars indicate standard error. Different letters on the graphs indicate significant differences ($p \leq 0.05$) in mean values as determined by a one-way ANOVA with Fisher LSD post-hoc analysis.

4.3.1.2. Nitrilase gene expression in maize grown under saline conditions

Maize nitrilase gene expression was analysed following salt treatment in hydroponics to determine whether the expression of *ZmNit2* or *ZmNit1* follows the trend seen with *AtNit2* where expression increased in a dose-dependent manner under saline conditions, primarily in shoot tissue (appendix figure 6.6) (Cackett, 2019). Maize shoot and root tissue were harvested separately from plants grown hydroponically on different concentrations of NaCl and used for RNA extraction and subsequent cDNA synthesis for RT-qPCR gene expression analysis.

Figure 4.3A shows that *ZmNit2* expression increases in maize in both root and shoot tissue in response to NaCl, in a dose-dependent manner. Figure 4.3B shows that expression of *ZmNit1* does not follow a dose-dependent expression pattern under saline conditions. Overall, this data shows that *ZmNit2* is upregulated by salinity and behaves similarly to *AtNit2,* despite no difference between the two tissue types being seen.

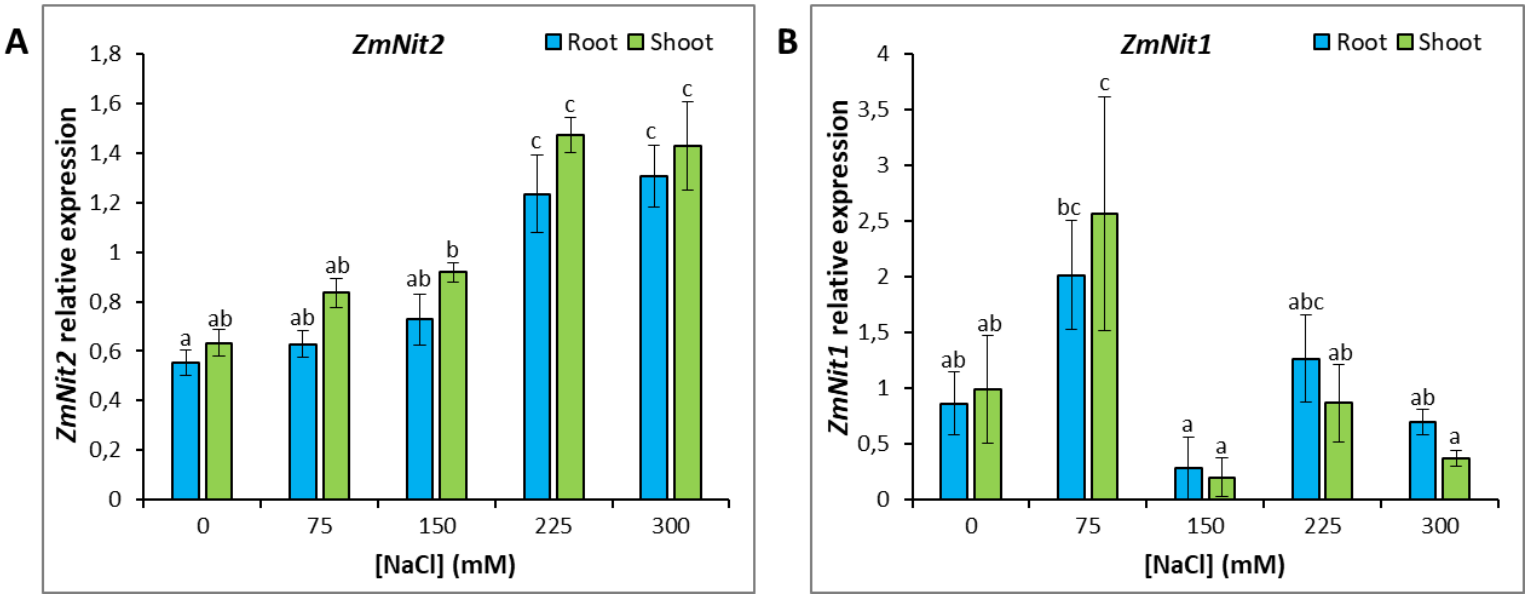

Figure 4.3: Nitrilase gene expression in maize grown under saline conditions

Maize plants were grown hydroponically in Hoagland's solution (control) for five days then transferred onto Hoagland's supplemented with the indicated concentrations of NaCl for nine days. Tissue from the second leaf or from the root of three plants in each treatment were harvested and pooled for RNA extraction and cDNA was synthesised for RT-qPCR gene expression analysis. The results are an average of three pooled tissue samples from independent biological experiments (n=3). **A**: *ZmNit2* expression, **B**: *ZmNit1* expression. Expression of each gene is shown relative to the *ZmMEP* reference gene. Error bars indicate standard error. Different letters on the graphs indicate mean values that are significantly different ($p \leq 0.05$) as determined by a one-way ANOVA with Fisher LSD post-hoc analysis.

4.3.2. Generation of a homozygous Arabidopsis line that overexpresses *ZmNit2*

4.3.2.1. The *ZmNit2* overexpression construct

AtNit2 overexpressor lines show improved salt tolerance, with reduced inhibition of growth and improved ion homeostasis relative to wild-type plants in the presence of NaCl (Cackett et al., 2022). To test whether overexpressing *ZmNit2* can also improve salt tolerance of Arabidopsis, a *ZmNit2* overexpression construct was generated and transformed into Arabidopsis.

Gateway Cloning Technology was used to clone the *Zea mays* (var. B73) *ZmNit2* coding sequence (CDS) into the pDONR™221 entry vector. After PCR confirmation and sequencing using the CDS flanking M13 primers (table 4.1), the *ZmNit2* CDS was transferred into the pB2GW7 Arabidopsis expression vector, downstream of the constitutive Cauliflower Mosaic Virus 35S promoter, creating pB2GW7-*ZmNit2* (figure 4.4). This construct was transformed into *E. coli* DH5α and colonies were screened from selection plates using colony PCR (data not shown). Subsequently, a single positive transformant was selected for plasmid DNA extraction and transformation into Agrobacterium.

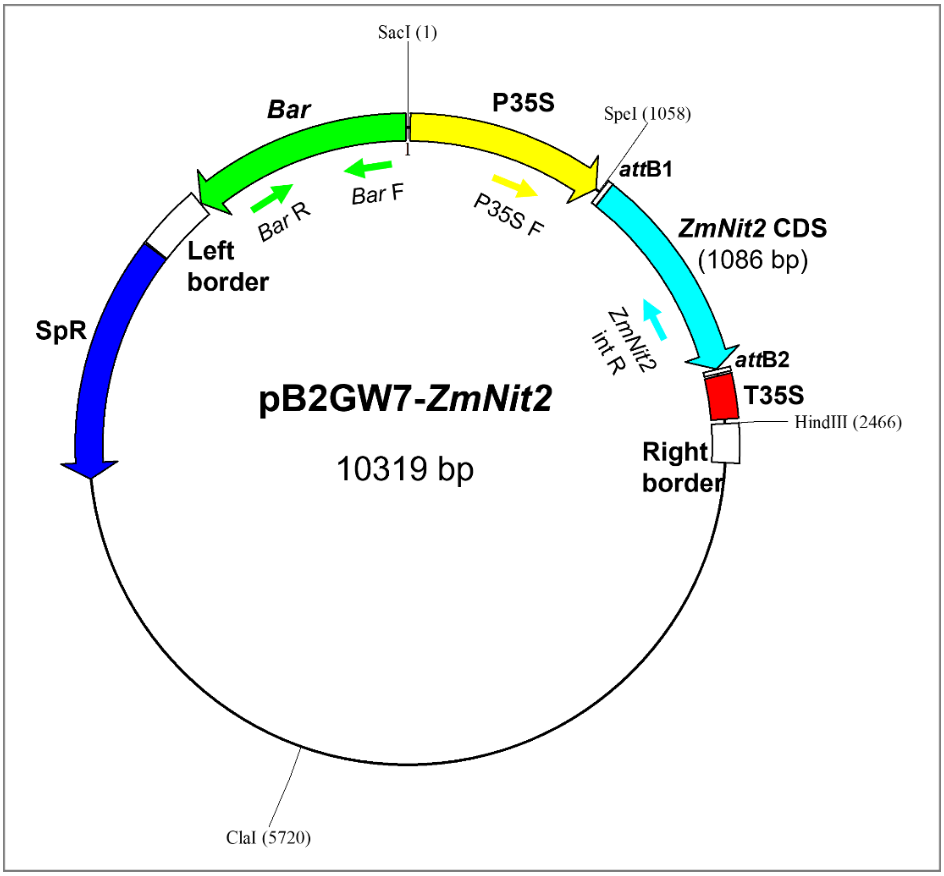

Figure 4.4: Map of the recombinant pB2GW7-*ZmNit2* generated via Gateway cloning

Expression of the *ZmNit2* coding sequence (**CDS**) is driven by the constitutive Cauliflower Mosaic Virus 35S promoter (**P35S**) and terminated by the 35S terminator sequence (**T35S**). Selection of the plasmid in positive *E. coli* and *A. tumefaciens* transformants is made possible by the spectinomycin resistance gene (**SpR**). The bialaphos acetyltransferase gene (***Bar***) confers resistance to glufosinate ammonium which allows for selection of positive Arabidopsis transformants. The region between the **left border** and **right border** inserts randomly into the Arabidopsis genome via *Agrobacterium*-mediated floral-dip transformation. The primers used for selection of bacterial transformants and transgenic Arabidopsis lines are shown by arrows inside the vector and are described in table 4.1.

4.3.2.2. Transient expression in tobacco and chlorophyll content under saline conditions

The process of generating homozygous *35S::ZmNit2* Arabidopsis lines was lengthy, so for an initial investigation, *ZmNit2* was transiently expressed in tobacco. Three days after vacuum infiltration of tobacco leaves with Agrobacterium containing the pB2GW7-*ZmNit2* vector or EV, tissue was harvested for RNA extraction and subsequent cDNA synthesis. Figure 4.5 shows the result of PCR analysis where it is evident that tobacco samples infiltrated with

pB2GW7-*ZmNit2* contained the *ZmNit2* product, whereas those infiltrated with EV did not, as expected (figure 4.5A). Figure 4.5B shows that all tobacco samples contained the *EF1α* reference gene, as expected, indicating that the cDNA was prepared correctly. This confirmed that the tobacco plants were correctly transiently expressing each construct and could be used for phenotypic analysis.

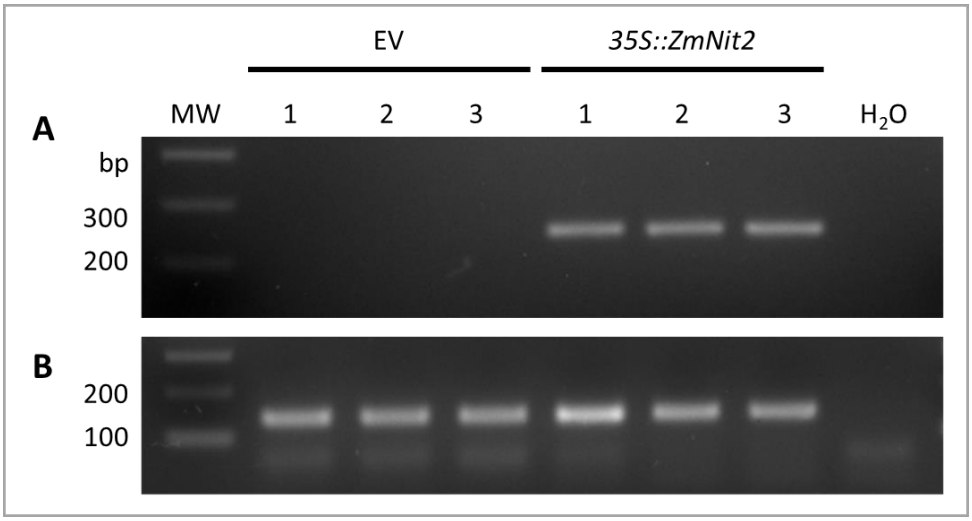

Figure 4.5: PCR confirmation of transient expression in tobacco

Tobacco plants were vacuum infiltrated with *A. tumefaciens* containing *35S::ZmNit2* or empty vector (EV) and tissue was harvested for RNA extraction and cDNA synthesis. An end-point PCR was used to confirm transient expression. **A:** *ZmNit2* PCR with an expected amplicon of 229 bp. **B:** *EF1α* control PCR with an expected band size of 135 bp. A no template H_2O negative control PCR reaction was included in both PCRs. The MW marker included is the New England Biolabs Quick-Load® 100 bp DNA ladder.

The chlorophyll content of *35S::AtNit2* plants was measured following salt assays where leaf discs of OE and WT plants were floated in PN media supplemented with various NaCl concentrations. Figure 4.6A shows that the total chlorophyll content in the leaf discs of the *35S::AtNit2* lines were significantly higher than WT under untreated conditions as well as 100 and 200 mM NaCl. The leaf discs floated in 300 mM NaCl were fully bleached in both lines. This data further demonstrates the salt tolerance of *35S::AtNit2* plants.

Figure 4.6B shows that the total chlorophyll content was higher in the tobacco leaf discs expressing *ZmNit2* compared with EV under all NaCl concentrations and untreated, however this was not significant under any treatment. However, in figure 4.6C it is evident that the leaf discs expressing *ZmNit2* remained greener and were more salt tolerant than those without *ZmNit2* expression. Interestingly, it was also apparent in both tobacco and Arabidopsis that the leaf discs of all genotypes floated on NaCl became larger and thicker than those floated on control media. It is thought that under saline conditions leaf morphology changes to decrease leaf surface area in order to increase nitrogen and chlorophyll concentration per unit area (James et al., 2002), but this result shows the opposite. This could be due to changes in cell expansion based on our hypothesis.

Overall, this data demonstrated that overexpressing *ZmNit2* warranted further investigation as a mechanism for improving salinity tolerance, and therefore pB2GW7-*ZmNit2* was transformed into Arabidopsis.

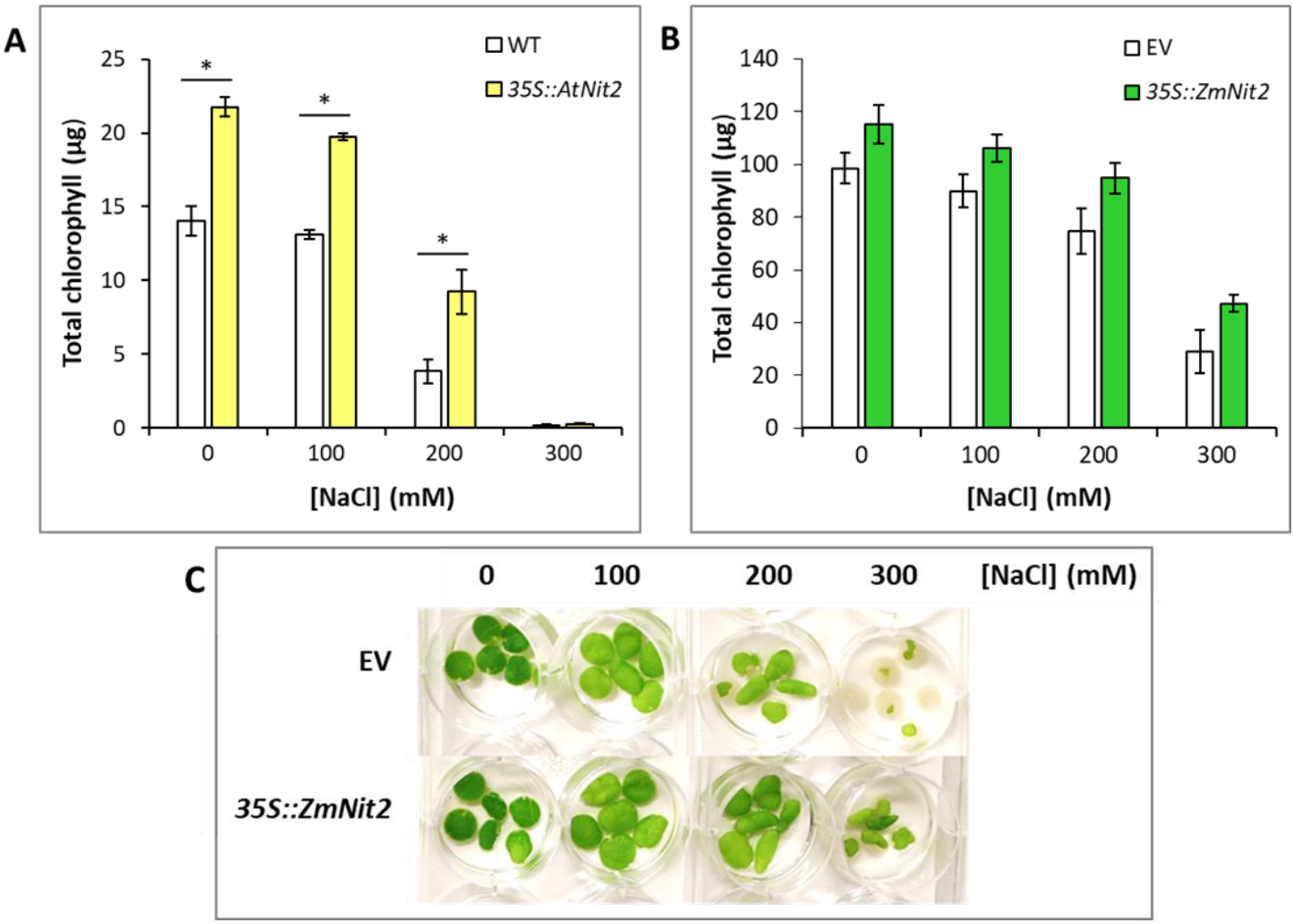

Figure 4.6: Chlorophyll content in *AtNit2* and *ZmNit2* overexpressing tissue

A: Total chlorophyll content of 3 leaf discs from *35S::AtNit2* and WT Arabidopsis controls treated with NaCl (n = 5). **B:** Total chlorophyll content of 6 tobacco leaf discs transiently expressing *35S::ZmNit2* or EV (n = 5). Error bars indicate standard error. T-tests were used to show a significant difference between OE and WT ($p < 0,05$). **C:** Representative picture to show phenotypic differences in leaf discs from tobacco transiently expressing *35S::ZmNit2* and EV controls after 3 days of floating in PN media supplemented with the indicated concentrations of NaCl.

4.3.2.3. Transformation of Arabidopsis with pB2GW7-*ZmNit2*

The pB2GW7-*ZmNit2* plasmid was transformed into *A. tumefaciens* GV3101. A colony PCR was conducted on ten colonies that grew on selective media using the P35S forward primer and *ZmNit2* internal reverse primer (table 2.1, figure 4.4).

Figure 4.7 shows that all ten Agrobacterium colonies and the positive control vector DNA had an amplicon at approximately 1357 bp, as expected, confirming the successful transformation of pB2GW7-*ZmNit2* into Agrobacterium. Empty pB2GW7 vector DNA was also previously transformed into Agrobacterium (chapter 2, figure 2.4C) to enable generation of an empty vector (EV) Arabidopsis line to be used as the background control in downstream phenotyping assays. A single Agrobacterium colony was selected (sample 1) to be used for Arabidopsis transformation.

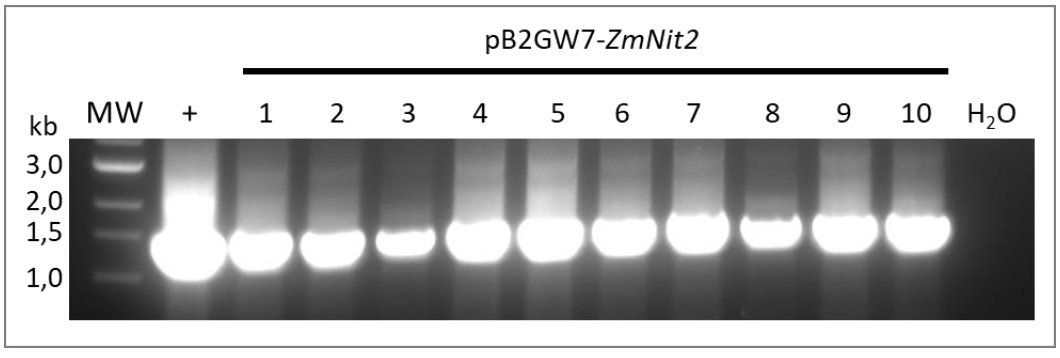

Figure 4.7: PCR confirmation of *A. tumefaciens* transformations with pB2GW7-*ZmNit2*

A colony PCR was performed on ten colonies from *A. tumefaciens* transformed with pB2GW7-*ZmNit2* using the P35S forward primer and *ZmNit2* internal reverse primer with an expected amplicon size of 1357 bp. A no template H_2O negative control PCR reaction was included with sequence-verified

pB2GW7-*ZmNit2* plasmid DNA used as a template in the positive control (**+**). The MW marker included is the New England Biolabs Quick-Load® 1 kb DNA ladder.

After confirming positive Agrobacterium transformation with the generated expression clone, Agrobacterium-mediated floral-dip transformation of Arabidopsis (No-0 ecotype) was performed with both pB2GW7-*ZmNit2* and pB2GW7 EV. The No-0 ecotype was used as the background for these lines as the *35S::AtNit2* line was generated in the No-0 background, enabling us to compare these lines. GFSA selection plates were used to isolate transgenic individuals from seeds collected from the transformed plants (T1 generation). Seedlings which were able to survive for 11 days on the selection plates were transferred onto soil.

Once the seedlings had established properly on soil, one leaf per line was harvested for DNA extraction and PCR analysis to confirm the presence of the transgene insertion. Figures 4.8 and 4.9 show that several transgenic lines were identified in the T1 generation for both the *35S::ZmNit2* and *35S* EV (No-0) Arabidopsis genotypes respectively. Figure 4.8 shows that 13 transgenic *35S::ZmNit2* lines were isolated that contained both the *Bar* gene (figure 4.8A) and the *ZmNit2* coding sequence downstream of the 35S promoter (figure 4.8B) as all 13 seedlings had a specific band amplified of the same size as the positive control pB2GW7-*ZmNit2* plasmid DNA.

Similarly, figure 4.9 shows that all six *35S* EV (No-0) seedlings that were able to grow on GFSA were verified by PCR analysis as they all contained the *Bar* PCR product (figure 4.9A), but no PCR product using the 35S forward primer and *ZmNit2* reverse primer (figure 4.9B). This result is significant in confirming that the EV transformed Arabidopsis plants are indeed missing the *ZmNit2* coding sequence downstream of the 35S promoter but do contain the pB2GW7 backbone and can thus be used as a background control in downstream phenotyping. All of these lines were then allowed to grow to maturity to self-fertilise and produce the next T2 generation

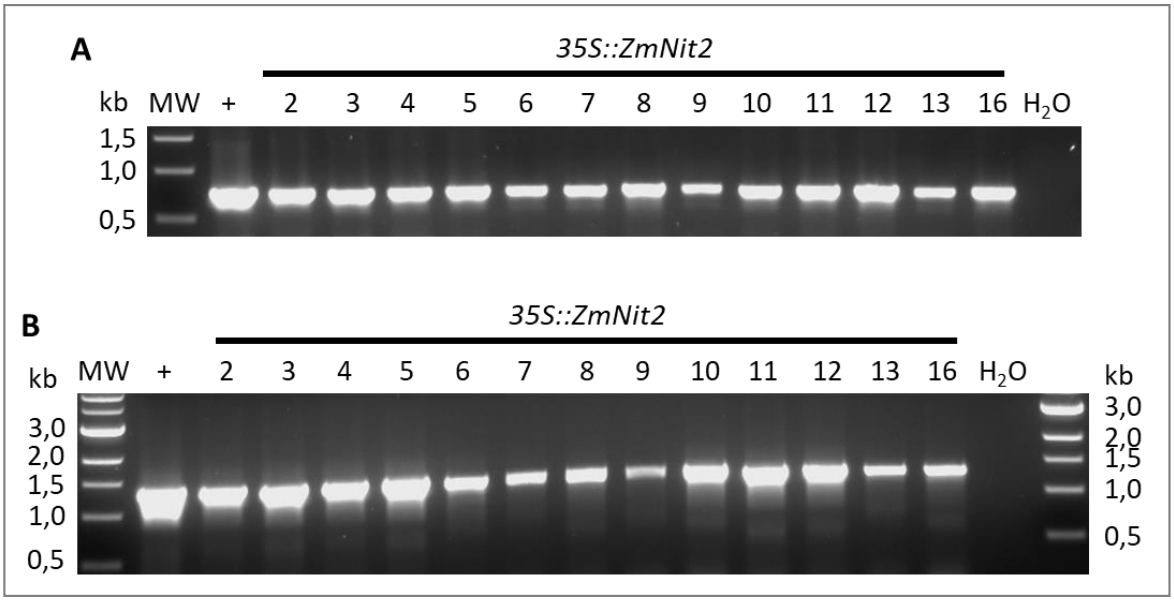

Figure 4.8: PCR confirmation of *35S::ZmNit2* Arabidopsis transformations

A PCR was performed on DNA extracted from 13 potentially transgenic Arabidopsis plants transformed with pB2GW7-*ZmNit2* using **A:** the *Bar* primer pair with an expected amplicon of 733 bp, and **B:** the P35S forward primer and *ZmNit2* internal reverse primer with an expected amplicon size of 1357 bp. A no template H_2O negative control PCR reaction was included with pB2GW7-*ZmNit2* #2 plasmid DNA used as a positive control (**+**) in both PCRs. The MW marker included is the New England Biolabs Quick-Load® 1 kb DNA ladder.

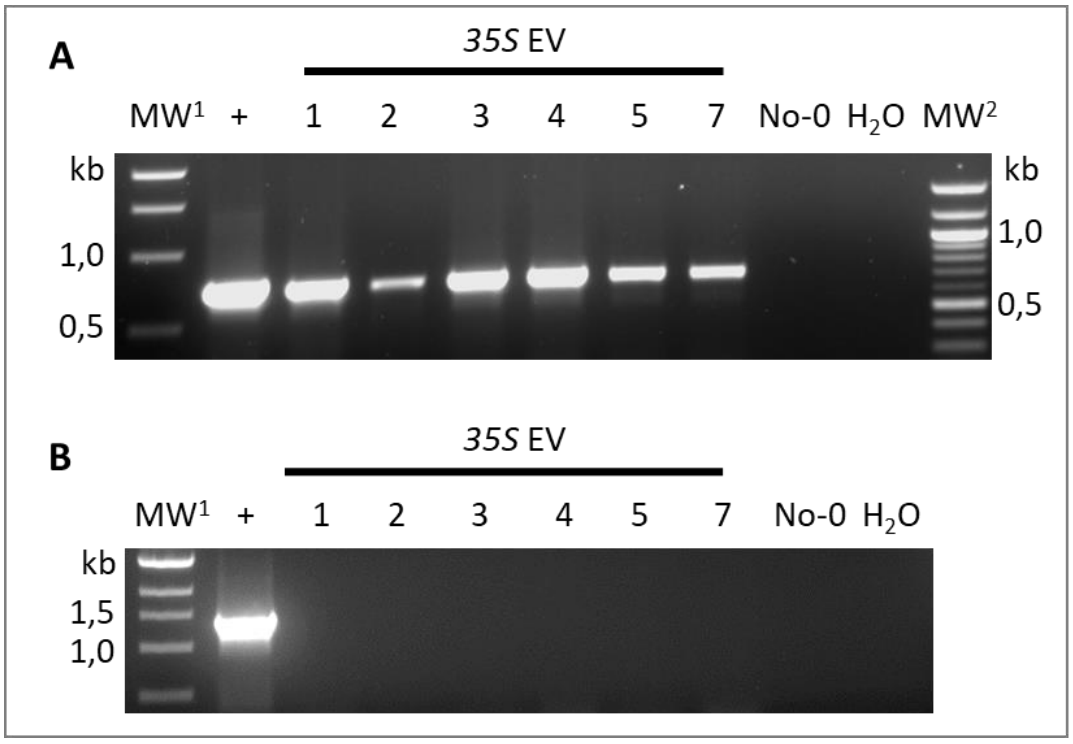

Figure 4.9: PCR confirmation of *35S* EV Arabidopsis transformations

A PCR was performed on DNA extracted from six potentially transgenic Arabidopsis plants transformed with pB2GW7 EV using **A:** the *Bar* primer pair with an expected amplicon of 733 bp, and **B:** the P35S forward primer and *ZmNit2* internal reverse primer with an expected amplicon size of 1357 bp. A No-0 wild-type (WT) DNA sample and a no template H_2O PCR reaction were included as negative controls with pB2GW7-*ZmNit2* #2 plasmid DNA used as a positive control (**+**) in both. The MW markers included are the New England Biolabs Quick-Load® 1 kb DNA ladder (**MW[1]**) and the Quick-Load® 100 bp DNA ladder (**MW[2]**).

4.3.2.4. Confirmation of *ZmNit2* expression

In the T2 generation, GFSA screening was used to identify lines which gave an approximate 3:1 ratio of transgenic (heterozygous or homozygous) to WT, which would indicate a single transgene insertion (appendix table 6.4). Several transgenic seedlings were transferred to soil to collect seed for future genotyping experiments. Another round of GFSA screening in the T3 generation led to identification of homozygous transgenic lines, which had 100% growth on selective media, which were then transferred to soil to collect seed for gene expression analysis and future phenotyping experiments. For each of the homozygous *35S::ZmNit2* and *35S* EV lines, two leaves from three of the transferred seedlings were pooled to form a single tissue sample for RNA extraction and subsequent cDNA synthesis. Expression of *ZmNit2* was determined by qPCR, relative to the *AtMON1* reference gene. Figure 4.10 shows that no *ZmNit2* expression was detected in the EV lines as expected, indicating that they are suitable for downstream use.

Variable levels of *ZmNit2* were observed in the *35S::ZmNit2* lines, as expected. Three overexpressor lines were selected to be carried forward based on having the highest *ZmNit2* expression – lines 2.2, 9.3 and 16.2. Additionally, EV lines 2.1 and 3.1 were selected for further analysis as they had the best germination frequencies and the most seeds available for subsequent use.

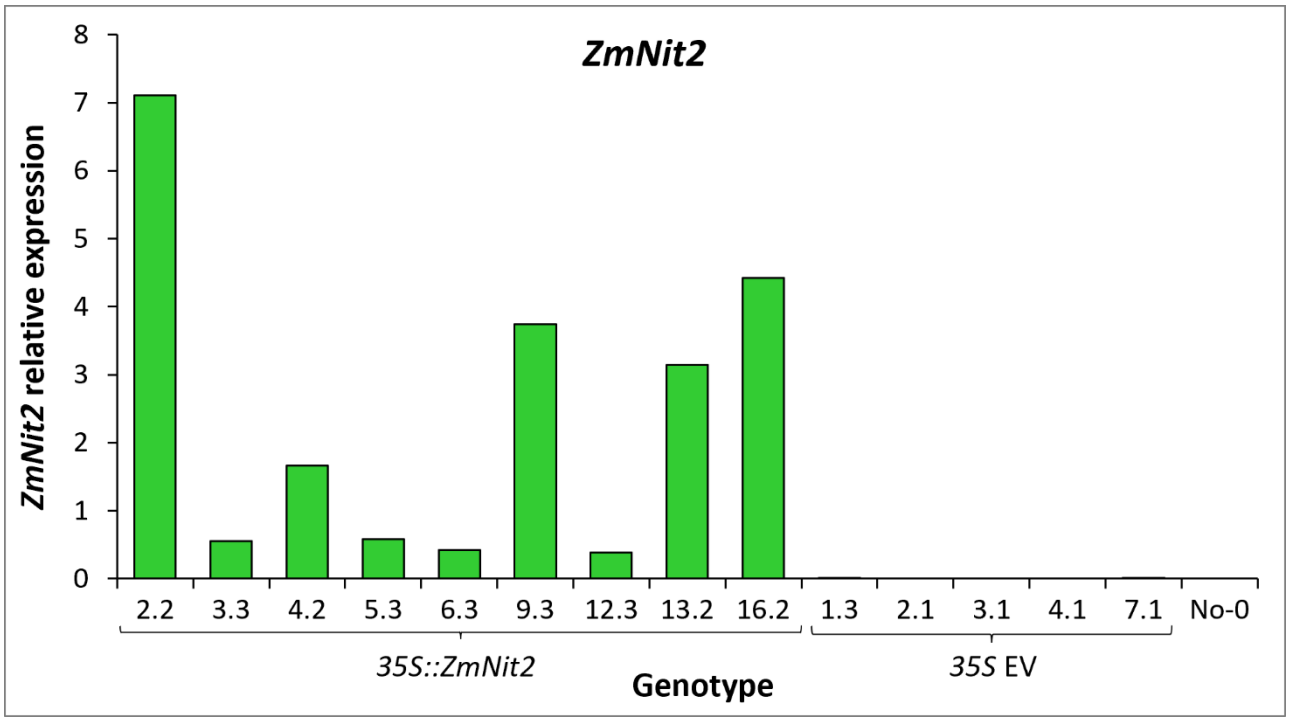

Figure 4.10: *ZmNit2* gene expression in homozygous T3 plants

Arabidopsis plants were grown on PN-agar supplemented with 10µg/mL GFSA for 11 days then transferred onto soil for two weeks. Tissue from two leaves of three plants were harvested and pooled for RNA extraction and cDNA was synthesised for RT-qPCR gene expression analysis. Expression of *ZmNit2* is shown relative to the *AtMON1* reference gene. No-0 WT Arabidopsis is included as a control.

For each of the selected lines, ten seedlings were harvested from PN-agar plates and used in DNA extractions and PCR to confirm homozygosity. For the *35S::ZmNit2* lines, PCR was conducted using the *35S* promoter forward primer and *ZmNit2* internal reverse primer and the results are shown in figure 4.11A. For the *35S* EV lines, PCR was conducted using the *Bar* primer pair (figure 4.11B). All ten of the seedlings from each line contained the specific transgene product, which, along with the growth on selection plates, indicates that these lines are all homozygous and could be further analysed.

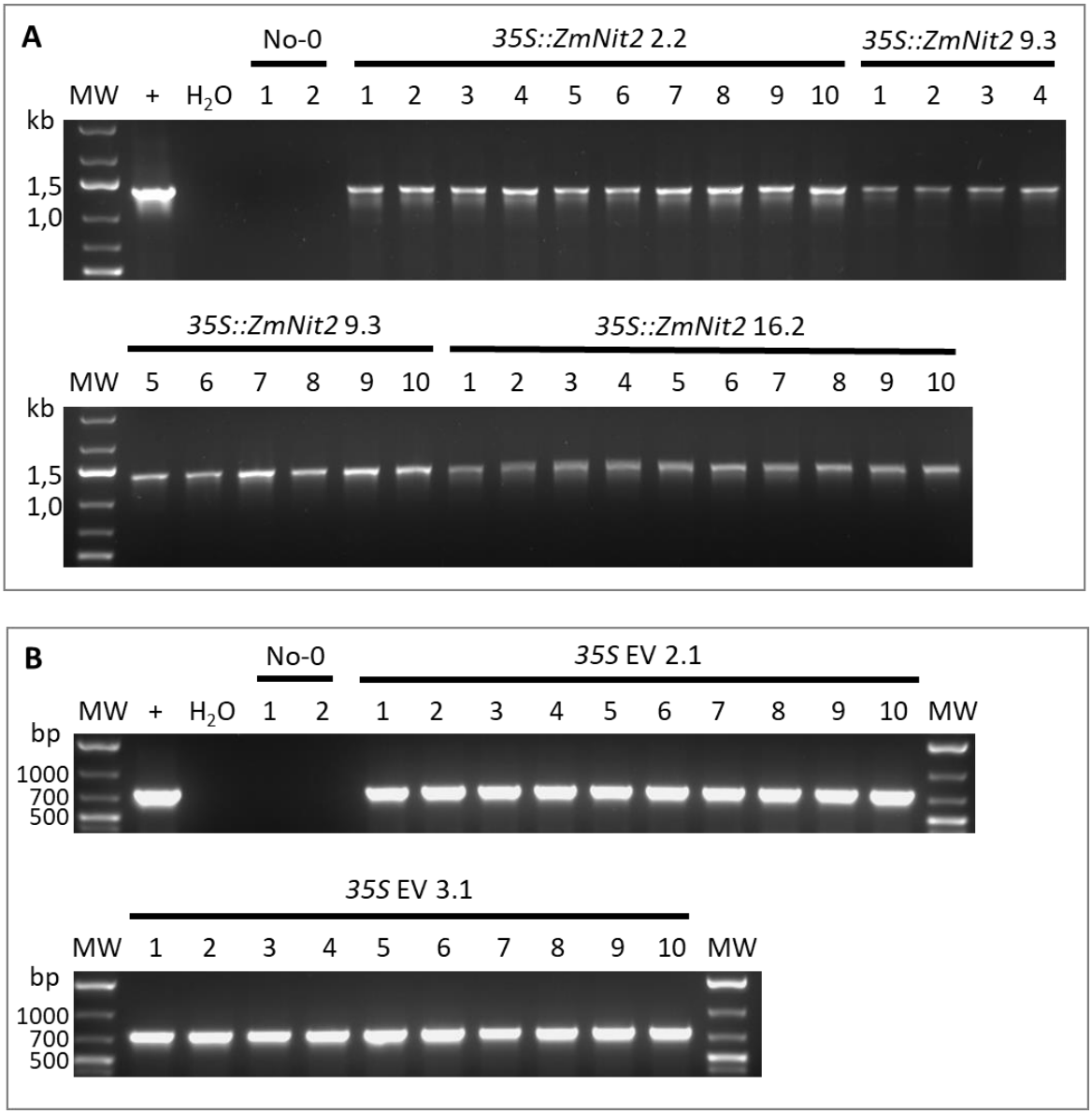

Figure 4.11: PCR confirmation of *35S::ZmNit2* homozygosity in the T3 generation

A PCR was performed on DNA extracted from ten seedlings off PN plates from T3 lines that were potentially homozygous for **A:** *ZmNit2,* using the P35S forward primer and *ZmNit2* internal reverse primer with an expected amplicon size of 1357 bp, and **B:** EV, using the *Bar* primer pair with an expected amplicon of 733 bp. No-0 WT DNA and a no template H_2O PCR reaction were used as negative controls with pB2GW7-*ZmNit2* #2 plasmid DNA used as a positive control (**+**) in both PCRs. The MW marker included is the New England Biolabs Quick-Load® 1 kb DNA ladder.

To be sure that these lines were indeed homozygous, another set of T3 seeds were screened on GFSA selection plates as before, with the same results observed where none of the lines had any GFSA-induced bleaching or death (data not shown). Ten seedlings were again

harvested from a single PN control plate for PCR analysis with the same results observed as in figure 4.11 above. Additionally, the remaining tissue from each PN plate was pooled and harvested for RNA extraction and subsequent cDNA synthesis and RT-qPCR gene expression analysis to determine the level of variation in expression of *ZmNit2* between plants in each line.

Figure 4.12 shows that there was some variation between each line and that each of the *35S::ZmNit2* homozygous OE lines selected showed significantly higher *ZmNit2* expression than the EV lines which had no *ZmNit2* expression, as expected. The actual values of the *ZmNit2* expression relative to *AtMON1* were lower than those previously seen in figure 4.10 which could be due to the fact that the tissue used was from a different developmental stage. Previously, *35S::ZmNit2* line 2.2 appeared to have the highest *ZmNit2* expression but in this experiment it appears to have significantly lower expression than lines 9.3 and 16.2. Lines 2.2 and 16.2 were chosen for phenotypic characterisation.

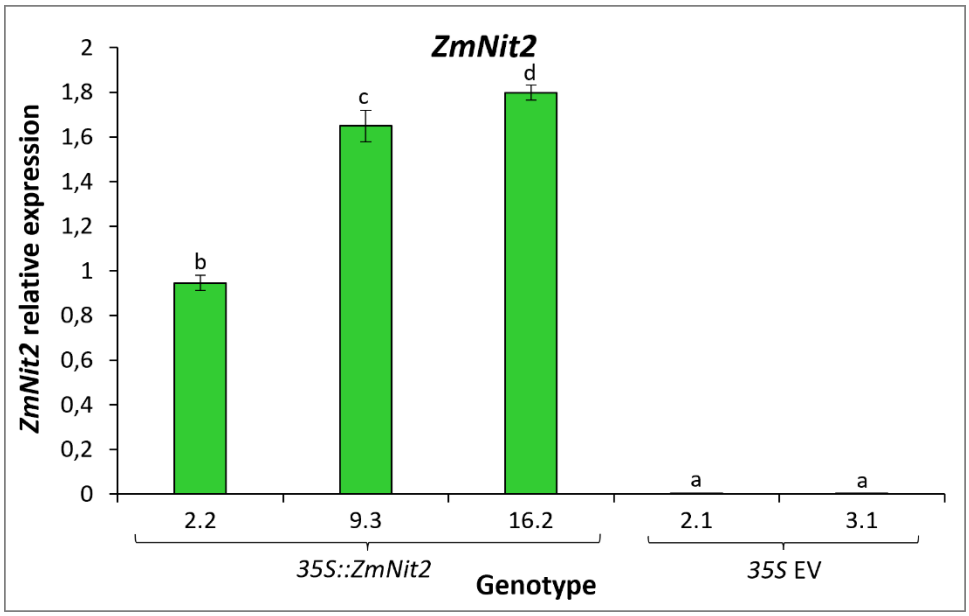

Figure 4.12: *ZmNit2* gene expression in homozygous T3 seedlings

Arabidopsis seedlings were grown on PN media for 11 days. Tissue was harvested and pooled for RNA extraction and cDNA was synthesised for RT-qPCR gene expression analysis. The results are an average of three pools of tissue (n=3). Expression of *ZmNit2* is shown relative to the *AtMON1* reference gene. Error bars indicate standard error. Different letters on the graphs indicate significant differences ($p \leq 0.05$) in mean values as determined by a one-way ANOVA with Fisher LSD post-hoc analysis.

4.3.3. Phenotypic characterisation of *35S::ZmNit2* Arabidopsis plants

4.3.3.1. Growth of *35S::ZmNit2* plants exposed to saline conditions early in development

To determine whether overexpressing *ZmNit2* had an impact on plant growth in salt early in development, *35S* EV and *35S::ZmNit2* plants were germinated and grown for two weeks on petri dishes containing untreated PN-agar (control) and PN-agar supplemented with differing concentrations of NaCl or iso-osmolar concentrations of sorbitol. The average biomass of the three lines was compared for each treatment to identify any phenotypic differences in their growth.

Figure 4.13A shows that the average mass per plant of each line was inhibited in a dose-dependent manner under saline conditions, as expected. The average plant mass of both *ZmNit2* OE lines were comparable under all treatment conditions. Notably, the *35S::ZmNit2* lines showed a lower plant mass than the EV line in untreated conditions, indicating a growth penalty for expressing the maize gene.

To account for the difference in the average plant mass between the lines in untreated conditions, the mass per plant was plotted relative to the untreated control for each line and the data is shown in figure 4.13B. Here, it is evident that the *ZmNit2* OE lines sustained growth better under saline conditions compared to the EV control, which is further depicted in figure 4.13C. Statistical analyses comparing each of the slopes showed that there was no significant difference between the two OE lines, and that both OE lines had a significantly less steep gradient than the EV line. This same trend is seen in sorbitol conditions (data not shown), indicating that *ZmNit2* might improve osmotic stress tolerance. Overall, this data indicates that Arabidopsis lines overexpressing *ZmNit2* are more tolerant of salt and sorbitol.

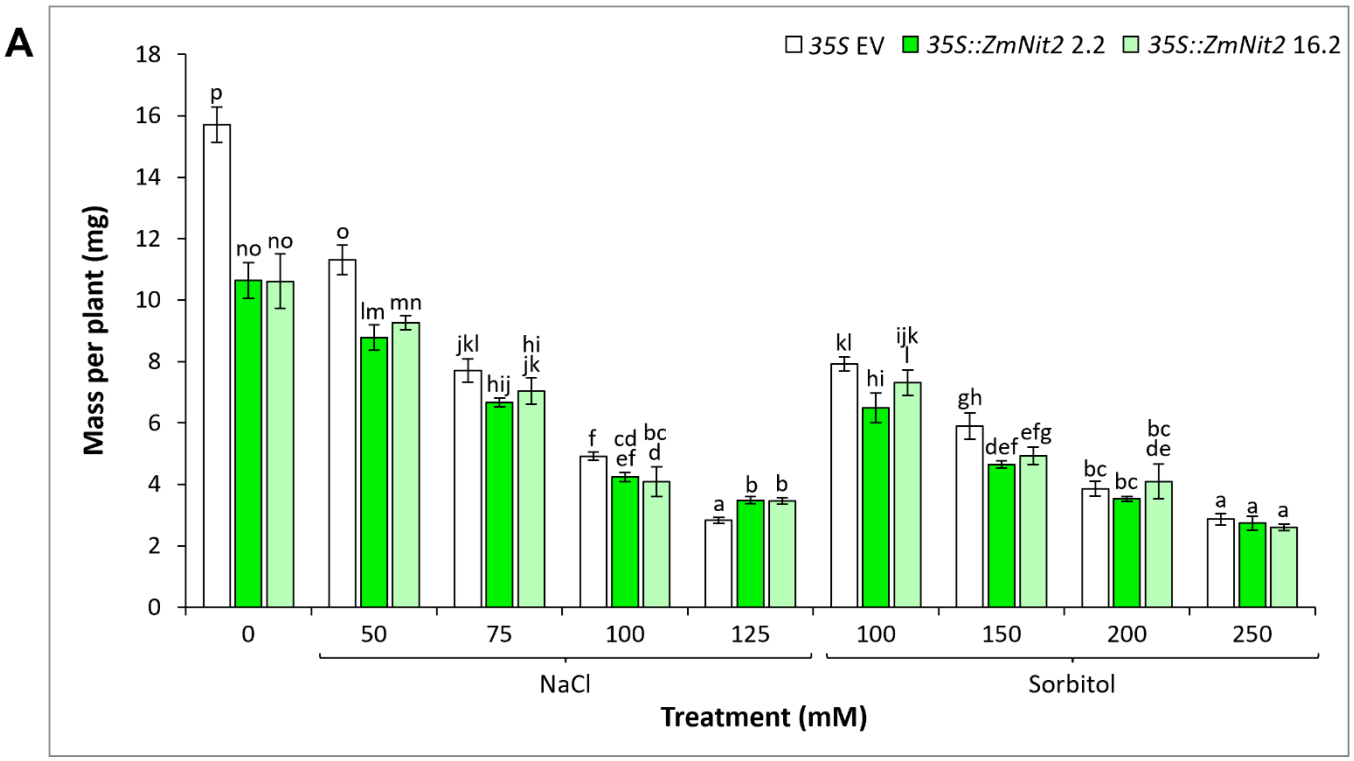
A
35S EV
35S::ZmNit2 2.2
35S::ZmNit2 16.2
Mass per plant (mg)
0
2
4
6
8
10
12
14
16
18
p
no no
o
lm mn
jkl hij hi jk
f cd ef bc d
a b b
kl hi ijk
gh def efg
bc bc bc de
a a a
0 50 75 100 125 100 150 200 250
NaCl
Sorbitol
Treatment (mM)

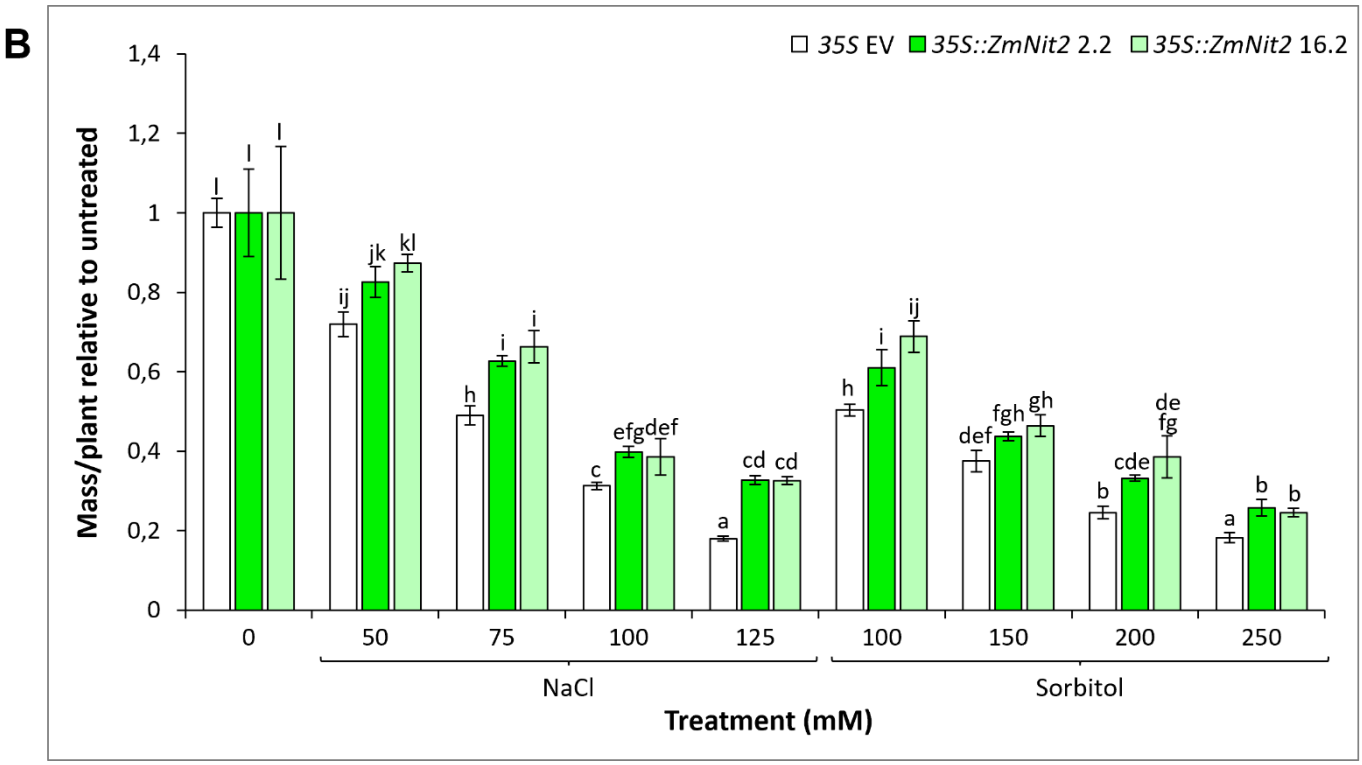
B
35S EV
35S::ZmNit2 2.2
35S::ZmNit2 16.2
Mass/plant relative to untreated
0
0,2
0,4
0,6
0,8
1
1,2
1,4
l l l
ij jk kl
h i i
c efg def
a cd cd
h i ij
def fgh gh
b cde de fg
a b b
0 50 75 100 125 100 150 200 250
NaCl
Sorbitol
Treatment (mM)

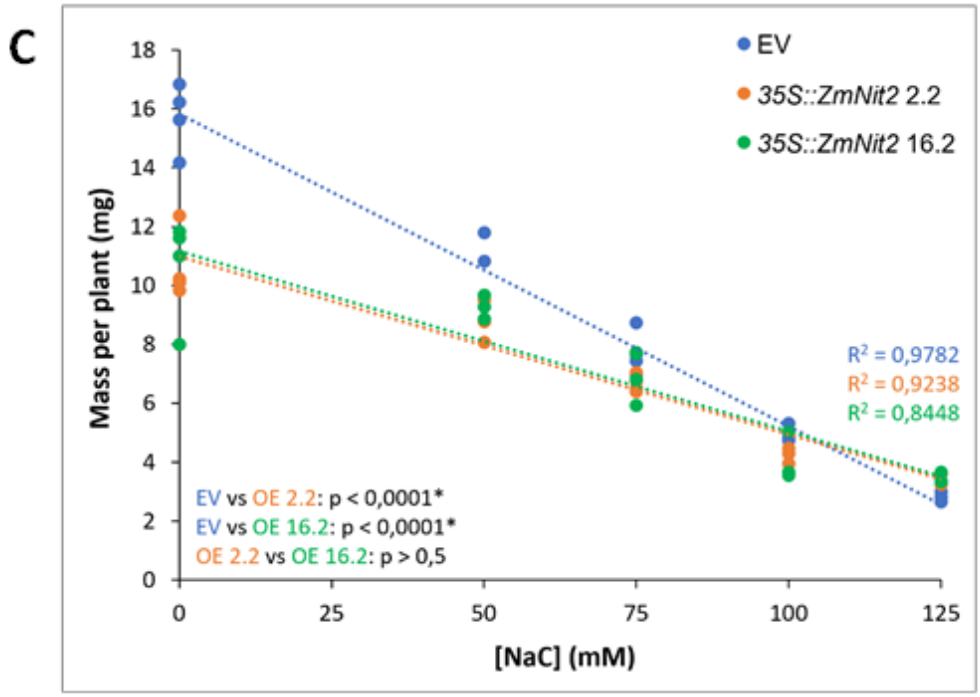

Figure 4.13: Growth of *35S::ZmNit2* plants exposed to saline conditions early in development

The EV and *35S::ZmNit2* plants were germinated and grown for two weeks on petri dishes containing untreated PN-agar (control) and PN-agar supplemented with the indicated concentrations of NaCl and sorbitol. **A:** The average mass per plant of each line. **B:** The average mass per plant plotted relative to the control (0 mM) for each line. Error bars indicate standard error. Different letters on the graphs indicate significant differences ($p \leq 0.05$) in mean values as determined by a one-way ANOVA with Fisher LSD post-hoc analysis **C:** The mass per plant is plotted as a regression analysis for NaCl conditions. The results show four replicates for each treatment with 50 seeds sown per plate (n=4). The experiment was repeated three times with comparable results. Each slope was compared statistically to one another to determine any significant differences and the results are shown in the bottom left corner with an asterisk indicating statistical significance.

4.3.3.2. Growth of *35S::ZmNit2* plants exposed to saline conditions later in development

To determine whether overexpressing *ZmNit2* has an impact on plant growth in saline conditions later in development (comparable to the effect seen by overexpressing *AtNit2*), *35S* EV, *35S::ZmNit2* 16.2, and *35S::AtNit2* plants were grown hydroponically in ¼ strength PN media for three weeks, then transferred onto ¼ strength PN media supplemented with or without 75 mM NaCl for a further week. The *35S* EV line was used as a control for both the

35S::ZmNit2 and *35S::AtNit2* lines. At the end of the experimental period, the shoot and root mass of each plant was recorded to determine the average per plant for each line in each treatment.

Figure 4.14A shows that the average shoot mass was significantly lower in all three genotypes in 75 mM NaCl compared to untreated conditions, as expected. There was no significant difference in average shoot mass between the genotypes in untreated conditions. However, the *35S::AtNit2* genotype showed a significantly higher average shoot mass in 75 mM NaCl compared to the EV and *35S::ZmNit2* line which were not significantly different to each other. This means that the *35S::AtNit2* plants show reduced salt inhibition of growth, as expected, whereas the *35S::ZmNit2* line experienced the same salt-induced inhibition of shoot growth as the EV control. Overall, this shows that overexpressing *ZmNit2* does not have the same effect in improving salt tolerance later in development as overexpressing *AtNit2* does.

Figure 4.14B shows that none of the genotypes tested displayed any growth phenotypes in response to 75 mM NaCl compared to untreated conditions, and there was no significant difference in average root mass between any of the genotypes under both untreated and 75 mM NaCl conditions. This experiment should be repeated with increased NaCl concentrations that inhibit root growth in order to determine if there are any differences between the genotypes.

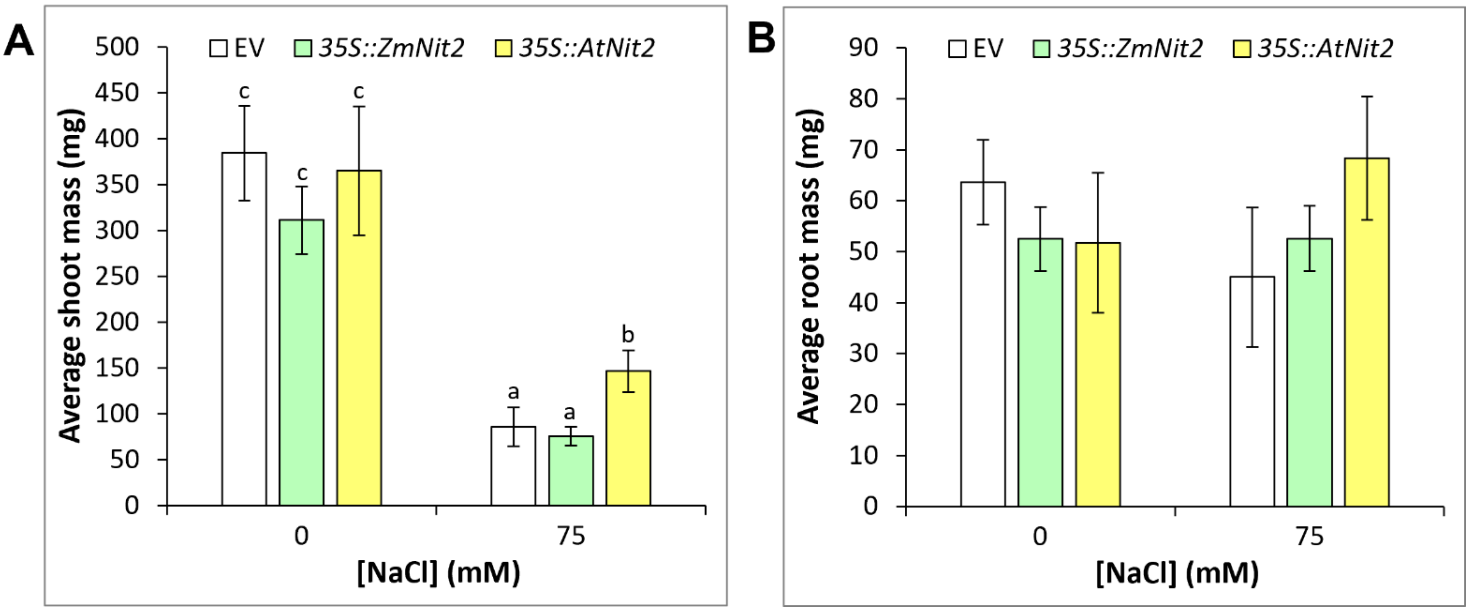

Figure 4.14: The average shoot and root mass of EV, *35S::ZmNit2* and *35S::AtNit2* plants after one week of salt treatment later in development

The *35S* EV, *35S::ZmNit2* and *35S::AtNit2* plants were grown hydroponically in ¼ strength PN media without salt stress for three weeks. Plants were then transferred onto PN media supplemented with 0 or 75 mM NaCl and grown under saline conditions for a further week. **A:** The average shoot mass per plant **B:** The average root mass per plant. The results are an average of six plants for each treatment for the EV and *35S::ZmNit2* lines and four plants for the *35S::AtNit2* line ($n \geq 4$). Error bars indicate standard error. Different letters on the graphs indicate significant differences ($p \leq 0.05$) in mean values as determined by a one-way ANOVA with Fisher LSD post-hoc analysis.

4.3.3.3. *AtEXP11* expression analysis in *35S::ZmNit2* plants

While overexpression of *ZmNit2* was sufficient to increase salt tolerance in terms of relative biomass production in seedlings (figure 4.13), it did not do so in older plants (figure 4.14), in contrast to *35S::AtNit2* where enhanced tolerance was seen at both developmental stages (Cackett, 2019). In addition to these phenotypes, *35S::AtNit2* also displays elevated expression of *EXPANSIN 11* (*AtEXP11*, AT1G20190), which is thought to function in plant cell expansion. In order to better understand whether expression of *ZmNit2* can phenocopy that of *AtNit2*, *AtEXP11* expression was analysed in the *ZmNit2* transgenics.

Arabidopsis No-0 WT, *35S::AtNit2, 35S* EV and *35S::ZmNit2* seeds were germinated and grown for 14 days on PN-agar, in triplicate. After two weeks, seedlings were pooled for each line from three separate plates for RNA extraction and subsequent cDNA analysis. RT-qPCR was used to analyse *AtEXP11* gene expression relative to *AtMON1*.

Figure 4.15 shows that *AtEXP11* expression is significantly higher in the *35S::AtNit2* line compared to the No-0 WT background as well as the *35S* EV and *35S::ZmNit2* lines. This same increase in *AtEXP11* expression is not seen when the maize *Nit2* gene is overexpressed, as the *35S::ZmNit2* line shows no significant difference in *AtEXP11* expression compared to the *35S* EV line. This indicates that *ZmNit2* might not be able to perform the same function in Arabidopsis as *AtNit2*, to cause *AtEXP11* upregulation.

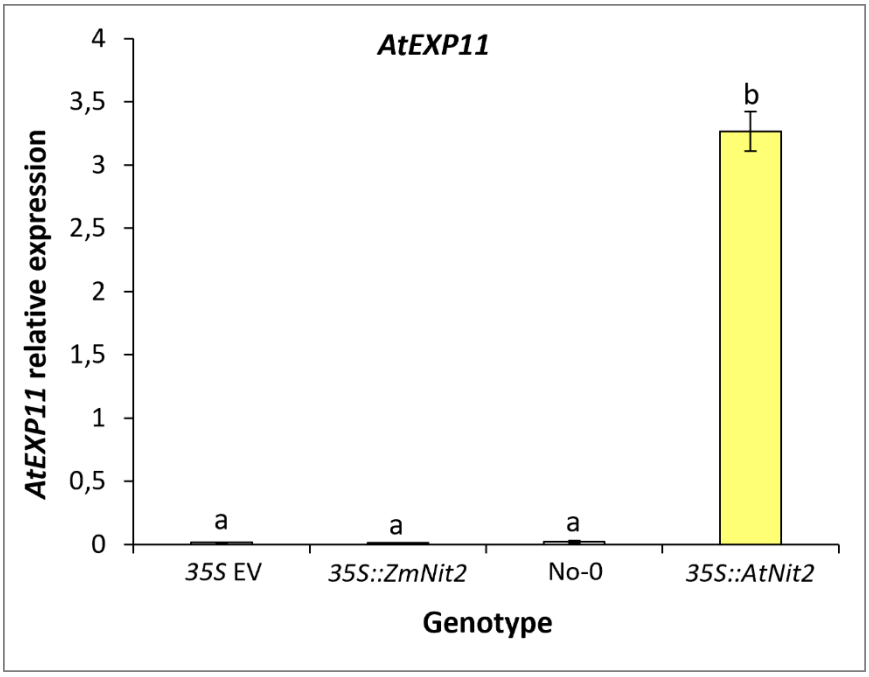

Figure 4.15: *AtEXP11* gene expression in *35S::ZmNit2* and *35S::AtNit2* lines

Arabidopsis seedlings were germinated and grown on PN media for 14 days. Tissue was harvested and pooled for RNA extraction and cDNA was synthesised for RT-qPCR gene expression analysis. The results are an average of three pools of tissue (n=3). Expression of *AtEXP11* is shown relative to the *AtMON1* reference gene. Error bars indicate standard error. Different letters on the graphs indicate significant differences ($p \leq 0.05$) in mean values as determined by a one-way ANOVA with Fisher LSD post-hoc analysis.

4.3.4. Investigating *ZmNit2* regulation

4.3.4.1. *ZmNit2* promoter analysis

Although *ZmNit2* was not able to directly phenocopy *AtNit2* in Arabidopsis, it does seem like *ZmNit2* plays a role in the response to salt stress, and *35S::ZmNit2* plants were more salt tolerant early in development. As a preliminary investigation into whether the work we are doing in Arabidopsis to uncover *AtNit2* regulation is relevant to maize, 1 kb of promoter DNA upstream of the *ZmNit2* translation start site was analysed *in silico* using PLACE to identify the predicted TFBS present in this region.

Table 4.2 lists the common TFBS present in both *Nit2* promoters, as well as other MYB TFBS present in the *ZmNit2* promoter region that are predicted in the PLACE database. Notably, six different predicted MYB TFBS are present on the positive strand in this region (shown in figure

4.16), even more than the five present in the *AtNit2* promoter. This suggests that one or more MYB TFs might play a role in *ZmNit2* regulation.

Table 4.2: TFBS present in 1 kb upstream of *ZmNit2*

Binding site name as per PLACE	Motif	Site in P*AtNit2?*	Site in P*ZmNit2*	# of sites in 1kb upstream of *ZmNit2*	Strand
MYBPZM	CC(A/T)ACC		CCAACC	2	+
MYBCOREATCYCB1	AACGG	✓	AACGG	2	+/-
MYBCORE	C(A/T/G/C)GTT(A/G)		C(C/G)GTTG	2	+
MYB2CONSENSUSAT	(T/C)AAC(T/G)G	✓	CAACGG	1	-
MYB4 binding site	A(A/C)C(A/T)A(A/C)C	✓	ACCAAAC	1	+
IBOXCORE	GATAA	✓	GATAA	1	+
TATABOX3	TATTAAT	✓	TATTAAT	2	+/-
TATABOX5	TTATTT	✓	TTATTT	2	-
WBOXNTERF3	TGAC(C/T)	✓	TGACC	1	+

Note: One of the MYBCORE sites is in the same location but on the opposite strand to the MYB2CONSENSUSAT/MYBCOREATCYCB1 site (which is at the same location on the negative strand)

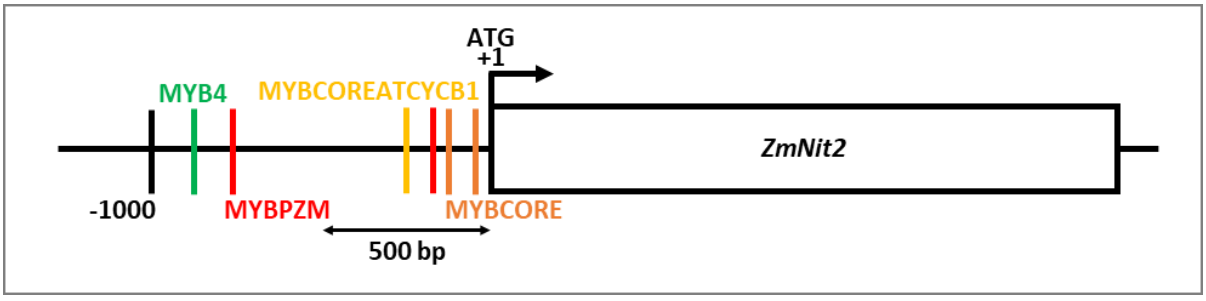

Figure 4.16: Schematic showing the presence of MYB binding sites in the *ZmNit2* promoter

In this schematic, the *ZmNit2* promoter positive strand is shown as a black line with the coding sequence indicated by a white box with a black outline. The translation start site (ATG) is labelled as +1 and all sites are labelled relative to this position. The MYBCORE binding sites (orange) are present at positions -27 and -110 in the *ZmNit2* promoter, with the MYBPZM sites (red) present at positions -127 and -747. The MYBCOREATCYCB1 (yellow) site and the MYB4 binding site (green) present at positions -239 and -845 respectively.

This promoter region was also manually searched for motifs similar to those in Arabidopsis to which the TFs identified in the Y1H experiment are proposed to bind to. The *ZmNit2* promoter region contains multiple NNATTA sites which is the canonical binding site for most homeodomain proteins (Tan & Irish, 2006), indicating that maize homeodomain proteins might also be able to bind to the *ZmNit2* promoter. Additionally, the putative binding site for HMGB9, AAATAAA, is also present in the *ZmNit2* promoter and may indicate that a homolog of HMGB9 is able to bind to the *ZmNit2* promoter and regulate its expression. There is also a GTAC motif present in the *ZmNit2* promoter which is predicted to be the binding site for SQUAMOSA promoter binding proteins in Arabidopsis (Yamasaki et al., 2009), implying that the SPL7 homolog in maize may be able to bind to the promoter of *ZmNit2.*

4.3.4.2. Maize TF homolog gene expression

To determine whether homologs of two of the TFs identified in the Y1H experiment are similarly regulated in maize under saline conditions, the maize homologs of AtHMGB9 and AtSPL7 were identified and their expression was analysed following salt treatment as in section 4.3.1.3.

4.3.4.2.1. AtHMGB9 homolog

When the Arabidopsis HMGB9 protein sequence was queried against the maize protein database, the top hit returned was ZmARID6 (GRMZM2G024976). When the reciprocal BLASTp was performed, the Arabidopsis HMGB15 and HMGB9 proteins were identified as the top two hits, with AtHMGB15 having a slightly higher percentage identity (46.77%) than AtHMGB9 (40.89%). However, AtHMGB15 and AtHMGB9 are paralogs of one another, sharing a 43% amino acid sequence identity, so this was not surprising (Xia et al., 2014). Very little is known about ZmARID6 but it has been annotated as a nuclear DNA binding transcription factor, with the same ARID domain as AtHMGB9. Therefore, *ZmARID6* gene expression was analysed.

Figure 4.17A shows that *ZmARID6* increased significantly in the root tissue under saline conditions, and significantly decreased in the shoot tissue under saline conditions. Additionally, *ZmARID6* expression varied significantly between the root and shoot tissue. Under untreated and low NaCl conditions, *ZmARID6* was expressed more in the shoot tissue

and this spatial expression was reversed under high NaCl conditions with a significantly higher *ZmARID6* expression in 300 mM NaCl in the root tissue. This data indicates that *ZmARID6* is differentially regulated under saline conditions in different tissue types. This data is similar to that seen in the Arabidopsis later development microarray where *AtHMGB9* expression decreased in the shoot tissue under high NaCl conditions (figure 3.9H), indicating that *ZmARID6* may be regulated similarly by saline conditions in maize shoot tissue compared to *AtHMGB9.* Additionally, *ZmARID6* shows an opposite expression pattern in shoots compared to *ZmNit2* (figure 4.3A), indicating that it is possible that it plays a role in *ZmNit2* repression in shoot tissue. However, in root tissue *ZmARID6* is upregulated under saline conditions similarly to *ZmNit2.* Overall, this data indicates that ZmARID6 may play a role in *ZmNit2* regulation, but this role might be different in different tissue types and needs further investigation.

4.3.4.2.2. AtSPL7 homolog

When the Arabidopsis SPL7 protein sequence was queried against the maize protein database, the top hit returned was ZmSBP11 (GRMZM2G109354; Zm00001eb349730). When the reciprocal BLASTp was performed, AtSPL7 was the top hit and therefore *ZmSBP11* expression was analysed under saline conditions.

Figure 4.17B shows that there was no significant differences in *ZmSBP11* expression in either tissue type under saline conditions and that there were no differences in expression levels between the two tissue types. This data is comparable to that seen in figure 3.9L where *AtSPL7* was shown to not differ under saline conditions in either tissue type in the later development microarray, indicating that *ZmSBP11* and *AtSPL7* may be similarly regulated under saline conditions. Although this data does not correspond to the upregulation of *ZmNit2* seen in figure 4.3A, the lack of regulation of *AtSBP11* expression under saline conditions does not mean that it does not play a role in *ZmNit2* regulation.

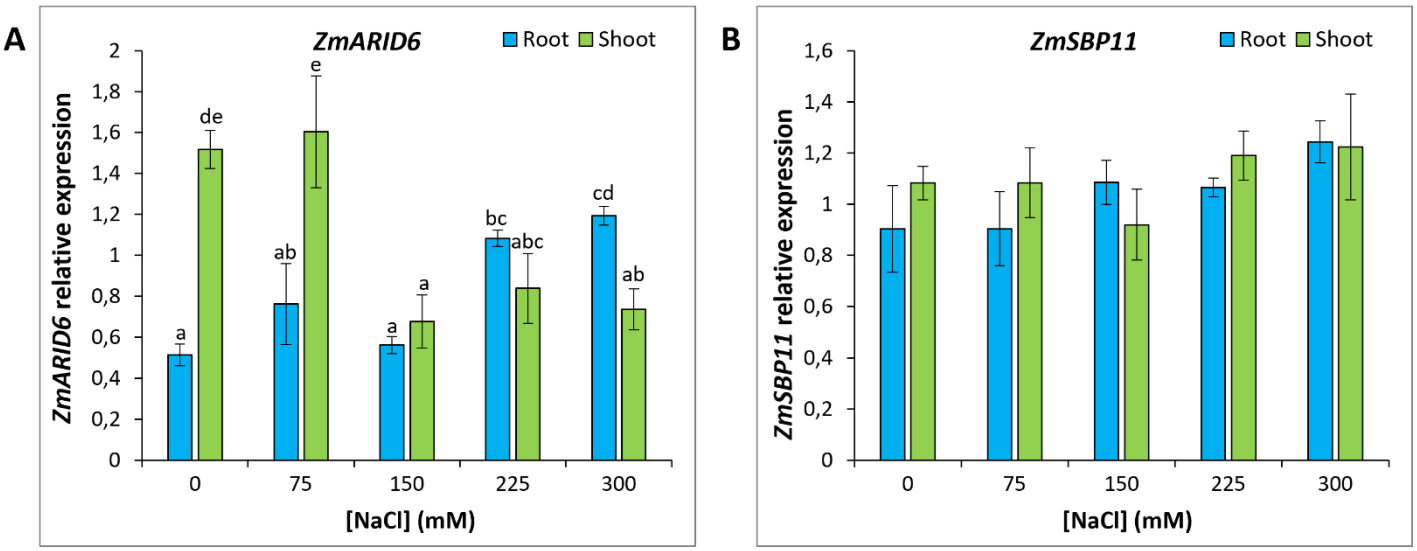

Figure 4.17: *ZmARID6* and *ZmSBP11* gene expression in maize grown under saline conditions

Maize plants were grown hydroponically in Hoagland's solution (control) for five days then transferred onto Hoagland's supplemented with the indicated concentrations of NaCl for nine days. For each treatment, tissue from the second leaf or from the root of three plants were harvested and pooled for RNA extraction and cDNA was synthesised for RT-qPCR gene expression analysis. The results are an average of three pooled tissue samples from independent biological experiments (n=3). **A**: *ZmARID6* expression, **B**: *ZmSBP11* expression. Expression of each gene is shown relative to the *ZmMEP* reference gene. Error bars indicate standard error. Different letters on the graphs indicate mean values that are significantly different ($p \leq 0.05$) as determined by a one-way ANOVA with Fisher LSD post-hoc analysis.

4.4. DISCUSSION

4.4.1. Salt stress negatively impacts the growth and development of the white maize variety, Kalahari Early Pearl

Maize is considered to be more sensitive to salt stress when compared to other important crops such as barley, cotton or sorghum, and it has been shown to be most sensitive to salinity during the vegetative growth stage (Maas et al., 1983). However, there is wide intraspecific genetic variation for salt resistance that exists within maize (Mansour et al., 2005). To date, no data have been shown analysing the change in growth or development of the Kalahari Early Pearl maize variety in response to saline conditions, presumably as it is only agriculturally relevant in Southern Africa.

Our findings here indicate that KEP shoot and root growth and development are inhibited by salinity as shoot and root fresh mass were significantly decreased in a dose-dependent manner, with low NaCl concentrations having more of an impact on shoot mass than root mass (figure 4.2). Moreover, this reduction in fresh mass was not due to a reduction only in leaf size, but to a complete stalling of plant development as illustrated by the reduction in leaf number (figure 4.1). Previous studies have shown that maize shoot growth is strongly inhibited during the first phase of salinity stress. One such studied exposed six day old seedlings to different NaCl treatments for 15 days in hydroponics, and saw that 150 mM NaCl was able to reduce fresh mass by 50-60% compared to untreated plants (Mansour et al., 2005). In another study, two maize lines with differing sensitivity to salt showed a 45-60% reduction in fresh weight in 100 mM NaCl treatment, with the salt-sensitive Pioneer 3906 variety having the higher percentage of fresh mass inhibition (Pitann, Kranz & Mühling, 2009). Szalai and Janda (2009) showed a 30% and 55% reduction in shoot and root fresh mass respectively in two-week old maize plants grown in media with 100 mM NaCl for a further seven days compared to those in control conditions. These results are comparable to ours seen in figure 2.2 where 150 mM NaCl resulted in approximately a 50% inhibition of shoot fresh mass when five day old KEP maize seedlings were exposed to saline conditions for a further nine days. However, in order to draw any conclusions as to whether KEP is a salt-sensitive or salt-tolerant maize variety, further experiments with a higher number of biological replicates should be conducted as well as experiments alongside maize lines with known salt phenotypes, such as the aforementioned salt-sensitive Pioneer 3906 variety and the more salt-tolerant SR03 variety (Pitann, Schubert & Mühling, 2009).

Salt stress also increased the root:shoot ratio in KEP, as expected (figure 4.2C). However, this increase was only significantly different from untreated in 150 and 225 mM NaCl conditions. This increased root growth compared to shoot growth under saline conditions correlates with previous studies, as this would allow for improved water and nutrient uptake and increased pumping of Na^+ back into the soil (Munns & Tester, 2008). As this increased root:shoot ratio was not observed under the highest NaCl concentration, this may indicate that KEP may not be salt tolerant under high salinity stress. Overall, these results illustrate how salinity slows KEP maize shoot and root growth early in development.

To further evaluate KEP salt tolerance in future, further phenotyping should be done to determine, for example, Na^+ and K^+ content, chlorophyll concentration and yield productivity.

4.4.2. *ZmNit2* increases in maize in response to salinity

Arabidopsis microarray assays have shown that *AtNit2* is significantly upregulated in response to NaCl early (figure 2.2E) and later in development (appendix figure 6.6), with a significantly higher induction in the shoot tissue compared to root tissue later in development (Cackett, 2019; Cackett et al., 2022). Expression of *ZmNit2* showed a dose-dependent increase in both root and shoot tissue with increasing NaCl concentrations (figure 4.3), although this was only significant in 225 and 300 mM NaCl compared to untreated. However, the relative *ZmNit2* expression was not significantly different between the root and shoot tissue at any tested NaCl concentration, differing from that seen in Arabidopsis. Analysis of expression of the other maize nitrilase, *ZmNit1,* showed no significant dose-dependent changes. This data agrees with the literature that *ZmNit2* is a homolog of *AtNit2* (Park et al., 2003). Although *ZmNit2* has been shown to be upregulated in maize tissues that show auxin-synthesising activity (Jensen & Bandurski, 1994), this is the first time *ZmNit2* expression has been measured under saline conditions in maize. Overall, these results suggest that *ZmNit2* upregulation occurs in KEP under saline conditions in both root and shoot tissue, in a dose-dependent manner, suggesting that *ZmNit2* may play a role in the maize salinity stress response.

4.4.3. Overexpressing *AtNit2* and *ZmNit2* improves chlorophyll retention

It is known that salt-tolerant species maintain photosynthesis better and show increased or unchanged chlorophyll content under salinity conditions, whereas chlorophyll levels decrease in salt-sensitive species, suggesting that this parameter can be considered a biochemical marker of salt tolerance in plants (Stepien & Johnson, 2009; Ashraf & Harris, 2013).

The chlorophyll content of *35S::AtNit2* leaf discs was significantly higher than WT under untreated and saline conditions (figure 4.6A), indicating that *35S::AtNit2* plants have a higher chlorophyll content and are more tolerant under saline conditions. Similarly, tobacco plants transiently expressing *ZmNit2* had a higher chlorophyll content than leaves infiltrated with the EV construct (control) under control and saline conditions, although this difference was

not statistically significant (figure 4.6B). However, when looking visually, it was apparent that the EV leaves became more yellow and senesced faster under saline conditions than the leaves expressing *35S::ZmNit2* (figure 4.6C). Overall, this indicates that increased *AtNit2* and *ZmNit2* expression both result in increased chlorophyll content in plants. The role of auxins in chlorophyll induction has previously been reported in algae and plants (Salazar-Iribe & De-la-Peña, 2020), and therefore the increased auxin biosynthesis in *35S::AtNit2* plants could result in the increased chlorophyll content that we see in these lines. By this hypothesis, it is possible that ZmNIT2 is also able to induce auxin accumulation in the tobacco leaves, resulting in the increased chlorophyll content that we observed.

4.4.4. Overexpressing *ZmNit2* in Arabidopsis improves salt tolerance, but only early in development

To determine whether *ZmNit2* is able to phenocopy *AtNit2*, Arabidopsis lines overexpressing *ZmNit2* were generated. The resulting homozygous transgenic *35S::ZmNit2* plants displayed varying levels of *ZmNit2* expression, while, as expected, no expression was detected in WT No-0 and the *35S* EV lines (figures 4.10 and 4.12). The variable levels of *ZmNit2* observed in the OE lines was expected due to the nature of Arabidopsis floral-dip transformation where the transgene is inserted randomly into the Arabidopsis genome. This means that the transgene DNA could have integrated near to or far from transcriptional activating elements or enhancers, or different regulatory elements or epigenetic markers, which would lead to variable expression levels (Gelvin, 2003).

Salt assays early and later in development were used to assess the phenotype of *35S::ZmNit2* plants in order to compare to *35S::AtNit2* lines. In early development assays, both *ZmNit2* OE lines tested maintained growth significantly better under both NaCl and sorbitol conditions, as measured by average plant fresh mass compared to the EV control line (figure 4.13). This result indicates that the *ZmNit2* OE lines were more tolerant to saline conditions. This result is comparable to that seen in *35S::AtNit2* plants which have been shown to survive and grow better under saline conditions compared to WT No-0 (Cackett et al., 2022). However, the *ZmNit2* OE lines suffered a growth penalty under control conditions which is not unexpected as there have been numerous examples showing that constitutive expression of genes encoding transcription factors, ion transporters or biosynthetic proteins can lead to

undesirable phenotypes, especially under non-stressed conditions (Karakas et al., 1997; Sheveleva et al., 1997; Kasuga et al., 1999; Cortina & Culiáñez-Macià, 2005; Hmida-Sayari et al., 2005; Suárez, Calderón & Iturriaga, 2009). This growth penalty in untreated conditions was also seen in the root and shoot biomass of the *35S::AtNit2* line later in development (Cackett, 2019), and therefore it appears that constitutively overexpressing both *AtNit2* and *ZmNit2* has detrimental effects on plant growth in the absence of stress.

Plants further along in development did not display the same phenotype under 75 mM as there was no significant difference in shoot (figure 4.14A) mass between the EV and *35S::ZmNit2* lines. This differed from the phenotype seen in *35S::AtNit2* plants which showed significantly higher shoot biomass production compared to the EV. The difference in root biomass under saline conditions between the genotypes could not be assessed as 75 mM NaCl was not high enough to alter root growth of any of the genotypes (figure 1.14B). In future, this experiment should be repeated with a range of NaCl concentrations.

Overall, this indicates that *ZmNit2* overexpression in Arabidopsis was able to reduce the salt- and sorbitol-induced inhibition of growth early in development but did not have any affect later in development.

4.4.5. *ZmNit2* overexpression does not alter *AtEXP11* expression

Plants overexpressing *AtNit2* show significant induction of *AtEXP11* expression compared to WT Arabidopsis (No-0) (Cackett, 2019), as confirmed in figure 4.15. AtEXP11 is part of the family of α-EXPANSINS responsible for cell wall loosening – a process activated following auxin-induced apoplast acidification by the plasma membrane H^+ ATPase (Barbez et al., 2017). This induction of *AtEXP11* was not seen in *35S::ZmNit2* plants (figure 4.15), indicating that overexpressing *ZmNit2* does not result in the same downstream affects as *AtNit2* and that *ZmNit2* is therefore unable to directly phenocopy *AtNit2.* However, there are multiple *EXP* genes, and analysis of other genes downstream of *Nit2* could prove fruitful in determining how *ZmNit2* overexpression is able to improve salt tolerance in Arabidopsis. Additionally, auxin levels should be measured in these lines.

4.4.6. ZmARID6 and ZmSBP11 could be candidates to investigate *ZmNit2* regulation

AtHMGB9 was identified as a putative repressor of *AtNit2* in chapter 3 and shows a downregulation of expression in Arabidopsis shoot tissue in response to salinity in the later development microarray as well as a decrease in two week old seedlings in the early development microarray under saline conditions (figures 3.9G and H). Similarly, the identified maize homolog, *ZmARID6,* was downregulated in KEP maize shoot tissue under saline conditions (figure 4.17A). However, in Arabidopsis there was no change in *AtHMGB9* expression in the root tissue in the later development microarray under saline conditions, but it does appear that *ZmARID6* expression is induced in maize root tissue under high salinity. This data indicates that *ZmARID6* could similarly be acting as a *ZmNit2* repressor in maize shoot tissue and more work should be done to investigate this if *ZmNit2* proves fruitful as a candidate for improving maize salt tolerance.

ZmSBP11 showed no significant change in expression in either KEP maize root or shoot tissue under saline conditions (figure 4.17B), mimicking that seen for *AtSPL7* in both the early and later development Arabidopsis microarrays where there was no significant change in *AtSPL7* expression under saline conditions (figures 3.9K and L). If further work in Arabidopsis shows that AtSPL7 plays a role in *ZmNit2* regulation, further work can be done to characterise the role that ZmSBP11 may play in *ZmNit2* regulation.

4.4.7. Summary

The South African maize variety, Kalahari Early Pearl, showed significant reductions in growth and development in both roots and shoots under saline conditions. The maize *AtNit2* homolog, *ZmNit2*, was induced by NaCl in both root and shoot tissue in a dose-dependent manner, and initial promoter analysis indicates that this gene may be similarly regulated to *AtNit2*. Overexpressing *ZmNit2* was sufficient to increase salt tolerance of Arabidopsis plants early in development, as observed by a decreased inhibition of growth under saline conditions, and larger plants under 125 mM NaCl conditions. However, no altered phenotype was observed later in development in response to 75 mM NaCl treatment. Overall, these results indicate that *ZmNit2* may play a role in the maize response to salt stress and validate that the work we are conducting in Arabidopsis is at least partly relevant to important crop plants such as maize. Further work needs to be conducted in this regard, including measuring

auxin levels in the *35S::ZmNit2* Arabidopsis lines, and characterisation of maize *ZmNit2* overexpressing and null mutant lines for changes in salt tolerance and auxin accumulation.

CHAPTER 5: FINAL DISCUSSION AND SUGGESTIONS FOR A WAY FORWARD

To engineer crops with enhanced salt tolerance, we need a better understanding of inherent plant molecular responses to salt stress. Our group has previously identified *AtNit2* as a candidate for enhancing plant growth under saline conditions to improve salt tolerance (Cackett et al., 2022). Thus, it is important to understand how this gene is regulated, and therefore investigating the regulation of *AtNit2* was the main aim of this research project. Additionally, this study aimed to investigate whether this work being conducted in Arabidopsis, a model plant not agriculturally important, is transferrable or relevant to maize, an important crop plant. As far as we know, this is the first time an unbiased approach was taken to identify potential *AtNit2* regulators and the first time any candidate TF regulators of *AtNit2* (other than AtATAF2) were characterised in Arabidopsis. It is also the first time a role for ZmNIT2 in salinity tolerance has been proposed. The main empirical and functional findings of this study are presented in detail in chapters 2-4. The aim of this final chapter is not only to highlight key findings in the context of the other literature, but to also acknowledge some caveats and limitations of aspects of this study, while also presenting some suggestions for a way forward.

5.1. *AtNit2* regulation

5.1.1. Identifying potential regulators of *AtNit2* through promoter analysis

In silico analysis of the *AtNit2* promoter sequence revealed the presence of five different MYB TFBS in the 1 kb of DNA upstream of the *AtNit2* translation start site (table 2.2; appendix figure 6.2), suggesting that one or more MYB TFs may be able to bind to and regulate *AtNit2* promoter activity. The first limitation to this lies in predicting the size of the gene promoter. Previous research has found that analysing the first 1 kb upstream of a gene translation start site in Arabidopsis is usually sufficient to identify the TFBS important in gene regulation (Riechmann, 2002), but there may be sites further upstream than this in the case of *AtNit2* that were not considered in this analysis. In fact, there is 2649 bp of DNA upstream of the 5' UTR of *AtNit2* before a long-noncoding RNA region (AT3G06765.1), with ~5 kb of DNA upstream of that before the first neighbouring gene (AT3G44290; see appendix figure 6.9)), meaning that the promoter region of *AtNit2* could actually span a much larger size. Indeed,

publicly available DAP-seq data in the Plant Cistrome Database (http://neomorph.salk.edu/dap_web/pages/index.php; O'Malley et al., 2016) reveals many TFBS upstream of *AtNit2*, with most further away than the 1368 bp tested in the Y1H experiment (see appendix figure 6.9). There could also be enhancer regions tens or hundreds of kb from the *AtNit2* locus, that may be important for *AtNit2* regulation which were not considered. Another caveat to this analysis is the fact that many TFBS are still unknown, meaning that many more TFBS could be present in the promoter region that are yet to be annotated. Additionally, most TFBS in the databases have been annotated based on experimental data from a single experiment, rather than compiling data from a diverse range of sources. For example, in the analysis of the *AtNit2* promoter region, the BS for AtATAF2 was not identified, but a paper has been published showing where this site is located (Huh et al., 2012). Many computational tools are available that analyse promoter DNA and predict TF binding based on a single source showing a specific TF bound to a particular section of DNA in a particular experiment *in vitro*, but it doesn't necessarily mean that that TF can actually bind to that particular promoter region *in planta*, or that other TFs can't bind that region. Subsequently, despite the *in silico* analysis identifying multiple MYB TFBSs in the putative *AtNit2* promoter region, one is unable to determine which of the large family of MYB TFs (if any) can bind to the *AtNit2* promoter region, and in what context, without actually testing for protein-DNA interaction *in vivo*.

As a preliminary approach to obtain some candidate TFs, the list of salt-specific genes upregulated early in Arabidopsis development was queried for any MYB TFs. Interestingly, two MYB TFs were significantly upregulated under saline conditions in the early development microarray; *AtMYB30* and *AtMYB2* (figure 2.2). However, Y1H analysis did not identify any direct binding of any MYB TFs to the *AtNit2* promoter DNA. This is in line with predictions from the Plant Cistrome Database (http://neomorph.salk.edu/dap_web/pages/index.php; O'Malley et al., 2016) where the only MYB TF predicted to bind upstream of *AtNit2* is AtMYB119 and this falls outside of the promoter region tested in the Y1H experiment (see appendix figure 6.9). This does not exclude AtMYB30 or AtMYB2 from being able to regulate *AtNit2* expression *in planta* as they may require post-translational modifications (PTMs) to be active that do not occur in yeast or may need to form part of a complex with another Arabidopsis TF. Additionally, they could play a role in indirectly regulating *AtNit2* by regulating

another gene upstream of *AtNit2* in the salt stress response or may only bind the *AtNit2* promoter under specific conditions or at certain developmental stages.

5.1.2. AtMYB30 may indirectly positively regulate *AtNit2* during the Arabidopsis salt stress response

Arabidopsis *35S::AtMYB30* OE lines maintained growth better under saline conditions early in development (figure 2.14), while the *atmyb30-2* mutant line displayed a greater degree of growth inhibition under saline conditions than WT (figure 2.15). However, phenotyping of another *atmyb30* mutant line should be performed as the two T-DNA mutant lines phenotyped in this study displayed slightly different results, with the *atmyb30-1* line not showing any significant difference in biomass compared to WT early in development (figure 2.15). In a recent study by Gong et al. (2020), a different *atmyb30* mutant was shown to be more sensitive to 125 mM NaCl, in agreement with our data for *atmyb30-2.* No changes in salt tolerance were seen in either the *atmyb30-2* or *35S::AtMYB30* lines later in development (figure 2.15). This data indicates that *AtMYB30* may play a positive role in the Arabidopsis salt stress response early, but not later in development. However, these phenotyping assays later in development should be repeated with more salt concentrations to determine whether any changes are seen in response to higher salinity. Previously, Mabuchi et al. (2018) showed that an *atmyb30* mutant line had significantly longer roots than WT, and an *AtMYB30* OE line had significantly shorter roots than WT under H_2O_2 (ROS) conditions, indicating that AtMYB30 regulates root cell elongation in response to ROS. It would therefore be interesting to analyse root elongation and architecture under saline conditions in the *AtMYB30*-misexpressing lines compared to WT, given that salinity stress leads to ROS accumulation and given the role of auxin in root responses to salinity stress (e.g., halotropism). Other auxin-related growth phenotypes, such as hypocotyl elongation, can also be tested in these lines, and IAA metabolite levels should be measured to understand the role of AtMYB30 in auxin-mediated plant growth. These analyses should also be conducted in the *AtMYB2* OE lines. Prior to this, the copy number of the transgene insertions should be assessed in all stable transformants, using Southern blot analysis or digital droplet (dd)PCR for example, to ensure a single insertion into the Arabidopsis genome (Głowacka et al., 2016). Single insertions are desirable in order to ensure segregation in a Mendelian fashion and to prevent gene silencing (Collier et

al., 2017). Additionally, multiple copies may have more effect both in terms of overexpression of the GOI as well as in terms of interfering with native genes at the site of insertion.

Interestingly, expression of *AtNit2* was significantly higher in the *AtMYB30* OE lines compared to the EV control line in both untreated and saline conditions (figure 2.17A). The *atmyb30* mutant lines did not display opposite results but instead also showed elevated *AtNit2* expression compared to WT, although only under saline conditions (figure 2.17B). If AtMYB30 was the main regulator of *AtNit2* expression in response to salt stress, acting only as either a direct activator or repressor, we would expect that the OE and KO lines would have opposite phenotypes; the fact that *AtNit2* expression is upregulated under saline conditions in both lines indicates that *AtNit2* regulation in the salt stress response is complex and there must be other mechanisms in place to ensure *AtNit2* induction under saline conditions. A major limitation to this project was only analysing gene expression at one time point after stress imposition for two weeks. As TF expression is usually altered after short exposure to stress conditions, and usually TF expression precedes target gene expression (Vom Endt, Kijne & Memelink, 2002), earlier time points would be particularly relevant to include in a future time course experiment. For example, in maize a time course was used for gene expression profiling with samples collected at 0, 0.5, 1, 2, 4, 8, 12, 24, 48, 72, 120 and 168 h after 100 mM NaCl treatment (Luo et al., 2021). As a result, many TFs that play a role in the salt stress response may not have been identified in our group's salinity stress transcriptomic experiments. Overall, these results are the first to indicate that *AtMYB30* might play a role in regulating *AtNit2,* although determining how and when, and whether this is important in the Arabidopsis salt stress response, requires further analyses.

Recently, AtMYB30 was linked to the Arabidopsis salt stress response for the first time (Gong et al., 2020). These researchers found that AtMYB30 plays a regulatory role in Arabidopsis salt tolerance by directly binding to and regulating *AtAOX1a* expression, thereby maintaining cellular redox homeostasis through enhanced alternative respiration. They showed this direct binding via three E1-like motifs (ACCAAAC) using Y1H analysis *in vivo,* and ChIP-qPCR *in planta*. They found that AtMYB30 needs to be SUMOlyated by AtSIZ1 before it is able to bind to the *AtAOX1a* promoter to upregulate its gene expression, and that when this SUMOlyation is abolished, plants are more sensitive to salt stress (Gong et al., 2020). Interestingly, despite the E1-like motif being present in the *AtNit2* promoter region (within fragments 3 and 4),

designated as 'MYB4 binding site' in table 2.2 and appendix figure 6.2, no binding was observed in our Y1H. It is possible that no direct binding was seen between AtMYB30 and the *AtNit2* promoter in the Y1H screening because AtMYB30 needs to be SUMOlyated prior to DNA binding. To assess whether AtMYB30 can bind to the *AtNit2* promoter using a different method, EMSA can be conducted. Additionally, an anti-AtMYB30 antibody can be obtained for ChIP-qPCR or ChIP-Seq under control and saline conditions which would determine whether AtMYB30 occupancy of the *AtNit2* promoter changes under saline conditions. In future, a more thorough investigation into the post-translational modification of AtMYB30 and AtMYB2 is also needed. Various *in silico* tools exist to predict PTM domains (reviewed in Audagnotto & Dal Peraro, 2017) which can be used as a first approach. Following this, PTM-antibody specific immunoprecipitation and western blot analysis can be used to confirm any predicted PTM. The results from this can then inform further protein-DNA interaction studies.

5.1.3. AtHMGB9 and AtSPL7 are putative repressors of *AtNit2*

In order to identify other TFs which may play a role in regulating *AtNit2* expression, a Y1H analysis was used. Six different TFs were identified that showed specific binding with one or more sections of the *AtNit2* promoter: AtHMGB9, AtSPL7, AtGL2, AtHB34, AtHB24 and AtHB28 (table 3.4). As far as we can tell, this is the first time that any of these TFs have been linked to *AtNit2.* Importantly, we don't exclude the importance of other TFs (that may not have been present in our TF library or were unidentifiable in the Y1H system) in transcriptional regulation of *AtNit2*, either under saline conditions or other conditions. As previously discussed, ascertaining the size of the full promoter region is difficult, so it is possible that some important TFs were not identified in this analysis as they may be further upstream of *AtNit2* than what I tested. Thus, the Y1H should be repeated with more promoter fragments further upstream of *AtNit2* than 1368 bp. Interestingly, none of the TFs identified in the Y1H screen were shown to bind in the DAP-seq experiment in the Plant Cistrome Database (http://neomorph.salk.edu/dap_web/pages/index.php; O'Malley et al., 2016). Additionally, AtATAF2 which has been shown to bind in the 117 bp region upstream of *AtNit2* (Huh et al., 2012) was not shown to bind under the conditions used in this DAP-seq experiment. Conversely, the TFs able to bind to the *AtNit2* promoter in this published DAP-seq experiment, such as AtREM19 (see appendix figure 6.9), which do fall within the promoter region tested, were not shown to bind in the Y1H experiment. This highlights how different TFs may only

bind in certain contexts and shows how important it is to determine under what conditions the TFs identified in the Y1H experiment may regulate *AtNit2*. In future, one possible way to determine the region of DNA containing the *AtNit2* regulatory elements is to perform an assay for transposase accessible chromatin with high-throughput sequencing (ATAC-seq) on plants grown under untreated and saline conditions to determine which regions of chromatin (and thus which TFBS) become more accessible during salinity stress. The regions that become more accessible under saline conditions upstream of *AtNit2* would likely contain important sites for binding of TFs during the salt-induced upregulation of *AtNit2*. These regions can then be used if the Y1H is repeated.

Based on our findings and previous literature, we hypothesise that AtHMBG9 binds to the AAATAAA motif present in the *AtNit2* promoter region within the two fragments that interacted via Y1H. To confirm this, the protoplast reporter assays can be repeated using a version of the *AtNit2* promoter with mutations in the AAATAAA sites to determine whether these are necessary for AtHMGB9 to alter *AtNit2* promoter activity. Additionally, EMSAs could be performed with sections of the promoter DNA containing these sites as well as with these sites mutated. Our findings showed that *AtHMGB9* expression is inhibited under saline conditions (figure 3.17B), and that *athmgb9* knock-down lines show slightly increased *AtNit2* expression under saline conditions (figure 3.17A). In line with this, reporter assays in Arabidopsis mesophyll protoplasts showed that AtHMGB9 is able to repress *AtNit2* promoter activity *in planta* (figure 3.12). Taken together, these results indicate that AtHMGB9 is a direct repressor of *AtNit2*. However, *athmgb9* knock-down lines showed slightly decreased salt tolerance (figure 3.16) implying that AtHMGB9 might be responsible for other important processes in the salt-stress response other than *AtNit2* regulation. To elucidate these, it would be interesting to obtain anti-AtHMGB9 antibody to perform a ChIP-seq analysis to determine which other DNA regions AtHMBG9 is able to bind to. Another TF identified by the Y1H, AtSPL7, appears to play a role in negatively regulating *AtNit2* transcription as *AtNit2* was slightly, but significantly, higher in an *atspl7* mutant line under control and saline conditions (figure 3.21A). However, AtSPL7 did not alter *AtNit2* promoter activity in untreated Arabidopsis mesophyll protoplasts (figure 3.12). This indicates that AtSPL7 may need to bind in combination with other co-factors to repress *AtNit2* promoter activity or may only play a role in *AtNit2* regulation under certain conditions. To test this, it would be interesting to

optimise a transient reporter assay in protoplasts under saline conditions. In future, EMSAs and ChIP-qPCR can be used as additional ways to test if AtSPL7 is able to directly bind the *AtNit2* promoter DNA, especially if a ChIP-qPCR can be performed under saline conditions. It would also be interesting to perform a pull-down assay with AtSPL7, or a yeast two-hybrid, to identify which other TFs AtSPL7 is able to bind to. If other TFs are identified that form a complex with AtSPL7, these can be tested in the protoplast reporter assays to assess whether *AtNit2* promoter activity is altered.

As AtHMGB9 and AtSPL7 are both potential repressors of *AtNit2*, it would be interesting to see whether overexpressing these genes prevents the salt-induced upregulation of *AtNit2* seen in Arabidopsis. However, as both of these TFs presumably regulate many genes, this makes mutant/OE analysis very complex. One way to prevent off-target effects is to overexpress these genes under multiple copies of the endogenous promoter. It is also possible that AtHMGB9 and/or AtSPL7 may only play a role in *AtNit2* regulation under different conditions and may not play a role in the salt-stress response at all. In future, this should be explored by analysing expression of these TFs, as well as the other TFs identified in the Y1H and *AtNit2*, under various conditions and at different developmental stages.

5.1.4. Investigating the role of AtHB34, AtHB24, AtHB28, and AtGL2 in *AtNit2* regulation

The same experiments to validate TF-DNA binding *in planta* should be conducted for these TFs as were performed for AtHMGB9 and AtSPL7. As previously mentioned, it is likely that the ZF-HD TFs act in the form of heterodimers with other members of the family (Tan & Irish, 2006). Thus, AtHB34, AtHB24 and AtHB28 should be tested in protoplast reporter assays alone, and in different combinations. For the same reason, T-DNA insertion mutants for each TF should be obtained, and different combinations of mutant lines should be cross-fertilised and double and triple mutants isolated. This will enable us to phenotype lines lacking each TF alone and in various combinations to test if any show alteration in *AtNit2* expression and salt tolerance. The aforementioned researchers also showed that AtHB34 may be redundant with AtHB23 and AtHB30 (Tan & Irish, 2006), so including these TFs in these analyses might also be necessary to obtain a phenotype. Based on this proposed redundancy, it would also be interesting to test whether overexpressing only one/two of these TFs might be sufficient to alter *AtNit2* expression and/or salt tolerance.

Of the six TFs identified in the Y1H screening, AtGL2 is the best characterised. Previous research has shown that *AtGL2* expression is downregulated by salinity stress (Beyrne, Iusem & González, 2019) which was consistent with our findings (figure 3.9I). This data suggests that if AtGL2 is involved in *AtNit2* regulation, it may be acting as a repressor early in development as its expression pattern is opposite to that of *AtNit2.* Based on the Y1H data and the available literature, we hypothesise that AtGL2 binds to the L1-box in the *AtNit2* promoter (TAAAATG) (which did not come up in the *in silico* promoter analysis as it was missing from the database). This should be tested using EMSAs with both the WT promoter region and a promoter with a mutation in this L1-box. If reporter assays in Arabidopsis protoplasts show that AtGL2 alters *AtNit2* promoter activity, this can also be repeated with the mutated promoter to determine whether this change in activity is abolished. Additionally, it would be interesting to obtain *atgl2* mutants and *AtGL2* overexpressing lines to test whether either have altered *AtNit2* expression and/or IAA levels, and to determine whether this impacts plant salinity tolerance.

Additionally, the role of *AtATAF2* in *AtNit2* regulation needs to be further investigated. To do this, *atataf2* mutant (Huh et al., 2012) should be obtained and characterised to determine if they lose the NaCl-induced *AtNit2* upregulation seen in WT plants. *AtATAF2*-misexpressing lines should also be characterised for auxin-related phenotypes such as changes in hypocotyl or root elongation, and changes in IAA metabolite levels. Despite not binding in our Y1H experiment, previous research has shown binding of AtATAF2 to the *AtNit2* promoter (Huh et al., 2012), so it would be interesting to test this TF in our hands in protoplast reporter assays, EMSAs, and ChIP-qPCR. Additionally, other TFs are predicted to have binding sites within the region upstream of *AtNit2* and these should be investigated in future studies. For example, in the Plant Cistrome Database, multiple NAC domain TFs are predicted to bind upstream of *AtNit2* as well as AtREM19 (see appendix figure 6.9).

5.1.5. When and where is *AtNit2* produced?

Arabidopsis reporter lines for *AtNit2* should be generated in order to investigate when and where *AtNit2* is produced. At the beginning of this research project, this was one of the aims. However, two different lines with the LucF gene downstream of different sized *AtNit2* putative promoter sequences (1 kb and ~1.3 kb) in two different reporter vectors (pBGWL7 and pART27) were generated, and neither was able to successfully report on *AtNit2* promoter

activity. It is possible that more transgenic lines need to be screened to identify a line with proper reporter activity, or perhaps a longer region of DNA upstream of *AtNit2* needs to be used. The aforementioned ATAC-seq should be able to inform this. A different reporter, such as GFP, could also be used. Additionally, a GUS reporter line could be used to determine *AtNit2* localisation throughout the salt stress response. If a successful reporter line is generated, mutations could also be introduced in specific TFBS to provide information on where and when that particular TF binds and regulates *AtNit2* expression. The *AtNit2* reporter line could also be crossed with a TF mutant line, such as *athmgb9,* to further characterise how the TF regulates *AtNit2* expression.

5.1.6. Determining the important regulatory regions for modulating the salt stress response

The aforementioned ATAC-seq experiment would provide insight into regulatory regions throughout the genome which are important for modulating the salt stress response This experiment can be paired with an RNA-seq analysis at several time-points to determine whether any changes in chromatin accessibility are associated with changes in gene expression. This will enable identification of other important salt stress responses and potential candidates for engineering salt tolerance. Increasing the copy number of regions that become more accessible under saline conditions upstream of important genes, e.g., *AtNit2,* could result in overexpression only under saline conditions which may mitigate the negative impact that overexpression of *AtNit2* has on root and shoot growth in untreated control conditions.

5.2. ZmNIT2 may play a role in the maize salt stress response

Expression of the maize *AtNit2* homolog, *ZmNit2*, was upregulated in the white maize variety Kalahari Early Pearl (KEP) in both root and shoot tissue in response to high NaCl treatments (figure 4.3). It would be interesting to repeat salt phenotyping experiments with maize plants grown for different lengths of time to determine whether *ZmNit2* is upregulated by salinity at different developmental stages. Although *AtNit2* is more highly expressed in Arabidopsis shoot tissue than in root tissue later in development (appendix figure 6.6), there was no significant difference in expression of *ZmNit2* between these tissue types in maize under the

conditions tested (figure 4.3), indicating that it might play a common role in the salt stress response in both tissue types and might have some different functions than AtNIT2.

As there is wide intraspecific genetic variation for salt resistance within maize (Mansour et al., 2005), it would be interesting to analyse the growth of multiple varieties under saline conditions to assess how tolerant each one is to salinity stress. Thereafter, *ZmNit2* gene expression levels can be compared between them to determine whether there is a link between the level of *ZmNit2* expression and degree of salt tolerance.

Researchers have shown that ZmNIT2 hydrolyses IAN to IAA (Park et al., 2003). Therefore, it is possible that maize plants grown under high NaCl conditions may induce *ZmNit2* expression to alter IAA levels, in an effort to maintain plant growth during salt stress. To investigate this further, ZmNIT2 protein expression and activity, and IAA metabolite levels, should be measured in maize grown under saline conditions. Critically, a limitation in the work presented in chapter 4 is that ZmNIT2 may exhibit different functions during heterologous expression in *Nicotiana* or Arabidopsis, and therefore analysis of a maize *zmnit2* mutant and characterisation of a maize transgenic line overexpressing *ZmNit2* should also be performed to assess whether altering *ZmNit2* expression in maize leads to any changes in salt tolerance. In order to definitively determine whether ZmNIT2 can phenocopy AtNIT2, it would be useful to complement an Arabidopsis *atnit2* mutant with *ZmNit2* under the control of the native *AtNit2* promoter. If this complementation could restore the WT phenotype then this would indicate that ZmNIT2 is functionally the same as AtNIT2. However, previous work on two different *atnit2* T-DNA mutant lines, and one *atnit2* RNAi line (with knocked down expression of all three *AtNit1* family genes) has been unable to identify any phenotypic changes compared to WT under saline conditions, meaning that there would be no known salt phenotype to test for complementation (Cackett et al., 2022). However, the *atnit2* RNAi line does have less total IAA levels (Lehmann et al., 2017), so if *ZmNit2* was transformed into this line we could investigate whether this is altered. Additionally, more *atnit2* mutant lines should be phenotyped, and they should be further characterised under saline conditions for different phenotypes such as halotropism, in order to identify a line with a measurable phenotype to be used in the complementation test.

As a preliminary analysis, *ZmNit2* was overexpressed in Arabidopsis. This *35S::ZmNit2* Arabidopsis line maintained growth better under saline conditions early in development and

had a higher fresh mass in 125 mM NaCl than EV (figure 4.13). Therefore, IAA metabolite levels should be measured in order to determine if this line is accumulating more IAA compared to the empty vector control under saline conditions, and thus may be responsible for modulating its growth. Different auxin-related phenotypes, such as hypocotyl elongation, could also be examined in the *35S::ZmNit2* Arabidopsis line. Despite *AtEXP11* expression not being upregulated in the *ZmNit2* OE in the same manner as it is in the *AtNit2* OE (figure 4.15), this does not exclude the possibility that the *ZmNit2* OE line may have altered expression of other genes proposed to act downstream in modulating growth in response to auxin. Therefore, the transcriptome of the *ZmNit2* OE could be analysed to see what is altered that might help it tolerate salt better compared to the EV control. Additionally, this can be compared to the transcriptomic changes in the *AtNit2* OE line to identify conserved genes that would presumably then represent core components of the plant salinity response.

Should it be determined that *ZmNit2* is a candidate for improving maize salt stress tolerance, it would be useful to express it under the control of different stress-inducible promoters, such as the *rd29A* promoter (Kasuga et al., 1999; Qiu et al., 2012), or multiple copies of its own promoter, to test which works best in improving salt tolerance without the negative growth penalties seen in control conditions when constitutively expressing *ZmNit2* (figure 4.13) and *AtNit2* (Cackett, 2019). Furthermore, if the aforementioned suggestions for identifying important TFBS for *AtNit2* induction under saline conditions to improve salt tolerance are followed, and similar regulation of *ZmNit2* is discovered, a promoter region could be engineered containing multiple copies of these TFBS. In this way, maize could be engineered to respond more robustly to salinity.

5.3. CONCLUSION

Overall, this study provides novel insights into the regulation of *AtNit2* by identifying several TFs that may bind to and regulate *AtNit2* expression. We propose that AtMYB30 may act as a positive regulator of *AtNit2* expression, though indirectly, and AtHMGB9 may act directly as a negative regulator. This study also shows that expression of *Nitrilase 2* in response to salt stress is conserved in maize, and *ZmNit2* is able to improve Arabidopsis salt tolerance, thus indicating a potential role for *ZmNit2* in engineering improved maize salt tolerance. In future, it will be important to understand the regulation of *Nit2* in the context of auxin-mediated salt

tolerance, and to understand the context under which the TFs identified in this study regulate *AtNit2*.

CHAPTER 6: APPENDIX

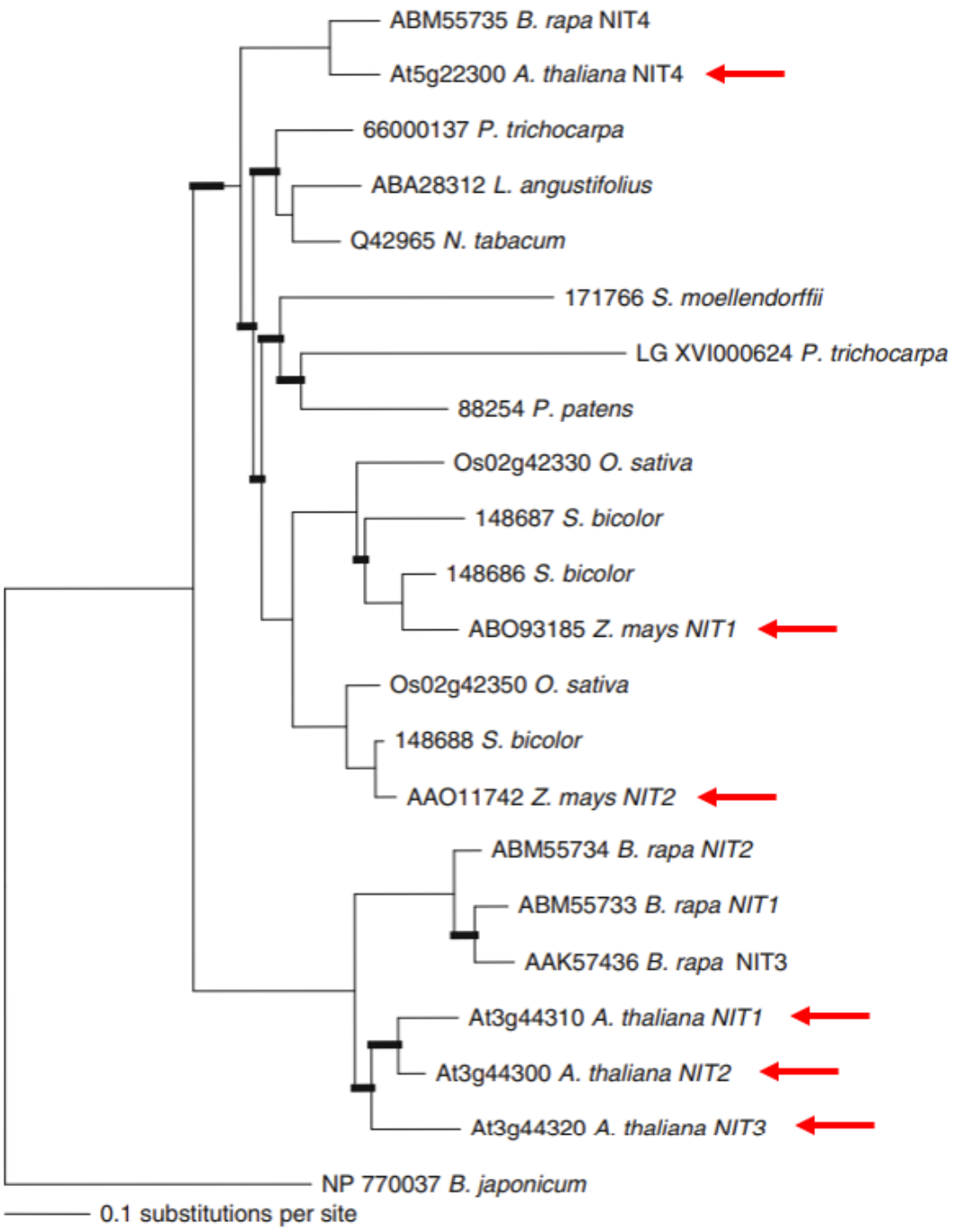

Appendix figure 6.1: Distribution of nitrilases within the plant kingdom (Abu-Zaitoon, 2014)

A phylogenetic analysis of plant nitrilases performed by Abu-Zaitoon (2014). Bold line branches indicate that the bootstrap values are less than 95%. The specific Arabidopsis and maize nitrilases of interest in this project are indicated with red arrows.

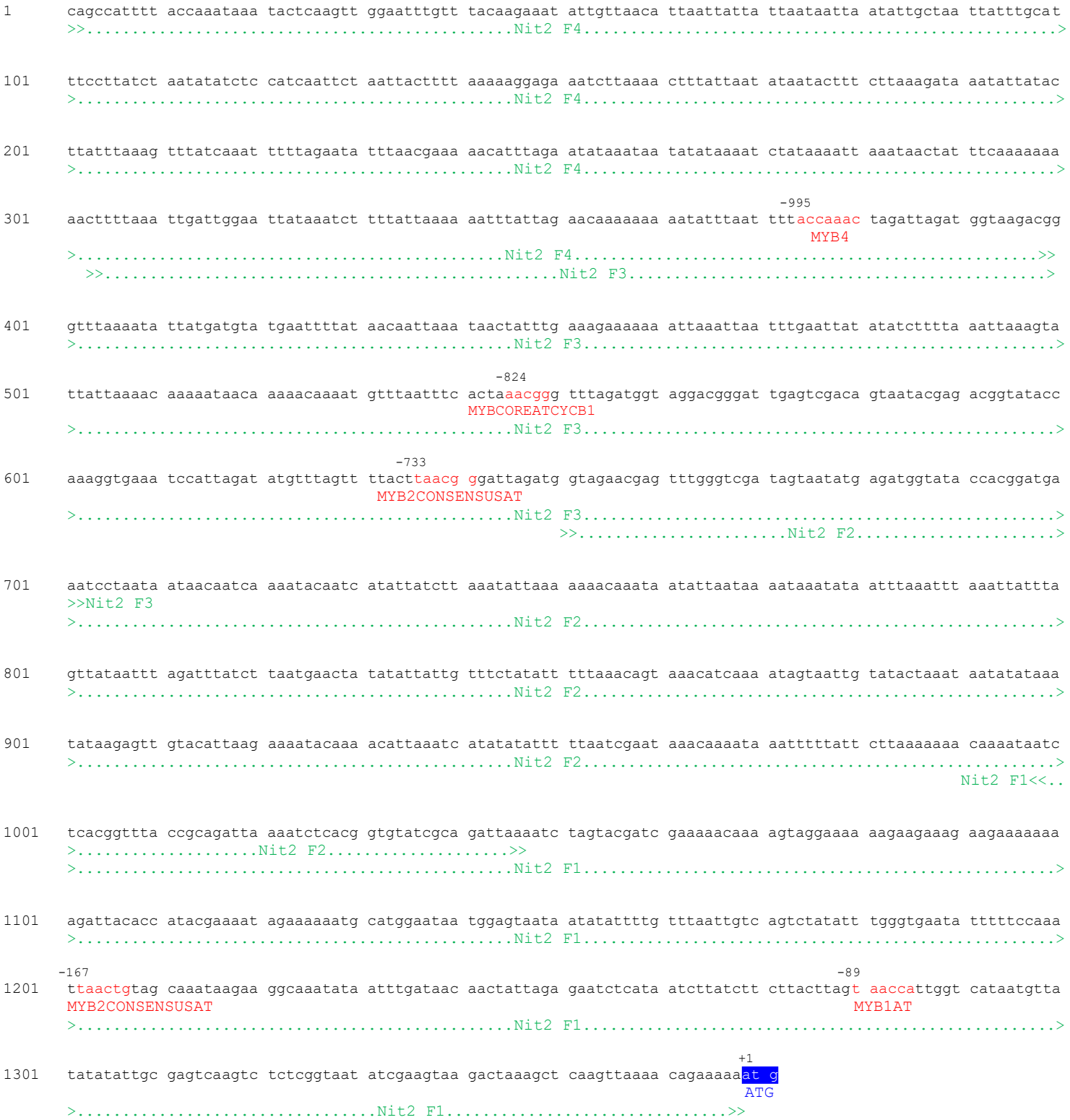

Appendix figure 6.2: The annotated *AtNit2* promoter

The full *AtNit2* promoter sequenced used in the transient reporter assays, with the promoter fragments used in the Y1H experiment annotated in green. The MYB TFBS are annotated in red. The positions of the TFBS are annotated relative to the ATG translation start site.

Appendix table 6.1: Transcription factors in the salt-specific gene list upregulated ≥ 2-fold

Gene accession number	Gene name/description	TF family	Fold change in response to NaCl
AT1G19350	*BRI1-EMS-SUPPRESSOR 1 (BES1)*	BES1	2.47
AT1G31140	*GORDITA (GOR)*	MADS-MIKC	7.30
AT1G51700	*DOF ZINC FINGER PROTEIN 1 (DOF1)*	C2C2-Dof	2.20
AT1G59530	*BASIC LEUCINE-ZIPPER 4 (bZIP4)*	bZIP	6.45
AT1G68800	*BRANCHED 2 (BRC2)*	TCP	3.41
AT1G68880	*BASIC LEUCINE-ZIPPER 8 (bZIP8)*	bZIP	2.66
AT1G75430	*BEL1-LIKE HOMEODOMAIN 11 (BLH11)*	HB-BELL	4.37
AT2G18490	*GA- AND ABA-RESPONSIVE ZINC FINGER (GAZ)*	C2H2	7.90
AT2G22200	*ETHYLENE RESPONSE FACTOR 56 (ERF56)*	ERF/AP2	2.16
AT2G28610	*PRESSED FLOWER (PRS)*	HB-WOX	2.83
AT2G42830	*SHATTERPROOF 2 (SHP2)*	MADS-MIKC	3.83
AT2G46400	*WRKY DNA-BINDING PROTEIN 46 (WRKY46)*	WRKY	5.42
AT2G47190	*MYB DOMAIN PROTEIN 2 (MYB2)*	MYB	2.95
AT3G17010	*REPRODUCTIVE MERISTEM 22 (REM22)*	B3	2.46
AT3G28857	*PACLOBUTRAZOL RESISTANCE 5 (PRE5)*	bHLH	2.32
AT3G28910	*MYB DOMAIN PROTEIN 30 (MYB30)*	MYB	2.31
AT3G50510	*LOB DOMAIN-CONTAINING PROTEIN 28 (LBD28)*	LOB	2.93
AT4G18170	*WRKY DNA-BINDING PROTEIN 28 (WRKY28)*	WRKY	2.68
AT4G18890	*BES1/BZR1 HOMOLOG 3 (BEH3)*	BES1	4.37
AT4G25490	*C-REPEAT/DRE BINDING FACTOR 1 (CBF1)*	ERF/AP2	4.90
AT5G01380	Homeodomain-like superfamily protein	Trihelix	3.39
AT5G04150	*bHLH101*	bHLH	2.94
AT5G13330	*RELATED TO AP2 6L (RAP2.6L)*	ERF/AP2	3.09
AT5G15160	*BANQUO 2 (BNQ2)*	bHLH	2.38
AT5G22570	*WRKY DNA-BINDING PROTEIN 38 (WRKY38)*	WRKY	7.20
AT5G26170	*WRKY DNA-BINDING PROTEIN 50 (WRKY50)*	WRKY	3.34
AT5G27810	MADS-box transcription factor family protein	MADS-M-type	2.99
AT5G39860	*PACLOBUTRAZOL RESISTANCE1 (PRE1)*	bHLH	3.36

Information on the "gene name/description" associated with each gene accession number is reported according to TAIR (https://www.arabidopsis.org/). The values in the "fold change in response to NaCl" column are the greatest fold changes seen for each gene across the four NaCl treatments, relative to the untreated control. Information on the TF families were obtained from http://plntfdb.bio.uni-potsdam.de.

Appendix table 6.2: Segregation ratios of the T2 Arabidopsis EV, *35S::AtMYB2,* and *35S::AtMYB30* lines (Col-0 BG)

Genotype	Line	PN %	GFSA %	Transgenic %
EV	5	32	98	306,3
	6	90	80	88,9
	11	86	64	74,4
	14	92	92	100,0
	15	74	58	78,4
	19	62	66	106,5
35S::AtMYB2	1	56	40	71,4
	6	34	28	82,4
	8	76	44	57,9
	14	90	56	62,2
	22	76	58	76,3
35S::AtMYB30	2	56	36	64,3
	5	72	68	94,4
	6	92	60	65,2
	12	46	58	126,1
	13	78	0	0,0
	15	76	56	73,7
	16	76	64	84,2
	17	74	68	91,9
	23	68	56	82,4
	24	70	66	94,3

Appendix figure 6.3: Dwarf phenotype of *35S::AtMYB30* line 2

Seeds of *35S::AtMYB30* lines 2.3 and 23.2 were planted on soil and allowed to grow for 4 weeks. Both genotypes were given the same amount of water and growth conditions.

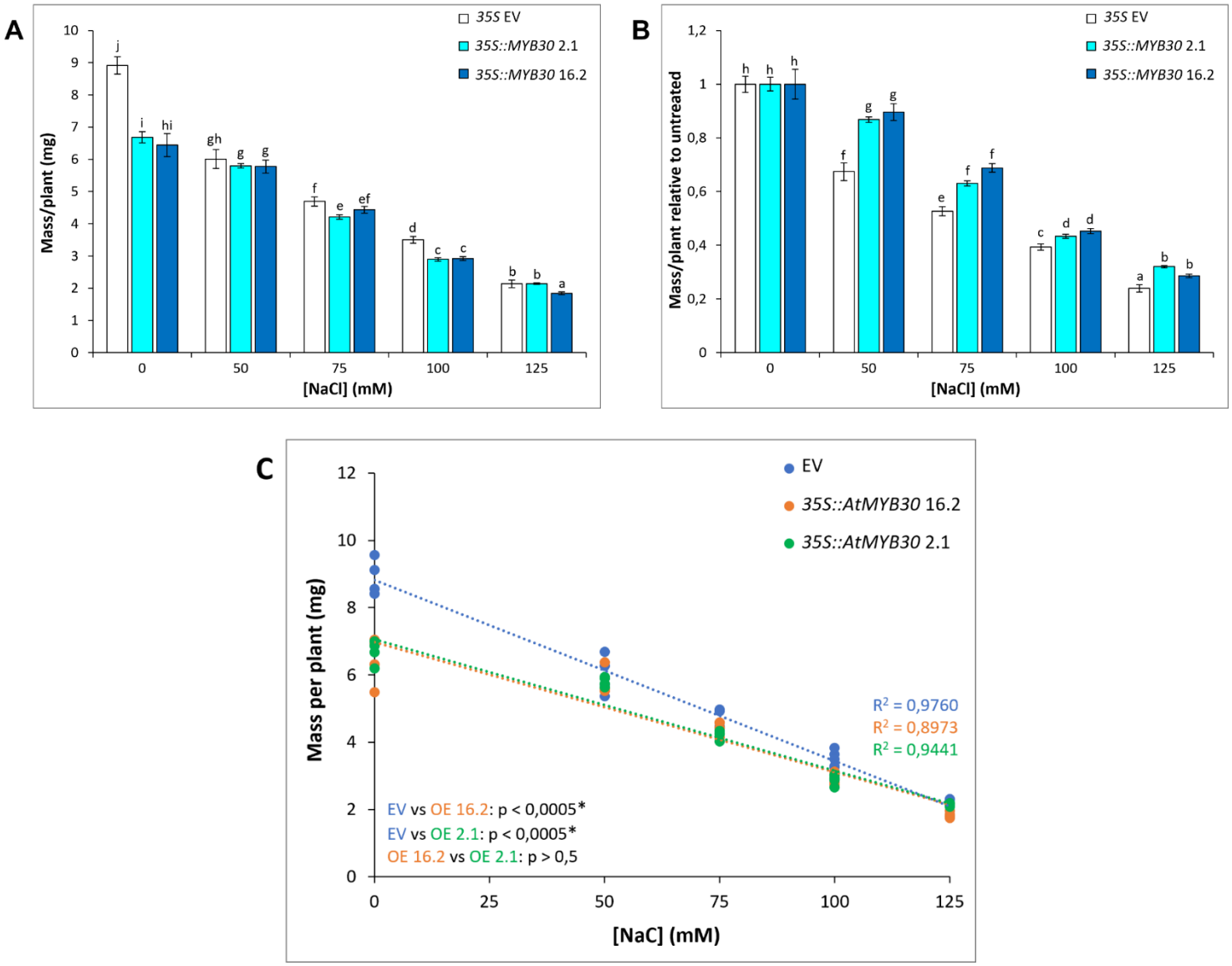

Appendix figure 6.4: Growth of additional *35S::AtMYB30* plants exposed to saline conditions early in development

Empty vector (*35S* EV) and *35S::AtMYB30* plants were germinated and grown for two weeks on petri dishes containing untreated PN-agar (control) and PN-agar supplemented with the indicated concentrations of NaCl. **A:** The average mass per plant of each line. **B:** The average mass per plant plotted relative to the control (0 mM) for each line. Error bars indicate standard error. Different letters on the graphs indicate significant differences ($p \leq 0.05$) in mean values as determined by a one-way ANOVA with Fisher LSD post-hoc analysis. **C:** The mass per plant is plotted as a regression analysis for NaCl conditions. The results show four replicates for each treatment with 50 seeds sown per plate (n=4). The experiment was repeated three times with comparable results. Each slope was compared statistically to one another to determine any significant differences and the results are shown in the bottom left corner with an asterisk indicating statistical significance.

Appendix table 6.3: Summary of yeast growth indicative of TF interaction with the *AtNit2* promoter fragments in the pairwise Y1H screen

TF	–Leu/-Trp/-His + 1 mM 3AT	–Leu/-Trp/-His + 10 mM 3AT	Specific interaction?
GeBP	1, 2 & EV +++ 3 & 4 +	-	-
HB34	3 +++	-	✓
HB24	2, 3 & 4 +++	3 & 4 +++ 2 +	✓
HB28	4 +++ 2 ++ 3 +	4 +	✓
DbSPR1	-	-	-
HMGB9	2 & 4 +++ 3 +	2 +++ 4 +	✓
DbSPR2	1, 2 & EV +++ 4 ++	-	-
TCP20	EV +++ 1, 2, 3 & 4 ++	-	-
TCP3	-	-	-
GL2	4 +++	4 +++	✓
SPL7	4 +++	4 +	✓

On each selection plate, yeast growth is scored as **+:** little growth (a few spots) , **++:** medium growth, or **+++:** strong growth. Where no growth is seen with the pHISLeu2 EV, the interaction is designated as specific with a tick.

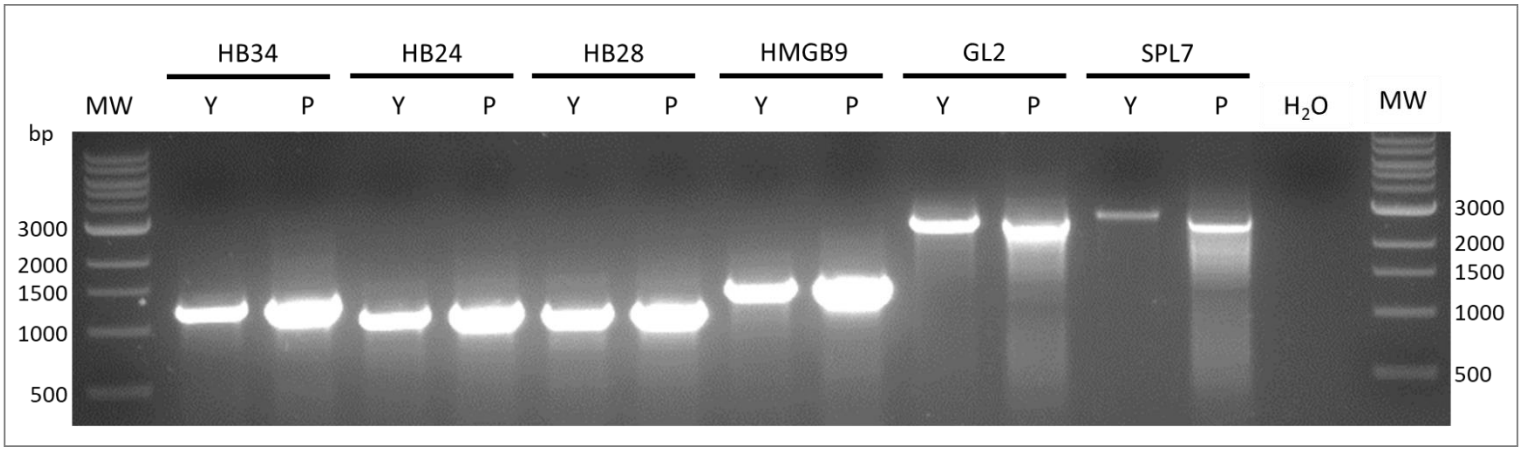

Appendix figure 6.5: PCR confirmation of the TFs present in the interacting yeast "prey" strains and *E. coli* version of the TF library

A PCR was performed using the pDEST22 primer pair on **Y:** yeast lysate samples from the interacting yeast on selective media, **P:** plasmid DNA extracted from the *E. coli* version of the TF library. A no template H_2O negative control was included. The MW marker included is the NEB Quick-Load® 1 kb DNA ladder.

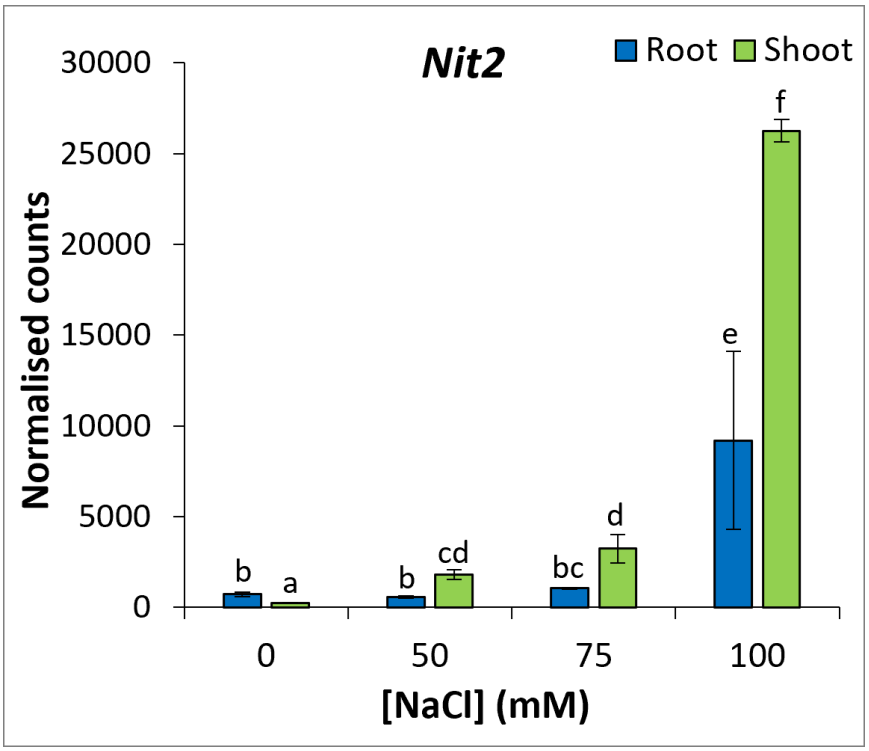

Appendix figure 6.6: *AtNit2* expression in the later development microarray

The later development microarray was performed on Arabidopsis Col-0 seedlings grown hydroponically for two weeks in untreated control conditions then transferred to media containing the indicated concentrations of NaCl for a further two weeks (blue bars: root, green bars: shoot). Error

bars indicate standard error. Different letters on the graphs indicate significant differences ($p \leq 0.05$) in mean fold change values as determined by Fisher LSD post-hoc analysis following a one-way ANOVA.

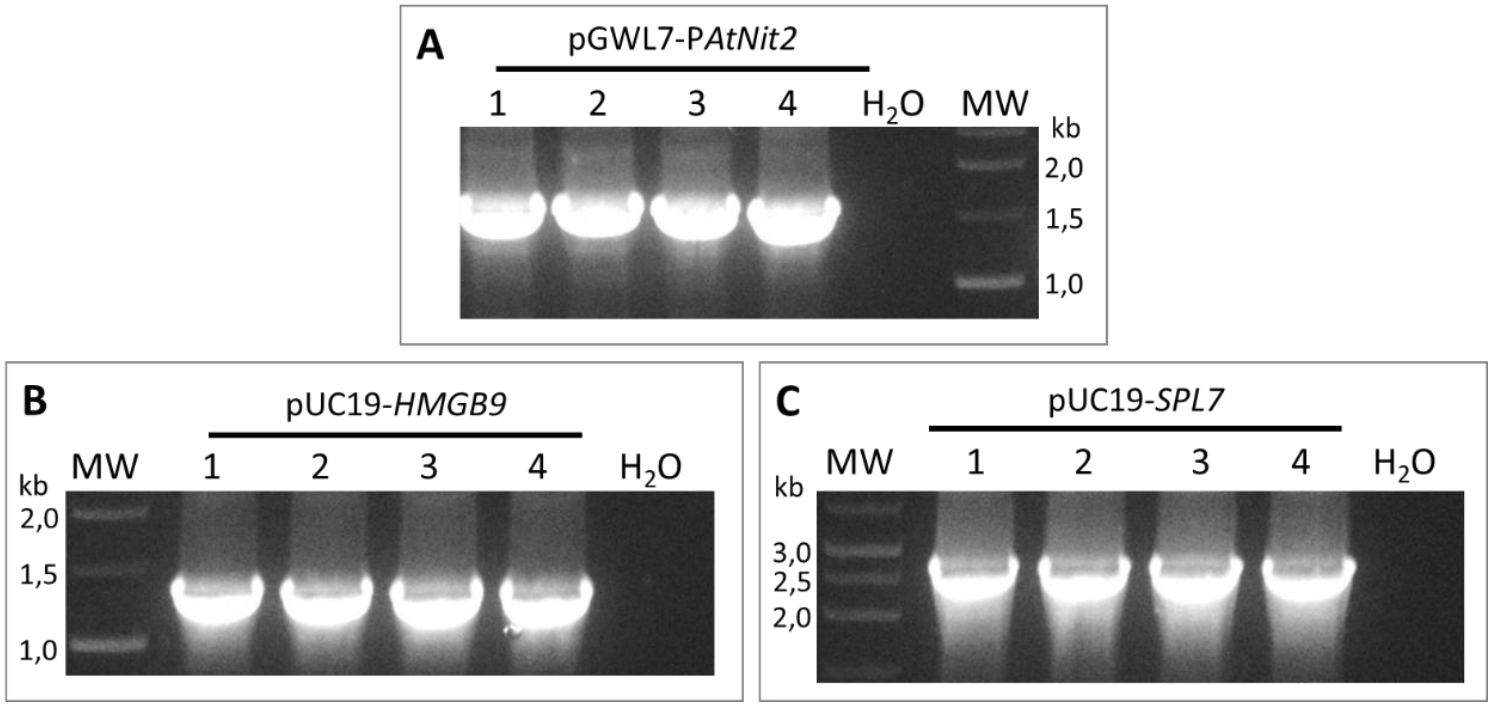

Appendix figure 6.6: PCR confirmation of successful *E. coli* transformations with pGWL7-P*AtNit2*, pUC19-*AtHMGB9* and pUC19-*AtSPL7*

Colony PCRs were performed on colonies from *E. coli* transformed with the following: **A:** pGWL7-P*AtNit2*, using the P*AtNit2* internal forward primer and the *Luc* reverse primer with an expected amplicon size of 1.6 kb, **B:** pUC19-*AtHMG9,* using the P35S forward primer and *AtHMGB9* FL reverse primer with an expected amplicon size of 1.4 kb, and **C:** pUC19-*AtSPL7,* using the P35S forward primer and *AtSPL7* FL reverse primer with an expected amplicon size of 2.8 kb. A no template H_2O negative control PCR reaction was included in each case. The MW marker included is the Promega 1 kb DNA ladder.

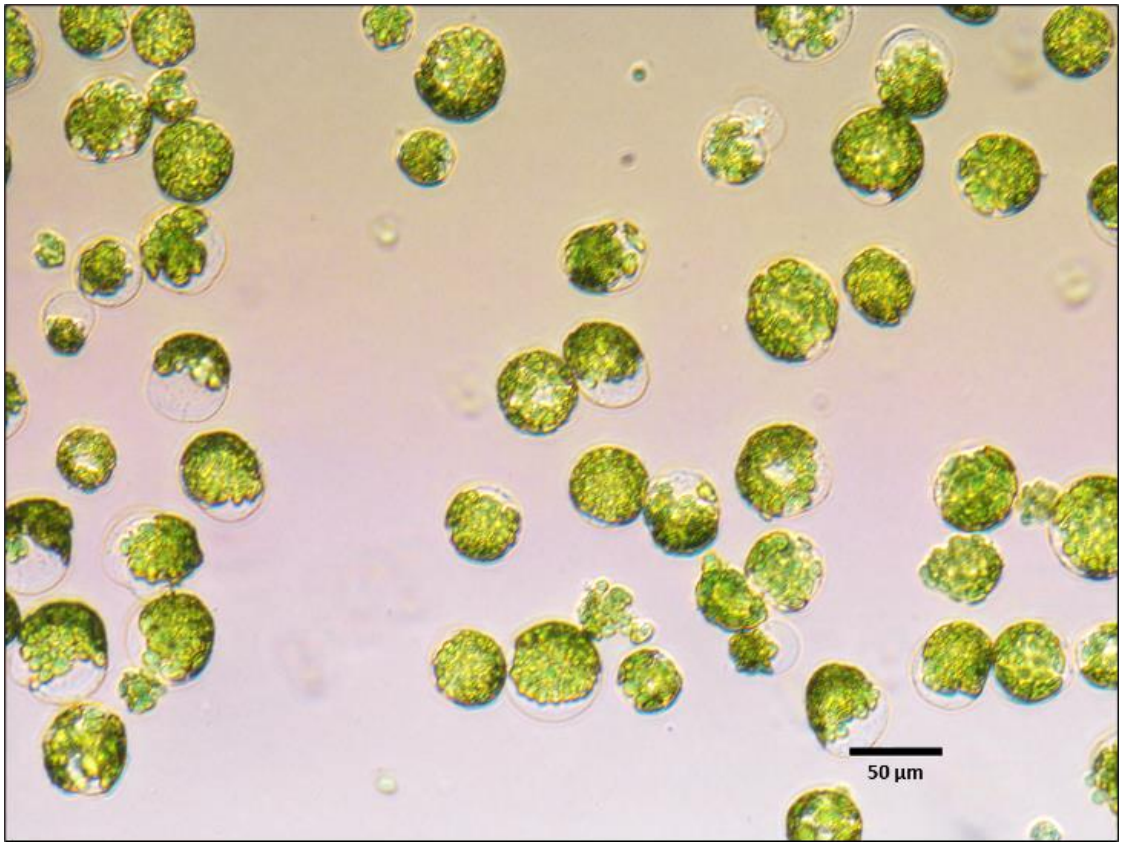

Appendix figure 6.7: Intact Arabidopsis mesophyll protoplasts

Representative image showing successful isolation of intact Arabidopsis mesophyll protoplasts of the correct size of ± 50 µm in diameter. The image was taken under bright-field settings.

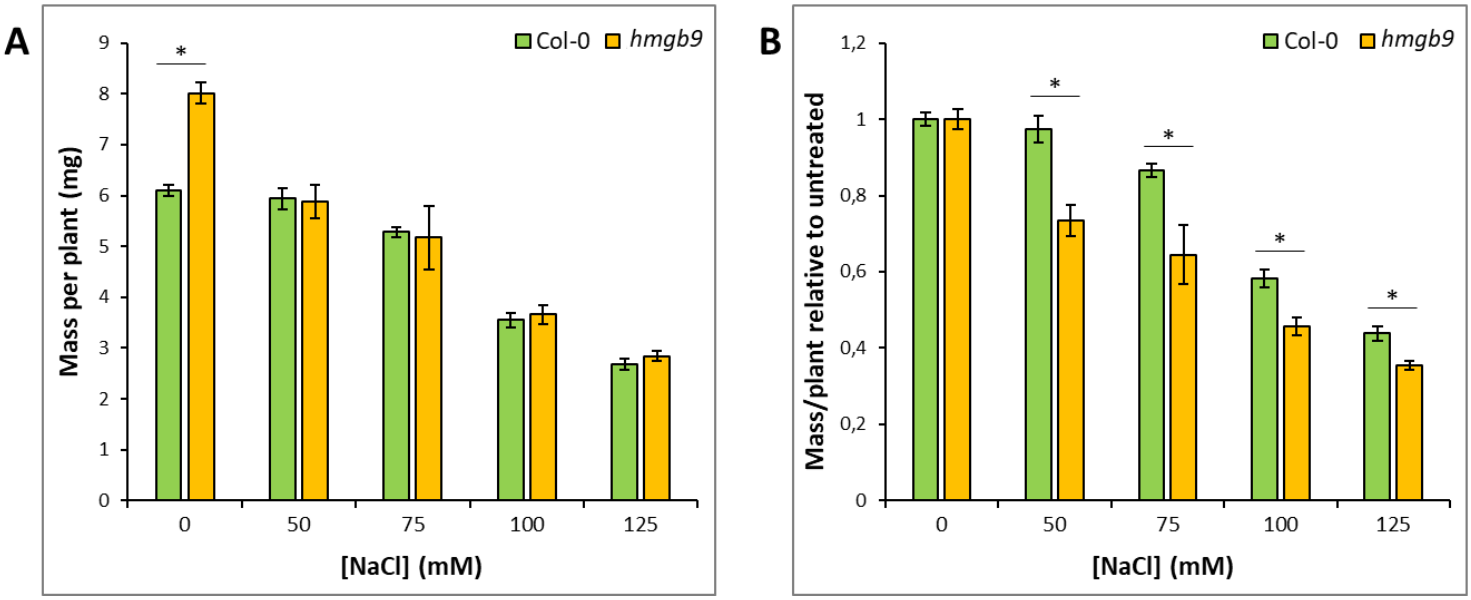

Appendix figure 6.8: Growth of *athmgb9* plants exposed to salinity early in development

Col-0 and *athmgb9* plants were germinated and grown for two weeks on petri dishes containing untreated PN-agar (control) and PN-agar supplemented with the indicated concentrations of NaCl. **A:** The average mass per plant of each line. **B:** The average mass per plant plotted relative to the control (0 mM) for each line. Error bars indicate standard error. The results show four replicates for each treatment with 50 seeds sown per plate (n=4). Asterisks represent statistical differences between the lines as determined from a two-tailed homoscedastic t-test ($p \leq 0.05$).

Appendix table 6.4: Segregation ratios of the T2 Arabidopsis EV and *35S::ZmNit2* lines (No-0 BG)

Genotype	Line	PN %	GFSA %	Transgenic %
35S::ZmNit2	**2**	40	28	70
	3	52	32	62,5
	4	42	28	66,7
	5	38	22	57,9
	6	58	35	60,3
	7	26	22	84,6
	8	38	26	68,4
	9	36	12	33,3
	10	28	24	85,7
	11	24	15	62,5
	12	54	43	79,6
	13	44	35	79,5
	16	40	23	57,5
35S EV	**1**	92	76	82,6
	2	96	70	72,9
	3	90	74	82,2
	4	68	54	79,4
	5	84	40	47,6
	7	76	64	84,2

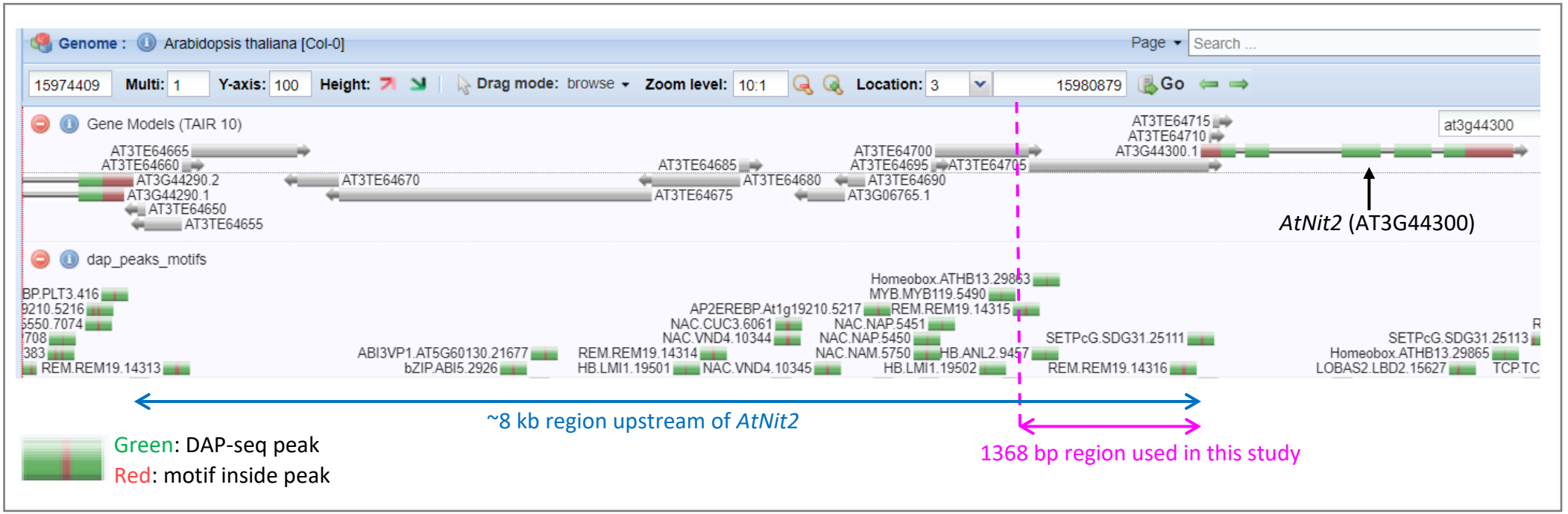

Appendix figure 6.9: Anno-J Networked Genome Browser screenshot showing DAP-seq data from the region surrounding *AtNit2*

The region surrounding the *AtNit2* gene (AT3G44300) is shown in the Anno-J Networked Genome Browser version X (21.3.30) with the DAP-seq data from O'Malley et al. (2016) (http://neomorph.salk.edu/aj2/pages/hchen/dap_ath_pub_models.php). The *AtNit2* gene is indicated by the black arrow. The next gene upstream of *AtNit2* (AT3G44290) is ~8 kb away (represented by the blue arrow). The 1368 bp region upstream of *AtNit2* used in this study is represented by the pink arrow. DAP-seq peaks are indicated by green boxes, with the inner red line representing the TF binding motif.

CHAPTER 7: REFERENCES

Abe, H., Urao, T., Ito, T., Seki, M. & Shinozaki, K. 2003. Arabidopsis AtMYC2 (bHLH) and AtMYB2 (MYB) Function as Transcriptional Activators in Abscisic Acid Signaling. *Society*. 15(January):63–78. DOI: 10.1105/tpc.006130.salt.

Abe, M., Takahashi, T. & Komeda, Y. 2001. Identification of a cis-regulatory element for L1 layer-specific gene expression, which is targeted by an L1-specific homeodomain protein. *The Plant Journal*. 26(5):487–494. DOI: 10.1046/j.1365-313x.2001.01047.x.

Abel, S. & Theologis, A. 1994. Transient transformation of Arabidopsis leaf protoplasts: a versatile experimental system to study gene expression. *The Plant Journal*. 5(3):421–427. DOI: 10.1111/j.1365-313X.1994.00421.x.

Abel, S. & Theologis, A. 2010. Odyssey of Auxin. *Cold Spring Harbor Perspectives in Biology*. 2(10):a004572–a004572. DOI: 10.1101/cshperspect.a004572.

Abogadallah, G.M. 2010. Sensitivity of *Trifolium alexandrinum* L. to salt stress is related to the lack of long-term stress-induced gene expression. *Plant Science*. 178(6):491–500. DOI: 10.1016/j.plantsci.2010.03.008.

Abu-Zaitoon, Y.M. 2014. Phylogenetic Analysis of Putative Genes Involved in the Tryptophan-Dependent Pathway of Auxin Biosynthesis in Rice. *Applied Biochemistry and Biotechnology*. 172:2480–2495. DOI: 10.1007/s12010-013-0710-4

Adem, G.D., Roy, S.J., Zhou, M., Bowman, J.P. & Shabala, S. 2014. Evaluating contribution of ionic, osmotic and oxidative stress components towards salinity tolerance in barley. *BMC Plant Biology*. 14(1):113. DOI: 10.1186/1471-2229-14-113.

Aharon, G.S., Apse, M.P., Duan, S., Hua, X. & Blumwald, E. 2003. Characterization of a family of vacuolar Na^+/H^+ antiporters in *Arabidopsis thaliana*. *Plant and Soil*. 253(1):245–256. DOI: 10.1023/A:1024577205697.

Al-shareef, N.O. & Tester, M. 2019. Plant Salinity Tolerance. *eLS*. 1–6. DOI: 10.1002/9780470015902.a0001300.pub3.

Alonso, J.M., Stepanova, A.N., Leisse, T.J., Kim, C.J., Chen, H., Shinn, P., Stevenson, D.K., Zimmerman, J., et al. 2003. Genome-wide insertional mutagenesis of *Arabidopsis thaliana*. *Science*. 301(5633):653–657. DOI: 10.1126/science.1086391.

Alqahtani, M., Roy, S.J. & Tester, M. 2019. Increasing Salinity Tolerance of Crops. *Encyclopedia of Sustainability Science and Technology.* 245–267. DOI: 10.1007/978-1-4939-8621-7_429.

Apel, K. & Hirt, H. 2004. Reactive oxygen species: Metabolism, oxidative stress, and signal transduction. *Annual Review of Plant Biology*. 55:373–399. DOI: 10.1146/annurev.arplant.55.031903.141701.

Apse, M.P. & Blumwald, E. 2007. Na^+ transport in plants. *FEBS Letters*. 581(12):2247–2254. DOI: 10.1016/j.febslet.2007.04.014.

Apse, M.P., Aharon, G.S., Snedden, W.A. & Blumwald, E. 1999. Salt Tolerance Conferred by Overexpression of a Vacuolar Na^+/H^+ Antiport in Arabidopsis. *Science*. 285(5431):1256–1258. DOI: 10.1126/science.285.5431.1256.

Araki, R., Mermod, M., Yamasaki, H., Kamiya, T., Fujiwara, T. & Shikanai, T. 2018. SPL7 locally regulates copper-homeostasis-related genes in Arabidopsis. *Journal of Plant Physiology*. 224–225(March):137–143. DOI: 10.1016/j.jplph.2018.03.014.

Ashraf, M. & Harris, P.J.C. 2013. Photosynthesis under stressful environments: An overview. *Photosynthetica*. 51(2):163–190. DOI: 10.1007/s11099-013-0021-6.

Assaha, D.V.M., Ueda, A., Saneoka, H., Al-Yahyai, R. & Yaish, M.W. 2017. The Role of Na^+ and K^+ Transporters in Salt Stress Adaptation in Glycophytes. *Frontiers in Physiology*. 8(509). DOI: 10.3389/fphys.2017.00509.

Athar, H.R. & Ashraf, M. 2009. Strategies for Crop Improvement Against Salinity and Drought Stress: An Overview. *Salinity and Water Stress*. 1–16. DOI: 10.1007/978-1-4020-9065-3_1.

Audagnotto, M., & Dal Peraro, M. 2017. Protein post-translational modifications: *In silico* prediction tools and molecular modeling. Computational and structural biotechnology journal. 15:307–319. DOI: 10.1016/j.csbj.2017.03.004

Baginsky, S., Hennig, L., Zimmermann, P. & Gruissem, W. 2010. Gene expression analysis, proteomics, and network discovery. *Plant Physiology*. 152(2):402–410. DOI: 10.1104/pp.109.150433.

Barberon, M. & Geldner, N. 2014. Focus Issue on Roots: Radial Transport of Nutrients: The Plant Root as a Polarized Epithelium. *Plant Physiology*. 166(2):528. DOI: 10.1104/PP.114.246124.

Barbez, E., Dünser, K., Gaidora, A., Lendl, T. & Busch, W. 2017. Auxin steers root cell expansion via apoplastic pH regulation in *Arabidopsis thaliana*. *Proceedings of the National Academy of Sciences of the United States of America*. 114(24):E4884–E4893. DOI: 10.1073/pnas.1613499114.

Barragán, V., Leidi, E.O., Andrés, Z., Rubio, L., de Luca, A., Fernández, J.A., Cubero, B. & Pardo, J.M. 2012. Ion exchangers NHX1 and NHX2 mediate active potassium uptake into vacuoles to regulate cell turgor and stomatal function in Arabidopsis. *Plant Cell*. 24(3):1127–1142. DOI: 10.1105/tpc.111.095273.

Bartel, B. & Fink, G.R. 1994. Differential regulation of an auxin-producing nitrilase gene family in *Arabidopsis thaliana*. *Proceedings of the National Academy of Sciences*. 91(14):6649–6653. DOI: 10.1073/pnas.91.14.6649.

Bartling, D., Seedorf, M., Mithofer, A. & Weiler, E.W. 1992. Cloning and expression of an Arabidopsis nitrilase which can convert indole-3-acetonitrile to the plant hormone, indole-3-acetic acid. *European Journal of Biochemistry*. 205(1):417–424. DOI: 10.1111/j.1432-1033.1992.tb16795.x.

Bassil, E., Tajima, H., Liang, Y.C., Ohto, M. aki, Ushijima, K., Nakano, R., Esumi, T., Coku, A., et al. 2011. The arabidopsis Na^+/H^+ antiporters NHX1 and NHX2 control vacuolar pH and K^+ homeostasis to regulate growth, flower development, and reproduction. *Plant Cell*. 23(9):3482–3497. DOI: 10.1105/tpc.111.089581.

Bednar, M. 2000. DNA microarray technology and application. *Medical Science Monitor*. 6(4):796–800.

Berthomieu, P., Conéjéro, G., Nublat, A., Brackenbury, W.J., Lambert, C., Savio, C., Uozumi, N., Oiki, S., et al. 2003. Functional analysis of AtHKT1 in Arabidopsis shows that Na^+ recirculation by the phloem is crucial for salt tolerance. *EMBO Journal*. 22(9):2004–2014. DOI: 10.1093/emboj/cdg207.

Beyrne, C.C., Iusem, N.D. & González, R.M. 2019. Effect of salt stress on cytosine methylation within *GL2*, an *Arabidopsis thaliana* gene involved in root epidermal cell differentiation. Absence of inheritance in the unstressed progeny. *International Journal of Molecular Sciences*. 20(18):1–13. DOI: 10.3390/ijms20184446.

Blumwald, E. 2000. Sodium transport and salt tolerance in plants. *Current Opinion in Cell Biology*. 12(4):431–434. DOI: 10.1016/S0955-0674(00)00112-5.

Böhmer, M. & Schroeder, J.I. 2011. Quantitative transcriptomic analysis of abscisic acid-induced and reactive oxygen species-dependent expression changes and proteomic profiling in Arabidopsis suspension cells. *The Plant Journal*. 67(1):105–118. DOI: 10.1111/j.1365-313X.2011.04579.x.

Bolle, C., Schneider, A. & Leister, D. 2016. Perspectives on Systematic Analyses of Gene Function in *Arabidopsis thaliana*: New Tools, Topics and Trends. *Advances in Genome Science*. 143–172. DOI: 10.2174/9781681081731116040009.

Bose, J., Rodrigo-Moreno, A., Lai, D., Xie, Y., Shen, W. & Shabala, S. 2015. Rapid regulation of the plasma membrane H^+-ATPase activity is essential to salinity tolerance in two halophyte species, *Atriplex lentiformis* and *Chenopodium quinoa*. *Annals of Botany*. 115(3):481–494. DOI: 10.1093/aob/mcu219.

Busch, W. & Lohmann, J.U. 2007. Profiling a plant: expression analysis in Arabidopsis. *Current Opinion in Plant Biology*. 10(2):136–141. DOI: 10.1016/j.pbi.2007.01.002.

Busoms, S., Terés, J., Yant, L., Poschenrieder, C. & Salt, D.E. 2021. Adaptation to coastal soils through pleiotropic boosting of ion and stress hormone concentrations in wild *Arabidopsis thaliana*. *New Phytologist*. 232(1):208–220. DOI: 10.1111/nph.17569.

Byrt, C.S., Platten, J.D., Spielmeyer, W., James, R.A., Lagudah, E.S., Dennis, E.S., Tester, M. & Munns, R. 2007. HKT1;5-Like Cation Transporters Linked to Na^+ Exclusion Loci in Wheat, *Nax2* and *Kna1*. *Plant Physiology*. 143(4):1918–1928. DOI: 10.1104/pp.106.093476.

Byrt, C.S., Xu, B., Krishnan, M., Lightfoot, D.J., Athman, A., Jacobs, A.K., Watson-Haigh, N.S., Plett, D., et al. 2014. The Na^+ transporter, TaHKT1;5-D, limits shoot Na^+ accumulation in bread wheat. *The Plant Journal*. 80(3):516–526. DOI: 10.1111/tpj.12651.

Cackett, L. 2019. Characterisation of auxin and auxin-related genes in the response of *Arabidopsis thaliana* to salt stress. University of Cape Town.

Cackett, L., Cannistraci, C.V., Meier, S., Ferrandi, P., Pěnčík, A., Gehring, C., Novák, O., Ingle, R.A., et al. 2022. Salt-Specific Gene Expression Reveals Elevated Auxin Levels in *Arabidopsis thaliana* Plants Grown Under Saline Conditions. *Frontiers in Plant Science*. 13(February):804716. DOI: 10.3389/fpls.2022.804716.

Carrió-Seguí, À., Romero, P., Sanz, A. & Peñarrubia, L. 2016. Interaction between ABA signaling and copper homeostasis in *Arabidopsis thaliana*. *Plant and Cell Physiology*. 57(7):1568–1582. DOI: 10.1093/pcp/pcw087.

Chakraborty, S. & Newton, A.C. 2011. Climate change, plant diseases and food security: An overview. *Plant Pathology*. 60(1):2–14. DOI: 10.1111/j.1365-3059.2010.02411.x.

Chan, R.L., Gago, G.M., Palena, C.M. & Gonzalez, D.H. 1998. Homeoboxes in plant development. *Biochimica et Biophysica Acta - Gene Structure and Expression*. 1442(1):1–19. DOI: 10.1016/S0167-4781(98)00119-5.

Chazen, O., Hartung, W. & Neumann, P.M. 1995. The different effects of PEG 6000 and NaCl on leaf development are associated with differential inhibition of root water transport. *Plant, Cell and Environment*. 18(7):727–735. DOI: 10.1111/j.1365-3040.1995.tb00575.x.

Chinnusamy, V., Jagendorf, A. & Zhu, J.-K. 2005. Understanding and Improving Salt Tolerance in Plants. *Crop Science*. 45(2):437–448. DOI: 10.2135/cropsci2005.0437.

Choi, W.G., Toyota, M., Kim, S.H., Hilleary, R. & Gilroy, S. 2014. Salt stress-induced Ca^{2+} waves are associated with rapid, long-distance root-to-shoot signaling in plants. *Proceedings of the National Academy of Sciences of the United States of America.* 111(17):6497–6502. DOI: 10.1073/pnas.1319955111.

Clapier, C.R., Iwasa, J., Cairns, B.R. & Peterson, C.L. 2017. Mechanisms of action and regulation of ATP-dependent chromatin-remodelling complexes. *Nature Reviews Molecular Cell Biology*. 18(7):407–422. DOI: 10.1038/nrm.2017.26.

Clough, S.J. & Bent, A.F. 1998. Floral dip: A simplified method for Agrobacterium-mediated transformation of *Arabidopsis thaliana*. *Plant Journal*. 16(6):735–743. DOI: 10.1046/j.1365-313X.1998.00343.x.

Collett, C.E., Harberd, N.P. & Leyser, O. 2000. Hormonal interactions in the control of Arabidopsis hypocotyl elongation. *Plant Physiology*. 124(2):553–561. DOI: 10.1104/pp.124.2.553.

Collier, R., Dasgupta, K., Xing, Y.P., Hernandez, B.T., Shao, M., Rohozinski, D., Kovak, E., Lin, J., et al. 2017. Accurate measurement of transgene copy number in crop plants using droplet digital PCR. *Plant Journal*. 90(5):1014–1025. DOI: 10.1111/tpj.13517.

Connolly, J.P., Augustine, J.G. & Francklyn, C. 1999. Mutational analysis of the engrailed homeodomain recognition helix by phage display. *Nucleic Acids Research*. 27(4):1182–1189. DOI: 10.1093/nar/27.4.1182.

Cortina, C. & Culiáñez-Macià, F.A. 2005. Tomato abiotic stress enhanced tolerance by trehalose biosynthesis. *Plant Science*. 169(1):75–82. DOI: 10.1016/j.plantsci.2005.02.026.

Cosgrove, D.J. 1993. Wall extensibility: its nature, measurement and relationship to plant cell growth. *New Phytologist*. 124(1):1–23. DOI: 10.1111/j.1469-8137.1993.tb03795.x.

Cramer, G.R. & Bowman, D.C. 1991. Kinetics of Maize Leaf Elongation: I. Increased yield threshold limits short-term, steady-state elongation rates after exposure to salinity. *Journal of Experimental Botany*. 42(11):1417–1426. DOI: 10.1093/JXB/42.11.1417.

Cramer, P., Bushnell, D.A. & Kornberg, R.D. 2001. Structural basis of transcription: RNA polymerase II at 2.8 ångstrom resolution. *Science*. 292(5523):1863–1876. DOI: 10.1126/science.1059493.

Di Cristina, M., Sessa, G., Dolan, L., Linstead, P., Baima, S., Ruberti, I. & Morelli, G. 1996. The Arabidopsis Athb-10 (GLABRA2) is an HD-Zip protein required for regulation of root hair development. *Plant Journal*. 10(3):393–402. DOI: 10.1046/j.1365-313X.1996.10030393.x.

Cubero-Font, P., Maierhofer, T., Jaslan, J., Rosales, M.A., Espartero, J., Díaz-Rueda, P., Müller, H.M., Hürter, A.L., et al. 2016. Silent S-Type Anion Channel Subunit SLAH1 Gates SLAH3 Open for Chloride Root-to-Shoot Translocation. *Current Biology*. 26(16):2213–2220. DOI: 10.1016/j.cub.2016.06.045.

Czemmel, S., Stracke, R., Weisshaar, B., Cordon, N., Harris, N.N., Walker, A.R., Robinson, S.P. & Bogs, J. 2009. The Grapevine R2R3-MYB Transcription Factor VvMYBF1 Regulates Flavonol Synthesis in Developing Grape Berries. *Plant Physiology*. 151(3):1513–1530. DOI: 10.1104/pp.109.142059.

Davey, M.R., Anthony, P., Power, J.B. & Lowe, K.C. 2005. Plant protoplasts: Status and biotechnological perspectives. *Biotechnology Advances*. 23(2):131–171. DOI: 10.1016/j.biotechadv.2004.09.008.

Davuluri, R. V., Sun, H., Palaniswamy, S.K., Matthews, N., Molina, C., Kurtz, M. & Grotewold, E. 2003. AGRIS: Arabidopsis Gene Regulatory Information Server, an information resource of Arabidopsis cis-regulatory elements and transcription factors. *BMC Bioinformatics*. 4:1–11. DOI: 10.1186/1471-2105-4-25.

Delessert, C., Kazan, K., Wilson, I.W., Straeten, D. Van Der, Manners, J., Dennis, E.S. & Dolferus, R. 2005. The transcription factor ATAF2 represses the expression of pathogenesis-related genes in Arabidopsis. *The Plant Journal*. 43(5):745–757. DOI: 10.1111/j.1365-313X.2005.02488.x.

Demidchik, V., Essah, P.A. & Tester, M. 2004. Glutamate activates cation currents in the plasma membrane of Arabidopsis root cells. *Planta*. 219(1):167–175. DOI: 10.1007/s00425-004-1207-8.

De Souza Miranda, R., Mesquita, R.O., Costa, J.H., Alvarez-Pizarro, J.C., Prisco, J.T. & Gomes-Filho, E. 2017. Integrative control between proton pumps and SOS1 antiporters in roots is crucial for maintaining low Na^+ accumulation and salt tolerance in ammonium-supplied *Sorghum bicolor*. *Plant and Cell Physiology*. 58(3):522–536. DOI: 10.1093/pcp/pcw231.

Di, D.-W., Zhang, C., Luo, P., An, C.-W. & Guo, G.-Q. 2016. The biosynthesis of auxin: how many paths truly lead to IAA? *Plant Growth Regulation*. 78(3):275–285. DOI: 10.1007/s10725-015-0103-5.

Ding, L. & Zhu, J.K. 1997. Reduced Na^+ uptake in the NaCl-hypersensitive *sos1* mutant of *Arabidopsis thaliana*. *Plant Physiology*. 113(3):795–799. DOI: 10.1104/pp.113.3.795.

Dubos, C., Stracke, R., Grotewold, E., Weisshaar, B., Martin, C. & Lepiniec, L. 2010. MYB transcription factors in Arabidopsis. *Trends in Plant Science*. 15(10):573–581. DOI: 10.1016/j.tplants.2010.06.005.

Dunlap, J.R. & Binzel, M.L. 1996. NaCl Reduces Indole-3-Acetic Acid Levels in the Roots of Tomato Plants Independent of Stress-Induced Abscisic Acid. *Plant Physiology*. 112(1):379–384. DOI: 10.1104/pp.112.1.379.

Edwards, K., Johnstone, C. & Thompson, C. 1991. A simple and rapid method for the preparation of plant genomic DNA for PCR analysis. *Nucleic Acids Research*. 19(6):1349. DOI: 10.1093/nar/19.6.1349.

Eisenstein, M. 2013. Plant breeding: Discovery in a dry spell. *Nature*. 501:S7–S9. DOI: 10.1038/501S7a.

Essah, P.A., Davenport, R. & Tester, M. 2003. Sodium influx and accumulation in arabidopsis. *Plant Physiology*. 133(1):307–318. DOI: 10.1104/pp.103.022178.

Eulgem, T., Rushton, P.J., Robatzek, S. & Somssich, I.E. 2000. The WRKY superfamily of plant transcription factors. *Trends in Plant Science*. 5(5):199–206. DOI: 10.1016/S1360-1385(00)01600-9.

Falhof, J., Pedersen, J.T., Fuglsang, A.T. & Palmgren, M. 2016. Plasma Membrane H^+-ATPase Regulation in the Center of Plant Physiology. *Molecular Plant*. 9(3):323–337. DOI: 10.1016/j.molp.2015.11.002.

Farooq, M., Hussain, M., Wakeel, A. & Siddique, K.H.M. 2015. Salt stress in maize: effects, resistance mechanisms, and management. A review. *Agronomy for Sustainable Development*. 35(2):461–481. DOI: 10.1007/s13593-015-0287-0.

Feki, K., Saibi, W. & Brini, F. 2015. Understanding Plant Stress Response and Tolerance to Salinity from Gene to Whole Plant. *Managing Salt Tolerance in Plants*. (October):1–18. DOI: 10.1201/b19246-2.

Fraenkel, E., Pabo, C.O., Fraenkel, E. & Pabo, C.O. 1998. Comparison of X-ray and NMR structures for the Antennapedia homeodomain-DNA complex. *Nature Structural and Molecular Biology*. 5(8):692–697. DOI: 10.1038/1382.

Frensch, J. & Hsiao, T.C. 1994. Transient Responses of Cell Turgor and Growth of Maize Roots as Affected by Changes in Water Potential. *Plant Physiology*. 104(1):247–254. DOI: 10.1104/PP.104.1.247.

Fukuda, A., Chiba, K., Maeda, M., Nakamura, A., Maeshima, M. & Tanaka, Y. 2004. Effect of salt and osmotic stresses on the expression of genes for the vacuolar H^+-pyrophosphatase, H^+-ATPase subunit A, and Na^+/H^+ antiporter from barley. *Journal of Experimental Botany*. 55(397):585–594. DOI: 10.1093/jxb/erh070.

Fuxman Bass, J.I., Reece-Hoyes, J.S. & Walhout, A.J.M. (in press). Gene-Centered Yeast One-Hybrid Assays. *Cold Spring Harbor Protocols*. (12):pdb.top077669. DOI: 10.1101/pdb.top077669.

Galvan-Ampudia, C.S., Julkowska, M.M., Darwish, E., Gandullo, J., Korver, R.A., Brunoud, G., Haring, M.A., Munnik, T., et al. 2013. Halotropism is a response of plant roots to avoid a saline environment. *Current Biology*. 23(20):2044–2050. DOI: 10.1016/j.cub.2013.08.042.

Garg, A.K., Kim, J.K., Owens, T.G., Ranwala, A.P., Do Choi, Y., Kochian, L. V. & Wu, R.J. 2002. Trehalose accumulation in rice plants confers high tolerance levels to different abiotic stresses. *Proceedings of the National Academy of Sciences of the United States of America*. 99(25):15898–15903. DOI: 10.1073/pnas.252637799.

Gaxiola, R.A., Rao, R., Sherman, A., Grisafi, P., Alper, S.L. & Fink, G.R. 1999. The *Arabidopsis thaliana* proton transporters, AtNhx1 and Avp1, can function in cation detoxification in yeast. *Proceedings of the National Academy of Sciences*. 96(4):1480–1485. DOI: 10.1073/pnas.96.4.1480.

Gelvin, S.B. 2003. Agrobacterium-Mediated Plant Transformation: the Biology behind the "Gene-Jockeying" Tool. *Microbiology and Molecular Biology Reviews*. 67(1):16–37. DOI: 10.1128/MMBR.67.1.16.

Gévaudant, F., Duby, G., Von Stedingk, E., Zhao, R., Morsomme, P. & Boutry, M. 2007. Expression of a constitutively activated plasma membrane H^+-ATPase alters plant development and increases salt tolerance. *Plant Physiology*. 144(4):1763–1776. DOI: 10.1104/pp.107.103762.

Gierth, M. & Mäser, P. 2007. Potassium transporters in plants - Involvement in K^+ acquisition, redistribution and homeostasis. *FEBS Letters*. 581(12):2348–2356. DOI: 10.1016/j.febslet.2007.03.035.

Głowacka, K., Kromdijk, J., Leonelli, L., Niyogi, K.K., Clemente, T.E. & Long, S.P. 2016. An evaluation of new and established methods to determine T-DNA copy number and homozygosity in transgenic plants. Plant, Cell & Environment. 39(4):908–917. DOI: 10.1111/pce.12693.

Glynn, S.E., Baker, P.J., Sedelnikova, S.E., Davies, C.L., Eadsforth, T.C., Levy, C.W., Rodgers, H.F., Blackburn, G.M., et al. 2005. Structure and Mechanism of Imidazoleglycerol-Phosphate Dehydratase. *Structure*. 13(12):1809–1817. DOI: 10.1016/j.str.2005.08.012.

GM Approval Database - MON-8746Ø-4. 2022. Available: https://www.isaaa.org/gmapprovaldatabase/event/default.asp?EventID=98 [2023, February 08].

Gong, F., Wu, X., Zhang, H., Chen, Y. & Wang, W. 2015. Making better maize plants for sustainable grain production in a changing climate. *Frontiers in Plant Science*. 6:1–6. DOI: 10.3389/fpls.2015.00835.

Gong, Q., Li, P., Ma, S., Indu Rupassara, S. & Bohnert, H.J. 2005. Salinity stress adaptation competence in the extremophile *Thellungiella halophila* in comparison with its relative *Arabidopsis thaliana*. *Plant Journal*. 44(5):826–839. DOI: 10.1111/j.1365-313X.2005.02587.x.

Gong, Q., Li, S., Zheng, Y., Duan, H., Xiao, F., Zhuang, Y., He, J., Wu, G., et al. 2020. SUMOylation of MYB30 enhances salt tolerance by elevating alternative respiration via transcriptionally upregulating *AOX1a* in Arabidopsis. *Plant Journal*. 102(6):1157–1171. DOI: 10.1111/tpj.14689.

Gosal, S.S., Wani, S.H. & Kang, M.S. 2010. Biotechnology and drought tolerance. *Water and Agricultural Sustainability Strategies*. 7528:229–259. DOI: 10.1080/15427520802418251.

Goyal, E., Amit, S.K., Singh, R.S., Mahato, A.K., Chand, S. & Kanika, K. 2016. Transcriptome profiling of the salt-stress response in *Triticum aestivum* cv. Kharchia Local. *Scientific Reports*. 6(June):1–14. DOI: 10.1038/srep27752.

Green, M.R. 2000. TBP-associated factors (TAF(II)s): Multiple, selective transcriptional mediators in common complexes. *Trends in Biochemical Sciences*. 25(2):59–63. DOI: 10.1016/S0968-0004(99)01527-3.

Grsic-Rausch, S., Kobelt, P., Siemens, J.M., Bischoff, M. & Ludwig-Müller, J. 2000. Expression and localization of nitrilase during symptom development of the clubroot disease in Arabidopsis. *Plant Physiology*. 122(2):369–378. DOI: 10.1104/pp.122.2.369.

Grsic, S., Sauerteig, S., Neuhaus, K., Albrecht, M., Rossiter, J. & Ludwig-Muller, J. 1998. Physiological analysis of transgenic *Arabidopsis thaliana* plants expressing one nitrilase isoform in sense or antisense direction. *Journal of Plant Physiology*. 153(3–4):446–456. DOI: 10.1016/S0176-1617(98)80173-9.

Gupta, B. & Huang, B. 2014. Mechanism of salinity tolerance in plants: Physiological, biochemical, and molecular characterization. *International Journal of Genomics*. DOI: 10.1155/2014/701596.

Hager, A. 2003. Role of the plasma membrane H^+-ATPase in auxin-induced elongation growth: Historical and new aspects. *Journal of Plant Research*. 116(6):483–505. DOI: 10.1007/s10265-003-0110-x.

Han, G., Wei, X., Dong, X., Wang, C., Sui, N., Guo, J., Yuan, F., Gong, Z., et al. 2020. Arabidopsis ZINC FINGER PROTEIN1 Acts Downstream of GL2 to Repress Root Hair Initiation and Elongation by Directly Suppressing bHLH Genes. *The Plant cell*. 32(1):206–225. DOI: 10.1105/tpc.19.00226.

Hansen, F.T., Madsen, C.K., Nordland, A.M., Grasser, M., Merkle, T. & Grasser, K.D. 2008. A novel family of plant DNA-binding proteins containing both HMG-box and AT-rich interaction domains. *Biochemistry*. 47(50):13207–13214. DOI: 10.1021/bi801772k.

Harvey, S., Kumari, P., Lapin, D., Griebel, T., Hickman, R., Guo, W., Zhang, R., Parker, J.E., et al. 2020. Downy Mildew effector HaRxL21 interacts with the transcriptional repressor TOPLESS to promote pathogen susceptibility. *PLoS Pathogens*. 16(8):1–30. DOI: 10.1371/JOURNAL.PPAT.1008835.

Haughn, G.W. & Somerville, C. 1986. Sulfonylurea-resistant mutants of *Arabidopsis thaliana*. *MGG Molecular & General Genetics*. 204(3):430–434. DOI: 10.1007/BF00331020.

Hazzouri, K.M., Khraiwesh, B., Amiri, K.M.A., Pauli, D., Blake, T., Shahid, M., Mullath, S.K., Nelson, D., et al. 2018. Mapping of HKT1;5 gene in barley using gwas approach and its implication in salt tolerance mechanism. *Frontiers in Plant Science*. 9(February):1–13. DOI: 10.3389/fpls.2018.00156.

Hickman, R., Hill, C., Penfold, C.A., Breeze, E., Bowden, L., Moore, J.D., Zhang, P., Jackson, A., et al. 2013. A local regulatory network around three NAC transcription factors in stress responses and senescence in Arabidopsis leaves. *Plant Journal*. 75(1):26–39. DOI: 10.1111/tpj.12194.

Higo, K., Ugawa, Y., Iwamoto, M. & Korenaga, T. 1999. Plant cis-acting regulatory DNA elements (PLACE) database: 1999. *Nucleic Acids Research*. 27(1):297–300. DOI: 10.1093/nar/27.1.297.

Hillebrand, H., Bartling, D. & Weiler, E.W. 1998. Structural analysis of the *nit2/nit1/nit3* gene cluster encoding nitrilases, enzymes catalyzing the terminal activation step in indole-acetic acid biosynthesis in *Arabidopsis thaliana*. *Plant Molecular Biology*. 36(1):89–99. DOI: 10.1023/A:1005998918418.

Hmida-Sayari, A., Gargouri-Bouzid, R., Bidani, A., Jaoua, L., Savouré, A. & Jaoua, S. 2005. Overexpression of Δ1-pyrroline-5-carboxylate synthetase increases proline production and confers salt tolerance in transgenic potato plants. *Plant Science*. 169(4):746–752. DOI: 10.1016/j.plantsci.2005.05.025.

Ho, C.K.M. & Strauss, J.F. 2004. Activation of the control reporter plasmids pRL-TK and pRL-SV40 by multiple GATA transcription factors can lead to aberrant normalization of transfection efficiency. *BMC Biotechnology*. 4:1–5. DOI: 10.1186/1471-6750-4-10.

Hoagland, D.R. & Arnon, D.I. 1950. The Water-Culture Method for Growing Plants without Soil. *California Agricultural Experiment Station Circular*. 347:29–31.

Holsters, M., Silva, B., Vliet, F., Genetello, C. & Schell, J. 1980. The Functional Organization of the Nopaline Plasmid pTiC58. *Plasmid*. 3:212–230.

Hong, S.M., Bahn, S.C., Lyu, A., Jung, H.S. & Ahn, J.H. 2010. Identification and Testing of Superior Reference Genes for a Starting Pool of Transcript Normalization in Arabidopsis. *Plant & Cell Physiology*. 51(10):1694–1706. DOI: 10.1093/pcp/pcq128.

Hoopes, G.M., Hamilton, J.P., Wood, J.C., Esteban, E., Pasha, A., Vaillancourt, B., Provart, N.J. & Buell, C.R. 2019. An updated gene atlas for maize reveals organ-specific and stress-induced genes. *Plant Journal*. 97(6):1154–1167. DOI: 10.1111/tpj.14184.

Horie, T. & Schroeder, J.I. 2004. Sodium transporters in plants. Diverse genes and physiological functions. *Plant Physiology*. 136(1):2457–2462. DOI: 10.1104/pp.104.046664.

Horie, T., Costa, A., Kim, T.H., Han, M.J., Horie, R., Leung, H.-Y., Miyao, A., Hirochika, H., et al. 2007. Rice OsHKT2;1 transporter mediates large Na^+ influx component into K^+-starved roots for growth. *The EMBO Journal*. 26(12):3003–3014. DOI: 10.1038/sj.emboj.7601732.

Howden, A.J.M. & Preston, G.M. 2009. Nitrilase enzymes and their role in plant-microbe interactions. *Microbial Biotechnology*. 2(4):441–451. DOI: 10.1111/j.1751-7915.2009.00111.x.

Huh, S.U., Lee, S.-B., Kim, H.H. & Paek, K.-H. 2012. ATAF2, a NAC transcription factor, binds to the promoter and regulates *NIT2* gene expression involved in auxin biosynthesis. *Molecules and Cells*. 34(3):305–313. DOI: 10.1007/s10059-012-0122-2.

Ingle, R.A., Stoker, C., Stone, W., Adams, N., Smith, R., Grant, M., Carré, I., Roden, L.C., et al. 2015. Jasmonate signalling drives time-of-day differences in susceptibility of Arabidopsis to the fungal pathogen *Botrytis cinerea*. *The Plant Journal*. 84(5):937–948. DOI: 10.1111/tpj.13050.

Initiative, T.A.G. 2000. Analysis of the genome sequence of the flowering plant *Arabidopsis thaliana*. *Nature*. 408(6814):796–815. DOI: 10.1038/35048692.

Iqbal, M. & Ashraf, M. 2007. Seed treatment with auxins modulates growth and ion partitioning in salt-stressed wheat plants. *Journal of Integrative Plant Biology*. 49(7):1003–1015. DOI: 10.1111/j.1672-9072.2007.00488.x.

Isayenkov, S. V. & Maathuis, F.J.M. 2019. Plant salinity stress: Many unanswered questions remain. *Frontiers in Plant Science*. 10(February). DOI: 10.3389/fpls.2019.00080.

James, R.A., Rivelli, A.R., Munns, R. & Caemmerer, S. von. 2002. Factors affecting CO_2 assimilation, leaf injury and growth in salt-stressed durum wheat. *Functional Plant Biology*. 29(12):1393. DOI: 10.1071/FP02069.

James, R.A., Blake, C., Byrt, C.S. & Munns, R. 2011. Major genes for Na+ exclusion, *Nax1* and *Nax2* (wheat *HKT1;4* and *HKT1;5*), decrease Na^+ accumulation in bread wheat leaves under saline and waterlogged conditions. *Journal of Experimental Botany*. 62(8):2939–2947. DOI: 10.1093/jxb/err003.

Jamil, A., Riaz, S., Ashraf, M. & Foolad, M.R. 2011. Gene expression profiling of plants under salt stress. *Critical Reviews in Plant Sciences*. 30(5):435–458. DOI: 10.1080/07352689.2011.605739.

Janicka-Russak, M., Kabała, K., Wdowikowska, A. & Kłobus, G. 2013. Modification of plasma membrane proton pumps in cucumber roots as an adaptation mechanism to salt stress. *Journal of Plant Physiology*. 170(10):915–922. DOI: 10.1016/j.jplph.2013.02.002.

Janowitz, T., Trompetter, I. & Piotrowski, M. 2009. Evolution of nitrilases in glucosinolate-containing plants. *Phytochemistry*. 70(15–16):1680–1686. DOI: 10.1016/j.phytochem.2009.07.028.

Jenrich, R., Trompetter, I., Bak, S., Olsen, C.E., Møller, B.L. & Piotrowski, M. 2007. Evolution of heteromeric nitrilase complexes in Poaceae with new functions in nitrile metabolism. *Proceedings of the National Academy of Sciences of the United States of America*. 104(47):18848–18853. DOI: 10.1073/pnas.0709315104.

Jensen, P.J. & Bandurski, R.S. 1994. Metabolism and Synthesis of Indole-3-Acetic Acid (IAA) in *Zea mays*. *Plant Physiology*. 106:343–351.

Ji, H., Pardo, J.M., Batelli, G., Van Oosten, M.J., Bressan, R.A. & Li, X. 2013. The salt overly sensitive (SOS) pathway: Established and emerging roles. *Molecular Plant*. 6(2):275–286. DOI: 10.1093/mp/sst017.

Jia, T., Zhang, K., Li, F., Huang, Y., Fan, M. & Huang, T. 2020. The AtMYB2 inhibits the formation of axillary meristem in Arabidopsis by repressing *RAX1* gene under environmental stresses. *Plant Cell Reports*. 39(12):1755–1765. DOI: 10.1007/s00299-020-02602-3.

Jiang, Y. & Deyholos, M.K. 2006. Comprehensive transcriptional profiling of NaCl-stressed Arabidopsis roots reveals novel classes of responsive genes. *BMC Plant Biology*. 6:1–20. DOI: 10.1186/1471-2229-6-25.

Jiang, X., Leidi, E.O. & Pardo, J.M. 2010. How do vacuolar NHX exchangers function in plant salt tolerance? *Plant Signaling and Behavior*. 5(7):792–795. DOI: 10.4161/psb.5.7.11767.

Jiang, K., Moe-Lange, J., Hennet, L. & Feldman, L.J. 2016. Salt stress affects the redox status of arabidopsis root meristems. *Frontiers in Plant Science*. 7(FEB2016):1–10. DOI: 10.3389/fpls.2016.00081.

Jinno, K., Kimura, W., Komatsu, M., Miura, M., Sakaoka, S., Nomoto, M., Tada, Y., Morikami, A., et al. 2019. Rapid and easy method for *in vitro* determination of transcription factor binding core motifs. *Bioscience, Biotechnology and Biochemistry*. 83(12):2276–2279. DOI: 10.1080/09168451.2019.1659719.

Joung, J.K., Ramm, E.I. & Pabo, C.O. 2000. A bacterial two-hybrid selection system for studying protein-DNA and protein-protein interactions. *Proceedings of the National Academy of Sciences of the United States of America*. 97(13):7382–7387. DOI: 10.1073/pnas.110149297.

Julkowska, M.M. & Testerink, C. 2015. Tuning plant signaling and growth to survive salt. *Trends in Plant Science*, 20(9), 586–594. DOI: 10.1016/j.tplants.2015.06.008.

Julkowska, M.M., Koevoets, I.T., Mol, S., Hoefsloot, H., Feron, R., Tester, M.A., Keurentjes, J.J.B., Korte, A., et al. 2017. Genetic Components of Root Architecture Remodeling in Response to Salt Stress. *The Plant Cell*. 29(12):3198–3213. DOI: 10.1105/tpc.16.00680.

Jung, J.H. & Park, C.M. 2011. Auxin modulation of salt stress signaling in Arabidopsis seed germination. *Plant Signaling and Behavior*. 6(8):1198–1200. DOI: 10.4161/psb.6.8.15792.

Kant, S., Kant, P., Raveh, E. & Barak, S. 2006. Evidence that differential gene expression between the halophyte, *Thellungiella halophila*, and *Arabidopsis thaliana* is responsible for higher levels of the compatible osmolyte proline and tight control of Na^+ uptake in *T. halophila*. *Plant, Cell and Environment*. 29(7):1220–1234. DOI: 10.1111/j.1365-3040.2006.01502.x.

Karakas, B., Ozias-Akins, P., Stushnoff, C., Suefferheld, M., Rieger, M. & Herbst, M. 1997. Salinity and drought tolerance of mannitol-accumulating transgenic tobacco. *Plant, Cell and Environment*. 20(5):609–616. DOI: 10.1111/j.1365-3040.1997.00132.x.

Karimi, M., Inzé, D. & Depicker, A. 2002. GATEWAY™ vectors for Agrobacterium-mediated plant transformation. *Trends in Plant Science*. 7(5):193–195. DOI: 10.1016/S1360-1385(02)02251-3.

Kasuga, M., Liu, Q., Miura, S., Yamaguchi-Shinozaki, K. & Shinozaki, K. 1999. Improving plant drought, salt, and freezing tolerance by gene transfer of a single stress-inducible transcription factor. *Nature Biotechnology*. 17(3):287–291. DOI: 10.1038/7036.

Knight, H., Trewavas, A.J. & Knight, M.R. 1997. Calcium signalling in *Arabidopsis thaliana* responding to drought and salinity. *Plant Journal*. 12(5):1067–1078. DOI: 10.1046/j.1365-313X.1997.12051067.x.

Kornberg, R.D. 1999. Eukaryotic transcriptional control. *Trends in Biochemical Sciences*. 24(12):46–49. DOI: 10.1016/S0968-0004(99)01489-9.

Korver, R.A., Koevoets, I.T. & Testerink, C. 2018. Out of Shape During Stress: A Key Role for Auxin. *Trends in Plant Science*. 23(9):783–793. DOI: 10.1016/j.tplants.2018.05.011.

Kreszies, T., Schreiber, L. & Ranathunge, K. 2018. Suberized transport barriers in Arabidopsis, barley and rice roots: From the model plant to crop species. *Journal of Plant Physiology*. 227(February):75–83. DOI: 10.1016/j.jplph.2018.02.002.

Kriechbaumer, V., Park, W.J., Piotrowski, M., Meeley, R.B., Gierl, A. & Glawischnig, E. 2007. Maize nitrilases have a dual role in auxin homeostasis and β-cyanoalanine hydrolysis. *Journal of Experimental Botany*. 58(15–16):4225–4233. DOI: 10.1093/jxb/erm279.

Kutz, A., Muller, A., Hennig, P., Kaiser, W.M., Piotrowski, M. & Weiler, E.W. 2002. A role for Nitrilase 3 in the regulation of root morphology in sulphur-starving *Arabidopsis thaliana*. *The Plant Journal*. 30(1):95–106. DOI: 10.1046/j.1365-313X.2002.01271.x.

Lee, T.I. & Young, R.A. 2000. Transcription of Eukaryotic Protein-Coding Genes. In *Annual review of Genetics*. V. 34. Weinheim, Germany: Wiley-VCH Verlag GmbH & Co. KGaA. 77–137. DOI: 10.1002/9783527678679.dg10113.

Lehmann, T., Janowitz, T., Sánchez-Parra, B., Alonso, M.-M.P., Trompetter, I., Piotrowski, M. & Pollmann, S. 2017. Arabidopsis NITRILASE 1 Contributes to the Regulation of Root Growth and Development through Modulation of Auxin Biosynthesis in Seedlings. *Frontiers in Plant Science*. 8(January):1–15. DOI: 10.3389/fpls.2017.00036.

Li, B., Byrt, C., Qiu, J., Baumann, U., Hrmova, M., Evrard, A., Johnson, A.A.T., Birnbaum, K.D., et al. 2016. Identification of a stelar-localized transport protein that facilitates root-to-shoot transfer of chloride in Arabidopsis. *Plant Physiology*. 170(2):1014–1029. DOI: 10.1104/pp.15.01163.

Li, L., Yu, X., Thompson, A., Guo, M., Yoshida, S., Asami, T., Chory, J. & Yin, Y. 2009. Arabidopsis MYB30 is a Direct Target of BES1 and Cooperates with BES1 to Regulate Brassinosteroid-Induced Gene Expression. *Plant Journal*. 58(2):275–286. DOI: 10.1111/j.1365-313X.2008.03778.x.Arabidopsis.

Li, Q., Lin, Y.-C., Sun, Y.-H., Song, J., Chen, H., Zhang, X.-H., Sederoff, R.R. & Chiang, V.L. 2012. Splice variant of the SND1 transcription factor is a dominant negative of SND1 members and their regulation in *Populus trichocarpa*. *Proceedings of the National Academy of Sciences*. 109(36):14699–14704. DOI: 10.1073/pnas.1212977109.

Li, X., Li, M., Zhou, B., Yang, Y., Wei, Q. & Zhang, J. 2019. Transcriptome analysis provides insights into the stress response crosstalk in apple (*Malus × domestica*) subjected to drought, cold and high salinity. *Scientific Reports*. 9(1):1–10. DOI: 10.1038/s41598-019-45266-0.

Liao, C., Zheng, Y. & Guo, Y. 2017. MYB30 transcription factor regulates oxidative and heat stress responses through ANNEXIN-mediated cytosolic calcium signaling in Arabidopsis. *New Phytologist*. 216(1):163–177. DOI: 10.1111/nph.14679.

Lin, W.C., Lu, C.F., Wu, J.W., Cheng, M.L., Lin, Y.M., Yang, N.S., Black, L., Green, S.K., et al. 2004. Transgenic tomato plants expressing the Arabidopsis *NPR1* gene display enhanced resistance to a spectrum of fungal and bacterial diseases. *Transgenic Research*. 13(6):567–581. DOI: 10.1007/s11248-004-2375-9.

Lin, Y., Zhang, C., Lan, H., Gao, S., Liu, H., Liu, J., Cao, M., Pan, G., et al. 2014. Validation of Potential Reference Genes for qPCR in Maize across Abiotic Stresses, Hormone Treatments, and Tissue Types. *PLoS ONE*. 9(5):e95445. DOI: 10.1371/journal.pone.0095445.

Liu, W., Li, R.-J., Han, T.-T., Cai, W., Fu, Z.-W. & Lu, Y.-T. 2015. Salt Stress Reduces Root Meristem Size by Nitric Oxide- Mediated Modulation of Auxin Accumulation and Signaling in Arabidopsis. *Plant Physiology*. 168(May):343–356. DOI: 10.1104/pp.15.00030.

Luo, Q., Teng, W., Fang, S., Li, H., Li, B., Chu, J., Li, Z. & Zheng, Q. 2019. Transcriptome analysis of salt-stress response in three seedling tissues of common wheat. *Crop Journal*. 7(3):378–392. DOI: 10.1016/j.cj.2018.11.009.

Luo, M., Zhang, Y., Li, J., Zhang, P., Chen, K., Song, W., Wang, X., Yang, J., et al. 2021. Molecular dissection of maize seedling salt tolerance using a genome-wide association analysis method. *Plant Biotechnology Journal*. 19(10):1937–1951. DOI: 10.1111/pbi.13607.

Luscombe, N.M., Austin, S.E., Berman, H.M. & Thornton, J.M. 2000. An overview of the structures of protein-DNA complexes. *Genome Biology*. 1(1):1–37.

Ma, J. & Ptashne, M. 1987. Deletion analysis of GAL4 defines two transcriptional activating segments. *Cell*. 48(5):847–853. DOI: 10.1016/0092-8674(87)90081-X.

Maas, E. V., Hoffman, G.J., Chaba, G.D., Poss, J.A. & Shannon, M.C. 1983. Salt sensitivity of corn at various growth stages. *Irrigation Science*. 4(1):45–57. DOI: 10.1007/BF00285556.

Maathuis, F.J.M., Ahmad, I. & Patishtan, J. 2014. Regulation of Na^+ fluxes in plants. *Frontiers in Plant Science*. 5(SEP):1–9. DOI: 10.3389/fpls.2014.00467.

Mabuchi, K., Maki, H., Itaya, T., Suzuki, T., Nomoto, M., Sakaoka, S., Morikami, A., Higashiyama, T., et al. 2018. MYB30 links ROS signaling, root cell elongation, and plant immune responses. *Proceedings of the National Academy of Sciences*. 115(20):E4710–E4719. DOI: 10.1073/pnas.1804233115.

Majda, M. & Robert, S. 2018. The role of auxin in cell wall expansion. *International Journal of Molecular Sciences*. 19(4). DOI: 10.3390/ijms19040951.

Mallik, R., Prasad, P., Kundu, A., Sachdev, S., Biswas, R., Dutta, A., Roy, A., Mukhopadhyay, J., et al. 2020. Identification of genome-wide targets and DNA recognition sequence of the Arabidopsis HMG-box protein AtHMGB15 during cold stress response. *Biochimica et Biophysica Acta - Gene Regulatory Mechanisms*. 1863(12):194644. DOI: 10.1016/j.bbagrm.2020.194644.

Manoli, A., Sturaro, A., Trevisan, S., Quaggiotti, S. & Nonis, A. 2012. Evaluation of candidate reference genes for qPCR in maize. *Journal of Plant Physiology*. 169(8):807–815. DOI: 10.1016/j.jplph.2012.01.019.

Mansour, M.M.F., Salama, K.H.A., Ali, F.Z.M. & Abou Hadid, A.F. 2005. Cell and plant responses to NaCl in *Zea mays* L. cultivars differing in salt tolerance. *Gen. Appl. Plant Physiol*. 31(1–2):29–41.

Marschner, H. 1995. The Mineral Nutrition of Higher Plants. In *Academic Press, London*.

Masucci, J.D., Rerie, W.G., Foreman, D.R., Zhang, M., Galway, M.E., Marks, M.D. & Schiefelbein, J.W. 1996. The homeobox gene *GLABRA 2* is required for position-dependent cell differentiation in the root epidermis of Arabidopsis thaliana. *Development*. 122(4):1253–1260.

Matthews, J.C., Hori, K. & Cormier, M.J. 1977. Purification and Properties of *Renilla reniformis* Luciferase. *Biochemistry*. 16(1):85–91. DOI: 10.1021/bi00620a014.

McNabb, D.S., Reed, R. & Marciniak, R.A. 2005. Dual luciferase assay system for rapid assessment of gene expression in *Saccharomyces cerevisiae*. *Eukaryotic Cell*. 4(9):1539–1549. DOI: 10.1128/EC.4.9.1539-1549.2005.

Meinke, D.W., Cherry, J.M., Dean, C., Rounsley, S.D. & Koornneef, M. 1998. *Arabidopsis thaliana*: A model plant for genome analysis. *Science*. 282(5389). DOI: 10.1126/science.282.5389.662.

Mercatelli, D., Scalambra, L., Triboli, L., Ray, F. & Giorgi, F.M. 2020. Gene regulatory network inference resources: A practical overview. *Biochimica et Biophysica Acta - Gene Regulatory Mechanisms*. 1863(6):194430. DOI: 10.1016/j.bbagrm.2019.194430.

Molina, C. & Grotewold, E. 2005. Genome wide analysis of Arabidopsis core promoters. *BMC Genomics*. 6:1–12. DOI: 10.1186/1471-2164-6-25.

Møller, I.S., Gilliham, M., Jha, D., Mayo, G.M., Roy, S.J., Coates, J.C., Haseloff, J. & Tester, M. 2009. Shoot Na^+ Exclusion and Increased Salinity Tolerance Engineered by Cell Type–Specific Alteration of Na^+ Transport in Arabidopsis. *The Plant Cell*. 21(7):2163–2178. DOI: 10.1105/tpc.108.064568.

Mukherjee, C., Zhu, D., Biehl, E.R., Parmar, R.R. & Hua, L. 2006. Enzymatic nitrile hydrolysis catalyzed by nitrilase ZmNIT2 from maize. An unprecedented β-hydroxy functionality enhanced amide formation. *Tetrahedron*. 62(26):6150–6154. DOI: 10.1016/j.tet.2006.04.069.

Munns, R. 1993. Physiological processes limiting plant growth in saline soils: some dogmas and hypotheses. *Plant, Cell and Environment*. 16(1):15–24. DOI: 10.1111/j.1365-3040.1993.tb00840.x.

Munns, R. 2002. Comparative physiology of salt and water stress. *Plant, Cell & Environment*. 25(2):239–250. DOI: 10.1046/j.0016-8025.2001.00808.x.

Munns, R. 2005. Genes and salt tolerance: bringing them together. *New Phytologist*. 167(3):645–663. DOI: 10.1111/j.1469-8137.2005.01487.x.

Munns, R. & Termaat, A. 1986. Whole-plant responses to salinity. *Australian Journal of Plant Physiology*. 13(1):143–160. DOI: 10.1071/PP9860143.

Munns, R. & Tester, M. 2008. Mechanisms of Salinity Tolerance. *Annual Review of Plant Biology*. 59(1):651–681. DOI: 10.1146/annurev.arplant.59.032607.092911.

Munns, R., Day, D.A., Fricke, W., Watt, M., Arsova, B., Barkla, B.J., Bose, J., Byrt, C.S., et al. 2020. Energy costs of salt tolerance in crop plants. *New Phytologist*. 225(3):1072–1090. DOI: 10.1111/nph.15864.

Nagahage, I.S.P., Sakamoto, S., Nagano, M., Ishikawa, T., Kawai-Yamada, M., Mitsuda, N. & Yamaguchi, M. 2018. An NAC domain transcription factor ATAF2 acts as transcriptional activator or repressor dependent on promoter context. *Plant Biotechnology*. 35(3):285–289. DOI: 10.5511/plantbiotechnology.18.0507a.

Nawrath, C. et al. 2013. Apoplastic Diffusion Barriers in Arabidopsis. Arabidopsis Book. [Online] DOI: 10.1199/tab.0167

Nemhauser, J.L., Mockler, T.C. & Chory, J. 2004. Interdependency of Brassinosteroid and Auxin Signaling in Arabidopsis. *PLoS Biology*. 2(9):e258. DOI: 10.1371/journal.pbio.0020258.

Normanly, J., Cohen, J.D. & Fink, G.R. 1993. *Arabidopsis thaliana* auxotrophs reveal a tryptophan-independent biosynthetic pathway for indole-3-acetic acid. *Proceedings of the National Academy of Sciences of the United States of America*. 90(21):10355–10359. DOI: 10.1073/pnas.90.21.10355.

Normanly, J., Grisafi, P., Fink, G.R. & Bartel, B. 1997. Arabidopsis mutants resistant to the auxin effects of indole-3-acetonitrile are defective in the nitrilase encoded by the *NIT1* gene. *The Plant Cell*. 9(10):1781–1790. DOI: 10.1105/tpc.9.10.1781.

O'Connor, T.R., Dyreson, C. & Wyrick, J.J. 2005. Athena: A resource for rapid visualization and systematic analysis of Arabidopsis promoter sequences. *Bioinformatics*. 21(24):4411–4413. DOI: 10.1093/bioinformatics/bti714.

O'Malley, R.C., Barragan, C.C. & Ecker, J.R. 2015. A user's guide to the Arabidopsis T-DNA insertion mutant collections. *Plant Functional Genomics: Methods and Protocols: Second Edition*. 323–342. DOI: 10.1007/978-1-4939-2444-8_16.

O'Malley, R.C., Huang, S.C., Song, L., Lewsey, M.G., Bartlett, A., Nery, J.R., Galli, M., Gallavotti, A., et al. 2016. Cistrome and Epicistrome Features Shape the Regulatory DNA Landscape. *Cell*. 165(5):1280–1292. DOI: 10.1016/j.cell.2016.04.038.

Oh, D.H., Leidi, E., Zhang, Q., Hwang, S.M., Li, Y., Quintero, F.J., Jiang, X., D'urzo, M.P., et al. 2009. Loss of Halophytism by interference with SOS1 expression. *Plant Physiology*. 151(1):210–222. DOI: 10.1104/pp.109.137802.

Ohashi, Y., Oka, A., Ruberti, I., Morelli, G. & Aoyama, T. 2002. Entopically additive expression of *GLABRA 2* alters the frequency and spacing of trichome initiation. *Plant Journal*. 29(3):359–369. DOI: 10.1046/j.0960-7412.2001.01214.x.

Okamoto, M., Kuwahara, A., Seo, M., Kushiro, T., Asami, T., Hirai, N., Kamiya, Y., Koshiba, T., et al. 2006. *CYP707A1* and *CYP707A2*, which encode abscisic acid 8'-hydroxylases, are indispensable for proper control of seed dormancy and germination in Arabidopsis. *Plant Physiology*. 141(1):97–107. DOI: 10.1104/pp.106.079475.

Ouwerkerk, P.B.F. & Meijer, A.H. 2011. Yeast One-Hybrid Screens for Detection of Transcription Factor DNA Interactions. In *Methods in Molecular Biology (Clifton, N.J.)*. V. 678. Humana Press, Totowa, NJ. 211–227. DOI: 10.1007/978-1-60761-682-5_16.

Panta, S., Flowers, T., Lane, P., Doyle, R., Haros, G. & Shabala, S. 2014. Halophyte agriculture: Success stories. *Environmental and Experimental Botany*. 107:71–83. DOI: 10.1016/j.envexpbot.2014.05.006.

Park, H.J., Kim, W.-Y. & Yun, D.-J. 2016. A New Insight of Salt Stress Signaling in Plant. *Molecules and Cells*. 39(6):447–459. DOI: 10.14348/molcells.2016.0083.

Park, W.J., Kriechbaumer, V., Müller, A., Piotrowski, M., Meeley, R.B., Gierl, A. & Glawischnig, E. 2003. The Nitrilase ZmNIT2 Converts Indole-3-Acetonitrile to Indole-3-Acetic Acid. *Plant Physiology*. 133(2):794–802. DOI: 10.1104/pp.103.026609.

Passioura, J.B. & Munns, R. 2000. Rapid environmental changes that affect leaf water status induce transient surges or pauses in leaf expansion rate. *Functional Plant Biology*. 27(10):941–948. DOI: 10.1071/PP99207.

Pasternak, T., Tietz, O., Rapp, K., Begheldo, M., Nitschke, R., Ruperti, B. & Palme, K. 2015. Protocol: An improved and universal procedure for whole-mount immunolocalization in plants. *Plant Methods*. 11(1):1–10. DOI: 10.1186/s13007-015-0094-2.

Piotrowski, M. 2008. Primary or secondary? Versatile nitrilases in plant metabolism. *Phytochemistry*. 69(15):2655–2667. DOI: 10.1016/j.phytochem.2008.08.020.

Piotrowski, M., Schönfelder, S. & Weiler, E.W. 2001. The Arabidopsis thaliana Isogene *NIT4* and Its Orthologs in Tobacco Encode β-Cyano-L-alanine Hydratase/Nitrilase. *Journal of Biological Chemistry*. 276(4):2616–2621. DOI: 10.1074/jbc.M007890200.

Pitann, B., Zörb, C. & Mühling, K.H. 2009. Comparative proteome analysis of maize (*Zea mays* L.) expansins under salinity. *Journal of Plant Nutrition and Soil Science*. 172(1):75–77. DOI: 10.1002/jpln.200800265.

Pitann, B., Kranz, T. & Mühling, K.H. 2009. The apoplastic pH and its significance in adaptation to salinity in maize (*Zea mays* L.): Comparison of fluorescence microscopy and pH-sensitive microelectrodes. *Plant Science*. 176(4):497–504. DOI: 10.1016/j.plantsci.2009.01.002.

Pitann, B., Schubert, S. & Mühling, K.H. 2009. Decline in leaf growth under salt stress is due to an inhibition of H^+-pumping activity and increase in apoplastic pH of maize leaves. *Journal of Plant Nutrition and Soil Science*. 172(4):535–543. DOI: 10.1002/jpln.200800349.

Prakash, L. & Prathapasenan, G. 1990. NaCl- and Gibberellic Acid-induced Changes in the Content of Auxin and the Activities of Cellulase and Pectin Lyase During Leaf Growth in Rice (*Oryza sativa*). *Annals of Botany*. 65(3):251–257.

Proctor, J.D. 2020. The functional characterisation of the XhABFA transcription factor from the resurrection plant *Xerophyta humilis*. University of Cape Town.

Pruneda-paz, J.L., Breton, G., Nagel, D.H., Kang, S.E., Bonaldi, K., Doherty, C.J., Ravelo, S., Galli, M., et al. 2014. A Genome-Scale Resource for the Functional Characterization of Arabidopsis Transcription Factors. *Cell Reports*. 8(2):622–632. DOI: 10.1016/j.celrep.2014.06.033.

Qadir, M., Quillérou, E., Nangia, V., Murtaza, G., Singh, M., Thomas, R.J., Drechsel, P. & Noble, A.D. 2014. Economics of salt-induced land degradation and restoration. *Natural Resources Forum*. 38(4):282–295. DOI: 10.1111/1477-8947.12054.

Qiu, Q.S., Barkla, B.J., Vera-Estrella, R., Zhu, J.K. & Schumaker, K.S. 2003. Na^+/H^+ exchange activity in the plasma membrane of Arabidopsis. *Plant Physiology*. 132(2):1041–1052. DOI: 10.1104/pp.102.010421.

Qiu, Q.S., Guo, Y., Quintero, F.J., Pardo, J.M., Schumaker, K.S. & Zhu, J.K. 2004. Regulation of Vacuolar Na^+/H^+ Exchange in Arabidopsis thaliana by the Salt-Overly-Sensitive (SOS) Pathway. *Journal of Biological Chemistry*. 279(1):207–215. DOI: 10.1074/jbc.M307982200.

Qiu, W., Liu, M., Qiao, G., Jiang, J., Xie, L. & Zhuo, R. 2012. An Isopentyl Transferase Gene Driven by the Stress-Inducible *rd29A* Promoter Improves Salinity Stress Tolerance in Transgenic Tobacco. *Plant Molecular Biology Reporter*. 30(3):519–528. DOI: 10.1007/s11105-011-0337-y.

Raffaele, S., Rivas, S. & Roby, D. 2006. An essential role for salicylic acid in AtMYB30-mediated control of the hypersensitive cell death program in Arabidopsis. *FEBS Letters*. 580(14):3498–3504. DOI: 10.1016/j.febslet.2006.05.027.

Rasheed, S., Bashir, K., Matsui, A., Tanaka, M. & Seki, M. 2016. Transcriptomic analysis of soil-grown *Arabidopsis thaliana* roots and shoots in response to a drought stress. *Frontiers in Plant Science*. 7(FEB2016). DOI: 10.3389/fpls.2016.00180.

Rask, L., Andreasson, E., Ekbom, B., Eriksson, S., Pontoppidan, B. & Meijer, J. 2000. Myrosinase: gene family evolution and herbivore defense in *Brassicaceae*. *Plant Molecular Biology*. 42:93–113. DOI: https://doi.org/10.1023/A:1006380021658.

Rayle, D.L. & Cleland, R. 1970. Enhancement of Wall Loosening and Elongation by Acid Solutions. *Plant Physiology*. 46(2):250–253. DOI: 10.1104/pp.46.2.250.

Rayle, D.L. & Cleland, R.E. 1992. The acid growth theory of auxin-induced cell elongation is alive and well. *Plant Physiology*. 99(4):1271–1274. DOI: 10.1104/pp.99.4.1271.

Redman, J.C., Haas, B.J., Tanimoto, G. & Town, C.D. 2004. Development and evaluation of an Arabidopsis whole genome Affymetrix probe array. *Plant Journal*. 38(3):545–561. DOI: 10.1111/j.1365-313X.2004.02061.x.

Reece-Hoyes, J.S. & Marian Walhout, A.J. 2012. Yeast One-Hybrid Assays: A Historical and Technical Perspective. *Methods*. 57(4):441–447. DOI: 10.1080/10810730902873927.

Regnard, G.L., Halley-Stott, R.P., Tanzer, F.L., Hitzeroth, I.I. & Rybicki, E.P. 2010. High level protein expression in plants through the use of a novel autonomously replicating geminivirus shuttle vector. *Plant Biotechnology Journal*. 8(1):38–46. DOI: 10.1111/j.1467-7652.2009.00462.x.

Ren, Z.H., Gao, J.P., Li, L.G., Cai, X.L., Huang, W., Chao, D.Y., Zhu, M.Z., Wang, Z.Y., et al. 2005. A rice quantitative trait locus for salt tolerance encodes a sodium transporter. *Nature Genetics.* 37(10):1141–1146. DOI: 10.1038/ng1643.

Rengasamy, P. 2010. Soil processes affecting crop production in salt-affected soils. *Functional Plant Biology*. 37(7):613–620. DOI: 10.1071/FP09249.

Reynolds, M. & Tuberosa, R. 2008. Translational research impacting on crop productivity in drought-prone environments. *Current Opinion in Plant Biology*. 11(2):171–179. DOI: 10.1016/j.pbi.2008.02.005.

Riechmann, J.L. 2002. Transcriptional Regulation: a Genomic Overview. *The Arabidopsis Book*. 1(1):e0085. DOI: 10.1199/tab.0085.

Ritchie, M.E., Phipson, B., Wu, D., Hu, Y., Law, C.W., Shi, W. & Smyth, G.K. 2015. Limma powers differential expression analyses for RNA-sequencing and microarray studies. *Nucleic Acids Research*. 43(7):e47. DOI: 10.1093/nar/gkv007.

Rodríguez-Rosales, M.P., Jiang, X., Gálvez, F.J., Aranda, M.N., Cubero, B. & Venema, K. 2008. Overexpression of the tomato K^+/H^+ antiporter LeNHX2 confers salt tolerance by improving potassium compartmentalization. *New Phytologist*. 179(2):366–377. DOI: 10.1111/j.1469-8137.2008.02461.x.

Rodríguez, H.G., Roberts, J.K.M., Jordan, W.R. & Drew, M.C. 1997. Growth, Water Relations, and Accumulation of Organic and Inorganic Solutes in Roots of Maize Seedlings during Salt Stress. *Plant Physiology*. 113(3):881–893. DOI: 10.1104/PP.113.3.881.

Rosso, M.G., Li, Y., Strizhov, N., Reiss, B., Dekker, K. & Weisshaar, B. 2003. An *Arabidopsis thaliana* T-DNA mutagenized population (GABI-Kat) for flanking sequence tag-based reverse genetics. *Plant Molecular Biology*. 53(1–2):247–259. DOI: 10.1023/B:PLAN.0000009297.37235.4a.

Roy, A., Dutta, A., Roy, D., Ganguly, P., Ghosh, R., Kar, R.K., Bhunia, A., Mukhobadhyay, J., et al. 2016. Deciphering the role of the AT-rich interaction domain and the HMG-box domain of ARID-HMG proteins of *Arabidopsis thaliana*. *Plant Molecular Biology*. 92(3):371–388. DOI: 10.1007/s11103-016-0519-y.

Roy, S.J., Negrão, S. & Tester, M. 2014. Salt Resistant Crop Plants. *Current Opinion in Biotechnology*. 26:115–124. DOI: 10.1016/j.copbio.2013.12.004.

Rudashevskaya, E.L., Ye, J., Jensen, O.N., Fuglsang, A.T. & Palmgren, M.G. 2012. Phosphosite Mapping of P-type Plasma Membrane H^+-ATPase in Homologous and Heterologous Environments. *Journal of Biological Chemistry*. 287(7):4904–4913. DOI: 10.1074/jbc.M111.307264.

Rus, A., Yokoi, S., Sharkhuu, A., Reddy, M., Lee, B.H., Matsumoto, T.K., Koiwa, H., Zhu, J.K., et al. 2001. AtHKT1 is a salt tolerance determinant that controls Na^+ entry into plant roots. *Proceedings of the National Academy of Sciences of the United States of America*. 98(24):14150–14155. DOI: 10.1073/pnas.241501798.

Sadowski, I. & Ptashne, M. 1989. A vector for expressing GAL4(1-147) fusions in mammalian cells. *Nucleic Acids Research*. 17(18):7539.

Salazar-Iribe, A. & De-la-Peña, C. 2020. Auxins, the hidden player in chloroplast development. *Plant Cell Reports*. 39(12):1595–1608. DOI: 10.1007/s00299-020-02596-y.

Sambrook, J., Fritsch, E.F. & Maniatis, T. 1989. *Molecular cloning: a laboratory manual*. Harbor Laboratory Press.

Sanan-mishra, N., Pham, X.H., Sopory, S.K. & Tuteja, N. 2005. Pea *DNA helicase 45* overexpression in tobacco confers high salinity tolerance without affecting yield. *Proceedings of the National Academy of Sciences*. 102(2):509–514.

Sasaki-Sekimoto, Y., Taki, N., Obayashi, T., Aono, M., Matsumoto, F., Sakurai, N., Suzuki, H., Hirai, M.Y., et al. 2005. Coordinated activation of metabolic pathways for antioxidants and defence compounds by jasmonates and their roles in stress tolerance in Arabidopsis. *The Plant Journal*. 44(4):653–668. DOI: 10.1111/j.1365-313X.2005.02560.x.

Schmidt, R.C., Müller, A., Hain, R., Bartling, D. & Weiler, E.W. 1996. Transgenic tobacco plants expressing the *Arabidopsis thaliana* Nitrilase II enzyme. *Plant Journal*. 9(5):683–691. DOI: 10.1046/j.1365-313X.1996.9050683.x.

Shabala, S. & Cuin, T.A. 2008. Potassium transport and plant salt tolerance. *Physiologia Plantarum*. 133(4):651–669. DOI: 10.1111/j.1399-3054.2007.01008.x.

Shavrukov, Y. 2013. Salt stress or salt shock: which genes are we studying? *Journal of Experimental Botany*. 64(1):119–127. DOI: 10.1093/jxb/ers316.

Sheen, J. 2002. A transient expression assay using Arabidopsis Mesophyll Protoplasts.

Sherf, B.A., Navarro, S.L., Hannah, R.R. & Wood, K. V. 1996. Promega Notes: Dual-Luciferase™ Reporter Assay: An Advanced Co-Reporter Technology Integrating Firefly and *Renilla* Luciferase. *Promega Notes Magazine*. (57):2.

Sheveleva, E., Chmara, W., Bohnert, H.J. & Jensen, R.G. 1997. Increased salt and drought tolerance by D-ononitol production in transgenic *Nicotiana tabacum* L. *Plant Physiology*. 115(3):1211–1219. DOI: 10.1104/pp.115.3.1211.

Shi, H., Quintero, F.J., Pardo, J.M. & Zhu, J.K. 2002. The putative plasma membrane Na^+/H^+ antiporter SOS1 controls long-distance Na^+ transport in plants. *Plant Cell*. 14(2):465–477. DOI: 10.1105/tpc.010371.

Spartz, A.K., Ren, H., Park, M.Y., Grandt, K.N., Lee, S.H., Murphy, A.S., Sussman, M.R., Overvoorde, P.J., et al. 2014. SAUR Inhibition of PP2C-D Phosphatases Activates Plasma Membrane H^+-ATPases to Promote Cell Expansion in Arabidopsis. *The Plant Cell*. 26(5):2129–2142. DOI: 10.1105/tpc.114.126037.

Stephenson, P., Stacey, N., Brüser, M., Pullen, N., Ilyas, M., O'Neill, C., Wells, R. & Østergaard, L. 2019. The power of model-to-crop translation illustrated by reducing seed loss from pod shatter in oilseed rape. *Plant Reproduction*. 32(4):331–340. DOI: 10.1007/s00497-019-00374-9.

Stepien, P. & Johnson, G.N. 2009. Contrasting responses of photosynthesis to salt stress in the glycophyte Arabidopsis and the halophyte *Thellungiella*: Role of the plastid terminal oxidase as an alternative electron sink. *Plant Physiology*. 149(2):1154–1165. DOI: 10.1104/pp.108.132407.

Stracke, R., Werber, M. & Weisshaar, B. 2001. The R2R3-MYB gene family in *Arabidopsis thaliana*. *Current Opinion in Plant Biology*. 4(5):447–456. DOI: 10.1016/S1369-5266(00)00199-0.

Su, J. & Wu, R. 2004. Stress-inducible synthesis of proline in transgenic rice confers faster growth under stress conditions than that with constitutive synthesis. *Plant Science*. 166(4):941–948. DOI: 10.1016/j.plantsci.2003.12.004.

Suárez, R., Calderón, C. & Iturriaga, G. 2009. Enhanced tolerance to multiple abiotic stresses in transgenic alfalfa accumulating trehalose. *Crop Science*. 49(5):1791–1799. DOI: 10.2135/cropsci2008.09.0573.

Sunarpi, Horie, T., Motoda, J., Kubo, M., Yang, H., Yoda, K., Horie, R., Chan, W.-Y., et al. 2005. Enhanced salt tolerance mediated by AtHKT1 transporter-induced Na_+ unloading from xylem vessels to xylem parenchyma cells. *The Plant Journal*. 44(6):928–938. DOI: 10.1111/j.1365-313X.2005.02595.x.

Szalai, G. & Janda, T. 2009. Effect of Salt Stress on the Salicylic Acid Synthesis in Young Maize (*Zea mays* L.) Plants. *Journal of Agronomy and Crop Science*. 195(3):165–171. DOI: 10.1111/j.1439-037X.2008.00352.x.

Taji, T., Seki, M., Satou, M., Sakurai, T., Kobayashi, M., Ishiyama, K., Narusaka, Y., Narusaka, M., et al. 2004. Comparative genomics in salt tolerance between Arabidopsis and Arabidopsis-related halophyte salt cress using arabidopsis microarray. *Plant Physiology*. 135(3):1697–1709. DOI: 10.1104/pp.104.039909.

Takahashi, K., Hayashi, K.I. & Kinoshita, T. 2012. Auxin activates the plasma membrane H^+-ATPase by phosphorylation during hypocotyl elongation in Arabidopsis. *Plant Physiology*. 159(2):632–641. DOI: 10.1104/pp.112.196428.

Tan, Q.K.G. & Irish, V.F. 2006. The Arabidopsis zinc finger-homeodomain genes encode proteins with unique biochemical properties that are coordinately expressed during floral development. *Plant Physiology*. 140(3):1095–1108. DOI: 10.1104/pp.105.070565.

Tang, M., Liu, X., Deng, H. & Shen, S. 2011. Over-expression of *JcDREB*, a putative AP2/EREBP domain-containing transcription factor gene in woody biodiesel plant *Jatropha curcas*, enhances salt and freezing tolerance in transgenic Arabidopsis thaliana. *Plant Science*. 181(6):623–631. DOI: 10.1016/j.plantsci.2011.06.014.

Teakle, N.L. & Tyerman, S.D. 2010. Mechanisms of Cl^- transport contributing to salt tolerance. *Plant, Cell and Environment*. 33(4):566–589. DOI: 10.1111/j.1365-3040.2009.02060.x.

Tester, M. & Davenport, R. 2003. Na^+ tolerance and Na^+ transport in higher plants. *Annals of Botany*. 91(5):503–527. DOI: 10.1093/aob/mcg058.

Thimann, K. V. & Mahadevan, S. 1964. Nitrilase: I. Occurrence, preparation, and general properties of the enzyme. *Archives of Biochemistry and Biophysics*. 105(1):133–141. DOI: 10.1016/0003-9861(64)90244-9.

Thompson, D.S., Wilkinson, S., Bacon, M.A. & Davies, W.J. 1997. Multiple signals and mechanisms that regulate leaf growth and stomatal behaviour during water deficit. *Physiologia Plantarum*. 100(2):303–313. DOI: 10.1111/J.1399-3054.1997.TB04787.X.

Tognetti, V.B., Bielach, A. & Hrtyan, M. 2017. Redox regulation at the site of primary growth: auxin, cytokinin and ROS crosstalk. *Plant, Cell & Environment*. 40(11):2586–2605. DOI: 10.1111/pce.13021.

Tominaga-Wada, R., Iwata, M., Sugiyama, J., Kotake, T., Ishida, T., Yokoyama, R., Nishitani, K., Okada, K., et al. 2009. The GLABRA2 homeodomain protein directly regulates *CESA5* and *XTH17* gene expression in Arabidopsis roots. *The Plant Journal*. 60(3):564–574. DOI: 10.1111/j.1365-313X.2009.03976.x.

Tyerman, S.D. 1992. Anion Channels in Plants. *Annual Review of Plant Physiology and Plant Molecular Biology*. 43(1):351–373. DOI: 10.1146/annurev.pp.43.060192.002031.

Urao, T., Yamaguchi-Shinozaki, K., Urao, S. & Shinozaki, K. 1993. An Arabidopsis MYB homolog is induced by dehydration stress and its gene product binds to the conserved MYB recognition sequence. *The Plant Cell*. 5:1529–1539. DOI: 10.1105/tpc.5.11.1529.

Vailleau, F., Daniel, X., Tronchet, M., Montillet, J.L., Triantaphylides, C. & Roby, D. 2002. A R2R3-MYB gene, *AtMYB30*, acts as a positive regulator of the hypersensitive cell death program in plants in response to pathogen attack. *Proceedings of the National Academy of Sciences*. 99(15):10179–10184. DOI: 10.1073/pnas.152047199\r152047199.

Vendruscolo, E.C.G., Schuster, I., Pileggi, M., Scapim, C.A., Molinari, H.B.C., Marur, C.J. & Vieira, L.G.E. 2007. Stress-induced synthesis of proline confers tolerance to water deficit in transgenic wheat. *Journal of Plant Physiology*. 164(10):1367–1376. DOI: 10.1016/j.jplph.2007.05.001.

Vorwerk, S., Biernacki, S., Hillebrand, H., Janzik, I., Müller, A., Weiler, E.W. & Piotrowski, M. 2001. Enzymatic characterization of the recombinant *Arabidopsis thaliana* nitrilase subfamily encoded by the *NIT 2/ NIT 1/ NIT 3*-gene cluster. *Planta*. 212(4):508–516. DOI: 10.1007/s004250000420.

Walcher, C.L. & Nemhauser, J.L. 2012. Bipartite Promoter Element Required for Auxin Response. *Plant Physiology*. 158(1):273–282. DOI: 10.1104/pp.111.187559.

Wang, J., Zhu, J., Zhang, Y., Fan, F., Li, W., Wang, F., Zhong, W., Wang, C., et al. 2018. Comparative transcriptome analysis reveals molecular response to salinity stress of salt-tolerant and sensitive genotypes of indica rice at seedling stage. *Scientific Reports*. 8(1):1–13. DOI: 10.1038/s41598-018-19984-w.

Wang, M., Wang, Y., Sun, J., Ding, M., Deng, S., Hou, P., Ma, X., Zhang, Y., et al. 2013. Overexpression of *PeHA1* enhances hydrogen peroxide signaling in salt-stressed Arabidopsis. *Plant Physiology and Biochemistry*. 71:37–48. DOI: 10.1016/j.plaphy.2013.06.020.

Wang, Q., Guan, C., Wang, P., Lv, M.-L., Ma, Q., Wu, G.-Q., Bao, A.-K., Zhang, J.-L., et al. 2015. AtHKT1;1 and AtHAK5 mediate low-affinity Na^+ uptake in Arabidopsis thaliana under mild salt stress. *Plant Growth Regulation*. 75(3):615–623. DOI: 10.1007/s10725-014-9964-2.

Wang, W., Vinocur, B. & Altman, A. 2003. Plant responses to drought, salinity and extreme temperatures: Towards genetic engineering for stress tolerance. *Planta*. 218(1):1–14. DOI: 10.1007/s00425-003-1105-5.

Wang, X., Goregaoker, S.P. & Culver, J.N. 2009. Interaction of the Tobacco Mosaic Virus Replicase Protein with a NAC Domain Transcription Factor Is Associated with the Suppression of Systemic Host Defenses . *Journal of Virology*. 83(19):9720–9730. DOI: 10.1128/jvi.00941-09.

Wang, Z., Gerstein, M. & Snyder, M. 2009. RNA-Seq: a revolutionary tool for transcriptomics. *Nature Reviews Genetics*. 10(1):57–63. DOI: 10.1038/nrg2484.

Weirauch, M.T., Yang, A., Albu, M., Cote, A.G., Montenegro-Montero, A., Drewe, P., Najafabadi, H.S., Lambert, S.A., et al. 2014. Determination and Inference of Eukaryotic Transcription Factor Sequence Specificity. *Cell*. 158(6):1431–1443. DOI: 10.1016/j.cell.2014.08.009.

Weng, Y.S. & Nickoloff, J.A. 1997. Nonselective URA3 colony-color assay in yeast *ade1* or *ade2* mutants. *BioTechniques*. 23(2):237–242. DOI: 10.2144/97232bm13.

De Wet, J.R., Wood, K. V., Helinski, D.R. & DeLuca, M. 1985. Cloning of firefly luciferase cDNA and the expression of active luciferase in *Escherichia coli*. *Proceedings of the National Academy of Sciences of the United States of America*. 82(23):7870–7873. DOI: 10.1073/pnas.82.23.7870.

White, P.J. & Broadley, M.R. 2001. Chloride in soils and its uptake and movement within the plant: A review. *Annals of Botany*. 88(6):967–988. DOI: 10.1006/anbo.2001.1540.

White, P.J. & Karley, A.J. 2010. Potassium. *Plant Cell Monographs*. 17:199–224. DOI: 10.1007/978-3-642-10613-2_9/COVER.

Woodward, A.W. & Bartel, B. 2005. Auxin: Regulation, Action, and Interaction. *Annals of Botany*. 95:707–735. DOI: 10.1093/aob/mci083.

Wu, H. 2018. Plant salt tolerance and Na^+ sensing and transport. *Crop Journal*. 6(3):215–225. DOI: 10.1016/j.cj.2018.01.003.

Wu, C.A., Yang, G.D., Meng, Q.W. & Zheng, C.C. 2004. The cotton *GhNHX1* gene encoding a novel putative tonoplast Na^+/H^+ antiporter plays an important role in salt stress. *Plant and Cell Physiology*. 45(5):600–607. DOI: 10.1093/pcp/pch071.

Wu, H., Shabala, L., Barry, K., Zhou, M. & Shabala, S. 2013. Ability of leaf mesophyll to retain potassium correlates with salinity tolerance in wheat and barley. *Physiologia Plantarum*. 149(4):515–527. DOI: 10.1111/ppl.12056.

Wu, H., Zhu, M., Shabala, L., Zhou, M. & Shabala, S. 2015. K^+ retention in leaf mesophyll, an overlooked component of salinity tolerance mechanism: A case study for barley. *Journal of Integrative Plant Biology*. 57(2):171–185. DOI: 10.1111/jipb.12238.

Xia, C., Wang, Y.-J., Liang, Y., Niu, Q.-K., Tan, X.-Y., Chu, L.-C., Chen, L.-Q., Zhang, X.-Q., et al. 2014. The ARID-HMG DNA-binding protein AtHMGB15 is required for pollen tube growth in *Arabidopsis thaliana*. *The Plant Journal*. 79(5):741–756. DOI: 10.1111/tpj.12582.

Xiang, C.C. & Chen, Y. 2000. cDNA microarray technology and its applications. *Biotechnology Advances*. 18(1):35–46. DOI: 10.1016/S0734-9750(99)00035-X.

Xu, G., Magen, H., Tarchitzky, J. & Kafkafi, U. 1999. Advances in Chloride Nutrition of Plants. *Advances in Agronomy*. 68(C). DOI: 10.1016/S0065-2113(08)60844-5.

Yamasaki, H., Hayashi, M., Fukazawa, M., Kobayashi, Y. & Shikanai, T. 2009. SQUAMOSA promoter binding protein-like7 is a central regulator for copper homeostasis in Arabidopsis. *Plant Cell*. 21(1):347–361. DOI: 10.1105/tpc.108.060137.

Yang, Y. & Guo, Y. 2018. Elucidating the molecular mechanisms mediating plant salt-stress responses. *New Phytologist*. 217(2):523–539. DOI: 10.1111/nph.14920.

Yang, A., Dai, X. & Zhang, W.H. 2012. A R2R3-type MYB gene, *OsMYB2*, is involved in salt, cold, and dehydration tolerance in rice. *Journal of Experimental Botany*. 63(7):2541–2556. DOI: 10.1093/jxb/err431.

Yanhui, C., Xiaoyuan, Y., Kun, H., Meihua, L., Jigang, L., Zhaofeng, G., Zhiqiang, L., Yunfei, Z., et al. 2006. The MYB transcription factor superfamily of Arabidopsis: Expression analysis and phylogenetic comparison with the rice MYB family. *Plant Molecular Biology*. 60(1):107–124. DOI: 10.1007/s11103-005-2910-y.

Yeo, A.R., Lee, À.S., Izard, P., Boursier, P.J. & Flowers, T.J. 1991. Short- and Long-Term Effects of Salinity on Leaf Growth in Rice (*Oryza sativa* L.). *Journal of Experimental Botany*. 42(7):881–889. DOI: 10.1093/JXB/42.7.881.

Yoo, J.H., Park, C.Y., Kim, J.C., Do Heo, W., Cheong, M.S., Park, H.C., Kim, M.C., Moon, B.C., et al. 2005. Direct interaction of a divergent CaM isoform and the transcription factor, MYB2, enhances salt tolerance in Arabidopsis. *Journal of Biological Chemistry*. 280(5):3697–3706. DOI: 10.1074/jbc.M408237200.

Yoo, S.D., Cho, Y.H. & Sheen, J. 2007. Arabidopsis mesophyll protoplasts: A versatile cell system for transient gene expression analysis. *Nature Protocols*. 2(7):1565–1572. DOI: 10.1038/nprot.2007.199.

Yu, C.-P., Lin, J.-J. & Li, W.-H. 2016. Positional distribution of transcription factor binding sites in *Arabidopsis thaliana*. *Scientific Reports*. 6:25164. DOI: 10.1038/srep25164.

Yu, L., Chen, H., Guan, Q., Ma, X., Zheng, X., Zou, C. & Li, Q. 2012. AtMYB2 transcription factor can interact with the *CMO* promoter and regulate its downstream gene expression. *Biotechnology Letters*. 34(9):1749–1755. DOI: 10.1007/s10529-012-0961-0.

van Zelm, E., Zhang, Y. & Testerink, C. 2020. Salt Tolerance Mechanisms of Plants. *Annual Review of Plant Biology*. 71:403–433. DOI: 10.1146/annurev-arplant-050718-100005.

Vom Endt, D., Kijne, J.W. and Memelink, J., 2002. Transcription factors controlling plant secondary metabolism: what regulates the regulators? *Phytochemistry*, *61*(2):107-114. DOI: 10.1016/S0031-9422(02)00185-1

Zhang, B. & Horvath, S. 2005. A General Framework for Weighted Gene Co-Expression Network Analysis. *Statistical Applications in Genetics and Molecular Biology*. 4(1):Article17. DOI: 10.2202/1544-6115.1128.

Zhao, Y. 2010. Auxin Biosynthesis and Its Role in Plant Development. *Annual Review of Plant Biology*. 61(1):49–64. DOI: 10.1146/annurev-arplant-042809-112308.

Zhao, C., Zhang, H., Song, C., Zhu, J.-K. & Shabala, S. 2020. Mechanisms of Plant Responses and Adaptation to Soil Salinity. *The Innovation*. 1(1):100017. DOI: 10.1016/j.xinn.2020.100017.

Zhang, M., Li, Y., Liang, X., Lu, M., Lai, J., Song, W. & Jiang, C. 2023. A teosinte-derived allele of an HKT1 family sodium transporter improves salt tolerance in maize. *Plant Biotechnology Journal.* 21(1):97–108. DOI: 10.1111/pbi.13927.

Zheng, Y., Jiao, C., Sun, H., Rosli, H.G., Pombo, M.A., Zhang, P., Banf, M., Dai, X., et al. 2016. iTAK: A Program for Genome-wide Prediction and Classification of Plant Transcription Factors, Transcriptional Regulators, and Protein Kinases. *Molecular Plant*. 9(12):1667–1670. DOI: 10.1016/j.molp.2016.09.014.

Zhu, J.K. 2002. Salt and drought stress signal transduction in plants. *Annual Review of Plant Biology.* 53: 243–273. DOI: 10.1146/annurev.arplant.53.091401.143329.

Zhu, B., Su, J., Chang, M., Verma, D.P.S., Fan, Y.L. & Wu, R. 1998. Overexpression of a Δ1-pyrroline-5-carboxylate synthetase gene and analysis of tolerance to water- and salt-stress in transgenic rice. *Plant Science.* 139:41-48. DOI: 10.1016/S0168-9452(98)00175-7.

Zou, C., Sun, K., Mackaluso, J.D., Seddon, A.E., Jin, R., Thomashow, M.F. & Shiu, S.H. 2011. Cis-regulatory code of stress-responsive transcription in *Arabidopsis thaliana*. *Proceedings of the National Academy of Sciences of the United States of America*. 108(36):14992–14997. DOI: 10.1073/pnas.1103202108.